STEROID 5-ALPHA REDUCTASE INHIBITORS, PHYSICOCHEMICAL PROPERTIES, AND PREFORMULATION STUDIES OF TEAK LEAF EXTRACT

KAMONLAK INSUMRONG

A Thesis Submitted to the Graduate School of Naresuan University
in Partial Fulfillment of the Requirements
for the Doctor of Philosophy in Chemistry- (Type 1.1)
2023

STEROID 5-ALPHA REDUCTASE INHIBITORS, PHYSICOCHEMICAL PROPERTIES, AND PREFORMULATION STUDIES OF TEAK LEAF EXTRACT

KAMONLAK INSUMRONG

A Thesis Submitted to the Graduate School of Naresuan University
in Partial Fulfillment of the Requirements
for the Doctor of Philosophy in Chemistry- (Type 1.1)
2023

Thesis entitled "Steroid 5-alpha reductase inhibitors, physicochemical properties, and preformulation studies of teak leaf extract"

By Kamonlak Insumrong

has been approved by the Graduate School as partial fulfillment of the requirements

for the Doctor of Philosophy in Chemistry- (Type 1.1) of Naresuan University

Oral Defense Committee

..... Chair
(Jukkarin Srivilai, Ph.D.)

..... Advisor
(Assistant Professor Nungruthai Suphrom, Ph.D.)

..... Co Advisor
(Associate Professor Kornkanok Ingkaninan, Ph.D.)

..... Co Advisor
(Associate Professor Neti Waranuch, Ph.D.)

..... Internal Examiner
(Associate Professor Boonjira Rutnakornpituk, Ph.D.)

Approved

.....
(Associate Professor Krongkarn Chootip, Ph.D.)
Dean of the Graduate School

Title	STEROID 5-ALPHA REDUCTASE INHIBITORS, PHYSICOCHEMICAL PROPERTIES, AND PREFORMULATION STUDIES OF TEAK LEAF EXTRACT
Author	Kamonlak Insumrong
Advisor	Assistant Professor Nungruthai Suphrom, Ph.D.
Co-Advisor	Associate Professor Kornkanok Ingkaninan, Ph.D. Associate Professor Neti Waranuch, Ph.D.
Academic Paper	Ph.D. Dissertation in Chemistry- (Type 1.1), Naresuan University, 2023
Keywords	Tectona grandis L.f. 5alpha-reductase inhibitors physicochemical properties stability skin penetration pre-formulation

ABSTRACT

The enzyme steroid 5α-reductase plays a pivotal role in the conversion of testosterone to dihydrotestosterone, a process linked to various androgen-dependent disorders. In the previous study, our research group explored the biological activities of *Tectona grandis* L.f. extracts, particularly their potential for addressing hair loss concerns. Notably, the hexane extract of *T. grandis* leaves exhibited promise as a 5α-reductase inhibitor. The objectives of the current study were therefore to purify and identify the 5α-reductase inhibitors from the *T. grandis* leaf-hexane extract. These isolated compounds were then used as bioactive compounds for the standardization of the extract. The physicochemical properties and stability profiles of extracts were also investigated. The study was extended to examine the skin penetration of extracts and their bioactive constituents, which will provide necessary information for the future formulation of products containing *T. grandis* leaves.

Three terpenoid compounds isolated from *T. grandis* leaves, namely (+)-eperua-8,13-dien-15-oic acid (1), (+)-eperua-7,13-dien-15-oic acid (2), and lupeol (3), were successfully identified by spectroscopic analysis. Their 5α-reductase inhibitory activity was assessed, revealing that compound 3 had weak inhibitory -activity while 1 and 2 exhibited potent inhibition. An HPLC method was developed for the quantitative

determination of two potent inhibitors (1 and 2) and quality control of *T. grandis* leaf extracts. Compounds 1 and 2 displayed higher content in the ethanolic extract than hexane extract suggesting that ethanol is a more preferable solvent for extraction. The quality control and extraction methods are beneficial for the continued development of *T. grandis* leaf extract as a hair loss treatment ingredient.

The appropriate vehicle for the *in-vitro* skin penetration study was determined using the shake flask method. Compounds 1 and 2 have poor solubility in distilled water while their solubility in HEPES buffer with 2% w/v of Tween20 was significantly greater. These findings suggest that the HEPES buffer may be an appropriate vehicle for further skin penetration study. The partition coefficients of 1 and 2 were hydrophobic compounds. As well, other physicochemical properties were also reported. The study of physicochemical properties provides information for designing and developing an appropriate formulation for a more effective assessment of bioactive compounds in pre-formulation studies.

Furthermore, there is currently no information in the literature on a pre-formulation study of two 5α-reductase inhibitors (1 and 2) in *T. grandis* extract, and their chemical stability is unknown. Therefore, this research aimed to determine how pH, temperature, and light affected the stability of 1 and 2 in crude ethanolic extract and ethanolic extract in PG with PEG-40 as a solubilizer. Moreover, these two extracts were also tested in buffered solution forms. Their residual concentrations of 1 and 2 were analyzed using the HPLC method. Compounds 1 and 2 were stable in acidic environments. Their degradations were extremely sensitive to light, particularly the degradation of 1 in the buffered solution form of ethanolic extract in PG. In the buffered solution form of ethanolic extract, both marker compounds exhibited rapid degradation under high temperatures. However, the addition of PG effectively reduced their degradation, particularly when protected from light. The calculated shelf-life of 1 and 2 was 1.48 years. Therefore, the extracts should be stored in a prepared extract form or otherwise in a slightly acidic environment with light protection. Additionally, the *in-vitro* skin penetration of 1 and 2 in both ethanolic extract and ethanolic extract in PG was evaluated using Franz diffusion cells. After 24 h, 1 demonstrated notably greater penetration in both extracts, showing significantly higher cumulative amounts (%) than

2. These observations indicate that the higher hydrophobicity of 1 facilitated its more efficient penetration into the stratum corneum. These studies provide valuable information that will aid in the further development of *T. grandis* extract-containing hair loss treatments.

ACKNOWLEDGEMENTS

I would like to express my deep gratitude to my advisor, Assistant Professor Dr. Nungruthai Suphrom, of the Faculty of Science at Naresuan University, for her invaluable advice, guidance, enthusiastic encouragement, giving good opportunities, and useful critiques of this research. I appreciate things that she has taught me, not only about research methodologies but about life as well. Without her assistance and encouragement, I might not have been able to complete this thesis.

I would also like to acknowledge my co-advisors, Associate Professor Dr. Kornkanok Ingkaninan and Associate Professor Dr. Neti Waranuch, both of the Faculty of Pharmaceutical Sciences, for their insightful comments, suggestions, and frequent assistance in the compilation of this work.

Special thanks are given to Dr. Wudtichai Wisuitiprot, of the Department of Thai Traditional Medicine at Sirindhorn College of Public Health, for his invaluable technical support, and to my colleague, Miss Nutchaninad Tanuphol for her advice on the research methodologies and her assistance with problem-solving in the lab. The author is also thankful to Dr. Trinop Promgool for his guidance to learn about structure elucidation, Dr. Eakkaluk Wongwad who contributed technical support in stability and in-vitro skin penetration studies and prepared the manuscript, and Dr. Ngamrayu Ngamdokmai for their kind help throughout my study.

In addition, I would like to thank Mr. Roy I. Morien of the Naresuan University Graduate School for editing this thesis and manuscript's grammar, syntax, and general expression.

This research was made possible in part by a generous grant from the Science Achievement Scholarship of Thailand (SAST), the NSRF via the Program Management Unit for Human Resources & Institutional Development, Research and Innovation [grant number C00SC65030008], and the Department of Chemistry, Faculty of Science, Naresuan University. I also would like to give special thanks to the Bioscreening unit, Cosmetics and Natural Products Research Center (COSNAT) in the Faculty of Pharmaceutical Sciences, Naresuan University for their laboratory facilities and valuable materials. I am also thankful to all staff members of the Department of Chemistry, Science lab centre, Faculty of Science, Naresuan University.

Finally, I am forever grateful to my family and friends for all their love and support during the period of this research.

Kamonlak Insumrong

TABLE OF CONTENTS

Page

LIST OF TABLES

Page

LIST OF FIGURES

Page

CHAPTER I
INTRODUCTION

1.1 Background and significance of the study

Testosterone is the most abundant androgen circulating in many androgen-sensitive tissues, and it can be converted to the more potent, dihydrotestosterone (DHT) by the steroid 5α-reductase enzyme, which requires nicotinamide adenine dinucleotide phosphate (NADPH) as a cofactor [1,2]. These androgenic hormones are capable of binding to androgen nuclear receptors and causing a variety of hormonal effects. A high level of DHT production can led to a variety of androgen-dependent disorders, including benign prostatic hyperplasia (BPH), androgenic alopecia (AGA), prostate cancer, female hirsutism, and acne [3,4].

Male pattern baldness, also known as androgenic alopecia (AGA), is the most common kind of hair loss, affecting both genders on a significant scale and exerting impacts on mental well-being and overall life quality. It is estimated that 0.2–2% of the world's population experiences hair loss [5,6]. AGA is inherited, androgen-dependent, related to 5α-reductase type 1, and presents in a distinct pattern. Therefore, the use of anti-androgens targeting 5α-reductase inhibition and/or androgen receptor blockers may be beneficial in the treatment of AGA. The US Food and Drug Administration (FDA) has only approved finasteride (5α-reductase type 2 inhibitor) and minoxidil (vasodilator) as treatments for AGA. However, these drugs can cause various adverse effects. For instance, topical minoxidil may cause scalp discomfort, itching, and allergic contact dermatitis [7], whereas oral finasteride may cause gynecomastia, altered sexual function including abnormal ejaculation, and even impairment of muscle growth [8,9]. Interestingly, it was necessary to discover and identify alternative 5α-reductase inhibitors. According to numerous research studies, many plants have been used to prevent or treat hair loss. Therefore, natural products may satisfy this requirement.

Tectona grandis L.f. is well-known locally as a teak tree (English) or sak (Thai) and is a member of the Lamiaceae family. It is a large deciduous tree that may reach a height of over 30 m under favorable conditions. Teak is a tropical plant that can

be founded in South and Southeast Asia and has a world-wide reputation for being a quality timber due to its exceptional physical and mechanical properties such as decay resistance, durability, elasticity, and strength. Teak wood is commonly used for furniture, carving, cabinetry, and door and window construction due to its superior texture, color, and finishing qualities [10]. Teak leaves have traditionally been used as a natural dye or coloring agent for textile production and food coloring. In addition, they have been identified as a new source of natural hair dyes derived from plants [11,12]. Besides its various applications, *T. grandis* plays a significant role in traditional Indian medicine. Various parts of this plant are attributed with several traditional uses, including anti-inflammatory, hair growth-promoting, skin diseases-treating, cooling, antibilious, anthelmintic, bronchitis, anuria, and urinary retention effects [13]. The seeds, fruit, roots, leaves, bark and wood of *T. grandis* have all been identified as potential sources of secondary metabolite constituents. These include anthraquinones, naphthoquinones [14,15], phenolic compounds [16], terpenoids [17], apocarotenoids [18], lignans, norlignans [19], fatty esters [20], phenylethanoid glycosides [21], and steroids or saponins [17,22]. The Indian system has traditionally employed *T. grandis* seeds as a hair tonic. From the literature, Jaybhaye et al. demonstrated the influence of petroleum ether extract derived from *T. grandis* seeds on the hair growth activity in albino mice. The study revealed that treatment with 5% and 10% petroleum ether extracts exhibited higher efficacy in promoting hair follicle growth compared to the positive control, minoxidil [23].

In a recent study conducted by Fachrunniza et al., a research study was undertaken to explore the biological activities of *T. grandis* in various parts, including the peels of fruit, seeds, leaves, fruits, woods, and barks. The investigation focused on the sequential solvent extraction with various solvents to prepare extracts, which were subsequently evaluated for their potential application in the treatment of hair loss. Hexane and ethyl acetate extracts of *T. grandis* leaf exhibited potent anti-testosterone activity and anti-inflammatory properties by inhibiting interleukin 1 beta (IL-1β) secretion in lipopolysaccharide (LPS)-stimulated RAW 264.7 cells. This discovery implies the potential utility of *T. grandis* leaf extract as a valuable active ingredient in pharmaceutical products targeting hair loss treatment [24]. Interestingly, the marker compounds for 5α-reductase inhibitory activity of this plant have not yet been

identified. Therefore, the objective of this study was to isolate and identify the 5α-reductase inhibitors from the leaf-hexane extract of *T. grandis* using bioassay-guided fractionation. The isolated 5α-reductase inhibitors will serve as quality control biomarkers for *T. grandis* leaf extract.

Furthermore, pre-formulation studies for the further development of products are still needed to improve their potency and stability. The preparation of extract with the proper extraction solvents should be considered for the continued development of products containing teak extract. Our preliminary results found that ethyl acetate and hexane extracts of *T. grandis* leaf exhibited significant 5α-reductase inhibition. However, these extracts contained gum components that could pose challenges for product development. Interestingly, the extraction of *T. grandis* leaf with 95% ethanol yielded an extract devoid of gum components. This ethanolic extract could inhibit 5α-reductase activity in the same range of concentration (μg/mL) as hexane extract and showed less cytotoxicity on Human Hair Follicle Dermal Papilla Cells (HFDPCs) than hexane extract. Thus, the ethanolic extract was used as a crude sample for the pre-formulation studies. Analytical techniques including Thin layer chromatography (TLC) and high-performance liquid chromatography (HPLC) were developed to analyze the bioactive constituents present in both *T. grandis* leaf hexane and ethanolic extract.

In the cosmetic, food and pharmaceutical industries, crude extracts are usually prepared in a carrier solvent. Propylene glycol (PG) and polyethylene glycol (PEG) are synthetic viscous liquids that are among the most widely used solvents in these industries. This synthetic alcohol can absorb water and maintain moisture in many product formulations. The FDA has authorized the usage of PG solvent in food products as it is generally considered as safe. It is utilized in pharmaceuticals, cosmetics, and foods to preserve moisture [25,26]. Thus, the crude *T. grandis* ethanolic extract prepared in PG solvent containing PEG-40 as a solubilizer is therefore one of the samples targeted for pre-formulation studies in the current investigation. The pre-formulation study is essential for ensuring that the final formulation of products is safe to use and maintains the quality of the extract. There is currently no information in the literature on a pre-formulation study of 5α-reductase inhibitors in *T. grandis* extract and their chemical stability is unknown. Therefore, the aim of this investigation was to

evaluate the effect of PG and PEG-40 on the stability of bioactive compounds in *T. grandis* leaf ethanolic extract and ethanolic extract in PG. Specifically, we assessed their chemical stability across diverse pH, temperature, and light conditions. We also investigated their physicochemical properties, including solubility, pH, color, zeta potential, viscosity, and partition coefficient. In addition, the effects of bioactive compounds in *T. grandis* leaf ethanolic extract and ethanolic extract in PG on the *in vitro* skin penetration behavior were investigated. The obtained information would be useful for future quality control, product design, and development.

1.2 Purposes of the study

1. To isolate and identify 5α-reductase inhibitors from *T. grandis* leaf hexane extract
2. To develop methods for analyzing of bioactive constituents in *T. grandis* leaf hexane and ethanolic extracts
3. To study the physicochemical properties of *T. grandis* leaf ethanolic extract and ethanolic extract in PG
4. To study the stability of bioactive compounds in *T. grandis* leaf ethanolic extract and ethanolic extract in PG
5. To investigate the *in vitro* skin penetration behavior of bioactive compounds in *T. grandis* leaf ethanolic extract and ethanolic extract in PG

1.3 Scope of the study

The dried leaf powder of *T. grandis* was extracted with hexane to produce a crude hexane extract. The extract was utilized to purify the 5α-reductase inhibitors. Additionally, another portion of the dried leaf powder was macerated using 95% ethanol to yielded the crude ethanolic extract. Moreover, solubilizing a crude ethanolic extract with PEG-40 hydrogenated castor oil and then adding PG resulted in ethanolic extract in PG. Both *T. grandis* leaf ethanolic extract and ethanolic extract in PG were used as crude samples for investigation of physicochemical properties and conducting pre-formulation studies. In this study, we aimed to isolate and characterize the 5α-reductase inhibitors present in the hexane extract of *T. grandis* leaf by combining chromatographic techniques with *in vitro* 5α-reductase inhibitory activity assay-guided

fractionation. The identification of the structures of isolated compounds were accomplished by the utilization of spectroscopic techniques. TLC and HPLC methods for the analysis of chemical constituents in the ethanolic extract of *T. grandis* leaf were developed. Moreover, the physicochemical properties (i.e. solubility, pH, color, zeta potential, viscosity, and partition coefficient) were studied. The degradation of 5α-reductase inhibitors in the *T. grandis* leaf ethanolic extract and ethanolic extract in PG was assessed in both prepared extract and diluted solution forms, after storage at the designed conditions. To conduct acid-base degradation studies, the ethanolic extract was maintained in four different pH solutions (2.0, 5.5, 7.4, and 9.0) at room temperature (25 °C) for a month. The optimal pH condition was used for the preparation of ethanolic extract and ethanolic extract in PG as buffered solution forms for other stability tests. To study the effect of temperature, both prepared extract and solution forms of ethanolic extract and ethanolic extract in PG were tested for six months under four different temperature conditions; 50, 60, 70, and 80 °C. In addition, the influence of light on the stability of both forms of ethanolic extract and ethanolic extract in PG was also tested by exposure to the samples in Q-SUN xenon test chambers under suitable conditions according to ICH guidelines. All samples were analyzed at various time intervals and the remaining 5α-reductase inhibitors were determined using a developed HPLC system. Moreover, the prepared extract form of ethanolic extract after being maintained under various conditions was evaluated for 5α-reductase inhibitory activity. For the further development of the extract and its constituents as tropical products, the skin penetration was also studied using a Franz diffusion cell, and the content of markers was quantitatively examined by HPLC analysis. The data from this pre-formulation study will be useful for further product design and development.

1.4 Expected output

1. The 5α-reductase inhibitors were successfully isolated and identified from the *T. grandis* leaf.

2. The TLC and HPLC methods for qualitative and quantitative analyses of bioactive constituents in *T. grandis* leaf ethanolic extract were developed.

3. The physicochemical properties of *T. grandis* leaf ethanolic extract and ethanolic extract in PG were studied.

4. The stability profiles of *T. grandis* leaf ethanolic extract and ethanolic extract in PG were demonstrated.

5. The *in vitro* skin penetration of *T. grandis* leaf ethanolic extract and ethanolic extract in PG was investigated.

CHAPTER II
LITERATURE REVIEW

2.1 Background of androgen hormones

Androgens, which are sex steroid hormones essential in both males and females, play a pivotal role in the development of anabolism, behavior, and secondary sexual characteristics such as pubic, axillary, and facial hair. They also contribute to the maturation of male muscle mass and skeletal integrity [27]. Testosterone, the predominant circulating androgen found in both genders, constitutes around 97% of which is bound to albumin and sex hormone-binding globulin, leaving only 3% available for biological activity. Testosterone synthesis primarily occurs in the Leydig cells of the testis, regulated by the hypothalamus and anterior pituitary glands, and is also produced in the ovaries of women [28,29]. The enzyme steroid 5α-reductase can metabolize testosterone to dihydrotestosterone (DHT) in most tissues, and nicotinamide adenine dinucleotide phosphate (NADPH) is used as a cofactor (Figure 1) [2].

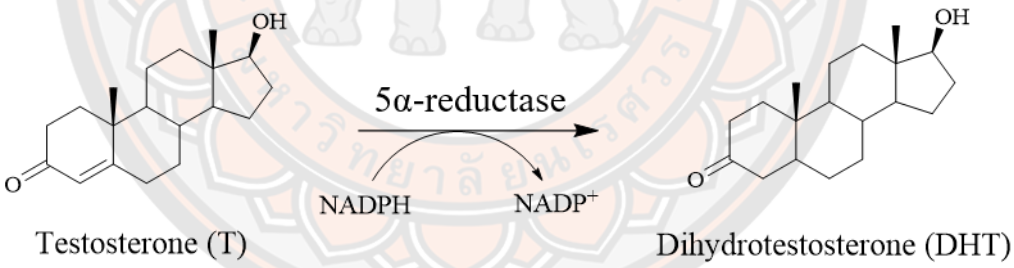

Figure 1 The enzymatic reaction of steroid 5α-reductase [2].

2.2 Steroid 5α-reductase

The enzyme steroid 5α-reductase (3-oxo-steroid-4-ene-dehydrogenase [5α-reductase; EC 1.3.99.5]) is a membrane-bond protein that utilizes NADPH as a cofactor to catalyze the reduction of 4-ene-3-oxosteroids to 5α-3-oxosteroids [2]. There are three isozymes of steroid 5α-reductase known as type 1 to type 3. These isozymes are localized within specific target cells [29]. Type 2 isozyme is primarily found in the genital skin, prostate, and scalp hair follicles, while type 1 is the dominant species expressed in hair follicles, sebaceous glands, and the liver.

Type 3 isozyme is predominantly expressed in various benign and malignant tissues [2,30,31]. The distribution of these three isozymes across different tissues is outlined in Table 1.

Table 1 Comparison of tissue distributions of steroid 5α-reductase isozymes [2,30,31].

Type of 5α-reductase	**Tissue distributions**
Type 1	"Sebaceous glands of the skin, sweat glands, dermal papilla cells, prostate cancer, fibroblasts from all areas, epidermal keratinocytes, hair follicles, liver, brain"
Type 2	"Normal prostate, genital skin, epididymis, seminal vesicles, hair follicles"
Type 3	"Malignant prostate, prostate cancer, breast cancer, lung carcinoma, skin and preadipocytes, and many other tissues"

Although some properties of type 1 and type 2 share some similarities, they differ in biochemical, pharmacological, and chromosomal location characteristics. For example, the optimal pH range of type 1 isoform covers a broad spectrum from neutral to basic (6.5-8.5), while type 2 isoform maintains activity within a narrower acidic pH range (4.5-5.5) [2,30,31] as described in Table 2.

Table 2 Characteristics of different steroid 5α-reductase isozymes [2,30,31].

Properties of isozyme	**Type 1**	**Type 2**	**Type 3**
Substrate testosterone K_m (affinity)	1,000-5,000 nM	4-100 nM	14,000 nM
Substrate progesterone K_m	300 nM	300 nM	-
Substrate corticosterone K_m	18,000 nM	4,000 nM	-
pH optimum	6.0-8.5	5.0-5.5	6.5-6.9
Hydro-lipophilicity	Hydrophobic	Hydrophobic	Hydrophobic
Amino acid count	259 residues	245 residues	318 residues
Molecular weight	29.46 kDa	27.00 kDa	36.51 kDa
Gene location	SRD5A1, 5p15	SRD5A2, 2p23	SRD5A3, 4q12
Gene designation	SRD5A1; 5α-reductase 1	SRD5A1; 5α-reductase 2	SRD5A1; 5α-reductase 3
Gene designation	5 exons, 4 introns	5 exons, 4 introns	5 exons, 4 introns
Finasteride inhibition (IC_{50})	26-500 nM	0.1-25 nM	17.4 nM
Dutasteride inhibition (IC_{50})	2-50 nM	0.5-35 nM	0.33 nM

Steroid 5α-reductase plays a crucial role in converting testosterone into the more potent DHT, which approximately 10 times more potent. DHT exhibits greater activity than testosterone due to its higher affinity for the androgen receptor [2,29]. Excessive DHT production results in various androgen-dependent disorders, including BPH, AGA, prostate cancer, hirsutism and acne [32].

2.3 Mechanism of action of androgens

2.3.1 Mechanism of the 5α-reductase action

The mechanism described for this process demonstrates the conversion of testosterone to DHT by the catalytic action of 5α-reductase, as depicted in Figure 2, where NADPH serve as the cofactor. The catalysis by 5α-reductase involves the creation of a binary complex between the enzyme and NADPH ($NADP^+$–enzyme) with

the substrate testosterone. The hydride ion (H^-) from NADPH directly donates to the C-5 position of testosterone. The enolate system forms as the enone in testosterone interacts with an electrophilic residue (Enz^+) in the active site of the enzyme. This process generates positively polarized species that accept a hydride ion from NADPH at C-5 of testosterone. Finally, enzyme-mediated tautomerization results in the formation of DHT, and the subsequent release of $NADP^+$ free the enzyme for further catalytic cycles [30,33].

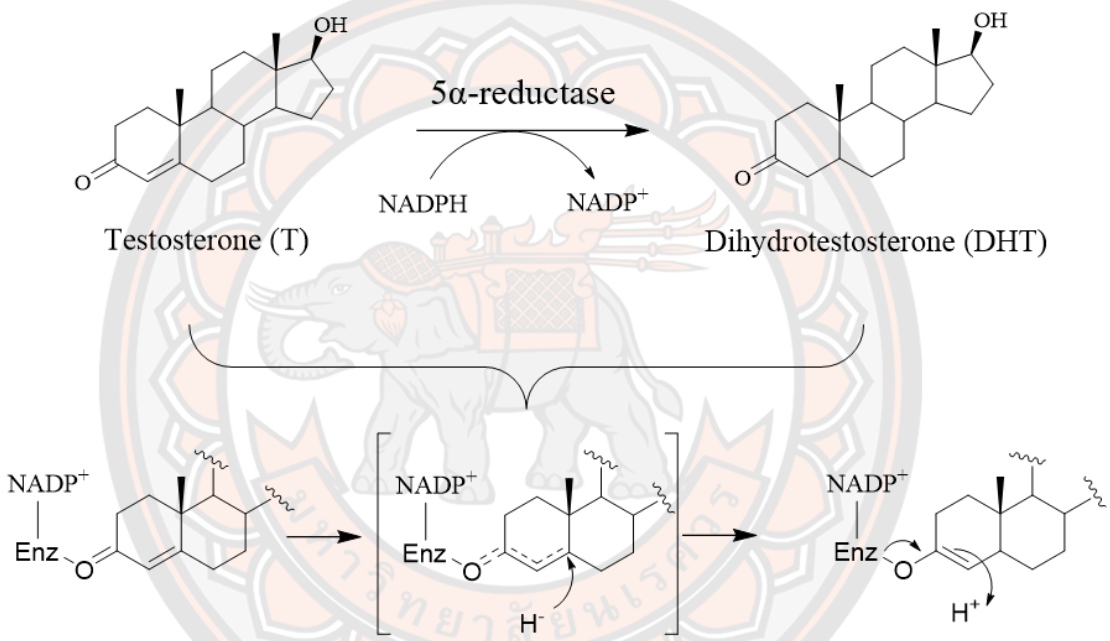

Figure 2 The purposed biochemical mechanism of 5α-reductase enzymatic reaction [30].

2.3.2 Mechanism of androgen action on human androgen receptors

The actions of testosterone and DHT are mediated through the androgen receptor (AR), which is a nuclear receptor (Figure 3). Testosterone undergoes passive diffusion through the cell membrane and is enzymatically converted to DHT. This alteration is essential for the subsequent binding to the androgen receptor. The complex of the androgen receptor undergoes sulfhydryl reduction and phosphorylation, enabling

it to adhere to specific gene sites. This interaction leads to the modification of RNA polymerase activity, ultimately giving rise to androgenic effects [34].

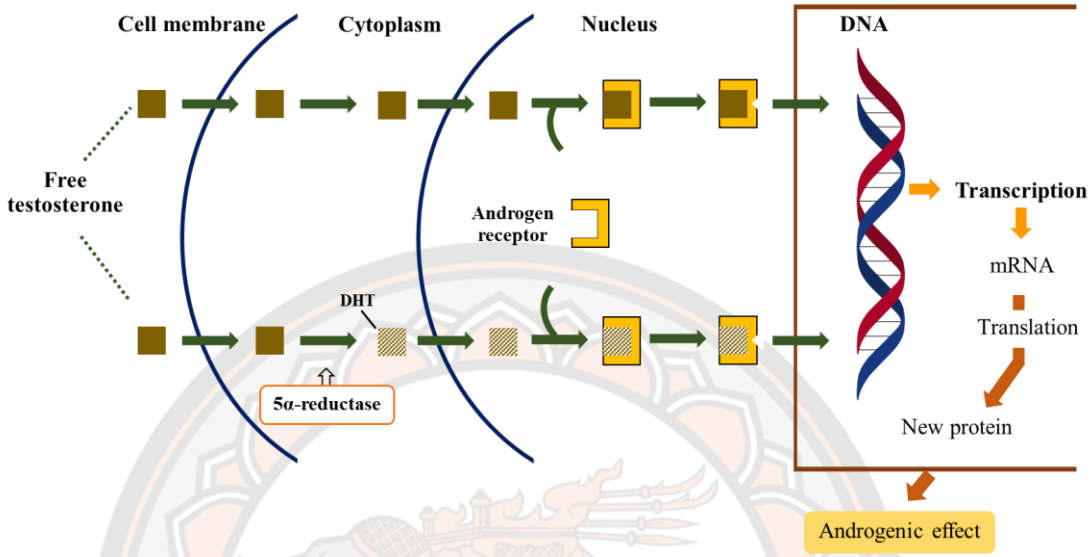

Figure 3 Cellular mechanism of androgens in the skin; DHT = dihydrotestosterone. Note: modified from Randall (1994) [4].

2.4 Androgen-dependent disorders

The overproduction of DHT can result in a variety of androgen-dependent disorders such as androgenic alopecia (AGA), benign prostatic hyperplasia (BPH), prostate cancer, hirsutism, and acne vulgaris.

2.4.1 Androgenic alopecia (AGA)

Androgenic alopecia (AGA) is a common androgen-dependent disorder marked by the gradual reduction of hair density, length, diameter, and pigmentation. The term of AGA, also known by synonyms like common baldness; male-pattern baldness; female-pattern alopecia; diffuse alopecia of women, was initially pathologically described by Orentreich in 1960 [35]. AGA, or hair loss, is a common dermatological condition that directly affects as an individual's self-esteem, social interactions, sexual well-being, and overall quality of life [36,37]. The estimated prevalence of hair loss among older men is as high as 70%. Recent research indicates

that 6% of women under 50 years of age are affected, whereas the condition afflicts 30-40% of women over the age of 70 [38].

Multifactorial etiologies of hair loss [39,40]

Several multiple factors leading to hair loss have been previously reported and summarized as follows:

General factors

1. Nutritional deficiency: Deficiency of certain vitamins such as B-complex and vitamin A, or an excess of vitamin A.

2. Hormonal variation: Androgenic hormones, particularly DHT, have been extensively recognized as the primary contributors to the pathophysiology of AGA or hair loss. Hormonal imbalances, such as elevated estrogens levels and insufficient progesterone levels, can lead to fluctuations throughout an individual's life and may contribute to excessive hair loss.

3. Post-acute-ailment: Hair loss can develop as a result of acute disorders that impair the immune system.

4. Medicine and drugs: Long-term usage of chemotherapy, cancer medication, steroids, antibiotics, antiepileptics, and antihypertensive drugs has been linked to hair loss.

Local factors

1. Local exposure to toxins: Excessive use of chemical-based shampoos, soaps, and lotions

2. Scalp carelessness: Unhygienic scalp care measures may cause hair loss.

3. Psychological Factors: Emotional stress, intense anxiety, depression, etc. are psychological factors causing hair loss.

4. Other factors: The factors include micro-inflammation of hair follicles and scalp, the toxins from industrial and water.

Classification of hair loss

The Hamilton-Norwood and Ludwig scales can be used to classify androgenic alopecia (AGA) or male and female pattern hair loss. As shown in Figure 4, the Hamilton-Norwood scale has classified male pattern baldness into 7 types. Typical hair loss typically begins with frontal thinning (type I), followed by a temporal

recession (type II), and subsequently a mid-frontal recession. In type III, hair loss occurs in a circular area on the vertex, often leading to type VII (very advanced hair loss) where hair density diminishes across the top of the scalp [36,41,42].

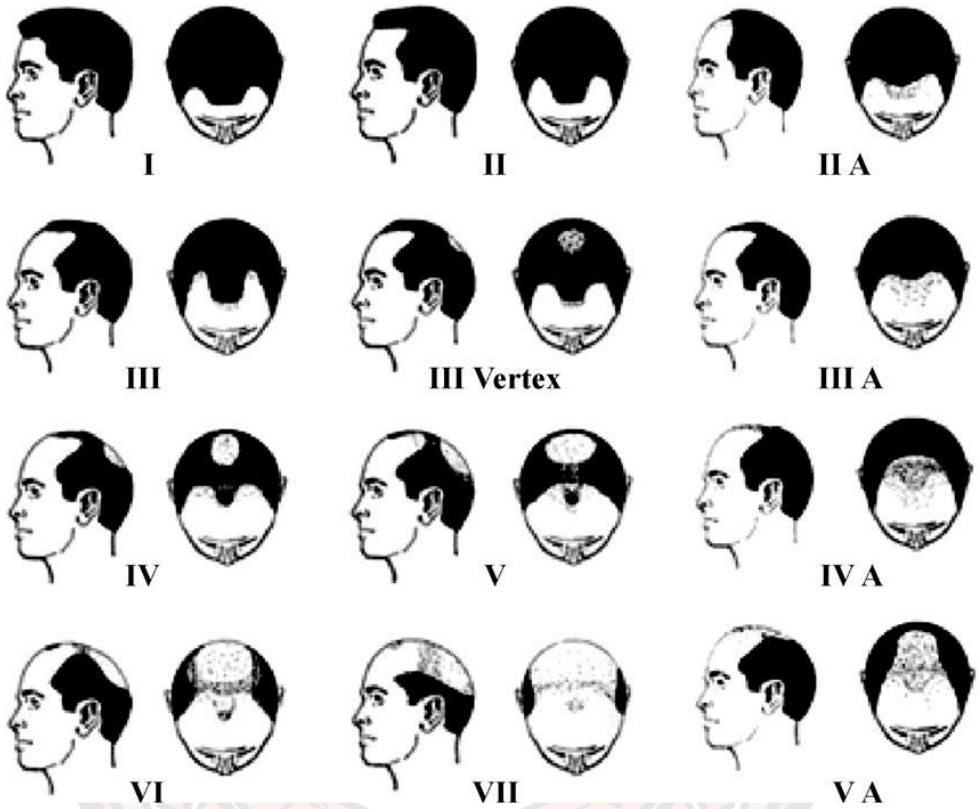

Figure 4 Norwood-Hamilton classification of male pattern baldness chart [41,42].

For female pattern baldness, Ludwig has classified the stages of hair loss from grade I to grade III (Figure 5). Based on various cases observed during several years, the stages of AGA in females may be described as follows:

"Grade I: Perceptible thinning of the hair on the crown, limited in the front by a line situated 1-3 cm behind the frontal hairline"

"Grade II: Pronounced rarefaction of the hair on the crown within the area seen in grade"

"Grade III: Full baldness (total denudation) within the area seen in Grades I and II"

Grade I **Grade II** **Grade III**

Figure 5 Schematic representation of three grades of female AGA [43].

Nowadays, the FDA has authorized only two drugs for the treatment of androgenetic alopecia. These drugs include topically applied minoxidil at concentration of 2% (for women) and 5% (for men), as well as administered orally finasteride at a dosage of 1 mg/day (for men), which is a type 2 steroid 5α-reductase inhibitor [44-46].

2.4.2 Acne

Acne is a dermatological condition affecting the pilosebaceous unit, primarily manifesting on the face, neck, and upper trunk. It is one of the most prevalent skin condition encountered by physicians, affecting approximately 85% of the population in the United States aged 12 to 24 years each year [47,48]. The pilosebaceous unit, which is a complex mini-organ comprising the hair follicle, sebaceous gland, keratinized follicular infundibulum, and sebaceous duct, plays a pivotal role. There are four main pathogenic factors that have an impact on acne, a multifactorial disorder that affects the pilosebaceous unit [49,50]. These factors consist of the following:

1) The excessive production of sebum due to androgen-induce activation of sebaceous glands.

2) The occurrence of aberrant keratinization of the follicles results in a blockage and subsequent formation of comedone.

3) *Propionibacterium acnes* colonizes the follicular duct and proliferates in teenagers.

4) The inflammatory response of the follicle and its adjacent dermal region

Although the exact pathogenesis of acne remains uncertain, it is evident that the primary mechanism behind sebum production is the stimulation of lipogenesis in the sebaceous glands. DHT produced locally in sebaceous glands by type 1 5α-reductase enhanced sebum production, and this enzyme is important in sebum production for the development of acne [51].

2.4.3 Benign prostatic hyperplasia (BPH)

BPH is a prevalent age-related male disease, affecting as much as 90% of men aged 80 and above [52]. It is clinically characterized by non-malignant enlargement of the prostate gland and is the most common cause of symptoms related to the lower urinary tract. Androgens, such as testosterone and DHT, are necessary for the continuous development and differentiated function of the prostate throughout life. They are also essential for the proliferation of stromal and epithelial cells in the prostate gland. The epithelial cell in this gland appears to express only the enzyme 5α-reductase type 1, whereas the stromal cell expresses both type 1 and type 2 of this enzyme. These isoenzymes play important roles in BPH, and their significances in prostate cancer are under investigation [53]. Presently, only finasteride (Proscar®) and dutasteride (Avordart®) are FDA-approved BPH treatments [54].

2.4.4 Hirsutism

Hirsutism is described as excessive terminal hair growth in the body of a female under the androgen-dependent areas. Typically, it is associated with hyperandrogenemia. More than 70-80% of hirsute women are influenced by androgenic factors [55]. These factors exert their influence on the body by affecting sex-specific regions, resulting in the transformation of short, straight, light-colored vellus hairs into bigger, curlier, and darker terminal hair [56]. Men typically have a higher degree of terminal hair in various regions of their bodies compared to women, mostly as a result of high levels of androgen during and after the period of puberty. Hirsutism arises in females as a result of an excessive production of androgens.

2.5 Medical treatment for AGA

The medication for AGA treatment can be generally categorized into two types: androgen-dependent and androgen-independent. Androgen-dependent treatments work by targeting androgens, such as androgen-receptor blockers or 5α-reductase inhibitors, to reduce DHT levels. The other mechanisms act against AGA as androgen-independent agents [46]. Nowadays, the FDA has approved only two drugs for the treatment of AGA, i.e., topically applied 2% (for women) or 5% (for men) minoxidil and orally administered finasteride (1 mg/day for men), which inhibits type 2 steroid 5α-reductase.

Minoxidil, a vasodilator, is a pyrimidine derivative known as 2,4-diamino-6-piperidinopyrimidine-3-oxide (Figure 6). It is employed in the treatment of scalp hair loss. Minoxidil was originally developed in the early 1970s as an oral treatment for hypertension [7]. Hypertrichosis (darkening of fine body hair) and the regrowth of hair in male pattern baldness were observed as side effects of this medicine in patients receiving oral minoxidil [57]. In 1998, FDA approved a topical solution minoxidil for the treatment of AGA in men, which was developed in response to one of these side effects. The topical formulation of the medicine with a 2% concentration was used to treat women [45], whereas the formulation with a 5% concentration solution or as the foam was recommended for men [44].

Topical minoxidil is an androgen-independent agent because this drug's effect does not involve either a hormonal factor or the inhibitory action of 5α-reductase [46]. While the precise biochemical mechanism behind its action on AGA remains unclear, it is believed to work by opening the potassium ion channels in vascular smooth muscle cells. This action promotes the release of vascular endothelial growth factor and hair growth promoters in the dermal papilla, ultimately increasing cutaneous blood flow. However, the use of topical minoxidil can cause adverse effects, including temporary increased hair shedding, contact dermatitis, and facial hypertrichosis. Additionally, minoxidil foam formulation containing propylene glycol may cause scalp irritation, itching, dryness, and erythema [7,46].

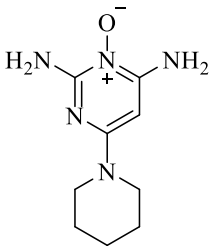

Minoxidil

Figure 6 Chemical structure of minoxidil [58].

Although oral finasteride and topical minoxidil agents are the most widely used for AGA, their adverse effects mentioned above are still limited to treatment. Therefore, there is a demand for new alternative treatments to prevent hair loss, and natural products may present a promising solution.

2.6 Anti-androgen drugs for 5α-reductase inhibition

In conventional modern pharmaceuticals, the only information available about 5α-reductase isozymes is their deduced primary sequence from cDNAs. This limitation arises because the enzyme is unstable during purification and its crystal structure remains unresolved. The first designs of inhibitors focused on modifying the structure of natural testosterone or its substrates. One approach involved substituting a carbon atom in the rings with a heteroatom like nitrogen, resulting in the creation of azasteroids [33]. The high-potential 5α-reductase inhibitors with clinical studies include finasteride (MK-906), dutasteride (GG745), epristeride, and 4-MA. Their structures are depicted in Figure 7.

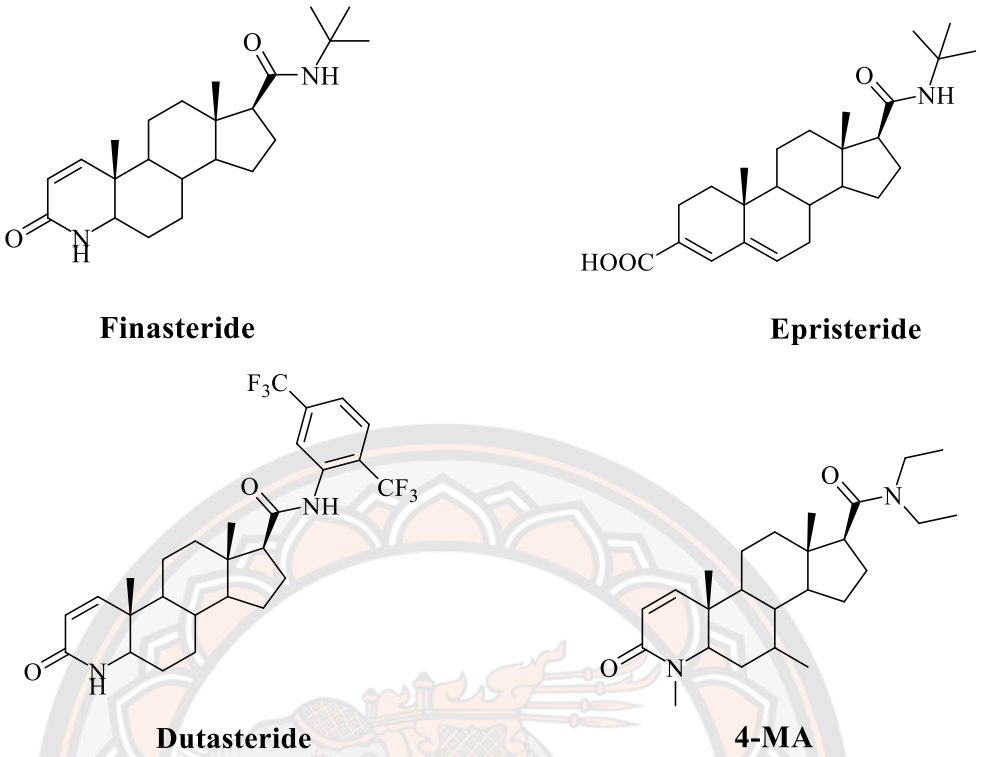

Figure 7 Chemical structures of steroid 5α-reductase inhibitors.

2.6.1 Finasteride

Finasteride, which is marketed as Proscar® for treatment of BPH and Propecia® for AGA, is classified as an androgen-dependent therapeutic drug. It was initially approved by the US FDA in 1992 for BPH and later, in late 1997 for AGA in men. Finasteride (17β-(*N-tert*-butylcarbamoyl)-4-aza-5 alpha-androstan-1-en-3-one) is a synthetic compound belonging to the 4-azasteroid class (Figure 7). It act as a specific inhibitor of type 2, 5α-reductase, effectively blocking the conversion of testosterone to DHT [33]. Finasteride exhibits potent inhibition of 5-reductase type 2, with an IC_{50} value of 69 nM, while its inhibition of 5α-reductase type 1 is less effective, with an IC_{50} value of 360 nM [59]. Finasteride (1 or 5 mg daily) suppressed intraprostatic DHT by 85% after 7 days of treatment in men with BPH [60]. The use of finasteride is not approved for females experiencing hair loss due to its absorption through the skin, potentially causing a teratogenic effect in male babies [8,46]. Nonetheless, ejaculation dysfunction, erectile dysfunction, and decreased libido are among the most frequently mentioned sexually adverse effects [61,62].

2.6.2 Epristeride

Epristeride or SKF105657, 3-androstene-3-carboxylic acids, is a potent type 2 5α-reductase inhibitor (Figure 7) used to treat BPH. This analog is approximately 400-fold more selective to type 2 than type 1 [63]. Epristeride is an uncompetitive inhibitory versus steroid substrate, and the proposed mechanism of 5α-reductase involves the formation of a ternary complex with epristeride, $NADP^+$, and enzyme [64]. However, this drug does not appear to lead to noticeable improvements in patient outcomes [65].

2.6.3 Dutasteride

Dutasteride (GG745), also known as 17β-*N*-[2,5-bis(trifluoromethyl)-phenyl)]-3-oxo-4-aza-5α-androst-1-ene-17-carboxamide, is a synthetic 4-azasteroid derivative (Figure 7). It received approval from the U.S. FDA in 2002 for the treating BPH under the brand name Avodart®. Dutasteride acts as a competitive inhibitor for both type 1 and type 2 isoforms of 5α-reductase. It suppressed DHT levels more effectively than finasteride (94.7% versus 70.8%) with the same concentration at 5 mg when patients with BPH were randomized to receive once-daily dosing for 24 weeks [66]. In addition, the administration of dutasteride at a dosage of 5 mg/day for a period of 6-10 weeks resulted in a significant reduction in intraprostatic DHT levels by 97% in individuals diagnosed with prostate cancer. Similarly, the use of a dosage of 3.5 mg/day for a duration of 4 months led to a remarkable decrease in intraprostatic DHT levels by 99% [67]. In another trial, the administration of dutasteride at dosages ranging from 3.5 to 5 mg/day resulted in a significant reduction of intraprostatic DHT levels, approaching maximum suppression. Furthermore, an *in vitro* study demonstrated the inhibitory effect of dutasteride on 5α-reductase type 3 [68].

2.6.4 4-MA

4-MA, chemically represented as [17β-*N*,*N*-diethylcarbamoyl-4-methyl-4-aza-5α-androstan-3-one], is a synthetic derivative of 4-azasteroid (Figure 7). It was initially identified as a potent dual inhibitor of both type 1 and type 2 5α-reductase isoforms, with IC_{50} values of 1.7 nM and 1.9 nM, respectively. However, it was

withdrawn from further clinical development due to its notably low affinity for androgen receptors and a lack of selectivity in relation to the 3β-hydroxysteroid dehydrogenase enzyme, along with concerns regarding its hepatotoxicity [69].

Finasteride and epristeride are well-known 5α-reductase inhibitors that are commercially available, but their multiple side effects limit their use. Herbal alternatives to 5α-reductase inhibition might be the answer to this problem [70].

2.7 Herbal 5α-reductase inhibitors

Herbal medications that inhibit 5α-reductase are one of the alternative treatments for androgen-dependent disorders. Many published articles have reported on the 5α-reductase inhibition effects of some medicinal plants. A summary of these studies, along with their IC_{50} or percentage (%) of inhibition values is provided in Table 3.

Table 3 Natural sources of steroid 5α-reductase inhibitors

Scientific name	Part used	Extraction solvents	Active compounds or crude extracts	Source of enzyme	IC_{50} or % enzymatic inhibition	Ref. no.
Acanthaceae						
Avicennia marina (AM)	Heartwood	Methanol	Methanolic AM extract and Avicequinone C	HHDPCs cells	AM extract (10 µg/mL): 52% inhibition Avicequinone C: IC_{50} = 38.8 ± 1.29 µM.	[71]
Araliaceae						
Panax ginseng	Rhizomes	50% Ethanol	Ginsenoside Ro and Ginsenoside Rg3	Rat epidermis	Ginsenoside Ro: IC_{50} = 259.4 µM Ginsenoside Rg3: IC_{50} = 86.1 µM	[72]
Asparagaceae						
Anemarrhena asphodeloides	Rhizomes	Diethyl ether	*cis*-Hinokiresinol and	Rat liver	*cis*-Hinokiresinol: IC_{50} = 0.31 mM 2,6,4′-Trihydroxy-4-methoxybenzophenone:	[73]

Scientific name	Part used	Extraction solvents	Active compounds or crude extracts	Source of enzyme	IC_{50} or % enzymatic inhibition	Ref. no.
			2,6,4′-Trihydroxy-4-methoxybenzophenone		IC_{50}>1.00 mM	
Asteraceae						
Carthamus tinctorius (CT)	Flowers	Distilled water	Distilled water CT extract	Rat epidermis	CT extract (2.5 mg/mL): 61.14% inhibition	[74]
Eclipta prostrata (HE)	Herba	75% Ethanol	75% Ethanolic HE extract	Rat epidermis	HE extract (2.5 mg/mL): 28.42% inhibition	[74]
Apiaceae						
Angelica sinensis (RA)	Radix	75% Ethanol	75% Ethanolic RA extract	Rat epidermis	RA extract (2.5 mg/mL): 17.19% inhibition	[74]
Angelica koreana	Roots	Methanol	Osthenol	LNCaP cells	Osthenol: IC_{50} = 0.1 µg/mL	[75]
Balsaminaceae						
Impatiens balsamina (IBA)	Aerial parts	35% Ethanol	Partitioned ethyl acetate extract Impatienol	Rat prostate	Partitioned ethyl acetate extract: IC_{50} = 52.9 µg/mL Impatienol: IC_{50} = 99.4 µg/mL	[76]

Scientific name	Part used	Extraction solvents	Active compounds or crude extracts	Source of enzyme	IC_{50} or % enzymatic inhibition	Ref. no.
Brassicaceae						
Brassica rapa	Pollens	SFE-CO_2	Linolenic acid Monolinolein	Rat liver	Linolenic acid: IC_{50} = 0.07 mM Monolinolein: IC50 = 0.18 mM	[77]
Cactaceae						
Cactus spp.	Flowers	Water	Water extract	Human hypertrophic prostate tissue	Water extract (1.3 mg/mL): 35.5%	[78]
Cynomoriaceae						
Cynomorium songaricum (CS)	Stems	75% Ethanol	75% Ethanolic CS extract	Rat epidermis	CS extract (2.5 mg/mL): 88.78% inhibition	[74]
Cupressaceae						

Scientific name	Part used	Extraction solvents	Active compounds or crude extracts	Source of enzyme	IC_{50} or % enzymatic inhibition	Ref. no.
Thujopsis dolabrata var. *homadae* (TD)	Barks	70% Acetone	70% Acetone TD extract	Rat liver	CP extract: IC_{50} = 42 µg/mL	[79]
Thuja occidentalis (TOS)	Fruits	95% Ethanol	95% Ethanolic TOS extract	HEK293 cells	TOS extract: IC_{50} = 2.6 µg/mL	[80]
Dipterocarpaceae						
Shorea laeviforia	Heartwood	Methanol	Valoneic acid dilactone Gallagyldilactone	Rat liver	Valoneic acid dilactone: IC_{50} = 129.1 µM Gallagyldilactone: IC_{50} = 91.2 µM	[81]
Fabaceae						
Pueraria thomsonii (PF)	Flowers	50% Ethanol	50% Ethanolic PF extract	Rat epidermis	PF extract (500 µg/mL): 60.2% inhibition	[82]
Acacia mangium (AMa)	Bark	70% Acetone	70% Acetone AMa extract	Rat liver	AMa extract: IC_{50} = 52 µg/mL	[79]
Acacia mearnsii (AMe)	Bark	70% Acetone	70% Acetone AMe extract	Rat liver	AMe extract: IC_{50} = 69 µg/mL	[79]

Scientific name	Part used	Extraction solvents	Active compounds or crude extracts	Source of enzyme	IC_{50} or % enzymatic inhibition	Ref. no.
Quercus acutissima	Cortex	Water	Tetragalloyl glucose Pentagalloyl glucose Eugeniin 1-Desgalloyl eugeniin Casuarinin Castalagin Stenophyllanin C (-)-Epicatechin gallate (-)-Epigallocatechin gallate	Rat liver	Tetragalloyl glucose: IC_{50} = 8.1 µM Pentagalloyl glucose: IC_{50} = 2.5 µM Eugeniin: IC_{50} = 10.9 µM 1-Desgalloyl eugeniin IC_{50} = 12.6 µM Casuarinin: IC_{50} = 10.5 µM Castalagin: IC_{50} = 8.0 µM Stenophyllanin C: IC_{50} = 7.2 µM, (-)-Epicatechin gallate: IC_{50} = 10-100 µM (-)-Epigallocatechin gallate: IC_{50} = 10-100 µM	[83]
Ganodermataceae						
Ganoderma lucidum (GL)	Radix	75% Ethanol	75% Ethanolic GL extract	Rat epidermis	GL extract (2.5 mg/mL): 85.86% inhibition	[74]

Scientific name	Part used	Extraction solvents	Active compounds or crude extracts	Source of enzyme	IC_{50} or % enzymatic inhibition	Ref. no.
	Fruits	Ethanol	Ganoderic acid DM, 5α-lanosta-7,9(11),24-triene-15α,26-dihydroxy-3-one	Rat liver	Ganoderic acid DM: IC_{50} = 10.6 µM 5α-lanosta-7,9(11),24-triene-15α,26-dihydroxy-3-one: IC_{50} = 41.9 µM	[84]
Sonneratia caseolaris (SC)	Barks	70% Acetone	70% Acetone SC extract	Rat liver	SC extract: IC_{50} = 47 µg/mL	[79]
Moraceae						
Artocarpus altilis	Leaves	Acetone	2-geranyl-2',3,4,4'-tetrahydroxydihydrochalcone	Rat liver	2-geranyl-2',3,4,4'-tetrahydroxydihydrochalcone: IC_{50} = 38 µM	[85]
Artocarpus incisus	Heartwoods	Methanol	Chlorophorin Artocapin	Rat liver	Chlorophorin: IC_{50} = 37 µM Artocapin: IC_{50} = 85 µM	[86]
Onagraceae						
Epilobium parviflorum	Stems and leaves	Water	Lyophilized aqueous extract	Human prostate	Lyophilized aqueous extract: IC_{50} = 0.16 g/L	[87]

Scientific name	Part used	Extraction solvents	Active compounds or crude extracts	Source of enzyme	IC_{50} or % enzymatic inhibition	Ref. no.
			Oenothein B		$IC_{50} = 2.2 \times 10^{-5}$ M Oenothein B: $IC_{50} = 2.2 \times 10^{-5}$ M	
Pinaceae						
Larix leptolepis (LL)	Barks	70% Acetone	70% Acetone LL extract	Rat liver	LL extract: $IC_{50} = 54$ µg/mL	[79]
Cryptomeria japonica (CJ)	Barks	70% Acetone	70% Acetone CL extract	Rat liver	CL extract: $IC_{50} = 39$ µg/mL	[79]
Piperaceae						
Piper nigrum	Leaves	Methanol	Piperine (-)-Cubebin (-)-3,4-dimethoxy-3,4-desmethylenedioxycubebin	Rat liver	Piperine: $IC_{50} = 0.48$ mM (-)-Cubebin: $IC_{50} = 0.44$ mM (-)-3,4-dimethoxy-3,4-desmethylenedioxycubebin: $IC_{50} = 1.03$ mM	[88]
Polygonaceae						

Scientific name	Part used	Extraction solvents	Active compounds or crude extracts	Source of enzyme	IC_{50} or % enzymatic inhibition	Ref. no.
Polygonum multiflorum Thunb (PM)	Root	50% Ethanol	50% Ethanolic PM extract Emodin	Rat ventral prostate	PM extract (500 µg/mL): 80.7% inhibition Emodin: IC_{50} = 40 µM	[89]
	Radix	75% Ethanol	75% Ethanol PM extract	Rat epidermis	PM extract (2.5 mg/mL): 90.25% inhibition	[74]
Salicaceae						
Salix rorida (SR)	Barks	70% Acetone	70% Acetone SR extract	Rat liver	SR extract: IC_{50} = 53 µg/mL	[79]
Populus nigra	Flowers and bud	50% Ethanol	Pinocembrin	Rat liver	Pinocembrin (100 nmol): 31% inhibition	[90]
Solanaceae						
Lycium barbarum (FL)	Fruits	75% Ethanol	75% Ethanol FL extract	Rat epidermis	FL extract (2.5 mg/mL): 26.51% inhibition	[74]
Theaceae						
Camellia sinensis	Seeds	*n*-Hexane	Kaempferol	HEK293 cells	NR	[91]
Umbelliferae						

Scientific name	Part used	Extraction solvents	Active compounds or crude extracts	Source of enzyme	IC_{50} or % enzymatic inhibition	Ref. no.
Torilis japonica	Fruits	Methanol	Torilin (-)-Guaiol Guaiazulene	Rat ventral prostate	Torilin: IC_{50} = 31.7 µM (-)-Guaiol: IC_{50} = 81.6 µM Guaiazulene: IC_{50} = 100.8 µM	[92]
	Leaves		Epicatechin-3-gallate Epigallocatechin-3-gallate	Rat liver	Epicatechin-3-gallate: IC_{50} = 5.3 µg/mL Epigallocatechin-3-gallate: IC_{50} = 6.8 µg/mL	[93]
Zingiberaceae						
Curcuma longa (Turmeric)	Rhizomes	Methanol	Methanolic turmeric extract	HEK293 cells	NR	[94]
Curcuma aeruginosa	Rhizomes	Hexane	Hexane *C. aeruginosa* extract, Germacrone	Rat liver	Hexane *C. aeruginosa* extract: IC_{50} = 0.22 mg/mL Germacrone: IC_{50} = 0.42 mg/mL	[95]
Kaempferia parviflora	Rhizomes	Ethanolic and	Ethanolic and supercritical fluid CO_2 extracts	Rat ventral prostate	Ethanolic and supercritical fluid CO_2 extract (0.32 mg/mL): 83.3% inhibition	[96]

Scientific name	Part used	Extraction solvents	Active compounds or crude extracts	Source of enzyme	IC_{50} or % enzymatic inhibition	Ref. no.
		supercritical fluid CO_2	5-Hydroxy-7,4'-imethoxyflavone		5-Hydroxy-7,4'-imethoxyflavone (0.32 mg/mL): 100% inhibition	
Alpinia officinarum	Rhizomes	Acetone	Acetone *A. officinarum* extract 1,7-Diphenylhept-4-en-3-one Dihydroyashabushiketol 5-Hydroxy-7-(4"-hydroxy-3"-methoxyphenyl)-1-phenyl-3-heptanone) 5-Hydroxy-7-(4"-hydroxyphenyl)-1-phenyl-3-heptanone)	Rat ventral prostate	Acetone *A. officinarum* extract (100 µg/mL): 51% inhibition 1,7-Diphenylhept-4-en-3-one: IC_{50} = 390 µM Dihydroyashabushiketol: IC_{50} = 230 µM 5-Hydroxy-7-(4"-hydroxy-3"-methoxyphenyl)-1-phenyl-3-heptanone): IC_{50} = 220 µM 5-Hydroxy-7-(4"-hydroxyphenyl)-1-phenyl-3-heptanone): IC_{50} = 220 µM	[97]

Note: NR = not reported

2.8 The *in vitro* assays for investigation of 5α-reductase inhibition

There are several *in vitro* assays for the investigation of 5α-reductase inhibitory activity. The experiments were conducted to investigate the substrate conversion process involving testosterone being transformed to DHT by the enzyme 5α-reductase, with NADPH serving as the co-factor (Figure 1).

The sources of the 5α-reductase enzyme can be obtained from various tissues such as prostate cancer (LNCaP cell), skin, liver, dermal papillae cell, keratinocyte cell, and fibroblast cell [30]. In this study, the LNCaP cell was used as the source of enzyme. This cell line was purchased from the ATCC (American Type Culture Collection), which isolated the left supraclavicular lymph node of a Caucasian male at age 50 years old (blood type B+) and cell morphology as given in Figure 8 [98]. This cell line can only express type 1 of 5α-reductase when cultivated under optimal conditions [99]. The determination of the indicator substance (whether it's a substrate, cofactor, or product) has been performed using many techniques including autoradiography, LC-MS, and HPLC.

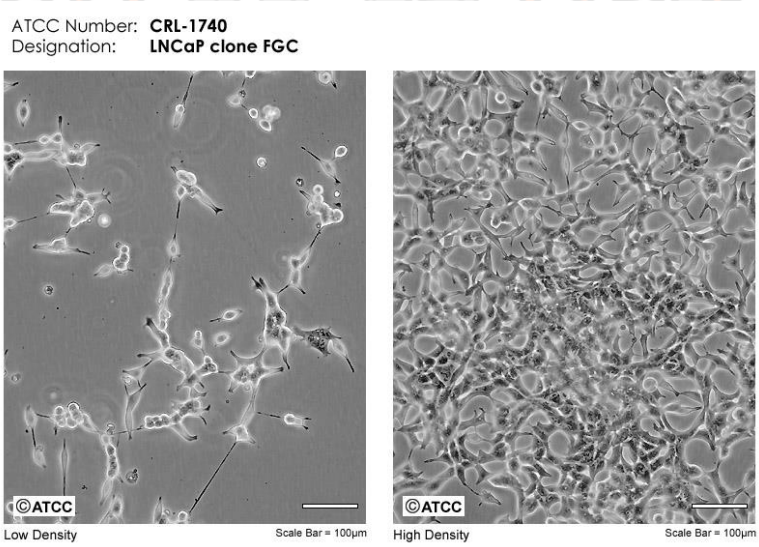

Figure 8 Morphology of LNCaP cell at low density (left) and high density (right) [98].

Various plants have been shown to possess potent anti-androgenic activity, as evidenced by the scientific literature. They might represent potential sources of anti-androgenic compounds. A recent finding from our research team reported that the

biological effects of *T. grandis* extract are associated with the prevention of hair loss. The result indicated that both hexane and ethyl acetate extracts of *T. grandis* leaf exhibited potent 5α-reductase inhibitory activity. Therefore, *T. grandis* leaf extracts could be used as an ingredient in alternative products of medicine or cosmetic for hair loss treatment.

2.9 *Tectona grandis* L.f.

2.9.1 Botanical description of *T. grandis*

Tectona grandis L.f., commonly referred to as the teak tree in English and sak in Thai, was formerly a member of Verbanaceae family and is now a member of Lamiaceae family. They are widely found in South and Southeast Asia. The teak tree is classified as a deciduous species and typically attains an average height of up to 30 m. The leaves exhibit an opposing arrangement and possess a broad elliptical shape, measuring approximately 30-50 cm in length and 15-20 cm in width. Teak trees produce small and fragrant flowers that form in large clusters, known as panicles, typically blooming from June to August. These panicles can contain numerous flower buds. Fruit is a drupe, initially pale green and later turning brown as it matures. The fruit has four chambers and is covered by a bladder-like structure. It is round, hard, and woody, enclosed within an inflated casing. The number of seeds found in each fruit generally ranges from 0 to 4. These seeds are characterized by their rectangular shape and brown color, and are enveloped within a rigid endocarp [100]. Teak wood is used in the timber industry due to its wood has good texture, color, and finishing qualities. It is used to make furniture, carving, houses, cabinets, doors, and windows [10,101].

2.9.2 Traditional uses

The utilization of teak in a diverse range of traditional treatments is attributed to the presence of medicinal properties in practically every component of the teak tree [13,23,102]. Flowers are used to treat acrid, bitter dry, bronchitis, and biliousness. Flowers and seeds have been used to treat diuretics or to increase urine flow. Wood has been used to treat headaches, biliousness, and burning pains, particularly in the liver region [13]. The bark is used for astringent, acrid, cooling,

constipating, anthelmintic, and depurative treatments. The root can also be used to treat urinary system-related troubles like anuria. Moreover, the seeds have been recommended as a hair growth promoter in India's traditional medical system [102].

2.9.3 Chemical constituents of *T. grandis*

Quinones, specifically naphthoquinones and anthraquinones, are the major chemical constituents present in teak trees. Furthermore, a wide range of compounds with varying structural complexities has been isolated from almost every part of teak. These compounds include terpenoids, apocarotenoids, phenolic compounds, flavonoids, steroids, saponins, phenylpropanoids like lignans and norlignans, phenylethanoid glycosides and fatty ester compounds [101]. The molecular formula and their parts of used containing these isolated compounds are presented in Table 4, while the chemical structures of all these compounds are depicted Figures 9-16. Some examples of the procedures for the isolation of quinones or other compounds found in *T. grandis* have been mentioned in this review.

In a study conducted by Kopa et al, in 2014 [103], they explored the chemical constituents of *T. grandis* methanolic extract. This investigation led to the isolation of a novel anthraquinone derivative known as grandiquinone A (3-acetoxy-8-hydroxy-2-methylanthraquinone), along with the identification of nine known compounds: "5,8-dihydroxy-2-methylanthraquinone, hydroxysesamone, 3-hydroxy-2-methylanthraquinone, quinizarine, betulinic acid, ursolic acid, tectograndone, corosolic acid, and sitosterol 3-*O*-β-D-glucopyranoside". Stepwise for the isolation of *T. grandis*, the methanolic extract was first diluted with water and subjected to ethyl acetate extraction, resulting in an EtOAc-soluble fraction (72 g). This fraction (70 g) was further chromatographed on a silica gel using *n*-hexane, EtOAc, and methanol as eluent in a gradient system, leading to the separation of five major fractions (A-E) based on TLC profiles. Fraction A (6 g) was subjected to column chromatography on silica gel using a gradient of *n*-hexane and EtOAc to yield 5,8-dihydroxy-2-methylanthraquinone (10 mg) and hydroxysesamone (40 mg). Grandiquinone A (2 mg) was separated from Fraction B (20 g) by silica gel column chromatography with *n*-hexane–EtOAc gradient. Fraction C (10 g) was purified on a Sephadex LH-20 column with elution using mixtures of *n*-hexane–dichloromethane–methanol (7:4:0.5), resulting in four

subfractions (C1–C4). Subfractions C1 (0.5 g), C2 (1.0 g), and C3 (52.5 mg) were further separated on a silica gel column, yielding 3-hydroxy-2-methylanthraquinone (5 mg), betulinic acid (50 mg), and ursolic acid, respectively. Moreover, fraction D yielded corosolic acid, quinizarine, and tectograndone, while sitosterol 3-*O*-β-D-glucopyranoside was obtained from fraction E.

Niamké et al. (2012) [104] discovered a new naphthoquinone compound, 4′,5′-dihydroxy-epiisocatalponol, in the heartwood of *T. grandis*. This part of used was extracted at 4 °C with acetone:water in the ratio of 80:20 v/v (500 mL). After evaporating the acetone, the remaining aqueous phase was further lyophilized. The residue (3.9 g) was dissolved in methanol (25 mL). This methanol solution, which had a concentration of 0.156 g/mL was then diluted 4-folds. It was then subjected to separate using semi-preparative HPLC, employing a reverse 5-µm C18 column (250 x 10 mm). During this process, the following condition were applied:

Mobile phase: line A consisted of 1% acetic acid in water (v/v), while line B comprised 50% methanol in acetonitrile (v/v). The gradient step was carried out using 30% B at 0-13 min, 30-100% B at 14-15 min, 100% B at 16-25 min, and 30% B at 26-28 min. Other parameters included a flow rate of 2.5 mL/min, a maximum pressure of 250 bar, a detection wavelength set at UV 254 nm, and an injection volume of 500 µL. A new naphthoquinone, identified as 4′,5′-dihydroxy-epiisocatalponol, was isolated as a slightly brownish solid with a retention time (t_R) of 9.7 min.

From the literature, the isolated compounds were separated using several column chromatographic techniques, including silica gel, Sephadex LH-20, and semi-preparative HPLC, leading to the isolation of quinones and various other compounds. Therefore, this data might be useful for finding the biomarkers in *T. grandis*.

Table 4 List of chemical constituents isolated from *T. grandis.*

Chemical constituents	Formula	Part used	Ref. no.
Naphthoquinones			
Lapachol (**1**)	$C_{15}H_{14}O_3$	Heartwood	[105-110]
		Root	[22]
Deoxylapachol (**2**)	$C_{15}H_{14}O_2$	Heartwood	[107,111-113]
5-Hydroxylapachol (**3**)	$C_{15}H_{14}O_4$	Root heartwood	[109]
Hydroxysesamone (**4**)	$C_{15}H_{14}O_5$	Leaves	[103]
α-Lapachone (**5**)	$C_{15}H_{14}O_3$	Roots	[22]
β-Lapachone (**6**)	$C_{15}H_{14}O_3$	Roots	[22]
Dehydro-α-lapachone (**7**)	$C_{15}H_{12}O_3$	Heartwood	[106,107,109]
		Roots	[22]
4′,5′-Dihydroxy-epiisocatalponol (**8**)	$C_{15}H_{18}O_4$	Heartwood	[104]
Tectol (**9**)	$C_{30}H_{26}O_4$	Heartwood	[114]
Dehydro-α-isodunnione (**10**)	$C_{15}H_{12}O_3$	Heartwood	[107]
Tecomaquinone-I (**11**)	$C_{30}H_{24}O_4$	Heartwood	[107,110]
Tectonaquinones A (**12**)	$C_{30}H_{24}O_5$	Heartwood	[110]
Tectonaquinones B (**13**)	$C_{25}H_{16}O_4$	Heartwood	[110]
Tectonaquinones C (**14**)	$C_{15}H_{12}O_3$	Heartwood	[110]
Anthraquinones			
Tectoquinone (**15**)	$C_{15}H_{10}O_2$	Heartwood	[107,110,115]
		Sapwood	[108]
		Saw dust	[116]
		Roots	[22]
2-Hydroxymethyl-anthraquinone (**16**)	$C_{15}H_{10}O_3$	Heartwood	[112,117]
2-Acetoxymethyl-anthraquinone (**17**)	$C_{15}H_{12}O_4$	Heartwood	[117]

Chemical constituents	Formula	Part used	Ref. no.
Anthraquinone-2-carbaldehyde (**18**)	$C_{15}H_8O_3$	Heartwood	[117]
Anthraquinone-2-carboxylic acid (**19**)	$C_{15}H_8O_4$	Heartwood	[117]
3-Hydroxy-2-methyl-anthraquinone (**20**)	$C_{15}H_{10}O_3$	Heartwood	[103,110]
Pachybasin (**21**)	$C_{15}H_{10}O_3$	Heartwood	[118]
Rubiadin (**22**)	$C_{15}H_{10}O_4$	Heartwood	[119]
Munjistin (**23**)	$C_{15}H_8O_6$	Heartwood	[119]
		Roots	[22]
2-Methylquinizarin (**24**)	$C_{15}H_{10}O_4$	Heartwood	[120]
		Roots heartwood	[109]
Quinizarine (**25**)	$C_{14}H_8O_4$	Leaves	[103]
1-Hydroxy-2-methyl anthraquinone (**26**)	$C_{15}H_{10}O_3$	Roots	[121]
		Stem	[112]
5,8-dihydroxy-2-methylanthraquinone (**27**)	$C_{15}H_{10}O_4$	Leaves	[103]
Obtusifolin (**28**)	$C_{16}H_{12}O_5$	Roots	[121]
		Saw dust	[116]
		Heartwood	[110]
9,10-Dimethoxy-2-methyl-1,4-anthraquinone (**29**)	$C_{17}H_{14}O_4$	Heartwood	[106]
5-Hydroxy-2-methyl anthraquinone (**30**)	$C_{15}H_{10}O_3$	Heartwood	[122]
1-Hydroxy-5-methoxy-2-methylanthraquinone (**31**)	$C_{16}H_{12}O_4$	Heartwood	[122]
1,5-Dihydroxy-2methylanthraquinone (**32**)	$C_{15}H_{10}O_4$	Heartwood	[122]

Chemical constituents	Formula	Part used	Ref. no.
5-Hydroxydigitolutein (**33**)	$C_{16}H_{12}O_5$	Tissue culture	[123]
Barleriaquinone-I (**34**)	$C_{15}H_{10}O$	Heartwood	[110,124]
Tectoleafquinone (**35**)	$C_{19}H_{14}O_6$	Leaves	[125]
Grandiquinone A (**36**)	$C_{17}H_{12}O_5$	Leaves	[103]
Tectograndone (**37**)	$C_{30}H_{20}O_{10}$	Leaves	[14,103]
Anthratectone (**38**)	$C_{27}H_{18}O_9$	Leaves	[15]
Naphthotectone (**39**)	$C_{17}H_{16}O_7$	Leaves	[15]
Monoterpene			
(6*RS*)-(*E*)-2,6-Dimethyl-2,7-octadiene-1,6-diol (**40**)	$C_{10}H_{18}O_2$	Leaves	[18]
Sesquiterpenes			
Iβ-6α-Dihydroxy-4(15)-eudesmene (**41**)	$C_{15}H_{26}O_2$	Leaves and Bark	
7-Epieudesm-4(15)-ene-1α,6α-diol (**42**)	$C_{15}H_{26}O_2$	Leaves and Bark	[17]
Diterpenes			
Abeograndinoic Acid (**43**)	$C_{20}H_{32}O_4$	Leaves and Bark	[17]
Phytol (**44**)	$C_{20}H_{40}O$	Leaves and Bark	[17]
7,11,15-Trimethyl-3-methylene-hexadecan-1,2-diol (**45**)	$C_{20}H_{40}O_2$	Leaves and Bark	[17]
Rhinocerotinoic acid (**46**)	$C_{20}H_{30}O_3$	Leaves and Bark	[17]
2-Oxokovalenic acid (**47**)	$C_{20}H_{30}O_3$	Leaves and Bark	[17]
19-Hydroxyferruginol (**48**)	$C_{20}H_{30}O_2$	Leaves and Bark	[17]
Tectograndinol (**49**)	$C_{20}H_{34}O_3$	Leaves	[126]
Solidagonal acid (**50**)	$C_{20}H_{30}O_3$	Leaves and Bark	[17]
Triterpenes			
Lupeol (**51**)	$C_{30}H_{50}O$	Bark	[127]
Betulin (**52**)	$C_{30}H_{50}O_2$	Bark	[127]
Betulinaldehyde (**53**)	$C_{30}H_{48}O_2$	Bark	[127]

Chemical constituents	Formula	Part used	Ref. no.
Betulinic acid (**54**)	$C_{30}H_{48}O_3$	Heartwood and Stem bark	[20]
		Bark	[128]
		Roots	[121]
		Leaves	[103]
Ursolic acid (**55**)	$C_{30}H_{48}O_3$	Leaves	[17,103]
Corosolic acid (**56**)	$C_{30}H_{48}O_4$	Leaves	[103]
Oleanolic acid (**57**)	$C_{30}H_{48}O_3$	Leaves and Bark	[17]
Maslinic acid (**58**)	$C_{30}H_{48}O_4$	Leaves and Bark	[17]
Methyl-2α,3α-dihydroxyurs-I2-en-28-oate (**59**)	$C_{30}H_{48}O_4$	Leaves and Bark	[17]
Euscaphic acid (**60**)	$C_{30}H_{48}O_5$	Leaves and Bark	[17]
Squalene (**61**)	$C_{30}H_{50}$	Roots	[112]
Polyterpene or rubber			
Caoutchouc or Indian rubber Polymer (**62**)	-	Wood	[129]
Apocarotenoids			
Tectoionol A (**63**)	$C_{13}H_{23}O_3$	Leaves	[18]
Tectoionol B (**64**)	$C_{13}H_{24}O_2$	Leaves	[18]
Annuionone D (**65**)	$C_{13}H_{20}O_3$	Leaves	[18]
3β-Hydroxy-7,8-dihydro-β-ionol (**66**)	$C_{13}H_{24}O_2$	Leaves	[18]
9(*S*)-4-Oxo-7,8-dihydro-β-ionol (**67**)	$C_{13}H_{22}O_2$	Leaves	[18]
3β-Hydroxy-7,8-dihydro-β-ionone (**68**)	$C_{13}H_{22}O_2$	Leaves	[18]
Phenolic compounds			
Gallic acid (**69**)	$C_7H_6O_5$	Leaves	[16]
Ellagic acid (**70**)	$C_{14}H_6O_8$	Leaves	[16]
Acetovanillone (**71**)	$C_9H_{10}O_3$	Leaves	[19]

Chemical constituents	Formula	Part used	Ref. no.
E-Isofuraldehyde (**72**)	$C_{10}H_{10}O_3$	Leaves	[19]
3-Hydroxy-1-(4-hydroxy-3,5-dimethoxyphenyl)propan-1-one (**73**)	$C_{11}H_{14}O_5$	Leaves	[19]
Evofolin A (**74**)	$C_{17}H_{18}0_6$	Leaves	[19]
Flavonoids			
Rutin (**75**)	$C_{27}H_{30}O_{16}$	Leaves	[16]
Quercitin (**76**)	$C_{15}H_{10}O_7$	Leaves	[16]
Steroids/ saponins			
β-Sitosterol (**77**)	$C_{29}H_{50}O$	Roots	[22]
Hydroxyenone (**78**)	$C_{29}H_{48}O_2$	Leaves and Bark	[17]
β-Sitosterol-β-D-[4′linolenyl-6′-(tridecan-4′″-one-1′″-oxy)] Glucuranopyranoside (**79**)	$C_{66}H_{110}O_8$	Stem bark	[20]
Stigmast-5-en-3-O-β-d-glucopyranoside (**80**)	$C_{35}H_{60}O_6$	Stem bark	[20]
Sitosterol 3-O-β-d-glucopyranoside (**81**)	$C_{60}H_{100}O_7$	Leaves	[103]
Phenylpropanoids: lignans			
Syringaresinol (**82**)	$C_{22}H_{26}O_8$	Leaves	[19,130]
Medioresinol (**83**)	$C_{21}H_{24}O_7$	Leaves	[19,130]
1-Hydroxypinoresinol (**84**)	($C_{20}H_{22}O_7$)	Leaves	[19]
Lariciresinol (**85**)	$C_{20}H_{24}O_6$	Leaves	[19,130]
Balaphonin (**86**)	$C_{20}H_{20}O_6$	Leaves	[19]
Zhebeiresinol (**87**)	$C_{14}H_{16}O_6$	Leaves	[19]
Phenylpropanoids: norlignans			
Tectonoelin A (**88**)	$C_{18}H_{16}O_6$	Leaves	[19]
Tectonoelin B (**89**)	$C_{19}H_{18}O_7$	Leaves	[19]
Phenylethanoid glycoside			
Verbascoside or acteoside (**90**)	$C_{29}H_{36}O_{15}$	Leaves	[21]

Chemical constituents	Formula	Part used	Ref. no.
Fatty esters			
7′-Hydroxy-*n*-octacosanoyl *n*-decanoate (**91**)	$C_{28}H_{56}O_3$	Stem bark	[20]
20′-Hydroxyeicosanyl linolenate (**92**)	$C_{38}H_{72}O_3$	Stem bark	[20]
18′-Hydroxy-*n*-hexacosanyl-*n*-decanoate (**93**)	$C_{36}H_{72}O_3$	Stem bark	[20]

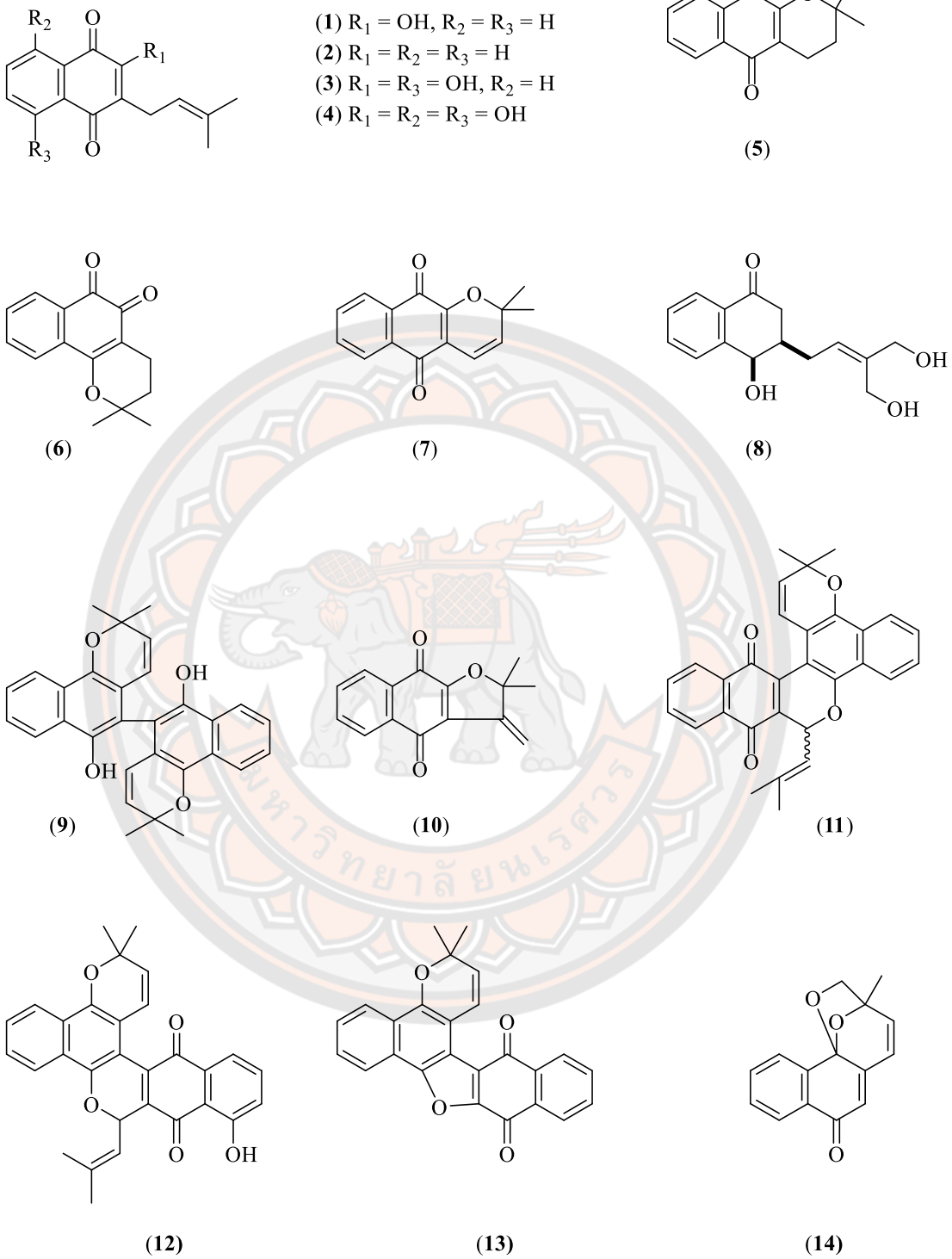

Figure 9 Chemical structures of naphthoquinones (**1-14**).

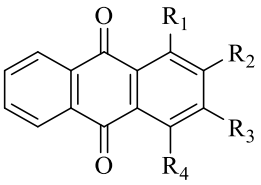

(**15**) $R_1 = R_3 = R_4 = H$, $R_2 = CH_3$
(**16**) $R_1 = R_3 = R_4 = H$, $R_2 = CH_2OH$
(**17**) $R_1 = R_3 = R_4 = H$, $R_2 = CH_2OAc$
(**18**) $R_1 = R_3 = R_4 = H$, $R_2 = CHO$
(**19**) $R_1 = R_3 = R_4 = H$, $R_2 = COOH$
(**20**) $R_1 = R_4 = H$, $R_2 = CH_3$, $R_3 = OH$
(**21**) $R_1 = OH = R_2 = R_4 = H$, $R_3 = CH_3$
(**22**) $R_1 = R_3 = OH$, $R_2 = CH_3$, $R_4 = H$
(**23**) $R_1 = R_3 = OH$, $R_2 = COOH$, $R_4 = H$
(**24**) $R_1 = R_4 = OH$, $R_2 = Me$ $R_3 = H$
(**25**) $R_1 = R_4 = OH$, $R_2 = R_3 = H$
(**26**) $R_1 = OH$, $R_2 = CH_3$, $R_3 = R_4 = H$

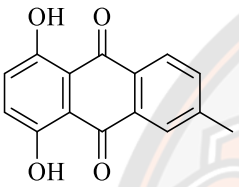

(**27**)

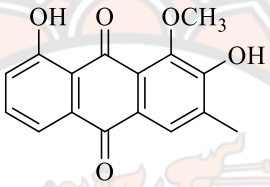

(**28**)

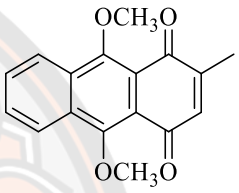

(**29**)

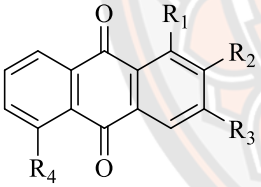

(**30**) $R_1 = H$, $R_2 = CH_3$, $R_3 = H$, $R_4 = OH$
(**31**) $R_1 = OH$, $R_2 = CH_3$, $R_3 = H$, $R_4 = OCH_3$
(**32**) $R_1 = OH$, $R_2 = CH_3$, $R_3 = H$, $R_4 = OH$
(**33**) $R_1 = OCH_3$, $R_2 = OH$, $R_3 = Me$, $R_4 = OH$
(**34**) $R_1 = R_2 = H$, $R_3 = CH_3$, $R_4 = OH$

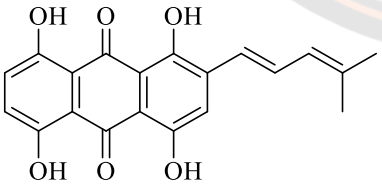

(**35**)

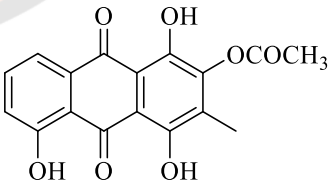

(**36**)

Figure 10 Chemical structures of anthraquinones (**15-36**).

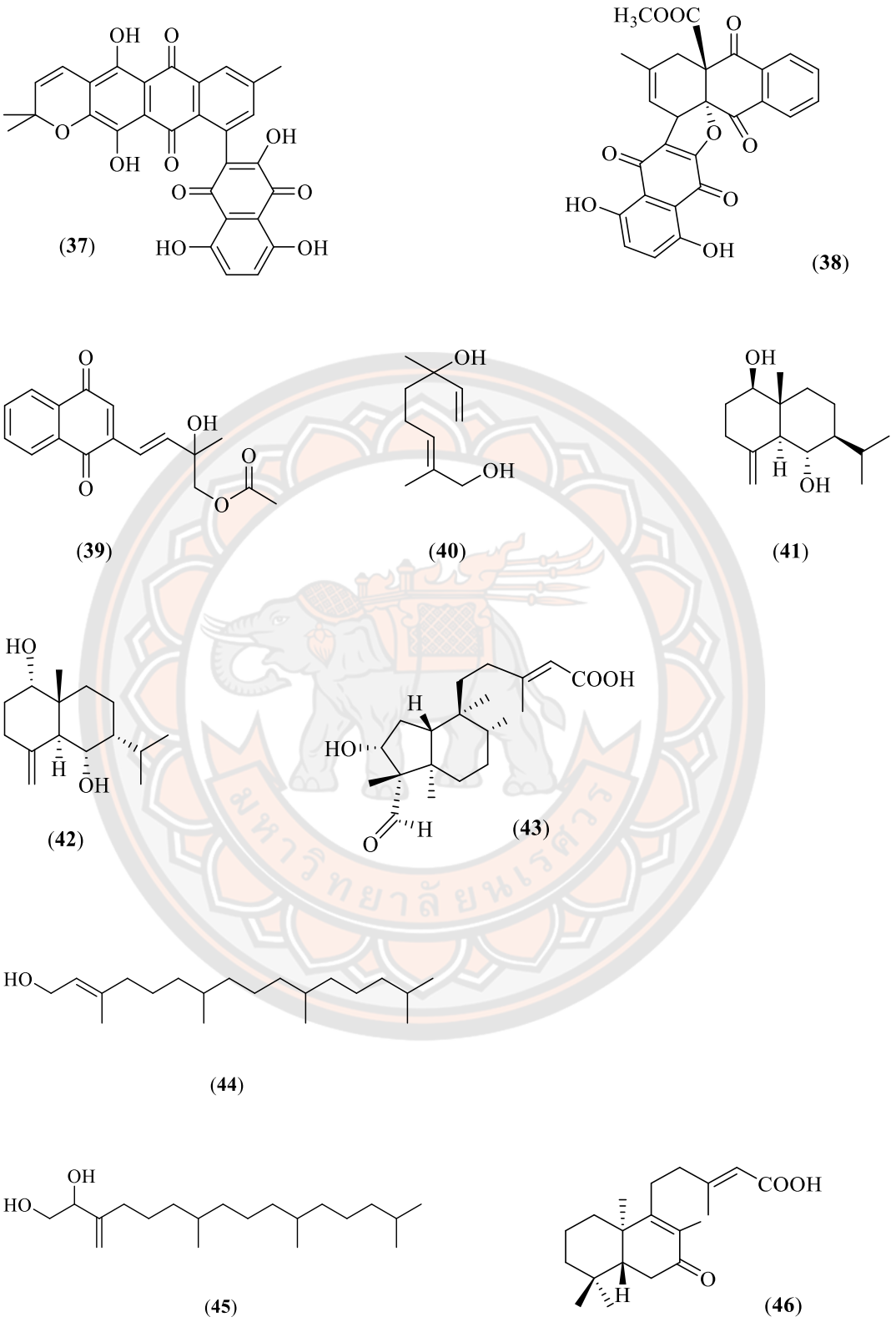

Figure 11 Chemical structures of anthraquinones (**37-39**) and terpenoids (**40-46**).

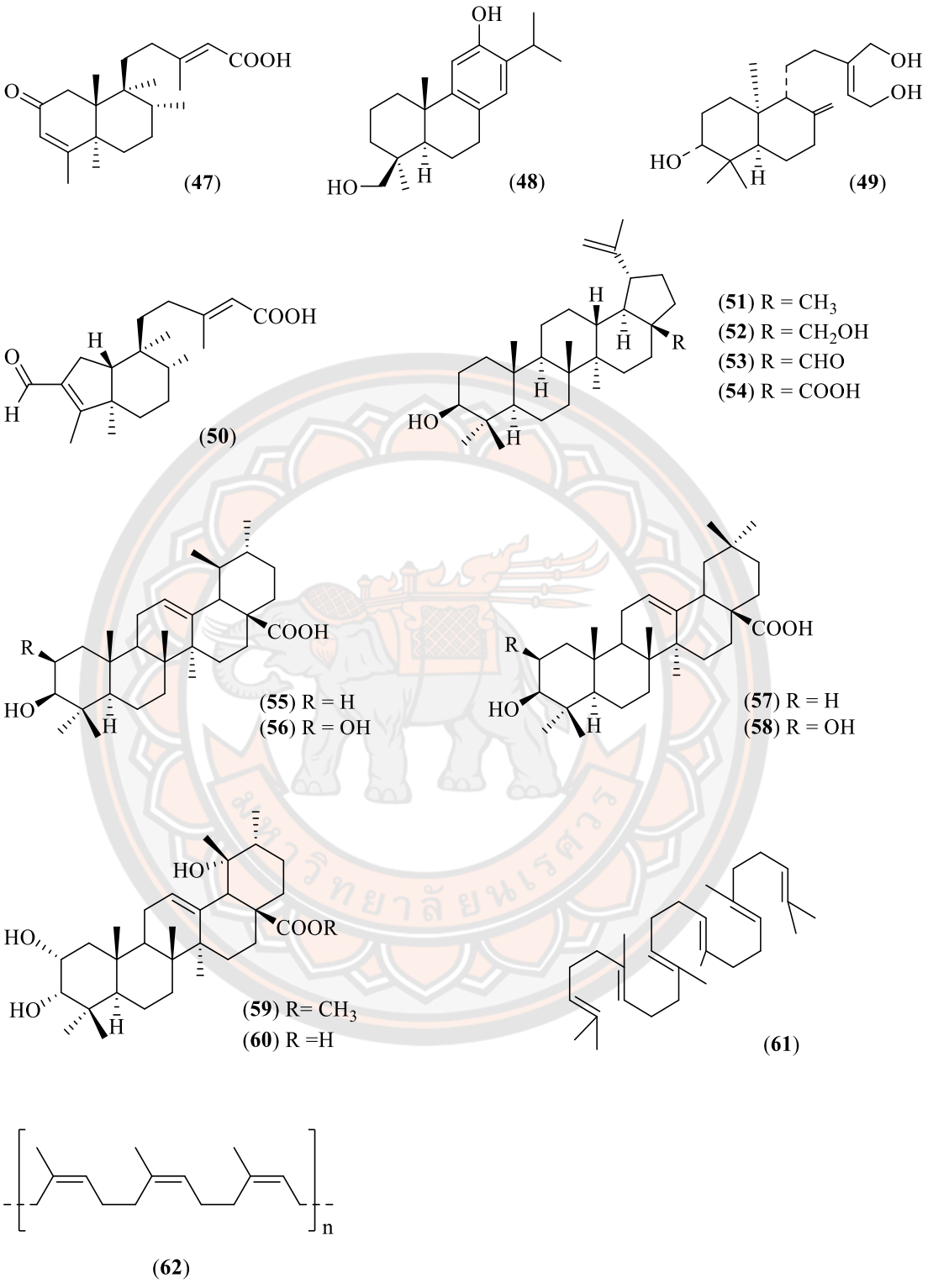

Figure 12 Chemical structures of terpenoids (**47-62**).

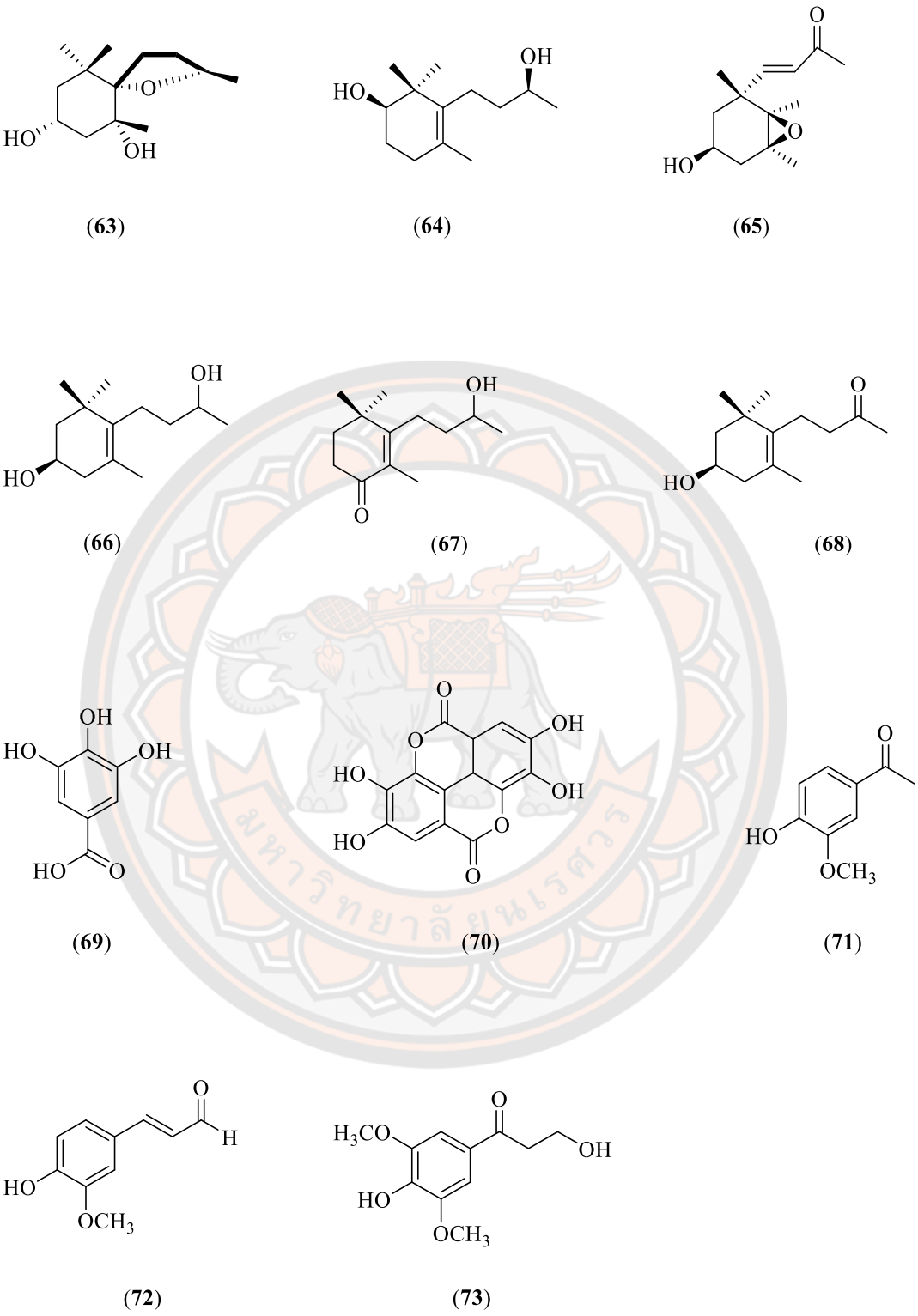

Figure 13 Chemical structures of apocarotenoids (**63-68**) and phenolic compounds (**69-73**)

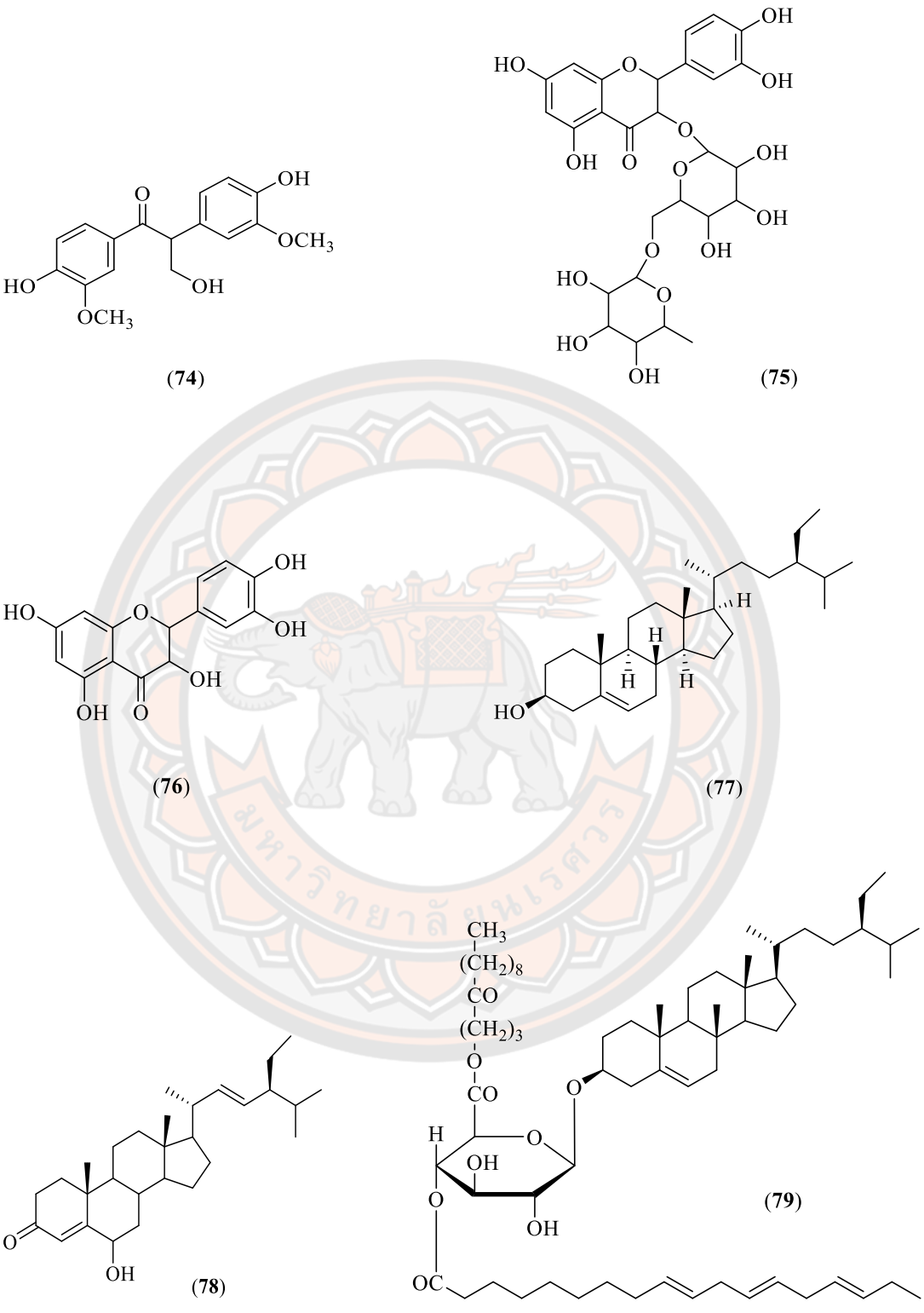

Figure 14 Chemical structures of phenolic compounds (**74**), flavonoids (**75-76**), steroids, and saponins (**77-79**).

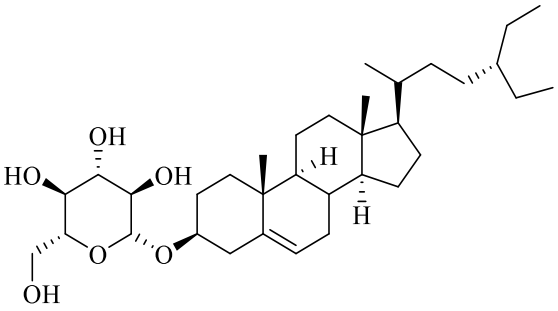

(**80**)

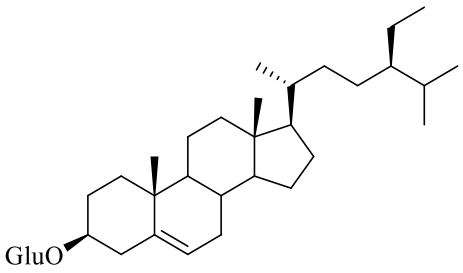

(**81**)

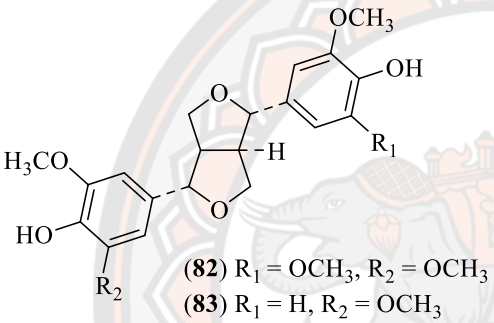

(**82**) $R_1 = OCH_3$, $R_2 = OCH_3$
(**83**) $R_1 = H$, $R_2 = OCH_3$
(**84**) $R_1 = H$, $R_2 = H$

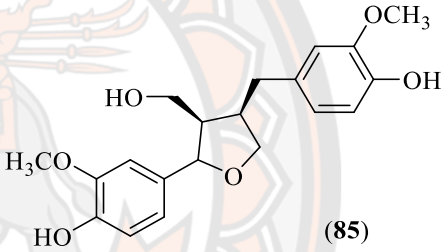

(**85**)

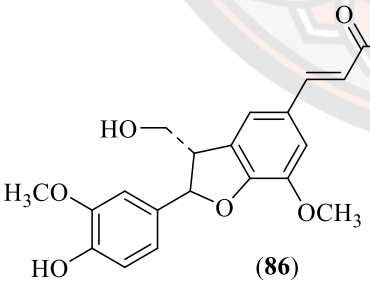

(**86**)

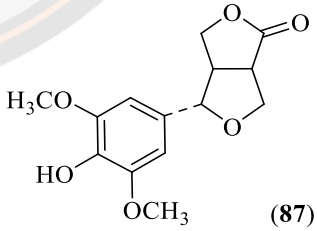

(**87**)

Figure 15 Chemical structures of steroids and saponins (**80-81**) phenylpropanoids (**82-87**): Note Glu = glucopyranoside).

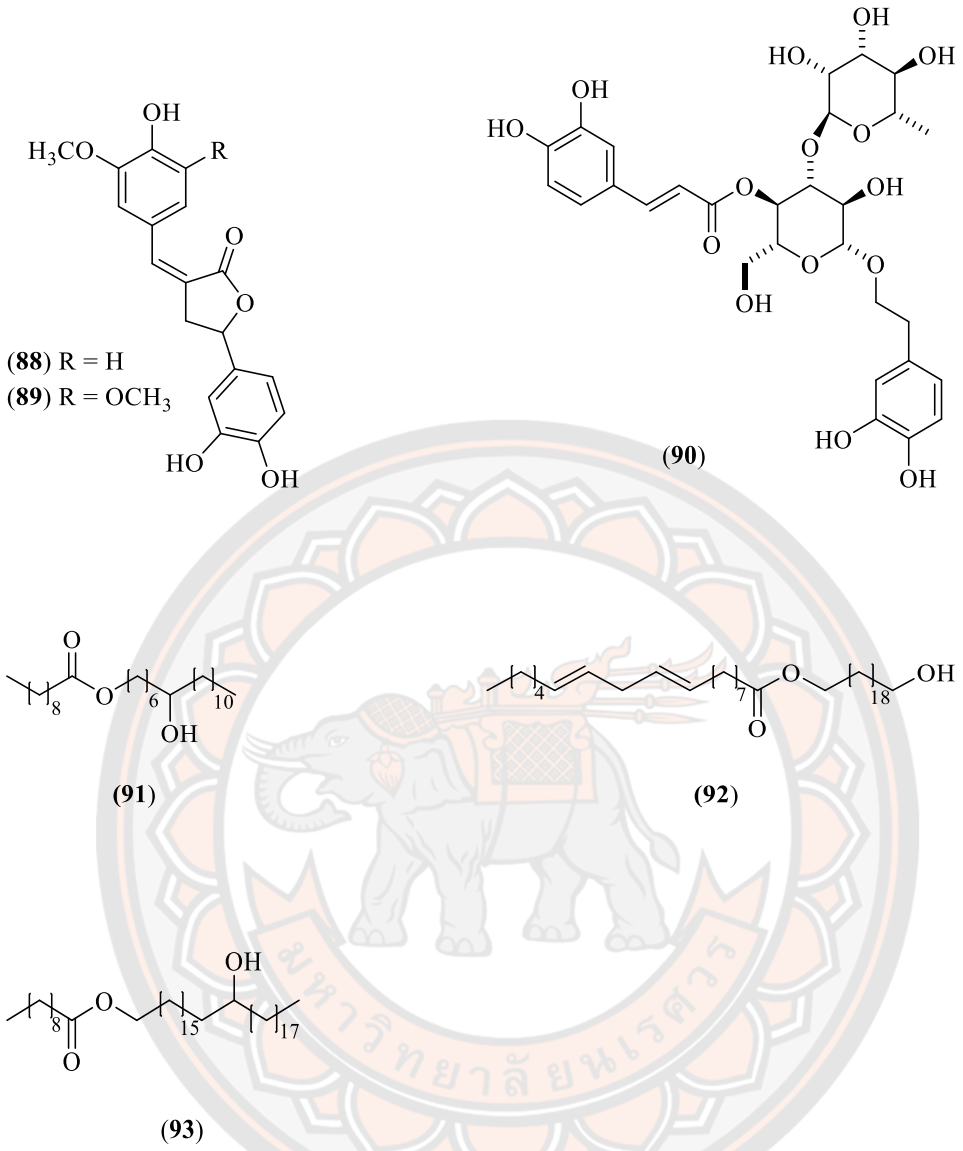

Figure 16 Chemical structures of phenylpropanoids (**88-90**) and fatty esters (**91-93**).

2.9.4 Pharmacology studies of *T. grandis*

Some isolated compounds from *T. grandis* as shown in Table 4 as well as several parts of *T. grandis* crude extract have been studied for their pharmacological activities such as wound healing, antibacterial activity, cytotoxic, hair growth, antioxidant, hypoglycemic, and anti-inflammatory properties. An overview of the pharmacological properties is summarized in Table 5.

Table 5 Overview of the pharmacological properties of *T. grandis*

Pharmacological activities	**Parts used**	**Active compounds or crude extracts**	**Ref. no.**
Wound healing activity	Leaf	Hydro-alcoholic extract	[131]
Antibacterial activity	Leaf and Bark	Chloroform extract	[132,133]
	Wood	Ethyl acetate extract	[132,133]
		5-Hydroxy-1,4-naphthalenedione (Juglone)	[134]
Synergistic *in vitro* antibacterial activity	Wood	Methanolic extract	[135]
Antiviral activity (against chikungunya virus)	Leaf	Ethanolic extract (Benzene-1-carboxylic acid-2-hexadecanoate)	[136]
Cytotoxicity	Wood	Methanolic extract	[132]
	Bark	Chloroform extract	[132]
		5-Hydroxylapachol, Lapachol	[109]
Hair growth activity	Seeds	Petroleum-ether extract	[23]
Antioxidant activity	Leaf, bark, and wood	Ethyl acetate extract	[132]
	Leaf	Methanolic extract	[137]
Hypoglycemia activity	Bark	Ethanolic extract	[138]
	Root	Methanolic extract	[139]
Anthelmintic activity	Fruits	Ethanolic extract	[140]
Anti-inflammatory activity	Flowers	Methanolic extract	[141]
	Stem	Hydro-alcoholic extract	[142]
Analgesic activity	Flowers	Methanolic extract	[141]
	Stem	Hydro-alcoholic extract	[143]

Pharmacological activities	Parts used	Active compounds or crude extracts	Ref. no.
Antifungal activity	roots and aerial parts	Methanolic extract, Phenolic acid 4′,5-′Dihydroxyepiisocatalponol	[104,144]
	Sawdust	Deoxylapachol	[116]
Anti-wood rot activity	Hardwood sawdust	Deoxylapachol	[116]
Diuretic activity	Leaf	Aqueous extract	[145,146]
Antiplasmodial activity	Leaf	Corosolic acid, 5,8-Dihydroxy-2-methylanthraquinone, Hydroxysesamone, Tectograndone	[103]
Antipyretic activity	Root	Methanolic extract	[147]
	Seeds	Methanolic extract	[148]
Gastroprotective activity	Root	Lapachol	[149]
	Leaf	Ethanolic extract, Verbascoside	[21]
Phytotoxicity	Dried leaf	2-Oxokovalenic acid, 19-hydroxyferruginol	[17]
Anti-COVID-19	NR	Barleriaquinone-I	[150]

Note: NR = not reported

Moreover, the traditionally acclaimed hair tonic was also confirmed by Jaybhaye et al. in 2010 [23]. They studied the effect of 5% and 10% petroleum ether extract of *T. grandis* seed on the hair growth rate in albino mice. The treatment was successful in producing more hair follicles than a standard positive control, minoxidil.

In the previous studies of our research team by Fachrunniza et al. (2020), they evaluated the effects of *T. grandis* extracts associated with hair loss treatment. Various parts of *T. grandis*, such as the roots, barks, woods, leaves, fruits, fruit peels , and seeds were sequentially extracted using different solvents. The crude extracts from different parts of *T. grandis* were tested for their 5α-reductase inhibition, anti-testosterone activity, cytotoxicity on HFDPCs, and anti-inflammatory effects by suppressing IL-1β secretion stimulated by RAW 264.7 cells. Notably, the leaf extract of *T. grandis*, obtained by hexane and ethyl acetate extraction, exhibited inhibition of 5α-reductase. Moreover, the cytotoxicity level in the hexane extract showed lower than ethyl acetate extract. Hexane extract demonstrated a comparable anti-testosterone activity profile to finasteride (used as a positive control) and exhibited the ability to inhibit IL-1β secretion. This discovery suggests that *T. grandis* might be a promising source for 5α-reductase inhibitors and serve as an ingredient in alternative medicine or cosmetic products for hair loss treatment [24].

In order to further develop products containing the potential plant extract for 5α-reductase inhibition, it is important to conduct qualitative and quantitative analyses of the 5α-reductase inhibitors in the extract. Moreover, the physicochemical properties, pre-formulation studies including stability profiles and skin penetration of the extract should be studied to provide useful information for further product design and development.

2.10 Methods for analysis the chemical components in extracts

2.10.1 Thin layer chromatography (TLC)

TLC is a conventional chromatography technique used to analyze the chemical constituents in extracts. Generally, a TLC plate is created using silica gel as a stationary phase on a sheet of aluminum foil, which is coated with a thin layer of adsorbent material. Then this plate is applied to the sample and developed using eluting solvents (mobile phase). Whether the compound travels up the TLC plate or is bound to the adsorbent depends on the physical properties (such as polarity and molecular structure) of each compound. The principle of solubility, known as “Like Dissolves Like”, is adhered to in this process. The analytes that exhibit lower solubility in the

mobile phase and possess a greater affinity for the stationary phase will be retained, whereas those analytes with higher solubility will elute to the top of the TLC plate as they are carried by the mobile phase [151]. After development, the TLC plate is subjected to visual inspection under daylight, and UV light at 254 and 366 nm to detect chemical components. In addition, the specific reagents are sprayed on TLC plate for detecting the group of compounds. For instance, anisaldehyde-sulfuric acid is used to detect steroids, essential oils, saponins, and sugars. Potassium hydroxide is employed for the detection of anthraquinone glycosides and their aglycones, while vanillin-sulfuric acid helps identify essential oils, phenols, steroids, and higher alcohols [152]. The retardation factor (R_f) value for each visualized spot is calculated by the following formula:

$$R_f = \frac{\text{Distance traveled by spot}}{\text{Distance traveled by solvent front}}$$

2.10.2 High-performance liquid chromatography (HPLC) and method validation

HPLC is a technique for the separation, identification, and quantification of compounds in a mixture. Generally, an HPLC system contained the basis modules: a solvent delivering, a pump, a sample injector, a column, a detector, and a data analysis unit (Figure 17).

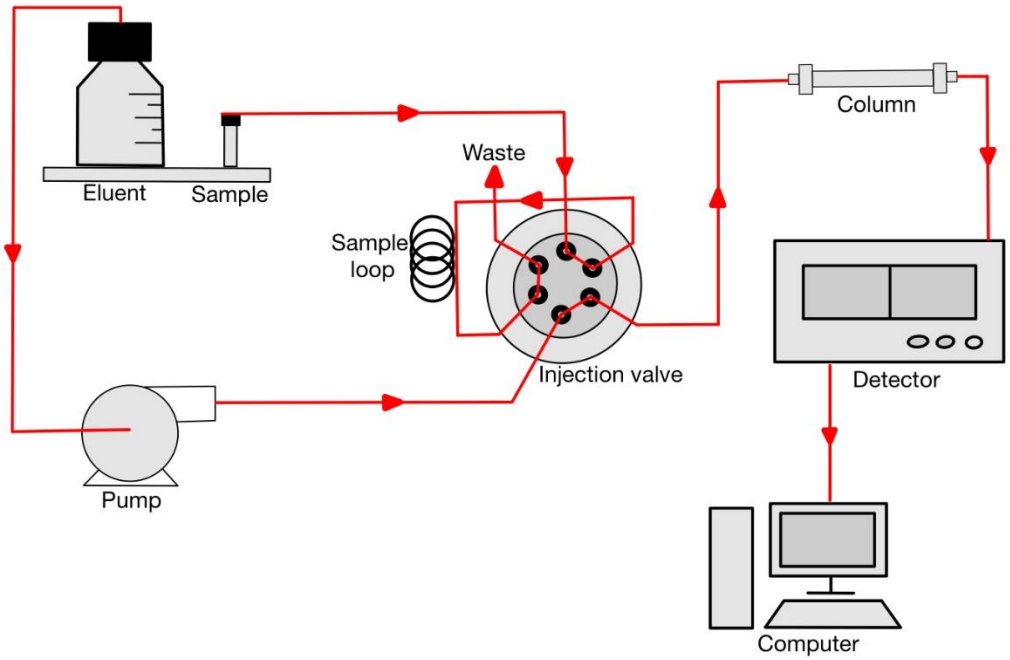

Figure 17 Schematic diagram of an HPLC system Note: modified from Juliane et al [153].

The principle of HPLC is a separation method that is based on sample (analyte) distribution between the stationary phase and mobile phase systems. Normal-phase, reverse-phase, size exclusion, chiral, ion exchange, and hydrophilic interactions are all common separation mechanisms supported by various packing materials [154]. Depending on the structure of the analyte, the compounds are retarded while they pass through the stationary phase. A range of detectors, including UV and fluorescence detectors, could be utilized based on the structural features of the analyte. After the substances have eluted from the column, the detection compartment recognizes them. The signals are recorded, transformed, and displayed in a chromatogram by the utilization computer software.

The HPLC method developed for the separation and quantification of active compounds in the extract is important for quality control. All analytical methods designed to analyze any sample will need to be validated. It also refers to various regulatory standards. The parameters described in this section are guidelines from the

International Conference on Harmonization (ICH, Q2R1) for aspects such as linearity, limits of detection (LOD) and quantification (LOQ), accuracy, as well as intra-day and inter-day precision. Additionally, the criteria for system suitability align with the standards established by the United States Pharmacopeia (USP 31).

Linearity: The linearity refers to the ca of HPLC method to yield results that exhibit a direct relationship with the concentration of the compound. A minimum of 5 concentrations is recommended for the performance of linearity [155]. Acceptance criteria; the correlation coefficient (R^2) is commonly used for this purpose, and curves with $R^2 \geqslant 0.999$ are usually considered to be linear. Moreover, it is required to perform data fitting to a regression line model represented as y = mx + b. The y-intercept should be equal to or less than 2% of the desired concentration response [156].

Limits of detection (LOD) and quantification (LOQ): The LOD represents the lowest detectable concentration of a compound that cannot be precisely as an exact value. The LOD is a parameter of the limit test that specifies whether an analyte's concentration is below or above a certain value. In an HPLC procedure, the LOQ represents the lowest concentration of a compound that can be accurately quantified while maintaining acceptable levels of accuracy and precision [155]. As for the acceptance criteria; the ICH references recommended a signal-to-noise ratio (S/N) for LOD as 3:1 and for LOQ as 10:1 [156].

The determination of LOD and LOQ values is performed by calculating the standard deviation based on the S/N ratio as in the following equation:

$$LOD = 3\ SD$$

$$LOQ = 10\ SD$$

Where SD refers to the standard deviation of the response, which is usually expressed as an analyte concentration in the sample.

Accuracy: Accuracy refers to the degree of closeness between the measured test results and the true values. The ICH guidelines suggest assessing accuracy by conducting a minimum nine determinations across a range of three concentration levels, which should include 25%, 50%, and 75% of the standard calibration curve. This typically involves performing three experiments, each with measurements at three different concentrations, thus ensuring a comprehensive

accuracy assessment for the entire analytical method. Accuracy should be expressed as the percent recovery, which is determined by assaying a known added amount of analyte in the sample. This recovery percentage should be calculated relative to the mean and the accepted true value, and it should be accompanied by confidence intervals to provide a comprehensive accuracy assessment [155]. The percentage recovery is calculated by the following equation:

$$\text{Recovery (\%)} = \frac{\text{C (Spiked)} - \text{C (Sample)}}{\text{C (Standard)}} \times 100$$

Where C represents the concentration in μg/mL. Acceptance criteria; The acceptable range for the % recovery value is 80.0-120.0 %.

Intra-day and inter-day precision: The precision of an analytical procedure is determined through two types of studies: intermediate precision (inter-day precision), which assesses variation between different days, and repeatability (intra-day precision), which assesses variation within the same day, all conducted at three concentration levels. Intra-day precision involves three replicate concentration analyses on the same day (n=3), while inter-day precision involves repeating each concentration on three different days (n=9). Precision is quantified as a relative standard deviation (RSD), typically expressed as a percentage, and calculated using the equation below:

$$\text{RSD (\%)} = \frac{\text{Standard deviation}}{\text{Mean}} \times 100$$

System suitability: The parameters of system suitability testing are method-dependent and are conducted on both HPLC systems by injecting five analyte concentrations to assess system accuracy and precision. The following parameters are determined: tailing factors, % RSD, resolution, and plate count [156]. The acceptance criteria for the system suitability testing are described in the USP 31 guideline (Table 6).

Table 6 Acceptance criteria for system suitability test according to USP 31 guideline [157].

Topic	USP 31
Resolution (*R*) *R*s between the peak of interest and the closest potential	> 1.5
Tailing factor (*T*)	≤ 2.0
Number of theoretical plate (*N*)	> 700
Relative standard deviation (RSD)	≤ 2 % (n=5)
	> 2 % (n=6)

2.11 Physicochemical properties

The assessment of the physicochemical properties of an extract is crucial for the development and design of a preferable formulation product. This assessment enables the enhancement of stability, solubility, and skin penetration, allowing for a more accurate evaluation of bioactive compounds in pre-formulation studies. In this study, measurements of physicochemical parameters such as solubility, pH, color, zeta potential, viscosity, and partition coefficient were focused, and some parameters are described.

2.11.1 Solubility

The solubility of an analyte is a fundamental and extensively utilized physicochemical property, holding significant importance in various applications. Typically, solubility experiments consist of 2 stages: (1) the preparation of organic solvents or saturated water, and (2) the determination of an analyte concentration in these organic solvents or the saturated water. Generally, solubility is commonly expressed in terms of concentration, denoted as mole fraction, molality, molarity, mass “g of solute per kg of solvent, g per dL (100 mL) of solvent” or other similar concentration units [158]. Both the USP (United States Pharmacopeia) and BP (British Pharmacopeia) classify the solubility, irrespective of the solvent used, based solely on quantification criteria. These criteria are detailed in Table 7.

Table 7 Descriptive solubility terms and solvent-to-solute ratio according to USP and BP criteria [159].

Descriptive term	**Part of the solvent required per part of solute**
Very soluble	< 1
Freely soluble	1 – 10
Soluble	10 – 30
Sparingly soluble	30 – 100
Slightly soluble	100 – 1000
Very slightly soluble	1000 – 10,000
Practically insoluble	≥ 10,000

2.11.2 Color measurement

Various color coordinate systems can be used to describe an object's color. Commission Internationale de l′éclairage (CIE) L* a* b* system is one of the most widely used systems. It was developed in 1976 for photoelectric measurement and the CIE L*a*b* color space (Figure 18), which provides more uniform color differences relative to human perception [160].

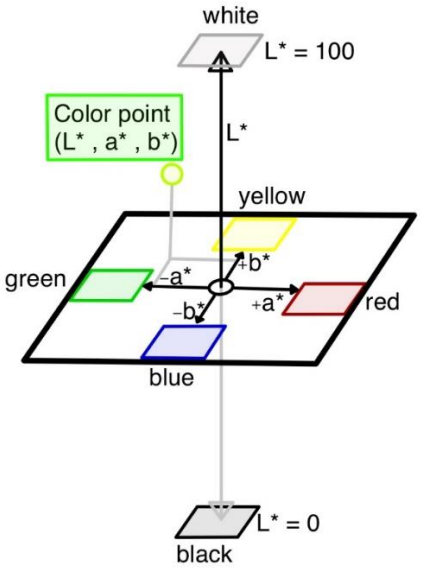

Figure 18 CIELAB color space. Note: modified from Beetsma et al [161].

The CIELAB coordinates (L*, a*, b*) are directly read. The parameter L* value is an estimate determination of luminosity, a characteristic that enables the representation of colors as values ranging from 0 (black) to 100 (white). In addition, the a* parameter is assigned positive values (+a*) to represent color in the redness colors, whereas negative values (-a*) are used to denoted colors in the greenness colors. Similarly, the parameter b* is assigned positive values (+b*) to indicate colors in the yellowness colors, while negative values (-b*) are used to represent colors in the blueness colors [160]. The calculation of the color difference (ΔE*) involves the utilization of L*, a*, and b* values, along with a comparison to the standard (excluding the sample) according to the following equation:

$$\Delta E^* = \sqrt{\Delta L^{*2} + \Delta a^{*2} + \Delta b^{*2}}$$

Deltas can exhibit positive (+) or negative (-) values for L* (ΔL*), a* (Δa*), and b* (Δb*) in the context of the colorimetry. The overall color difference, denoted as Delta E (ΔE*), is consistently positive [162].

"ΔL* (L* sample – L* standard) = (+ = lighter, – = darker)"

"Δa* (a* sample – a* standard) = (+ = redder, – = greener)"

"Δb* (b* sample – b* standard) = (+ = yellower, – = bluer)"

2.11.3 Zeta potential

The zeta potential analysis is a crucial parameter for estimating the stability of nanoparticle (NP) dispersions in solution. NPs with a net charge in an ionic solution composed of an ion layer (with a charge opposite to that of NPs) can absorb near their surface; this is known as the Stern layer. The loosely associated ions are contained in a second diffuse outer layer (Figure 19). These two layers are collectively known as the EDL (electrical double layer). The zeta potential refers to the electrostatic potential observed at the boundary known as the "slipping plane", and it is associated with the surface charge of the NPs [163]. Zetasizer has the capability to concurrently determine the velocities of the numerous charged particles in the solution through electrophoretic light scattering (ELS) [164].

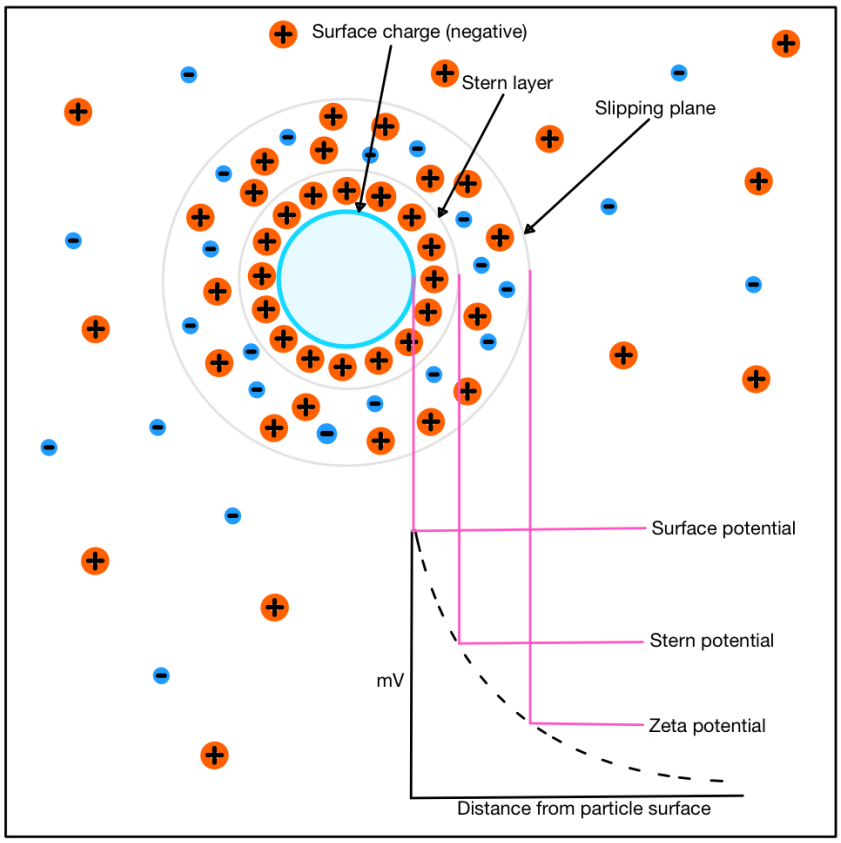

Figure 19 Schematic illustration of the EDL phenomenon occurring at the interface between a liquid medium and a negatively charged particle. Note: modified from Pate et al [165].

Normally, zeta potential analyses are beneficially used to optimize emulsions, suspensions, and dispersions in formulation products. The magnitude of particle zeta potential typically ranges from +100 mV to −100 mV. The zeta potential value can serve as an indicator of the colloidal stability of the solution (Table 8).

Table 8 The colloidal stability behavior for ranges of zeta potential [166]

Zeta potential value (mV)	Colloidal stability behavior
0 to ± 5	"Flocculation or coagulation"
± 10 to ± 30	"Incipient instability"
± 30 to ± 40	"Moderate stability"
± 40 to ± 60	"Good stability"
more than ± 60	"Excellent stability"

The widely accepted threshold for the zeta potential of stable aqueous suspensions is a value exceeding +30 mV or falling below than −30 mV, indicating strong cationic and anionic properties, respectively. Particles exhibiting zeta potential values below +25 mV or above −25 mV will eventually undergo agglomeration as a result of intermolecular forces such as hydrogen bonding, van der Waals interactions, and hydrophobic interactions [163,166].

2.11.4 Viscosity

The viscosity of a fluid refers to its ability to resist deformation and absorb stress, with the specific degree of resistance being influenced by the rate at which deformation occurs. The relationship between shear stress (τ) and shear rate (D) is expressed by the following equation.

$$\tau = \eta D$$

where η is the dynamic viscosity.

The viscosity of non-Newtonian liquids exhibits variability in response to changes in shear rate, while the Newtonian liquids maintain a constant viscosity across all shear rates and are only affected by the variables pressure and temperature.

The SI unit of τ and D is Pascal (Pa) and per second (s^{-1}), respectively. The dynamic viscosity is measured in Pascal second (Pa.s) in the SI unit. For practical purposes, a sub-multiple is often more convenient: 1 mPa.s is equal to 10^{-3} Pa.s, which corresponds to one centipoise (cP) in the now-obsolete centimeter-gram-second (cgs) system [167].

2.11.5 Partition coefficient

The partition coefficient ($P_{o/w}$) characterizes the solubility ability of the plant extracts or compounds in a biphasic system consisting of lipids (such as fats, oils, and organic solvents, commonly *n*-octanol) and water, which are immiscible. The partition coefficient is described in simple terms as the ratio of the concentration of a solute dissolved in an organic portion versus the aqueous portion. The solute that is mainly dissolved in the aqueous portion is called as “water-liking” or hydrophilic, whereas those that are predominantly dissolved in lipids are called “lipid liking” or lipophilic. The partition coefficient, also known as the $K_{o/w}$ or $P_{o/w}$ value, serves as an indicator of the potential for a substance to be absorbed by various living organisms, including plants, animals, and humans, as well as whether it is more likely to be transported and dispersed by water. The log $P_{o/w}$ value is a fixed parameter defined by the following equation:

$$\text{Partition coefficient, } P_{o/w} = \frac{[\text{organic}]}{[\text{aqueous}]}, \quad \log P_{o/w} = \log_{10} (\text{partition coefficient})$$

Where [ ] represent the concentration of the solute in both the organic and aqueous partitions [168].

A negative Log $P_{o/w}$ value suggests that the compound has a stronger attraction to the aqueous phase, indicating its more hydrophilic. When log $P_{o/w} = 0$, the compound is evenly distributed between two phases. Conversely, a positive Log $P_{o/w}$ value indicates a higher concentration partitioned in the organic phase, signifying its lipophilic properties. For example, a Log $P_{o/w} = 1$ indicates a partitioning ratio of a 10:1 between the organic and aqueous phases [168]. Several published articles reported on the determination of $P_{o/w}$ of plant extracts and compounds. For instance, the log $P_{o/w}$ of germacrone in *Curcuma aeruginosa* Roxb. extract was determined using the HPLC method [169], the log $P_{o/w}$ of eurycomamone in *Eurycoma longifolia* Jack extract was established using the HPLC method [170], and the analysis of log $P_{o/w}$ for three plant extracts, namely barberry (*Berberis vulgaris* L.), cornelian cherry (*Cornus mas* L.) and

mahonia (*Mahonia aquifolium* Nutt.), was conducted using the UV spectroscopy technique [171].

2.12 Stability studies

The stability of natural plant extracts is crucial for ensuring the quality, safety, and efficacy of the final product available in the market. Several factors (i.e. pH, temperature, and light) may influence the chemical degradation of crude extracts and their active compounds. In most cases, either hydrolysis or oxidation is present in the reaction [172].

2.12.1 Effect of pH

The effect of pH stability in extracts containing bioactive compounds has been reported. For example, Wongwad et al (2020) determined the effect of pH on bioactive compounds such as benzophenones (iriflophenone 3,5-C-β-D-diglucoside and iriflophenone 3,5-C-β-D-glucoside) and xanthones (mangiferin) in *Aquilaria crassna* leaf extract. The pH rate profiles of these compounds suggested that they exhibit stability under environments ranging from neutral to acidic [173]. Sipahli et al (2016) investigated the effect of pH on the chemical stability of crude anthocyanins in *Hibiscus sabdariffa* extract with pH ranges from 1 to 9 [174]. They found that crude anthocyanins degraded more slowly at an acidic pH range. In addition, Suphrom et al (2014) also studied the effect of pH (ranging from 2.0 to 9.0) on sesquiterpenoids as a germacrone compound in *Curcuma aeruginosa* Roxb. extract, which compound was unaffected by pH (2.0-9.0) [175].

2.12.2 Effect of temperature

The bioactive compounds found in extracts, such as terpenoids, flavonoids, and phenolics, are known to exhibit heat instability and are susceptible to degradation over a period of time. The thermal degradation kinetics model is a frequently employed approach to characterize the degradation process of these chemical substances. This model can provide the valuable data for monitoring and forecasting the long-term quality and shelf-life-related alterations in plant extracts containing bioactive compounds. Several stability studies of bioactive compounds in

diverse plant species have been reported using this technique. For example, Oancea et al (2018) conducted a study on the degradation of polyphenolic compounds, focusing on the major anthocyanin compounds like pelargonidin-3-sophoroside and delphinidin-3-glucoside, as well as catechin hydrate, which is a major flavonoid compounds found in *Sambucus nigra* L. extract [176], and sour cherry (*Prunus cerasus*) extract [177]. In addition, Beelders et al (2015) investigated the degradation of benzophenones and xanthones in *Cyclopia genistoides* (L.) Vent. [178]. Similarly, Wongwad et al (2020) documented the degradation of these compounds in a different plant (*Aquilaria crassna*) [173]. Moreover, Suphrom et al (2014) also studied the degradation of an antiandrogenic compound, germacrone, in *Curcuma aeruginosa* Roxb. extract at various temperatures. Their finding indicated that the pure solid form of germacrone was highly sensitive to temperature changes, while the degradation process was slower when the compound was stored in the dried extract [175].

2.12.3 Effect of light

Light is one of the important factors in the chemical stability of plant extract, with ultraviolet (UV) rays known to stimulate redox reactions [172]. To assess photostability, ICH guidelines offer various methods for testing plant extracts and drug substances. Specific requirements for visible and UV exposure are outlined as follows:

- Visible light: A minimum of 1.2 million lux-hours for visible light
- Ultraviolet light: An integrated UV energy of 200 w-hour/m^2 within the range of 300-400 nm for ultraviolet light

Commonly, the ID65 serves as the light source, and it is activated using a Window-Q filter in the Q-SUN chamber. This choice is made because it effectively replicates sunlight entering an indoor environment [179]. Several instances of Q-SUN chamber set points with a Window-Q filter are given in Table 9.

Table 9 The set points of a Window-Q filter in a Q-SUN chamber at a 420 nm control point [179]

Set Point (420 nm)	**UV Irradiance**	**Illuminance**	**Test Duration**	**UV Dosage**	**Visible Light Dosage**
0.62 W/m^2	28.3 W/m^2	50.4 klx	24 hours	673 W-hour/m^2	1.21 million lux-hour
1.10 W/m^2*	49.7 W/m^2	89.5 klx	13.5 hours	671 W-hour/m^2	1.21 million lux-hour
1.47 W/m^2	66.5 W/m^2	119.6 klx	10 hours	665 W-hour/m^2	1.20 million lux-hour

Note: *1.10 W/m^2 is a typical set point in photostability tests.

Many published articles on the rapid photodegradation of chemical compounds in plant extracts have been reported. For example, Bilia et al (2001) studied the photodegradation of *Hypericum perforatum* L., and observed a slight decrease in flavonoids when exposure to light [180]. This finding was subsequently confirmed by Kopleman et al (2001) [181]. Moreover, the stability of the active ingredient known as azadirachtin-A in *Azadirachtin indica* oil was examined by Barrek et al (2004) across several settings, including pH levels, temperature variations, and exposure to various light sources such as UV radiation, darkness, and daylight. Additionally, they identified the degradation products of this compound using HPLC–MS and HPLC–MS–MS techniques [182].

2.13 Skin penetration study

In the human body, the skin is the largest organ. It has a barrier function to prevent foreign molecules penetration into the body. The skin is a viable route for drug delivery. Transdermal delivery has become popular as a viable alternative to delivering drugs through intact skin. These systems provide several advantages, such as passing initial metabolism, ensuring patient adherence across diverse medical conditions, and enabling controlled and sustained release of drugs [183]. The transdermal system is generally suitable for routine *in vitro* studies of drug penetration. The assessment of

drug absorption through the skin is frequently conducted using Franz diffusion cells [184]. Various types of membranes, including synthetic artificial membranes like cellulose acetate (CA) and Strat-M membranes, as well as animal skin such as rodent skin and pig skin, and human skin derived from cosmetic surgeries biopsies, and human cadavers, can be effectively employed in the Franz diffusion cell system. Animal and human skins are the most preferred among these membranes because they are the most similar to *in vivo* human skin. Nevertheless, both of these models have limitations, including cost, human skin availability, and ethical concerns related to animal skin usage [185]. The utilization of synthetic artificial membranes is frequently employed for assessment of the penetration of active ingredients. It is mimicked because these membranes contain either the domains of hydrophilic or lipophilic skin [186].

2.13.1 Synthetic Strat-M® membrane

Strat-M® is a synthetic artificial membrane designed as a viable alternative to human skin model. It offers improve predictability of diffusion in human skin while avoiding issues like lot-to-lot variation, safety concerns, and storage limitations. As shown in Figure 20, the composition of this membrane was intentionally engineered to replicate the structural characteristics and lipid chemistry found in the epidermal layer of human skin. The Strat-M® membrane is characterized by an approximate thickness of 300 µm and is consists of an outer layer supported by two layers of polyethersulfone (PES) and a bottom layer supported by a polyolefin non-woven fabric [187].

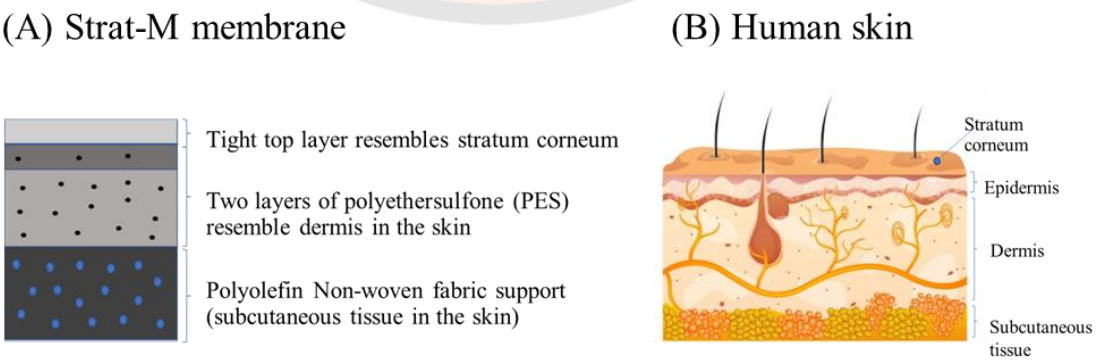

Figure 20 The structure of artificial Strat-M® membrane (A) [187] and normal human skin (B) [188].

2.13.2 The classical scheme of skin absorption

The stratum corneum serves as the principal barrier for drug permeation through the various layers of skin. Nevertheless, there are some mechanisms for the transportation of natural compounds, such as tree penetration pathways (intracellular, intercellular, and follicular routes). The intracellular pathway is conductive to the penetration of lipophilic drug substances. The intercellular pathway is suitable for the transmission of hydrophilic drug substances. In contrast, the follicular or transappendageal pathway enables direct and rapid transfer of substances to the upper segment (infundibulum) region via the eccrine (sweat) glands or hair follicles (Figure 21) [189,190]. Substances typically pass through the skin via a combination of all pathways, with the relative importance of each route dependent on the physicochemical properties of the substance [191].

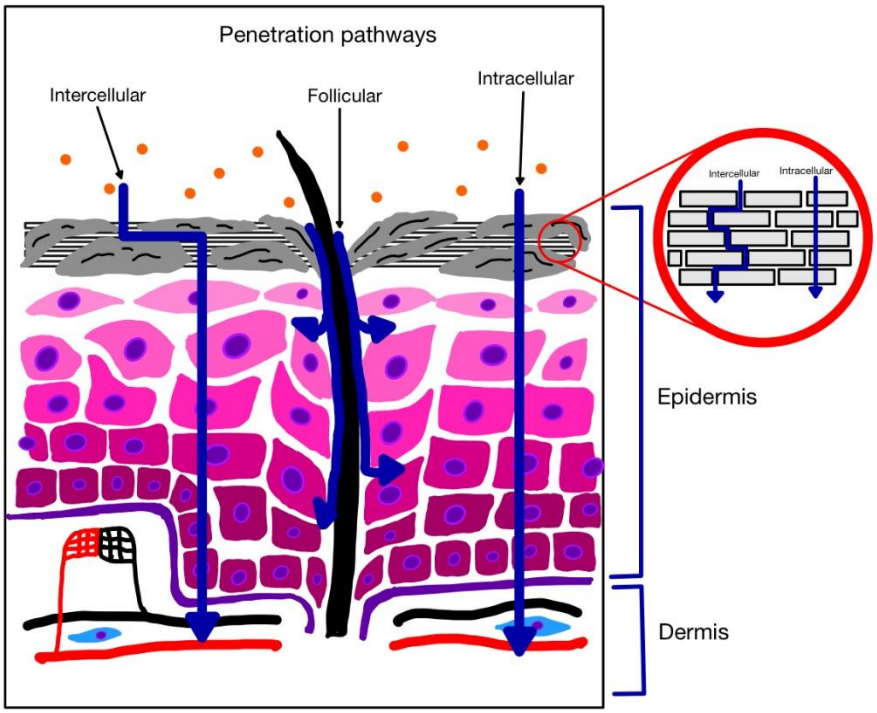

Figure 21 Potential routes for drug penetration through various skin layers include follicular, intra-, and intercellular pathways. The close-up in the upper right inset provides a detailed view of the stratum corneum, highlighting the intracellular pathway and the convoluted intercellular pathway Note: modified from Bolzinger et al [192].

2.13.3 Franz diffusion cell system

The Franz cell apparatus (Figure 22) is composed of the donor chamber on top, which is separated from the receiver chamber below.

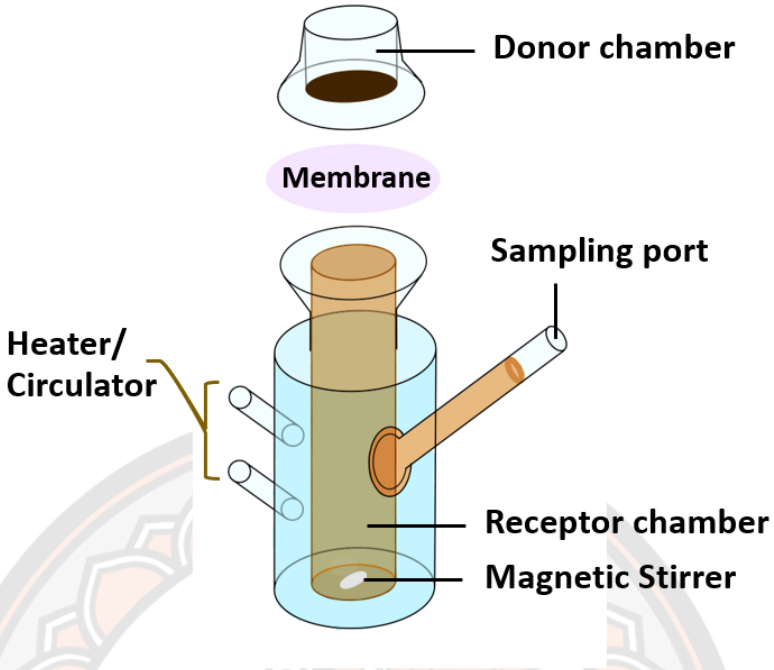

Figure 22 Franz diffusion cell [193].

The system is maintained at a constant temperature using a heated water jacket. The solution within the receiver chamber is homogeneously mixed throughout the experiment using a magnetic bar stirring. In the donor chamber, the tested samples are placed in contact with the glossy side of the Strat-M™ membrane. After collection of the sample at various times, all samples are analyzed using the validated HPLC method.

CHAPTER III
RESEARCH METHODOLOGY

3.1 General experimental procedures

Thin layer chromatography (TLC) analysis was conducted using a 20 × 20 cm aluminum sheet coated with TLC silica gel 60 F254 (Merck, Darmstadt, Germany). For the chromatographic isolation of the extract constituents, silica gel columns (granule size 0.040–0.063 mm, Merck, Darmstadt, Germany), Sephadex LH-20 columns (particle size dry 18–111 µm, GE Healthcare, Uppsala, Sweden), and SiliaBond® C18 columns (particle size 40-63 µm, SiliCycle, Quebec, Canada) were employed. For quantitative analysis of marker compounds in *T. grandis* extracts, two experiments involving different machines of high-performance liquid chromatography (HPLC) were conducted: stability studies and determination of partition coefficient. For the stability studies, HPLC analysis was carried out using Agilent Technology system (model 1260 infinity with fraction collector, Santa Clara, CA, USA) coupled with a Phenomenex Luna C18(2) column (150 × 4.6 mm, 5 µm particle size, USA). The partition coefficient was determined using HPLC with a Shimadzu LC-20AT system and a Shimadzu SPD-20A UV/Vis detector. HPLC analysis utilized a Phenomenex Luna C18 column (150 × 4.6 mm, 5 µm particle size) along with a guard column (5 µm Phenomenex C18, 4 mm × 3 mm). For gas chromatography-mass spectrometry (GC-MS) analysis, an Agilent Technology model 6890 instrument (Palo Alto, CA, USA) was employed, and separation was achieved using a fused silica capillary Hewlett Packard HP-5MS column (0.25 mm x 30 m i.d., 0.25 µm film thickness), coupled with a mass selective detector (MS). Fourier-transform infrared (FT-IR) spectra were obtained using the attenuated total reflectance (ATR) mode on a PerkinElmer Spectrum GX instrument (Perkin Elmer, Waltham, MA, USA). Optical rotations were determined using a POLAX-2L polarimeter from Atago, Japan. HPLC analysis was carried out on an Agilent 1260 Infinity instrument equipped with an ESI interface and coupled to a 6540 ultrahigh definition accurate mass Q-TOF mass spectrometer (Agilent Technologies, Palo Alto, CA, USA). Nuclear magnetic resonance (NMR) spectra were recorded on a Bruker AV400 spectrometer (Bruker, Billerica, MA, USA), operating at 400 MHz for proton

and 100 MHz for carbon nuclei. Absorbance measurements were conducted using the hybrid Multi-Mode Detection Synergy H1 instrument (model H1MF) manufactured by Bio-TeK Instruments (Winooski, VT, USA). The color of the extracts was assessed using Konica Minolta (Thailand). Zeta potential measurements were conducted using a zeta potential analyzer (Malvern Zetasizer Nano ZS, UK). An ultrasonic processor, Sonics Vibracell™ VCX130 with probe V18, was employed for sonication (Newtown, CT, USA). U-shaped 96-deep-well plates were used (Agilent Technologies, Santa Clara, CA, USA) and were covered with well-cap mats sourced from Thermo Scientific (Waltham, MA, USA). Franz diffusion apparatus was performed by Logan Instruments Corp (model, FDC-6, Somerset, NJ, USA). The Strat-M membrane transdermal diffusion test model, which includes discs sized at 25 mm), was bought from Merck Millipore (Cork, Ireland). Accelerated light stability and weathering chamber were performed by Q-LAB (model Q-SUN XE-1-BC, USA). Viscosity was measured by an AMETEK Brookfield viscometer (model DV3TRVCJ0, USA). The pH value was recorded using Mettler Toledo (Bangkok, Thailand). An orbital shaker (Biosan, Latvia) was used for solubility testing.

3.2 Chemical reagents

The solvents used in this study, including hexane, acetone, methanol (MeOH), ethanol (EtOH), ethyl acetate (EtOAc), dimethyl sulfoxide (DMSO), and dichloromethane (DCM), were of analytical reagent (AR) grade and were obtained from RCI Labscan Ltd (Bangkok, Thailand). Acetonitrile (CH_3CN), graded for HPLC was bought from RCI Labscan Ltd (Bangkok, Thailand). Additionally, β-Nicotinamide adenine Dinucleotide Phosphate (NADPH, tetrasodium salt) was obtained from OYC (Tokyo, Japan). Hydroxylamine hydrochloride was purchased from Carlo Erba Reagent (Milan, Italy). The Roswell Park Memorial Institute (RPMI) 1640 Medium, supplemented with L-glutamine, fetal bovine serum (FBS), and antibiotics (consisting of 100 unit/mL penicillin G and 100 µg/mL streptomycin) were bought from GIBCO (Grand Island, NY, USA). Disodium ethylenediaminetetraacetate dihydrate (EDTA) was purchased from Bio-Rad laboratories life science group (Hercules, California). Phenylmethanesulfonyl fluoride (PMSF), 2-amino-2-(hydroxymethyl)-1,3-propanediol (Trizma® base), 2-[4-(2-hydroxyethyl)piperazin-1-

yl]ethanesulfonic acid (HEPES), testosterone, sodium pyruvate, sodium bicarbonate, and D-(+)-glucose monohydrate, butylated hydroxytoluene, and benzophenone were obtained from Sigma-Aldrich (St. Louis, MO, USA). Additionally, potassium chloride (KCl), di-sodium hydrogen orthophosphate anhydrous (Na_2HPO_4), potassium dihydrogen orthophosphate (KH_2PO_4), and propylene glycol (PG) were ordered from Ajax Finechem (New South Wales, Australia). Polyethylene glycol-40 (PEG-40) hydrogenated castor oil was obtained from Phitsanuchemicals (Phitsanulok, Thailand). Tween20® was purchased from AppliChem GmbH (Darmstadt, Germany). Formic acid was purchased from KemAus (Australia). Toluene and octyl methoxycinnamate were purchased from Merck (Damstadt, Germany). Benzyl benzoate was purchased from Thai-China Flavours & Fragrances Industry (Phra Nakhon Si Ayutthaya, Thailand).

3.3 Plant materials and extraction

Fresh mature leaves of *T. grandis* (teak) were gathered in September 2019 from Banna district, Nakhon Nayok Province, Thailand. The identification and authentication of plant material was conducted by Assistant Professor Pranee Nangngam, Ph.D., from the Faculty of Science, Naresuan University. The voucher specimen with the collection number 05721 was deposited at the Department of Biology, Faculty of Science, Naresuan University, Phitsanulok, Thailand. The voucher specimen and characteristics of *T. grandis* leaves are shown in Figure 23.

Figure 23 The voucher specimen (left) and fresh mature leaves (right) of *T. grandis*

The fresh mature leaves of *T. grandis* (TG) were cleaned, chopped, and subjected to a drying process at a temperature of 55 °C for three days. The dried plant material was finely ground by a mechanical grinder and sieved through a 60-mesh sieve. The extraction of *T. grandis* leaf powder was conducted separately by maceration with two organic solvents: hexane and 95% ethanol. For the preparation of crude hexane extract, 1.5 kg of *T. grandis* leaf powder was macerated with hexane (6.0 L) at room temperature. This maceration process was repeated three times, with each round lasting at least five days and involving occasional shaking. Afterward, the solvent was combined and removed by evaporating under reduced pressure, resulting in the production of a dark brown viscous crude hexane extract, yielding 127 g (8.47% yield). To prepare the crude ethanolic extract, a 292 g sample of leaf powder was macerated with 95% ethanol (1.17 L). Following a similar procedure as previously described for the hexane extract, a dark green viscous crude ethanolic extract was obtained, yielding 32.90 g (11.27% yield). In addition, an ethanolic extract in PG was produced for used as a sample in stability and skin penetration tests. A crude ethanolic extract was initially solubilized with PEG-40 hydrogenated castor oil at a ratio of 1:3 w/w. Subsequently, PG was added at a ratio of 1:4 w/w to yield a dark brown liquid of ethanolic extract in PG (Figure 24). All obtained extracts were stored at -20 °C until use.

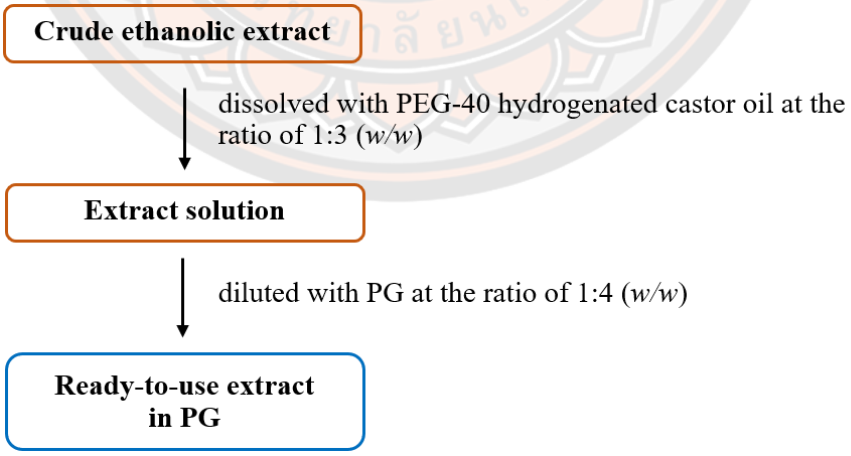

Figure 24 Schematic diagram of the preparation of ethanolic extract in PG

3.4 Isolation and identification of 5α-reductase inhibitors from *T. grandis* leaf extract

To isolate the 5α-reductase inhibitors, a 100 g sample of the hexane extract was dissolved in 100 mL of hexane to provide a hexane solution. This solution was carefully added to 100 mL of chilled acetone, resulting in the separation of 47.00 g of an acetone-soluble portion and 54.56 g of acetone-insoluble residue. The 47.00 g acetone-soluble portion was subsequently dried and suspended in MeOH to obtain 33.08 g methanol-soluble portion (hTG) and 13.01 g methanol-insoluble residue. Of this hTG extract, 18.46 g was further fractionated using a sephadex LH-20 column (2.5 × 73 cm). MeOH was employed as the mobile phase during this fractionation process, leading to the separation of seven fractions, labeled as hTG.A–hTG.G. In order to determine the active compounds, a process known as activity-guided fractionation was used. This involved utilizing an *in vitro* experiment to assess the inhibitory activity of the fraction obtained against 5α-reductase. Among these fractions the highest 5α-reductase inhibitory activity was observed in hTG.B. A part of fraction hTG.B (9.85 g) was subsequently subjected to separate using a sephadex LH-20 column (2 × 88 cm), employing MeOH as mobile phase. This process yielded six fractions, designated as hTG.B1–hTG.B6. These obtained fractions were further assessed for their ability to inhibit 5α-reductase activity. Two major fractions, hTG.B3 and hTG.B4 exhibited the highest levels of inhibitory activity. The active fraction, hTG.B4 (5.06 g, orange viscous), was re-fractionated using a silica gel column (5 × 13 cm). Elution was carried out using a stepwise gradient of hexane and EtOAc ranging from 99.5:0.5 to 0:100% *v*/*v*, yielding seven sub-fractions labeled as hTG.B4/1–hTG.B4/7. A total of 529.9 mg of sub-fraction hTG.B4/3 was further chromatographed with a silica gel column (1.5 × 13 cm). The elution process was carried out using a gradient mixture of hexane and EtOAc, ranging from a ratio of 95:0.5 to 0:100% *v*/*v*). This resulted the separation of the mixture into seven fractions, labeled as hTG.B4/3.1–hTG.B4/3.7. From these sub-fractions, hTG.B4/3.1 (90.0 mg, white solid) was selected for further purification and was processed on a reversed-phase C18 column (1.5 × 20 cm) with MeOH as the eluent, yielding three sub-fractions, identified as hTG.B4/3.1.1–hTG.B4/3.1.3. The white solid powder of hTG.B4/3.1.1 (61.1 mg) was subsequently dissolved with MeOH and

subjected to HPLC utilizing an Agilent 1260 infinity system with a fraction collector (USA). A Phenomenex Luna® C18(2) column (250 × 10 mm, 10 µm particle size) was employed. The condition for HPLC were as follow: an injection volume of 50 µL, a flow rate of 5 mL/min and detection at 220 nm. The mobile phase consisted acetonitrile:water (90:10 v/v) in an isocratic manner. Two pure compounds; **1** (19.5 mg, t_R: 11.03 min) and **2** (16.3 mg, t_R: 10.12 min) were successfully isolated (Figure 25). In addition to these compounds, an active fraction, hTG.B3 (1.71 g, brownish syrupy), was also loaded on a sephadex LH-20 column (2 × 88 cm) using MeOH as an eluent to produce four sub-fractions, labeled as hTG.B3/1–hTG.B3/4. A subfraction hTG.B3/3 (319.3 mg) was further re-fractionated over the silica gel column, with sequential elution using a gradient comprising hexane, dichloromethane (CH_2Cl_2), and MeOH, yielding nine sub-fractions identified as hTG.B3/3.1–hTG.B3/3.9.

Sub-fraction hTG.B3/3.3 (6.1 mg) was subjected to a C18 column (1.5 × 20 cm, MeOH) as a reversed-phase system to obtain compound **3** (3.7 mg, colorless needle-shaped crystals). As well, the purification of fraction hTG.B3/3.4 (5.4 mg) using the same step as hTG.B3/3.3 led to the isolation of compound **3** (1.7 mg, Figure 26). The identification of all the previously known isolated compounds was confirmed by comparing their physical properties and spectral data with those previously reported in the literature.

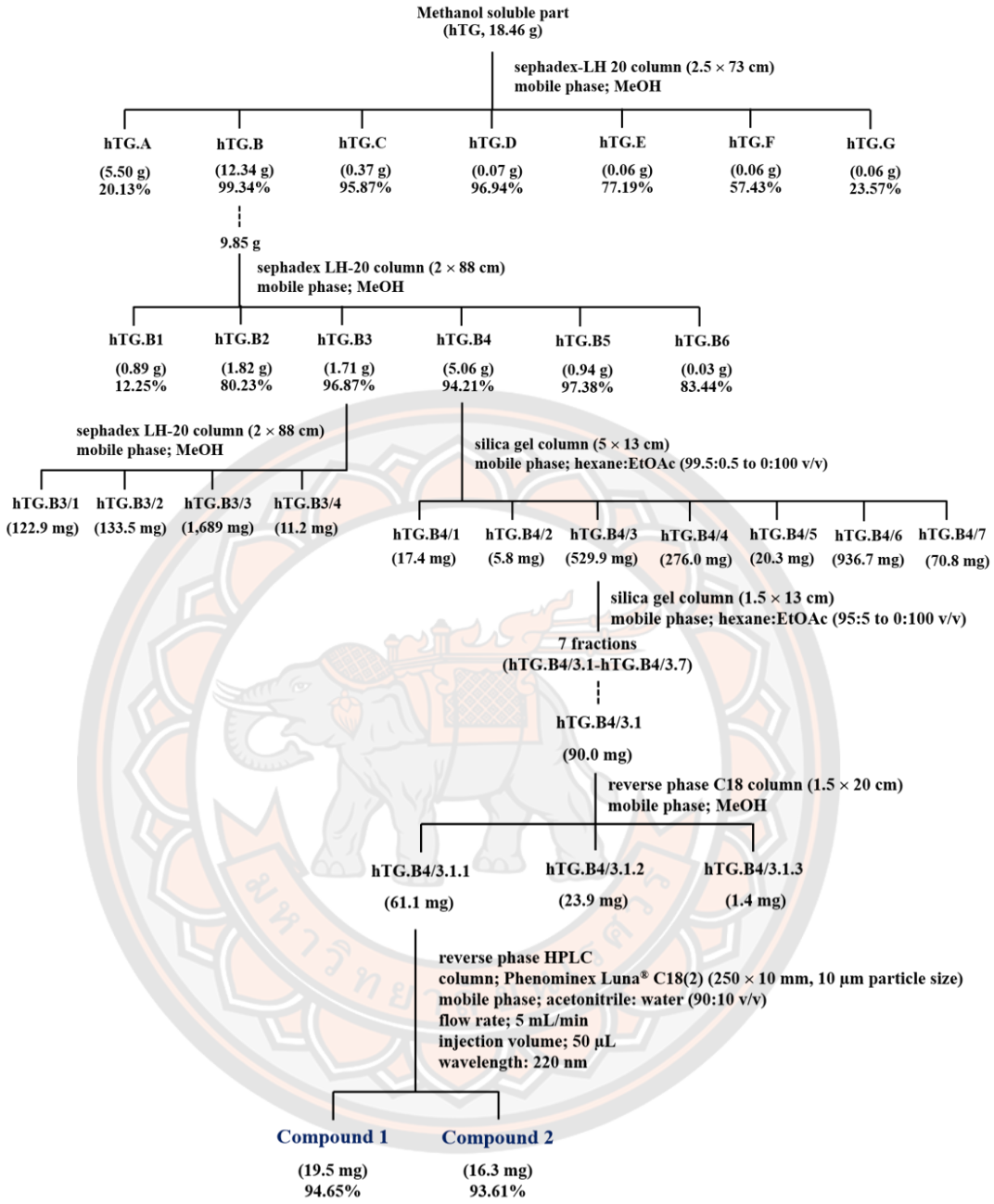

Figure 25 Schematic diagram of the fractionation process for hTG extract and the percentages represent the inhibition of 5α-reductase activity tested at the final assay concentration of 100 µg/mL

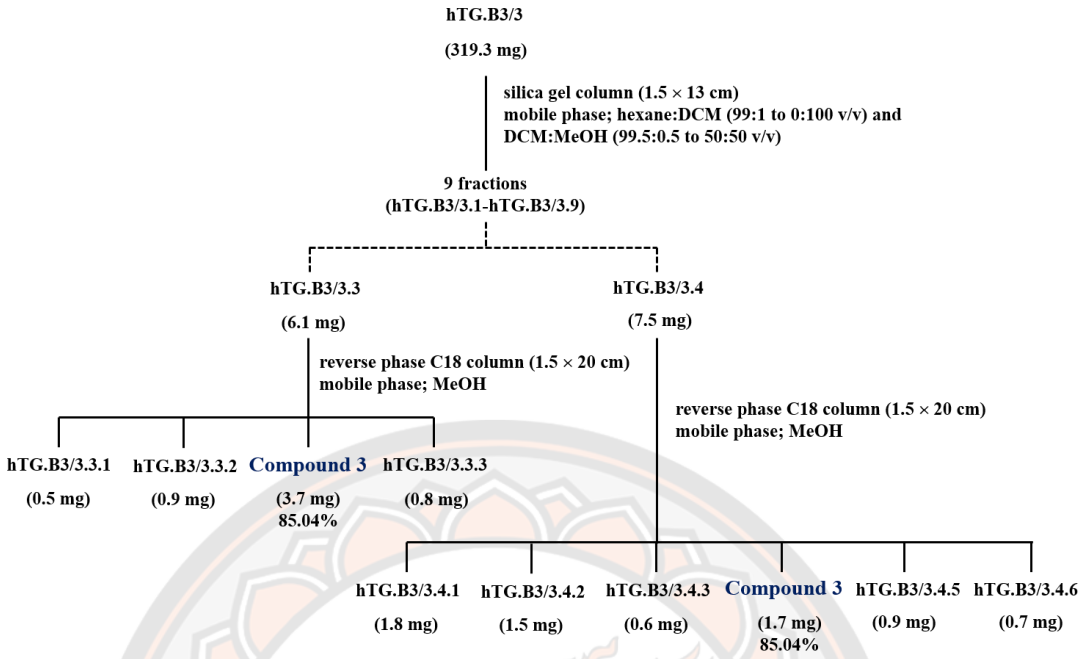

Figure 26 Schematic diagram of the fractionation process for sub-fraction hTG.B3/3 and the percentages represent the inhibition of 5α-reductase activity tested at the final assay concentration of 100 µg/mL

3.4.1 Specific rotation

The optical rotation of chiral compounds **1** and **2** was determined by measuring the specific rotation of compounds. In our experiment, samples were dissolved in MeOH with a concentration of 1.25 g/mL, loaded into a 0.5 dm sample cell, and observed at 25 °C. The calculation of the specific rotation was performed by the following equation:

$$[\alpha]_D^T = \frac{\alpha}{cl}$$

Where: [α] represents the specific rotation, α is the observed rotation in degrees, *c* is the concentration in g/mL, *l* is the path length in dm, and T is the temperature in °C at which the experiment was conducted.

3.4.2 GC-MS conditions for identification of compound **3**

In this study, GC-MS analysis was performed for the identification of compound **3**. The sample was dissolved in DCM and subsequently injected into the GC-MS system. The GC-MS instrument utilized was an apparatus from Hewlett Packard, equipped with a mass selective detector and an Agilent HP-5MS fused-silica capillary column (30 m x 0.25 mm i.d., 0.25 μm film thickness). Helium gas served as the carrier gas, with a constant flow of 1.0 mL/min. Operating conditions were as follows: the injector was set at 250 °C and operated in split mode (1 μL) with a split ratio of 10:1 v/v. The oven temperature was initially maintained at 70 °C for 3 min, then programmed to increase at a rate of 5 °C/min until reaching 280 °C, where it was held for 15 min. The temperature of the transfer line heater was specifically set at 280 °C. Mass scanning covered a range from 50 to 700 amu in full scan mode. The identification of compound **3** relied on computer-assisted matching of its recorded mass spectra fragmentation patterns, with a requirement of achieving a match of at least 90% against a Wiley7n spectral library.

3.5 Measurement of 5α-reductase inhibitory activity

3.5.1 Cell culture and enzyme preparation

According to the literature, androgen-dependent LNCaP cells were reported as the source of 5α-reductase, which predominantly provided type 1 [99]. Thus, in this study, 5α-reductase was obtained in the form of a crude enzyme from LNCaP cells (ATCC® CRL-1740TM) using the extraction protocol outlined by Fachrunniza et al. with minor modification [24]. This protocol was adapted from the method originally developed by Srivilai et al. [194]. In the assay, the cells were grown in phenol red RPMI-1640 powder, which was supplemented with 10% fetal bovine serum and 1 % antibiotics. They were maintained in culture flasks (175 cm^2) at 37 °C in a humidified atmosphere with 5% CO_2. The medium was changed every 3-4 days, and cell detachment was achieved using 0.25% trypsin in a phosphate buffer (PBS) solution without Mg^{2+} and Ca^{2+}, which also included 0.2 g/L EDTA. The enzyme preparation was performed when the cell line reached 80% confluence. The growth medium was removed, and the cells were washed with a tris-HCl buffer solution at pH 7.4. This

buffer contained 10 mM tris-HCl buffer, 50 mM KCl, 1 mM EDTA, and 0.5 mM phenylmethanesulfonyl fluoride). The cells were then detached from the culture surface, followed by centrifugation at 1900 × g for 10 min. Afterward, the cell pellets were gathered and resuspended in tris-HCl buffer at pH 7.4, reaching a concentration of $\geq 9 \times 10^7$ cells/mL. The obtained cell pellets were placed in an ice bath and further homogenized using a sonication probe. The total protein content of crude enzyme used in the 5α-reductase inhibitory assay was found to be a minimum of 75 µg protein equivalent. This determination was made using the Pierce bicinchoninic acid (BCA) protein assay (Pierce, Rockford, IL, USA).

3.5.2 Enzymatic 5α-reductase inhibition assay

The assessment of the *in vitro* inhibitory activity of the test samples against the conversion of testosterone to DHT by steroid 5α-reductase was conducted using the methodology outlined by Srivilai et al. [194]. After the enzymatic reaction, the production of DHT was quantitated using LC-MS to determine 5α-reductase activity. Curcumin and finasteride, which are known 5α-reductase inhibitors [33,195], were used as the positive controls in this experiment. In the enzymatic assay, the reaction was carried out on U-shaped 96-deep-well plates, which were sealed with well-cap mats. The reaction mixture consisted of the test sample, which was dissolved in DMSO (10 µL), along with 34.7 µM of testosterone in PG and water (20 µL), and 1 mM NADPH in tris-HCl buffer pH 7.4 (50 µL). The reaction was initiated by addition of homogenized crude enzyme (80 µL). The final reaction volume was then adjusted to 200 µL by adding tris-HCl buffer with a pH of 7.4 (40 µL). The enzymatic reaction was conducted under controlled conditions in a water bath equipped with a shaker, operating at a temperature of 37 °C for a duration of 60 min. Subsequently, the reaction was terminated by the addition of 10 mg/mL HM in 80% v/v ethanol (200 µL). The solution was thereafter incubated for a further 60 min at a temperature of 60 °C in order to achieve full derivatization of all the DHT that had been produced. Following incubation, the mixture solution was subjected to centrifugation at 1700 × g for 10 min, and the resulting supernatant was collected for quantifying the production of DHT using LC-MS analysis. Two control groups, namely C_0 and C_{60}, were established and made by

containing all the solutions, along with 10 µL of DMSO, without the addition of any test sample. The reaction in the C_0 control group was halted at 0 min by the addition of HM, prior to the initiation of the enzymatic reaction. Conversely, the reaction in the C_{60} control group continued with the enzymatic reaction and was stopped after a 60 min incubation period, which allowed for a complete enzymatic reaction to occur. Table 10 summarizes the volume of all reagent solutions as well as the incubation times for the three assay groups of the 5α-reductase inhibitory activity assay.

Table 10 Summary of 5α-reductase inhibitory activity assay groups, reagents, and incubation times, shown in chronological order from left to right

Groups	Sample/ DMSO (µL)	T (µL)	Tris buffer (µL)	NADPH (µL)	Enzyme (µL)	HM (µL)	Incubation at 37 °C (min)	HM (µL)	Incubation at 60 °C (min)
Control C0	10	20	40	50	80	200	60	-	60
Control C60	10	20	40	50	80	-	60	200	60
Sample	10	20	40	50	80	-	60	200	60

Note: T = testosterone and HM = hydroxylamine hydrochloride

The production of DHT was assessed using LC-MS. To determine the inhibition caused by the test sample, it was quantified by measuring the area under the curve (AUC) of the extracted ion chromatogram (EIC) of derivatized-DHT (*m/z* $[M + H]^+$, 306.2428). The inhibition of the enzymatic reaction was calculated using the following equation:

$$5\alpha - \text{reductase inhibitory activity } (\%) = \left[1 - \frac{\text{AUC of sample} - \text{AUC of } C_0}{\text{AUC of } C_{60} - \text{AUC of } C_0}\right] \times 100$$

3.5.3 LC-MS method for the measurement of DHT [194]

For LC-MS analysis, an HPLC system connected to a Q-TOF LC/MS was used, equipped with dual electrospray ionization (ESI) in positive mode, and *m/z* values were scanned within the range of 100-1200 amu. The stationary phase employed in this study was a Phenomenex Luna® C18(2) reversed-phase column (150 mm x 4.6 mm, 5 µm). Nitrogen was employed as the nebulizing gas at 30 psi, and the drying gas flowed

at 10 L/min and was maintained at 350 °C. The elution of the compounds was achieved using a mobile phase system with a gradient composition. This system consisted of purified water containing 0.1% (v/v) formic acid (solvent A), and acetonitrile containing 0.1% (v/v) formic acid (solvent B). The mobile phase system was first set at a concentration of 60% of solvent B. Subsequently, the concentration of solvent B was raised linearly to 80% over a period of 8 min. This concentration was maintained for a duration of 4 min, following which a post-run period of 2 min was set. The total analysis run-time was 14 min, with the column temperature maintained at 35 °C. The flow rate was set at 0.5 mL/min, and a 20 µL injection volume was used. The mass data were subsequently analyzed using Agilent MassHunter Qualitative Analysis software version B06.00.

3.6 Qualitative and quantitative analyses of *T. grandis* leaf extracts

3.6.1 TLC analysis

The TLC technique was employed to conduct chromatographic fingerprints and preliminary phytochemical screening of teak leaf extracts. It is a technique used to separate a wide range of phytochemical components. The hexane and ethanolic extracts were prepared at a concentration of 10 mg/mL by dissolving individuals with DCM and MeOH, respectively, and then 2.0 µL of each extract was subjected to a TLC silica plate (TLC silica gel 60 F_{254} aluminium sheet). This plate was developed in a pre-saturated TLC chamber with hexane:EtOAc (7:3 v/v). The plate was examined under visible light, UV at 254 and 366 nm after development. Subsequently, the plate was immersed in various specific reagents for the identification of compounds, which included anisaldehyde-sulfuric acid for detecting essential oils, steroids, saponins, and sugars. Additionally, a solution consisting of 5% potassium hydroxide in methanol was employed to detect anthraquinone glycosides and their aglycones. Lastly, bromocresol green was utilized to detect carboxylic acids [152]. The photos of the developed TLC plate with or without coloration were taken.

3.6.2 High-performance liquid chromatography (HPLC) analysis

3.6.2.1 Reference solutions

The two isolated 5α-reductase inhibitors (**1** and **2**) with a purity of 99% were precisely measured and solubilized in methanol and subsequently diluted using the same solvent to get the required concentration. Prior to being introduced into the HPLC system, all reference solutions were subjected to filtration through a 0.45 µm nylon membrane.

3.6.2.2 Chromatographic conditions

The HPLC system employed in this study was an Agilent 1260 infinity instrument, which was equipped with a G1315D diode array detector. The chromatographic separation was conducted using a Phenomenex Luna C18(2) column with dimensions of 150 mm × 4.6 mm and a particle size of 5 µm. The mobile phase was prepared by combining acetonitrile and 0.1% formic acid in purified water at a volumetric ratio of 85:15 (v/v). The isocratic elution system was set to operate at a flow rate of 0.8 mL/min under ambient temperature conditions, and the UV chromatogram was captured at a wavelength of 220 nm. Each injection had a volume of 20 µL.

3.6.2.3 Validation of HPLC Method

The HPLC method for quantitative analysis of active compounds in *T. grandis* leaf extract was validated for various parameters, including linearity, limit of detection (LOD), limit of quantification (LOQ), accuracy, intra-day, and inter-day precision. This validation process followed the guidelines outlined by International Conference on Harmonization (ICH) [196] and United States Pharmacopeia (USP 31) for system suitability.

System suitability

To assess system suitability, five replicate injections of compounds **1** and **2** were introduced into the HPLC system. The following parameters were determined: retention time, peak area, plate count, tailing factors, resolution, and relative standard deviation (%RSD).

Linearity

The linearity ranges of **1** and **2** were evaluated by conducting triplicate analyses at eight different concentration levels, ranging from 1.56 to 200 µg/mL. To establish a calibration curve, the average peak areas were plotted against their corresponding concentrations, and parameters such as slope, y-intercept, and the squared regression coefficient (r^2) were calculated.

Limits of detection (LOD) and quantification (LOQ)

The LOD and LOQ were determined under the current chromatographic conditions using the spiking sample blank technique. This involved adding the lowest known concentration of standard reference solutions and performing 10 replicate analyses. The LOD and LOQ were established by calculating the standard deviation (SD) of the response, which is often denoted as the concentration of the analyte in the sample. This calculation was based on the signal–to–noise ratio (S/N) of 3 for LOD and 10 for LOQ.

Accuracy

The method's accuracy was assessed by the utilization of the spike sample technique. Solution containing mixtures of **1** and **2** at three distinct concentration levels (15, 75, and 135 µg/mL) were introduced into the crude ethanolic extract solution, including the designated range at 25, 50, and 75% of their respective calibration curves. This procedure was repeated three times. The accuracy was determined by employing the subsequent equation and presenting the results as a percentage of the recovery. The concentration, denoted as C, is expressed in units of µg/mL. The appropriate percentage of recovery value should be 80.0-120.0 %

$$\text{Recovery (\%)} = \frac{\text{C (spiked)} - \text{C (non - spiked)}}{\text{C (Standard)}} \times 100$$

Precision

The precision of the methodology was assessed by both repeatability (intra-day precision) and intermediate precision (inter-day precision) investigations. The

experiments were conducted by examining three different concentration levels, namely 20, 75, and 150 µg/mL. The intra-day precision was assessed by performing three replicates tests of each concentration within a single day, resulting in a sample size of three (n = 3). The inter-day precision was assessed by performing triplicate analyses over a period of three consecutive days. The precision was determined by calculating the relative standard deviation (RSD) as a percentage, using the given equation:

$$\text{RSD (\%)} = \frac{\text{Standard deviation}}{\text{Mean}} \times 100$$

*3.6.2.4 HPLC quantification of 5α-reductase inhibitors (**1** and **2**) in T. grandis leaf extracts*

The hexane and ethanolic extracts were weighed individually and dissolved in methanol to achieve a final concentration of 100 µg/mL. Each extract solution was subsequently filtered through a nylon membrane (0.45 µm) prior being loaded into the HPLC system in triplicate. The quantification of **1** and **2** in *T. grandis* leaf extracts were determined by utilizing the respective calibration curves and the results were expressed as % w/w.

3.7 Study on physicochemical properties of *T. grandis* extracts

Various physicochemical parameters of crude ethanolic extract and ethanolic extract in PG, including solubility, pH, color, zeta potential, viscosity, and partition coefficient measurements were studied according to the method described in OECD guidelines.

3.7.1 Solubility

To determine the optimal vehicle solvent for the *in vitro* skin penetration study, the solubility of **1** and **2** in the ethanolic extract was evaluated using two different solvents: distilled water and HEPES buffer pH 7.4 (containing 25 mM HEPES and 2% w/v of Tween20®). The shaking flask method was used as described in OECD guideline No. 105 [197]. Briefly, excess quantities of extract were added to 1 mL of each solvent and then shaken at 220 rpm (37 ± 2°C) using an orbital shaker. This process was done

in triplicate. After 24, 48, and 72 h, the tubes were collected and centrifuged at 600 g. The clear solutions of distilled water and HEPES buffer (diluted 100 times by methanol) solvents were then filtered through a 0.45 μm membrane and analyzed using the HPLC method.

3.7.2 pH determination

The pH values of crude ethanolic extract and ethanolic extract in PG were determined. Each extract was weighed at 100 mg and further saturated with 40 mL of distilled water to produce a dispersion-like sample. These saturated aqueous solutions were transferred to a beaker and the pH value was determined using a pH meter.

3.7.3 Color measurements

The measurement of visual color was conducted with a colorimeter. The measurements were carried out using the standard CIE illuminant D65. The color parameters were assessed using L*, a*, and b* values, where L* represents lightness (ranging from 0 for black to 100 for white), a* indicates greenness (-a*), and redness is denoted as (+a*), while blueness is reflected by (-b*) and yellowness by (+b*). For the sample preparation, the crude ethanolic extract and ethanolic extract in PG were distributed into the sample chamber with a controlled area (width 2 cm × length 2 cm × depth 1 mm) as shown in Figure 27. Five measurements were taken on each sample in three replicates (n=3).

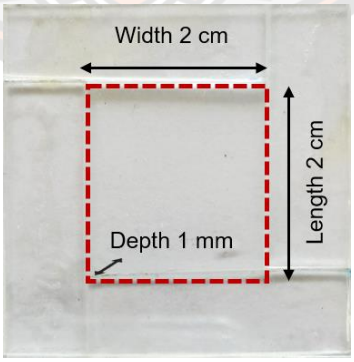

Figure 27 Sample chamber for color measurement

3.7.4 Zeta potential measurement

Zeta potential was employed to quantitatively determine the stability of suspensions. The crude ethanolic extract was dissolved in water (0.5 mg/mL), then the saturated aqueous solution was transferred into the DTS 1070 cuvette by syringe. After that, the sample was measured for the zeta potential value using a zeta potential analyzer in three replicates (n=3).

3.7.5 Viscosity measurement

The viscosity measurement of the ethanolic extract in PG was performed with a viscometer using a CP42 spindle at a constant temperature of 25 °C. This extract was rotated at 65 rotations per minute. The experiment was determined in triplicate (n=3).

3.7.6 Determination of partition coefficient of compounds **1** and **2**

The partition coefficients *n*-octanol/water ($P_{o/w}$) of **1** and **2** were determined using the HPLC method in accordance with the OECD test guideline no. 117 [198]. This approach applies to log $P_{o/w}$ values between 0 and 6. In brief, the reference substances used in this study were benzene (log $P_{o/w}$ = 2.177), toluene (log $P_{o/w}$ = 2.720), benzophenone (log $P_{o/w}$ = 3.200), benzyl benzoate (log $P_{o/w}$ = 3.969), butylated hydroxytoluene (log $P_{o/w}$ = 5.319), and octyl methoxycinnamate (log $P_{o/w}$ = 5.921). The test reference substances and test compounds (**1** and **2**) were dissolved at a concentration of 500 µg/mL in methanol. The HPLC analysis was conducted using a Shimadzu equipped with column C18, as above described. The specific HPLC conditions included an injection volume of 20 µL, a UV detector set at 254 nm, and a column temperature maintained at 25 °C. The compounds were eluted at 1.0 mL/min using an isocratic mode of 60% acetonitrile in water. The capacity factor (*k*) of reference and tested compounds was calculated using the equation follow:

$$k = \frac{t_R - t_0}{t_0}$$

In this analysis, t_R represents the retention time of the sample under examination, while t_0 stands for the dead time. The experiment was determined in triplicate (n=3), and a correlation curve was constructed. This curve involved plotting the octanol/water

partition coefficient (log $P_{o/w}$) of reference compounds against their average log *k* values. Subsequently, the log $P_{o/w}$ values of compounds **1** and **2** were calculated.

3.8 Stability studies

The samples were prepared in glass vials and subsequently stored under designed conditions. Three sample vials were randomly taken at various intervals and the remaining contents of two marker compounds (**1** and **2**) were determined using the validated HPLC method. Prior to analysis, all samples were stored at a temperature of −80 °C.

3.8.1 Effect of pH

Acid-base degradation studies were conducted to identify the pH at which compounds **1** and **2** in *T. grandis* extract exhibit the highest stability. Four different pH levels were tested: 2.0, 5.5, 7.4, and 9.0. Phosphate buffer solutions were used to prepare the buffer solution systems. One gram of crude ethanolic extract was combined with 2.5 mL) of PEG-40 before being incorporated into a buffer solution to achieve a final volume of 100 mL. Subsequently, 1 mL of this buffered solution form was transferred into individual light-protected glass vials and kept at a room temperature (25 °C) for 30 days. These samples were randomly collected at 0, 3, 5, 7, 15, and 30-day intervals.

3.8.2 Effect of temperature

The chemical degradation of prepared extract and buffered solution forms of crude ethanolic extract and ethanolic extract in PG was determined after kept at various temperatures. A total of 10 mg of the prepared extracts were placed in glass vials for testing. Additionally, *T. grandis* crude ethanolic extract and ethanolic extract in PG at a concentration of 10 mg/mL were prepared in a combination solution of PEG-40 and buffer solution pH 5.5 (2.5:97.5 v/v) for solution form testing. All samples were protected from light and stored for 6 months at four different temperatures: 50, 60, 70, and 80 °C. The samples were analyzed at various times (0, 30, 60, 90, 120, 150, and 180 days).

3.8.3 Effect of light

The prepared extract and buffered solution forms of crude ethanolic extract and ethanolic extract in PG were stored according to ICH guidelines for photostability testing [199]. The samples were placed in a xenon test chamber for 13.5 h with the following parameters: 420 nm wavelength at 1.10 W/m^2, UV irradiance at 49.7 W/m^2, illuminance at 89.5 Klx, and visible light dose at 1.21 million lux-h. All samples were conducted in triplicate, and the remaining contents of **1** and **2** were analyzed.

3.8.4 Prediction of shelf life by the Q10 method

A Q10 method is a predictive tool utilized for estimating the duration of product stability. It is operates on the assumption that the ratio of time to equal harm at two temperatures, which increased at a constant rate for every 10 °C increase in temperature [200,201]. The shelf life of **1** and **2** in crude ethanolic extract and ethanolic extract in PG of prepared extract forms at 30 °C (Zone IV mean kinetic temperature) was calculated using the following equation:

$$t_{90}(\mathrm{T2}) = \frac{t_{90}\ (\mathrm{T1})}{\mathrm{Q}^{(\Delta \mathrm{T}/10)}}$$

where t_{90} (T2) is the estimated shelf life at 30 °C and t_{90} (T1) is the time at tested temperature (50 °C) which the active compounds **1** and **2** remained 90% or higher. The Q value is set at 3. The ∆T is the temperature differences between T2 and T1 in degree Celsius (°C).

3.8.5 Quantitative analysis of the remaining contents of compounds **1** and **2** in samples

The remaining contents of **1** and **2** were determined by HPLC using the validated HPLC method described above in high-performance liquid chromatography (HPLC) analysis in section number 3.6.2. In brief, the experiment was conducted using an HPLC-UV equipped with a C18(2) column (150 × 4.6 mm, 5 µm particle size). The mobile phase consisted of an 85:15 (v/v) mixture of acetonitrile and 0.1% (v/v) formic acid in purified water. An isocratic elution system was employed with a flow rate of 0.8

mL/min, UV detection set at 220 nm, and an injection volume of 20 µL. The linearity of compounds **1** and **2** at concentrations ranging from 1.56-200 µg/mL was determined by correlation coefficient (r^2) values of 0.9997 for **1** and 0.9995 for **2**. The retention time for **1** was 14.52 min and 13.15 min for **2**.

3.8.6 Preliminary identification of temperature-induced degradation products

To identify the temperature degradation products of compounds **1** and **2**, the solid mixtures of **1** and **2** (6.3 mg) were kept at 80 °C for 14 days. The mixtures **1** and **2** at day 0 (before the test) and day 14 (after the test) were characterized using TLC and LC-MS. For TLC analysis, the sample was solubilized in methanol to obtain a concentration of 20 mg/mL, and then 2.0 µL of this solution was subjected to a TLC silica plate (TLC silica gel 60 F254 aluminium sheet). The mobile phase was a 7:3 (v/v) mixture of hexane and ethyl acetate. After development process, the plate was examined under UV light at 254 nm. For LC-MS analysis, an Agilent 1260 Infinity Series HPLC system was couple to a Q-TOF LC/MS. This setup featured dual electrospray ionization (ESI) operating in negative mode, with *m/z* scanning conducted over the range of 50-500 amu. Reversed-phase column Phenomenex Luna C18(2) (150 mm x 4.6 mm, 5 µm) was employed as the stationary phase. An isocratic mobile phase system containing acetonitrile and purified water (85:15 v/v), both of which contained 0.1% (v/v) formic acid for ionization enhancement, was used to elute the compounds. The flow rate and injection volume were set at 0.8 mL/min and 20 µL, respectively.

After 14 days of storage at 80 °C, TLC fingerprints and LC-MS profiles revealed polar degradation compounds of mixtures **1** and **2**. The 6.3 mg of sample was subjected to fractionation using a silica gel column. An eluent gradient of hexane and ethyl acetate was employed, resulting in the separation of the sample into four sub-fractions labeled as A, B, C and D. The major polar spot for fraction C was observed at R_f = 0.43, which was then identified using the LC-MS technique under the aforementioned analysis conditions.

3.9 *In vitro* skin penetration study

Following OECD test 428 [202], a Franz diffusion cell was used to evaluate the skin penetration of crude ethanolic extract and ethanolic extract in PG. As a model,

a synthetic membrane (Strat-M™) was employed. The Franz cell apparatus is comprised of a 1.76 cm^2 donor chamber on top, which is separated from the 7 mL receiver compartment below. The system was maintained at a temperature of 37°C using a heated water jacket. The solution in the receiver chamber was continually circulated at 600 rpm using a magnetic stir bar. The receiver chamber solution was prepared by combining 2% *w/v* of Tween20® in an aqueous HEPES (25 mM) buffer at pH 7.4. The synthetic membrane was allowed to reach thermal equilibrium at 37°C for 30 min. Test sample solutions were prepared using two methods: (i) crude ethanolic extract was initially dissolved with PEG-40 hydrogenated castor oil in a 1:3 *w/w* ratio to produce an extract solution, which was then diluted with water in a 1:4 *w/w* ratio to produce the ethanolic extract solution; and (ii) ethanolic extract was prepared using the same procedure as described above, except that in the final step, water was replaced by PG solvent to provide the ethanolic extract in PG. A schematic diagram of preparation and the formula ingredients of these extracts are depicted in Figure 28 and Table 11, respectively. In the donor chamber, 100 µL of each tested sample solution was placed in contact with the shiny side of a Strat-M™ membrane. At 4, 8, 12, 16, 20, and 24 h, the receiver solution (500 µL) was sampled and substituted with an equivalent volume of fresh medium. The amounts of the two active compounds in the samples were analyzed using the HPLC method. After 24 h, the remaining test sample on the membrane surface was lightly brushed with a cotton-tipped swab until it appeared shiny. Each cotton-tipped swab and membrane was extracted by sonication with methanol for 15 min. The quantities of the two active compounds in the samples were then measured using HPLC and the percentages of the compounds remaining in the different compartments, relative to the quantity added to the synthetic membrane, were calculated. The experiment was done in triplicate for each sample.

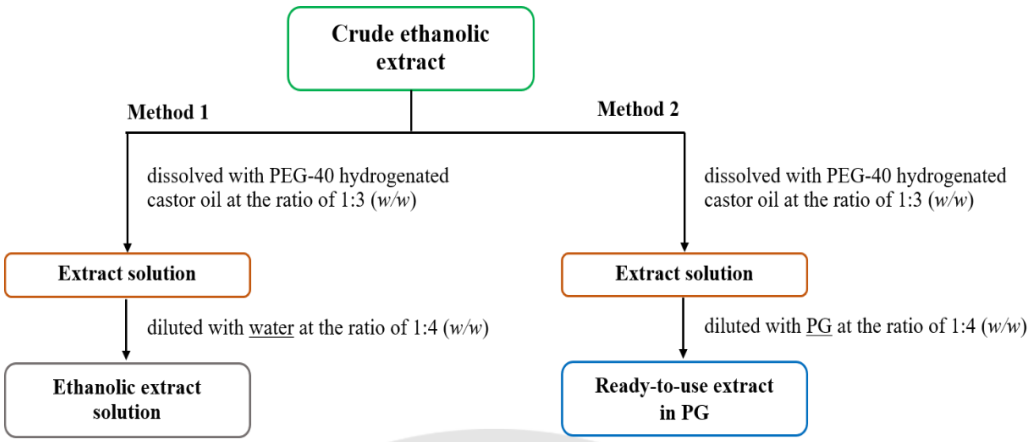

Figure 28 Schematic diagram of the preparation of the tested sample solutions

Table 11 The formula ingredients of ethanolic extract solution and ethanolic extract in PG

Formula ingredients	**Amounts in the formulation (% *w/w*)**
Ethanolic extract solution	
Crude ethanolic extract	5
PEG-40 hydrogenated castor oil	15
Water	80
Ethanolic extract in PG	
Crude ethanolic extract	5
PEG-40 hydrogenated castor oil	15
PG	80

3.10 Statistic analysis

The data were expressed as the mean ± standard deviation (SD) of a minimum of three experiments. To compare statistical differences, a one-way analysis of variance (ANOVA) was employed, followed by Duncan's test. In all cases, a significance level of $p < 0.05$ indicated statistical significance.

CHAPTER IV
RESULT AND DISCUSSION

4.1 Extraction yield of plant material

The leaf powder of *T. grandis* was extracted separately with two organic solvents: hexane and 95% ethanol. This process yielded a dark brown viscous crude hexane extract (127 g, 8.47% yield) and a dark green viscous crude ethanolic extract (32.90 g, 11.27% yield). The physical appearance of these extracts is shown in Figure 29.

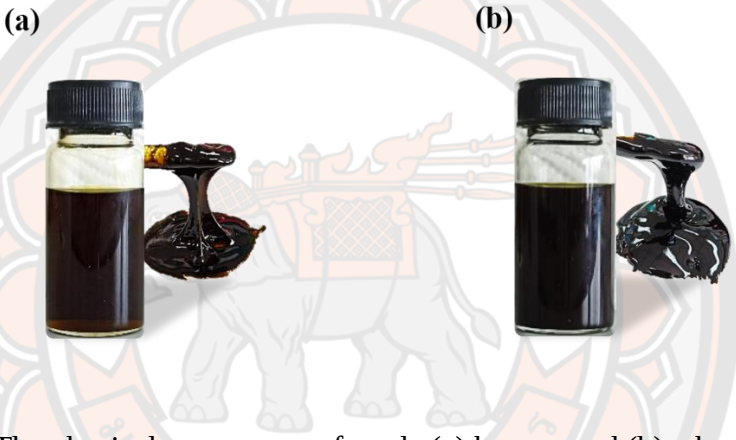

Figure 29 The physical appearance of crude (a) hexane and (b) ethanolic extracts

In addition, the ethanolic extract was dissolved in PEG-40 hydrogenated castor oil and PG solvents to produce an ethanolic extract in PG (as mentioned in 3.3). The formula ingredients of this extract are summarized in Table 12. The ethanolic extract in PG appears to be a dark brown liquid (Figure 30).

Table 12 The formula ingredients of ethanolic extract in PG

Formula ingredients	Amounts in ethanolic extract in PG (% *w/w*)
Crude ethanolic extract	5
PEG-40 hydrogenated castor oil	15
PG	80

Figure 30 The physical appearance of ethanolic extract in PG

4.2 Isolation and identification of 5α-reductase inhibitors from *T. grandis* leaf extract

To isolate the 5α-reductase inhibitors from *T. grandis* leaf-hexane extract, the extract underwent a process where chilled acetone was added to remove gum components. The portion that remained after the removal of gum components (referred as the acetone-soluble portion) was then evaporated and subsequently dissolved in MeOH to produce a crude extract labeled as hTG. In order to separate the bioactive compounds from hTG extract, a fractionation process guided by an *in vitro* 5α-reductase test was initially conducted. The hTG extract was fractionated and purified, yielding three known compounds. The identification of the chemical structures of these three isolated compounds were accomplished through the analysis of spectroscopic data, as well as the comparison of their spectra and physical properties with existing data from previously published data [203-206]. These compounds, shown in Figure 31, were identified as follows: two eperuane-type diterpenes, namely (+)–eperua-8,13-dien-15-oic acid (**1**) and (+)–eperua-7,13-dien-15-oic acid (**2**), along with a lupane-type triterpene known as lupeol (**3**).

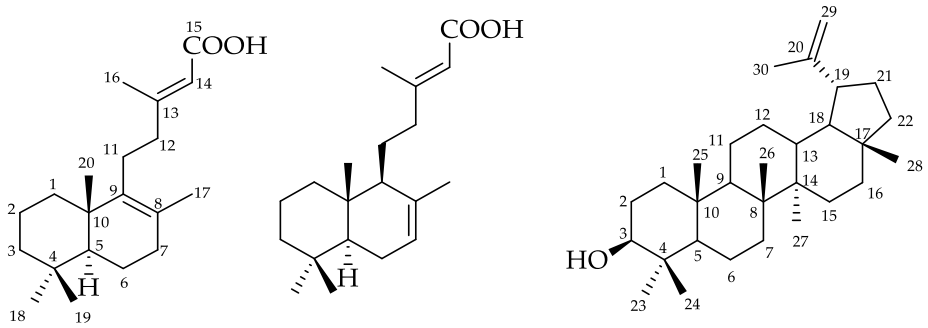

1 **2** **3**

Figure 31 Chemical structures of three compounds isolated from *T. grandis* leaf extract.

Compound **1** was obtained as a white solid with the molecular formula $C_{20}H_{32}O_2$ as determined by HRESI-MS in negative ion mode at *m/z* 303.2374 $[M\text{-}H]^-$ (Calcd for $C_{20}H_{31}O_2$, 303.2403) (Figure 46). The melting point of **1** was 121–122 °C. The UV spectrum of **1** (Figure 47) showed the absorption maxima (λ_{max} (log ε)) at 209 nm (6.71). The FT-IR (ATR) spectrum of **1** (Figure 48) showed the absorption bands at 2919, 2844 cm^{-1} (C–H stretching), 1688 cm^{-1} (C=O stretching of conjugated acid), 1634 cm^{-1} (C=C stretching of conjugated alkene), 1440 cm^{-1} (O–H bending of carboxylic acid), 1241 cm^{-1} (C–O stretching), and 869, 926 cm^{-1} (C=C bending).

The ^1H NMR (in $CDCl_3$) spectrum of **1** (Figure 49) showed the signal of olefinic methine proton at δ_H 5.71 (*br s*, 1H, H-14), aliphatic methine proton at δ_H 1.14 (*m*, 1H, H-5), seven methylene protons at δ_H 1.14, 1.81 (*m*, 2H, H-1), δ_H 1.48 (*m*, 2H, H-2), δ_H 1.14, 1.40 (*m*, 2H, H-3), δ_H 1.64 (*m*, 2H, H-6), δ_H 1.97, 2.03 (*m*, 2H, H-7), δ_H 2.04, 2.20 (*m*, 2H, H-11), δ_H 2.20 (*m*, 2H, H-12), and five methyl protons at δ_H 2.20 (*d*, *J* = 1.1 Hz, 3H, H-16), δ_H 1.57 (*s*, 3H, H-17), δ_H 0.88 (*s*, 3H, H-18), δ_H 0.83 (*s*, 3H, H-19), δ_H 0.94 (*s*, 3H, H-20). The ^1H–^1H COSY spectrum was used to determine the connectivity of each proton. The ^1H–^1H COSY correlation of **1** (Figures 55-56 and Table 13) revealed a vicinal correlation between H-1 and H-2, while H-2 displayed connectivity with H-1 and H-3. Additionally, the vicinal correlation of H-3 and H-2 was observed. Moreover, the vicinal correlation between H-5 and H-6 revealed their

connectivity. Then, H-6 demonstrated connectivity with H-5 and H-7, while H-7 demonstrated connectivity with H-6. The observed vicinal correlation between H-11 with H-12 confirmed their connectivity.

The ^{13}C NMR and DEPT-135 data of **1** (Figures 50 and 51) revealed the presence of 20 carbon atoms, including seven methylene carbon signals at δc 37.2 (C-1), δc 19.2 (C-2), δc 41.9 (C-3), δc 19.2 (C-6), δc 33.8 (C-7), δc 26.5 (C-11), δc 42.0 (C-12), an aliphatic methine carbon at δc 52.1 (C-5), an olefinic methine carbon at δc 114.5 (C-14), five methyl carbons at δc 19.4 (C-16), δc 19.7 (C-17), δc 33.5 (C-18), δc 21.8 (C-19), δc 20.3 (C-20), and five quaternary carbons at δc 33.5 (C-4), δc 126.9 (C-8), δc 139.5 (C-9), δc 39.3 (C-10), δc 163.8 (C-13). The downfield signal at δc 171.5 (C-15) was assigned as carbonyl carbon (carboxylic acid).

The confirmation of ^{1}H and ^{13}C chemical shift assignments was accomplished using HMQC and HMBC correlation spectra. The HMQC spectrum (Figures 52 and 53) showed carbons and protons connected by one bond. The HMBC long-range correlation and full assignments of **1** were shown in Figure 54 and Table 13. The HMBC correlations from two methyl protons at H-18 (δ_H 0.88) and H-19 (δ_H 0.83) to C-4 (δc 33.5), C-3 (δc 41.9) and C-5 (δc 52.1), indicated that two methyl protons (H-18 and H-19) are connected to C-4. The methine proton H-5 (δ_H 1.14) exhibited HMBC correlations with another methyl carbon at C-20 (δc 20.3), and quaternary carbon (C-10: δc 39.3). In addition, the methyl protons H-20 (δ_H 0.94) were also coupling with the methine carbon (C-5: δc 52.1), suggesting ring closure. Additional HMBC correlations of H-1 (δ_H 1.14, 1.81)/C-9 (δc 139.5) and H-6 (δ_H 1.64)/C-4 (δc 33.5) established the connection between two cyclic rings. A vinyl methyl signal of H-17 was observed at δ 1.57. The chemical shift of the methylene proton (H-7) was nearly identical (δ1.97 and 2.03). This information indicated that H-7 was adjacent to the double bond and that the carbon next to this methylene was also quaternary. HMBC correlations were additionally supported by the cross-peak couplings of H-17 to C-7 (δc 33.8, $^{3}J_{CH}$), C-8 (δc 126.9, $^{2}J_{CH}$), and C-9 (δc 139.5, $^{3}J_{CH}$).

The present of adjacent carbons C-11, C-12, and C-13 was inferred from the coupling of H-11 (δ_H 2.04, 2.20) and H-12 (δ_H 2.20) to C-13 (δc 163.8), as evidenced by $^{3}J_{CH}$ and $^{2}J_{CH}$ HMBC correlations. Furthermore, a trisubstituted double bond was

identified between C-13 (δc 163.8) and C-14 (δc 115.1) based on HMBC correlations of $^{2}J_{CH}$ and $^{3}J_{CH}$ from the methyl proton H-16 (δ_H 2.20) to C-12 (δc 42.0), C-13 and C-14, as well as from the olefinic proton H-14 (δ_H 5.71) to C-12 (δ_C 42.0). The coupling of H-14 (δ_H 5.71) and H-16 (δ_H 2.20) with C-15 (δc 171.5) confirmed the presence of a carboxylic group on the side chain of **1**.

The relative configuration of **1** was assigned by the analysis of the ^{1}H–^{1}H NOESY spectrum (Figures 57 and 58). Notably, NOESY correlations were observed between H-20 (δ_H 0.94) and H-11 (δ_H 2.04, 2.20). In addition, the methyl proton signal at δ_H 0.88 (H-18) displayed cross-peaks with aliphatic methine proton at δ_H 1.14 (H-5), while the cross-peak between H-20 and H-5 was absent, suggesting that H-20 and H-5 have different orientations. The experiment of optical rotation of **1** provided $[\alpha]_D^{25}$ +80 (*c* 1.25, MeOH). Comparing with the reported spectroscopic data [203] (see Table 14 for details), this compound was identified as (+)-eperua-8,13-dien-15-oic acid.

Compound **2** was obtained as a colorless solid with the molecular formula $C_{20}H_{32}O_2$ as determined by HRESI-MS in negative ion mode at *m/z* 303.2352 $[M\text{-}H]^-$ (Calcd for $C_{20}H_{31}O_2$, 303.2403), as shown in Figure 59. The melting point of **2** was 101−102 °C. The UV spectrum of **2** (Figure 60) showed the absorption maxima (λ_{max} (log ε)) at 216 nm (6.72). The FT-IR (ATR) spectrum of **2** (Figure 61) revealed absorption bands at 2959, 2922, 2841 cm^{-1} (C–H stretching), 1693 cm^{-1} (C=O stretching of carboxylic acid), 1634 cm^{-1} (C=C stretching of alkene), 1455 cm^{-1} (O–H bending of carboxylic acid), and 1241 cm^{-1} (C–O stretching).

The ^{1}H NMR (in $CDCl_3$) spectrum of **2** (Figure 62) exhibited signals that were quite similar to those of **1**. The spectrum revealed five methyl protons attached to quaternary carbons; δ_H 2.18 (*d*, *J* = 1.1 Hz, 3H, H-16), δ_H 1.69 (*br s*, 3H, H-17), δ_H 0.87 (*s*, 3H, H-18), δ_H 0.85 (*s*, 3H, H-19), and δ_H 0.75 (*s*, 3H, H-20). In addition, two olefinic methine protons at δ_H 5.41 (*br s*, 1H, H-7), δ_H 5.70 (*br s*, 1H, H-14), two aliphatic methine protons at δ_H 1.17 (*m*, 1H, H-5), δ_H 1.62 (*m*, 1H, H-9), and six methylene protons at δ_H 0.94, 1.83 (*m*, 2H, H-1), δ_H 1.42 (*m*, 2H, H-2), δ_H 1.17, 1.42 (*m*, 2H, H-3), δ_H 1.95 (*m*, 2H, H-6), δ_H 1.42, (*m*, 2H, H-11), δ_H 2.12, 2.37 (*m*, 2H, H-12) were observed. In comparison to ^{1}H NMR of **1**, there were significant differences in the ring

at H-7 (δ_H 5.41) and H-9 (δ_H 1.62), indicating that the methylene proton (H-7) in **1** was replaced by a vinyl proton in **2** and that H-9 contained an additional proton.

The ^{13}C NMR (in $CDCl_3$) and DEPT-135 data of **2** (Figures 63 and 64) indicated the presence of 20 carbon atoms, consisting of six methylene carbons, two aliphatic methine carbons, two olefinic methine carbons, five methyl carbons, four quaternary carbons and a carbonyl carbon (carboxylic acid). Comparing the shifts of C-1, C-20, and C-11 in **2** with those in **1**, it was observed that C-1 experienced a deshielding effect ($\Delta\delta$ = 2.1 ppm), C-20 showed shielding ($\Delta\delta$ = -6.6 ppm), and C-11 was only slightly affected ($\Delta\delta$ = -1.1 ppm) due to the change in the position of the olefinic linkage from Δ^8 to Δ^7. To further confirm the assignment of ^1H and ^{13}C chemical shifts, HMQC (Figures 65 and 66) and HMBC correlation spectra (Figures 67-69 and Table 13) were employed. The HMBC experiment revealed two and three-bond correlations from the olefinic proton at H-7 (δ_H 5.41) to C-5 and C-9 (with δc 50.2 and δc 54.6, respectively). This observation confirmed that the double bond is located at C-7. Based on HMBC correlations with C-8 (δc 134.8, $^2J_{CH}$), C-7 (δc 123.0, $^3J_{CH}$), and C-9 (δc 54.6, $^3J_{CH}$), the methyl proton at H-17 (δ_H 1.69) was assigned to attach directly to the quaternary carbon, C-8 (δc 134.8, $^2J_{CH}$). Additional HMBC correlations of H-1 (δ_H 0.94, 1.83)/C-9 (δc 54.6) and H-6 (δ_H 1.95)/C-4 (δc 33.1) established the linkage between two cyclic rings. Other key HMBC correlations were observed between two methylene protons (H-11: δ_H 1.42 and H-12: δ_H 2.12, 2.37) to C-9 (δc 54.6), indicating that the side chain part was connected to the C-9 position. In addition, the vicinal correlations between H-9, H-11, and H-12 for ^1H–^1H COSY correlation were observed (Figures 70-71 and Table 13), indicating their connectivity. The orientations of methyl protons (H-18 and H-20) and aliphatic methine proton (H-5) in **2** were assigned to be the same as in **1** by the similar NOESY correlations (Figures 72 and 73). The cross-peak correlation was not observed between H-20 and H-9, whereas it was observed between H-9 and H-5, indicating that H-20 and H-9 have distinct orientations. The experiment of optical rotation of **2** yielded $[\alpha]_D^{25}$ +80 (*c* 1.25, MeOH). Therefore, all of these assignment data and comparing them with the reported data [204,205] allowed for the structure of **2** to be determined as (+)-eperua-7,13-dien-15-oic acid (see reported data in Table 14 for details).

Compound **3** was obtained as needle-shaped crystals. The EI-MS analysis (Figure 74) revealed a molecular ion peak at *m/z* 426.39 $[M]^+$, along with other fragment peaks at 393(5), 315(18), 207(85), 189(100), 161(40), 135(82), 119(51), 95(89), 69(62). These mass spectral data are consistent with the molecular formula $C_{30}H_{50}O$. The melting point of **3** was found to be in the range of 212–215 °C. The optical rotation in our experiment yielded $[\alpha]_D^{25}$ +43 (*c* 0.23, $CHCl_3$). In the UV spectrum (Figure 75), an absorption maximum (λ_{max} (log ε)) of **3** was observed at 283 nm (4.81).Additionally, the FT-IR (ATR) spectrum of **3** (Figure 76) displayed characteristic absorption bands at 3347 cm^{-1} (O–H stretching), 3066 cm^{-1} (C–H stretching of alkene), 2941, 2871, 2852 cm^{-1} (C–H stretching), 1637 cm^{-1} (C=C stretching), 1451 cm^{-1} (C–H bending).

The ^1H NMR (in $CDCl_3$, 400 MHz) spectrum of **3** (Figure 77 and Table 15) indicated the presence of six aliphatic methine protons at δ_H 3.81 (*dd*, *J* = 11.2, 5.0 Hz, 1H, H-3), δ_H 0.67 (*m*, 1H, H-5), δ_H 1.33 (*m*, 1H, H-9), δ_H 1.65 (*m*, 1H, H-13), δ_H 1.38 (*m*, 1H, H-18), δ_H 2.38 (*dt*, *J* = 11.0, 5.8 Hz 1H, H-19), eleven methylene protons at δ_H 0.89, 1.65 (*m*, 2H, H-1), δ_H 1.62 (*m*, 2H, H-2), δ_H 1.36, 1.53 (*m*, 2H, H-6), δ_H 1.39 (*m*, 2H, H-7), δ_H 1.31, 1.40 (*m*, 2H, H-11), δ_H 1.08, 1.62 (*m*, 2H, H-12), δ_H 1.05, 1.60 (*m*, 2H, H-15), δ_H 1.50 (*m*, 2H, H-16), δ_H 1.29 (*m*, 2H, H-21), δ_H 1.17 (*m*, 2H, H-22), δ_H 4.56, 4.69 (*br d*, 2H, H-29), and seven methyl protons at δ_H 0.96 (*s*, 3H, H-23), δ_H 0.76 (*s*, 3H, H-24), δ_H 0.83 (*s*, 3H, H-25), δ_H 1.03 (*s*, 3H, H-26), δ_H 0.94 (*s*, 3H, H-27), δ_H 0.79 (*s*, 3H, H-28), δ_H 1.68 (*s*, 3H, H-30).

The ^{13}C NMR (in $CDCl_3$) data indicated the presence of 30 carbon atoms (Figure 78 and Table 15), including six aliphatic methine carbons at δc 79.2 (C-3), 55.4 (C-5), 50.6 (C-9), 38.2 (C-13), 48.5 (C-18), 48.1 (C-19), eleven methylene carbons at δc 38.9 (C-1), 27.6 (C-2), 18.5 (C-6), 34.4 (C-7), 21.1 (C-11), 25.3 (C-12), 27.6 (C-15), 35.7 (C-16), 30.0 (C-21), 40.2 (C-22), 109.5 (C-29), seven methyl protons at δc 28.1 (C-23), 15.5 (C-24), 16.1 (C-25), 16.3 (C-26), 14.7 (C-27), 18.1 (C-28), 19.5 (C-30), and six quaternary carbons at δc 39.0 (C-4), 41.0 (C-8), 37.3 (C-10), 43.0 (C-14), 43.2 (C-17), 151.1 (C-20). These assignments were compared to previously reported data [206] (see Table 15 for details). Compound **3** (with a purity of 97%) was identified by comparing its recorded mass spectrum to those present in the Wiley7n standard library. Using all obtained spectral data and comparing them to the literature, the ^1H NMR, ^{13}C

NMR, and MS are in agreement with lupeol, which was previously isolated from *T. grandis* bark [206].

Table 13 NMR data of **1** and **2** (in $CDCl_3$) measured at 400 (^1H) and 100 (^{13}C) MHz

Position	**1**				**2**			
	^{13}C (ppm)[a], mult.[b]	^1H (ppm)[a], mult. (*J* in Hz)	^1H–^1H COSY	HMBC	^{13}C (ppm)[a], mult.[b]	^1H (ppm)[a], mult. (*J* in Hz)	^1H–^1H COSY	HMBC
1	37.2, CH_2	1.14, *m* 1.81, *m*	2	2, 5, 9, 10, 20	39.3, CH_2	0.94, *m* 1.83, *m*	2	2, 9, 10, 20
2	19.2, CH_2	1.48, *m*	1, 3	3, 10, 18	18.9, CH_2	1.42, *m*	1, 3	4, 10
3	41.9, CH_2	1.14, *m* 1.40, *m*	2	2, 4, 5, 18, 19	42.4, CH_2	1.17, *m* 1.42, *m*	2	1, 4, 5, 18, 19
4	33.5, C	–	–	–	33.1, C	–	–	–
5	52.1, CH	1.14, *m*	6	4, 6, 7, 9, 10, 18, 19, 20	50.2, CH	1.17, *m*	6	4, 7, 8, 9, 10, 18, 19, 20
6	19.2, CH_2	1.64, *m*	5, 7	4, 5, 7, 8, 10	23.9, CH_2	1.95, *m*	5, 7	10
7	33.8, CH_2	1.97, *m* 2.03, *m*	6	5, 6, 8, 9, 17	123.0, CH	5.41, *br s*	6	5, 9, 17
8	126.9, C	–	–	–	134.8, C	–	–	–
9	139.5, C	–	–	–	54.6, CH	1.62, *m*	11	8, 10, 12
10	39.3, C	–	–	–	37.0, C	–	–	–
11	26.5, CH_2	2.04, *m* 2.20, *m*	12	8, 9, 12, 13	25.4, CH_2	1.42, *m*	9, 12	8, 9, 12, 13
12	42.0, CH_2	2.20, *m*	11	11, 13, 14	43.8, CH_2	2.12, *m* 2.37, *m*	11	9, 11, 13, 14, 16
13	163.8, C	–	–	–	163.6, C	–	–	–

Position	**1**				**2**			
	^{13}C (ppm)[a], mult.[b]	^{1}H (ppm)[a], mult. (*J* in Hz)	^{1}H–^{1}H COSY	HMBC	^{13}C (ppm)[a], mult.[b]	^{1}H (ppm)[a], mult. (*J* in Hz)	^{1}H–^{1}H COSY	HMBC
14	114.5, CH	5.71, *br s*	–	12, 15, 16	115.1, CH	5.70, *br s*	–	12, 15, 16
15	171.5, C	–	–	–	171.4, C	–	–	–
16	19.4, CH_3	2.20, *d* (1.1)	–	12, 13, 14	19.4, CH_3	2.18, *d* (1.1)	–	12, 13, 14, 15
17	19.7, CH_3	1.57, *s*	–	7, 8, 9	22.3, CH_3	1.69, *br s*	–	7, 8, 9
18	33.5, CH_3	0.88, *s*	–	3, 4, 5, 19	33.3, CH_3	0.87, *s*	–	3, 4, 5, 19
19	21.8, CH_3	0.83, *s*	–	3, 4, 5, 18	22.0, CH_3	0.85, *s*	–	3, 4, 5, 18
20	20.3, CH_3	0.94, *s*	–	1, 5, 9, 10	13.7, CH_3	0.75, *s*	–	1, 5, 9, 10

[a] Assignments were based on ^{1}H, ^{13}C, and HMQC experiments; [b] Multiplicities were established by DEPT experiment.

Table 14 ^{1}H (500 MHz, $CDCl_3$) and ^{13}C NMR (125 MHz, $CDCl_3$) data of **1** [203] and **2** [204,205] reported in the literature

Position	**1**		**2**	
	^{13}C (ppm), mult.	^{1}H (ppm), mult. (*J* in Hz)	^{13}C (ppm), mult.	^{1}H (ppm), mult. (*J* in Hz)
1	37.0, CH_2	1.14, *m*	39.2, CH_2	0.97, *m*
		1.81, *m*		1.85, *m*
2	19.0, CH_2	1.64, *m*	18.8, CH_2	1.47, *m*
				1.56, *m*
3	41.9, CH_2	1.14, *m*	42.2, CH_2	1.18, *m*
		1.40, *m*		1.42, *m*
4	33.3, C	–	33.0, C	–
5	51.8, CH	1.14, *m*	50.1, CH	1.19, *m*
6	19.0, CH_2	1.64, *m*	23.8, CH_2	1.88, *m*
				2.00, *m*
7	33.6, CH_2	1.95, *dd* (17.6, 6.4)	122.8, CH	5.42, *br s*
		2.05, *m*		
8	126.8, C	–	134.6, C	–
9	139.3, C	–	54.4, CH	1.65, *m*
10	39.1, C	–	36.8, C	–
11	26.3, CH_2	2.04, *m*	25.3, CH_2	1.36, *m*
		2.19, *m*		1.63, *m*
12	41.8, CH_2	2.19, *m*	43.6, CH_2	2.13, *m*
				2.40, *m*
13	163.9, C	–	163.6, C	–
14	114.1, CH	5.72, *d* (1.0)	115.0, CH	5.71, *br d* (0.9)
15	170.8, C	–	171.9, C	–
16	19.5, CH_3	2.20, *d* (1.0)	19.3, CH_3	2.20, *br d* (0.9)
17	19.2, CH_3	1.58, *s*	22.2, CH_3	1.71, *br s*
18	33.3, CH_3	0.89, *s*	33.1, CH_3	0.87, *s*
19	21.7, CH_3	0.83, *s*	21.8, CH_3	0.89, *s*
20	20.1, CH_3	0.95, *s*	13.6, CH_3	0.77, *s*

Table 15 NMR data of **3** (in $CDCl_3$) recorded at 400 (^1H) and 100 (^{13}C) MHz and that of **3** (in $CDCl_3$) from reported data at 500 (^1H), and 125 (^{13}C) MHz

Position	**3**		Reported data [206]	
	^{13}C (ppm)	^1H (ppm), mult. (*J* in Hz)	^{13}C (ppm)[a], mult.[b]	^1H (ppm), mult. (*J* in Hz)
1	38.9	0.89, *m*	38.7, CH_2	0.94, *m*
		1.65, *m*		1.64, *m*
2	27.6	1.62, *m*	27.5, CH_2	1.61, *m*
3	79.2	3.18, *dd* (11.2, 5.0)	79.3, CH	3.18, *dd* (11.0, 5.3)
4	39.0	–	39.8, C	–
5	55.4	0.67, *m*	55.5, CH	0.69, *m*
6	18.5	1.36, *m*	19.0, CH_2	1.39, *m*
		1.53, *m*		1.52, *m*
7	34.4	1.39, *m*	34.2, CH_2	1.38, *m*
8	41.0	–	41.1, C	–
9	50.6	1.33, *m*	50.9, CH	1.30, *m*
10	37.3	–	37.2, C	–
11	21.1	1.31, *m*	21.2, CH_2	1.29, *m*
		1.40, *m*		1.43, *m*
12	25.3	1.08, *m*	25.3, CH_2	1.10, *m*
		1.62, *m*		1.70, *m*
13	38.2	1.65, *m*	38.5, CH	1.62, *m*
14	43.0	–	42.8, C	–
15	27.6	1.05, *m*	27.2, CH_2	0.96, *m*
		1.60, *m*		1.61, *m*
16	35.7	1.50, *m*	35.9, CH_2	1.48, *m*
17	43.2	–	43.2, C	–
18	48.5	1.38, *m*	48.5, CH	1.39, *m*
19	48.1	2.38, *dt* (11.0, 5.8)	47.8, CH	2.38, *m*
20	151.1	–	151.2, C	–
21	30.0	1.29, *m*	30.1, CH_2	1.27, *m*
22	40.2	1.17, *m*	40.3, CH_2	1.19, *m*
23	28.1	0.96, *s*	28.4, CH_3	0.97, *s*
24	15.5	0.76, *s*	15.6, CH_3	0.77, *s*
25	16.1	0.83, *s*	16.2, CH_3	0.84, *s*
26	16.3	1.03, *s*	16.1, CH_3	1.04, *s*

Position	**3**		Reported data [206]	
	^{13}C (ppm)	^{1}H (ppm), mult. (*J* in Hz)	^{13}C (ppm)[a], mult.[b]	^{1}H (ppm), mult. (*J* in Hz)
27	14.7	0.94, *s*	14.8, CH_3	0.96, *s*
28	18.1	0.79, *s*	18.1, CH_3	0.80, *s*
29	109.5	4.56, *br d*	109.5, CH_2	4.56, *br d*
		4.69, *br d*		4.68, *br d*
30	19.5	1.68, *s*	19.8, CH_3	1.70, *s*

[a] Assignments of reported data were based on ^{1}H, ^{13}C, and HSQC experiments;

[b] Multiplicities were established by the DEPT-135 experiment.

Various classes of terpenoids such as sesquiterpenes (eudesmane- and oppositane-types), diterpenes (phytane- and eperuane-types), and triterpenes (ursane-, oleanane-, and lupane-types) have been previously reported in *T. grandis* leaves and bark [17,127]. Compounds **1** and **2** have been previously identified both in natural sources and through chemical synthesis. They were initially isolated and characterized as components in the MeOH extract of *Sindora siamensis* Miq. leaves [203]. Compound **1** has also been synthesized from sclareol by superacidic cyclization of alcohols [207-209], whereas **2** can be synthesized through MnO_2 and $AgNO_3$ oxidation of labda-7,13 *E*-diene-15-ol [210]. Furthermore, the enantiomer of **2**, (-)-eperua-7,13-dien-15-oic acid, had been separated from various plants including *Copaifera langsdorffii* [211], *Isodon scoparius* [212], and *Hymenaea coubarril* [205]. Moreover, **3** has been previously found in several plants, such as *T. grandis* [127], *Wrightia tinctoria* R.Br. [213], *Oxystelma esculentum* (L. f.) Sm. [214], and *Taraxacum officinale* (L.) Weber ex F.H.Wigg. [215]. It should be noted that this study represents the first report of the isolation and characterization of two eperuane-type diterpenes (**1** and **2**) as the chemical components in *T. grandis* leaf.

4.3 Steroid 5α-reductase inhibitory activity

The 5α-reductase inhibitory activity was assessed using LNCaP cell as a source of enzyme. In the screening, the percentages of enzymatic inhibition of *T. grandis* leaf extracts and three isolated compounds were determined at the final

concentration of 100 µg/mL. All samples exhibited greater than 80% inhibitory activity against steroid 5α-reductase. Therefore, the concentrations that could inhibit 50% of enzymatic activity (IC_{50}) of all samples were further determined. Two reference 5α-reductase inhibitors, finasteride and curcumin, were determined using assay as previously described by Srivilai et al. (2017) [195]. Their IC_{50} values on 5α-reductase are presented in Table 16 and the IC_{50} graphs for **1** and **2** are illustrated in Figures 81 and 82, respectively.

Table 16 The IC_{50} values of the three isolated compounds (**1-3**) and two 5α-reductase inhibitors against 5α-reductase activity. The data represent the means ± SD of triplicate tests.

Samples	**IC_{50} (µg/mL)**	**IC_{50} (µM)**
Isolated compounds		
(+)-Eperua-8,13-dien-15-oic acid (**1**)	4.31 ± 0.87	14.19 ± 2.87^{b}
(+)-Eperua-7,13-dien-15-oic acid (**2**)	4.45 ± 0.10	14.65 ± 0.31^{b}
Lupeol (**3**)	>170	>400
Positive controls [195]		
Curcumin	4.95 ± 0.15	13.40 ± 0.40^{b}
Finasteride	0.28 ± 0.01	0.73 ± 0.03^{a}

The mean IC_{50} values (µM) from each sample were compared using one-way ANOVA, followed by Duncan's test. Values that do not share the same letter are considered significantly different from each other ($p < 0.05$).

The finding indicated that the ethanolic extract exhibited more potent 5α-reductase inhibition with as IC_{50} value of 23.91 ± 0.17 µg/mL compared to the hexane extract, which had an IC_{50} of 26.45 ± 0.69 µg/mL. The isolated diterpenes **1** and **2** displayed 5α-reductase inhibitory activity with IC_{50} values of 14.19 ± 2.87 µM (equivalent to 4.31 ± 0.87 µg/mL) for **1** and 14.65 ± 0.31 µM (equivalent to 4.45 ± 0.10 µg/mL) for **2**. Both compounds **1** and **2** exhibited significantly greater inhibition compared to triterpene (**3**) but was less potent than a positive drug, finasteride. Notably,

there was no statistically significant difference in the inhibitory activity between the two potent compounds (**1** and **2**) and the natural 5α-reductase inhibitor, curcumin. The interpretation of structure–activity relationships was limited due to the relatively small number of compounds studied. Nevertheless, the significance of α,β unsaturated carboxylic acid in the side chains of **1** and **2** in relation to their 5α-reductase inhibitory activity is worthy of consideration. Conversely, the reason behind the lower inhibitory activity of **3** remains largely unexplored, suggesting that additional factors might be involved, which needs to be further studied. The literature has also highlighted the important role of the carboxyl group in inhibiting 5α-reductase [84,216]. For example, it was shown that ganoderic acid TR displayed higher level of inhibitory activity than 5α-lanosta-7,9(11),24-triene-15α,26-dihydroxy-3-one. These two compounds exhibit structural similarity, with the only difference residing in the position of C-26: ganoderic acid TR contains a carboxyl group, while 5α-lanosta-7,9(11),24-triene-15α,26-dihydroxy-3-one features a hydroxyl group at this position. Hence, these results strongly indicate that the presence of a carboxyl group in the 17β-side chain of ganoderic acid TR is crucial for its inhibitory activity. In contrast, the methyl ester of ganoderic acid TR displayed significantly reduced inhibitory potency against 5α-reductase. Furthermore, the presence of unsaturation at C-24 and C-25 emerged as critical requirement for the three most potent inhibitors, namely ganoderic acid TR, ganoderic acid DM, and 5α-lanosta-7,9(11),24-triene-15α,26-dihydroxy-3-one. Conversely, the fully saturated triterpenoids exhibited lower efficacy. The research conducted by Srivilai et al. [217] provided insights into the essential role of α,β unsaturated ketone groups in sesquiterpenes for inhibiting 5α-reductase.

In addition, the presence of a double bond in the cyclic ring of **1** and **2** may also be the key point for 5α-reductase inhibitory activity, as described in the literature. For instance, Guarna et al. conducted a study in 2001, investigating the effect of C-ring modifications in benzo[c] quinonlizin-3-ones on the inhibitory activity against 5α-reductase (type 1). In their research, they synthesized and evaluated several derivatives of octahydro- and decahydrobenzo[c]quinolizine-3-one, which featured either partially or fully saturated C-rings. These compounds were assessed for their potential to inhibit 5α-reductase type 1. Among the various derivatives, they found that

octahydrobenzo[c]quinolizine-3-one, featuring a double bond at the position 6a-10a, exhibited notable and selective inhibition of 5α-reductase type 1 (IC_{50} = 58 nM). The inhibitory potency of this compound was notably higher, about 345-fold, than that of the corresponding 6a-10a saturated *trans*-fused decahydrobenzo[c]quinolizine-3-one, which had an IC_{50} value of 20,000 nM. The finding strongly indicates that the removal of the double bond in the C-ring caused a significant decrease of 5α-reductase inhibitory potency [218].

In terms of their pharmacological properties, compound **1** and **2** have previously been reported to possess histone deacetylase (HDAC) inhibitory activity [203]. On the other hand, **3** has demonstrated various pharmacological activities, including anti-inflammatory activity [219], antimalarial activity [220], and apoptogenic activity [221,222]. Additionally, it has exhibited potent androgen receptor inhibitory activity [223]. Although **3** has been shown to have the anti-androgenic effect via the androgen receptor inhibition, there is a lack of information regarding the inhibitory activity of **1** and **2** on 5α-reductase. The enzymatic activity of 5α-reductase exhibited by these compounds is being reported for the first time in this study.

Standardization and quality control are imperative to maintain consistent levels of bioactive compounds in *T. grandis* extract, a crucial requirement for product development involving this extract. Therefore, a quantitative investigation was then undertaken on the two markers (**1** and **2**) present in the extracts obtained from hexane extraction, as previously suggested. Additionally, ethanol was utilized as a solvent due to its cost-effectiveness and environmentally friendly alternative.

4.4 Qualitative and quantitative analyses of teak leaf extract

4.4.1 TLC analysis

TLC separation is the most used technique for analyzing phytochemical constituents in extracts. The TLC fingerprint was employed for the propose of sample quality control. In this study, TLC fingerprint profiles of both hexane and ethanolic *T. grandis* leaf extracts were carried out using the hexane:EtOAc (7:3 v/v) as a mobile phase system (Figure 32).

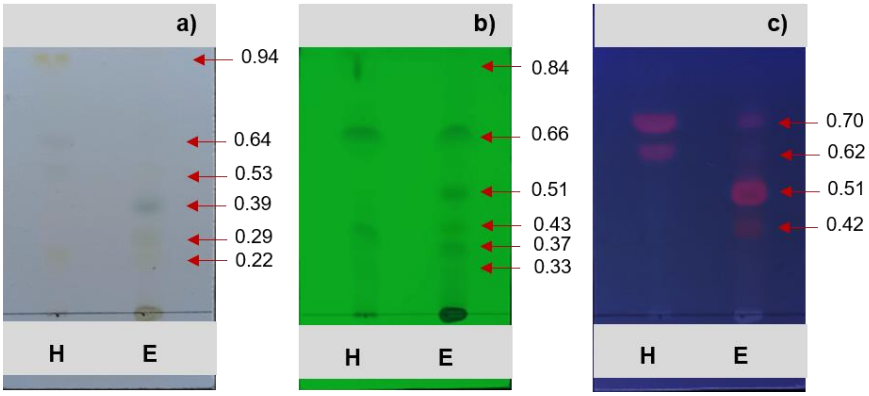

Figure 32 TLC fingerprints of hexane and ethanolic extracts (10 mg/mL) using hexane:EtOAc (7:3 v/v) as mobile phase: visualized without staining under a) daylight, b) 254 nm UV light, and c) 366 nm UV light. R_f values are indicated. (H = hexane extract and E = ethanolic extract)

More spots were observed in hexane extract than that in ethanolic extract when illuminated with daylight (Figure 32a). As depicted in Figures 32b and 32c, distinct quenching and fluorescence spots were observed at the short UV wavelength (254 nm) and long UV wavelength (366 nm), respectively. In comparison to leaf hexane extract, leaf ethanolic extract had the most visible spots under 254 nm. Visualization at 366 nm revealed fewer spots for both extracts.

The preliminary study on phytochemical components of the extracts was conducted following the same procedure as that used for the TLC method. Qualitative phytochemical analysis was employed to determine the presence or absence of various groups of secondary metabolites. Most spots turned purple color after being post-derivatized with anisaldehyde-sulfuric acid spray, indicating that they contained essential oils, steroids, or terpenoids. After straining with anisaldehyde-sulfuric acid, the results also demonstrated that the heavy purple spot was presented on the top of the TLC plate of hexane extract while that of ethanolic extract was not presented (Figure 33a). We suspected that this spot was derived from gum components, which might be a problem for future product developments. Therefore, ethanol is a preferable extraction solvent for removing gum components.

Moreover, a bromocresol green reagent was used to detect the carboxylic acid group of compounds **1** and **2** (R_f = 0.68) in hexane and ethanolic extracts. Bot extracts contained yellow spots on a light blue background, indicating the presence of carboxylic groups (Figure 33b). In addition, quinone compounds were not found in any extracts after being sprayed with a 5% potassium hydroxide reagent, as shown in Figure 33c.

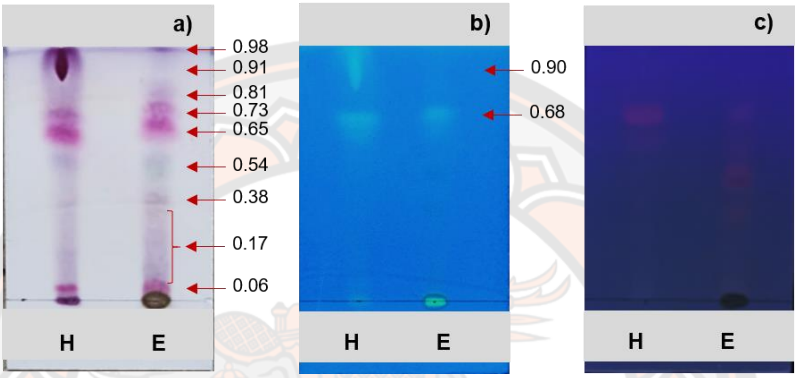

Figure 33 TLC fingerprints of hexane and ethanolic extracts (10 mg/mL) using hexane:EtOAc (7:3 v/v) as mobile phase: visualized after stain with a) anisaldehyde-sulfuric acid, b) bromocresol green, and c) 5% potassium hydroxide. R_f values are indicated. (H = hexane extract and E = ethanolic extract)

However, TLC profiles provide qualitative information regarding the presence and absence of secondary metabolites. To determine the consistent levels of 5α-reductase inhibitors in *T. grandis* leaf extracts, standardization and quality control are required. Thus, we employed the HPLC method for the quantitative determination of bioactive compounds.

4.4.2 Quantitative HPLC analysis of 5α-reductase inhibitors in *T. grandis* leaf extract

An HPLC method was established and validated following ICH guidelines to quantitatively determine the presence of two active compounds, **1** and **2**. For effective separation, a wavelength of 220 nm was chosen for quantitative analysis. Compounds

1 (t_R 14.52 min) and **2** (t_R 13.15 min) in both hexane and ethanolic extracts from *T. grandis* leaf were efficiently separated within 15 min. This separation was achieved using an isocratic elution system consisting of acetonitrile and formic acid in purified water as the mobile phase (Figure 34).

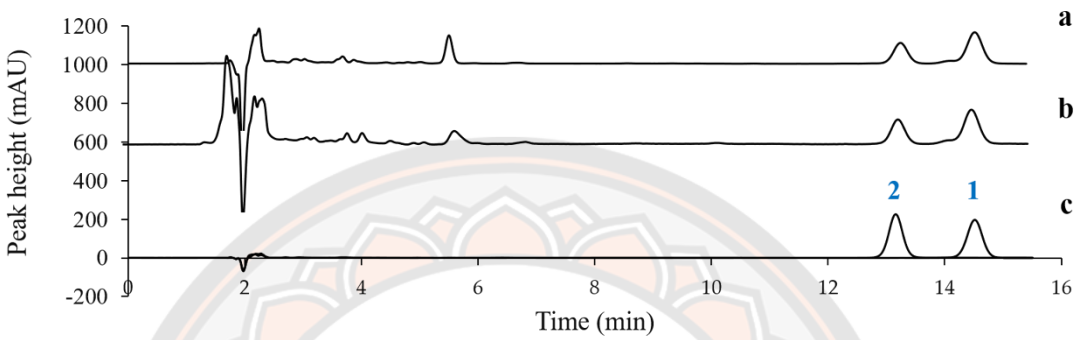

Figure 34 HPLC-DAD chromatograms of (a) 100 µg/mL *T. grandis* leaf-hexane extract, (b) 100 µg/mL *T. grandis* leaf-ethanolic extract, and (c) a mixture of 50 µg/mL isolated compounds **1** and **2**.

4.4.2.1 System suitability

The tailing factors (*T*) of compounds **1** and **2** on the chromatogram (Figure 34) were 0.98 and 0.99, respectively, indicating peak symmetry ($T<2$). The resolution (*R*) values of 2.73 and 23.84, respectively, indicated that the peaks of compounds **1** and **2** can be separated from those of other compounds ($R>1.5$). The number of theoretical plates ($N>700$) determined the efficiency of the column, and the result showed that the *N* of compounds **1** and **2** were 14801 and 13934 respectively (Table 17). These results suggest that the HPLC system and operating conditions are suitable.

Table 17 HPLC method system suitability data for **1** and **2** quantifications

Parameters	Values ± % RSD	
	1	**2**
Retention time (min)	14.52 ± 0.05	13.15 ± 0.06
Peak area (mAU*s)	5118.75169 ± 0.35	5646.97637 ± 0.44
Tailing factor (*T*)	0.98 ± 0.42	0.99 ± 0.85
Resolution (*R*)	2.73 ± 0.34	23.84 ± 0.30
Number of theoretical plate (*N*)	14801 ± 1.12	13934 ± 0.45

4.4.2.2 Linearity

The plot of peak area versus the concentrations (1.56–200 µg/mL) of **1** and **2** demonstrated good linearity for this method, with an r^2 value of 0.9997 for **1** (Figure 83) and 0.9995 for **2** (Figure 84). The method exhibited high sensitivity with LOD value of 0.09 µg/mL for **1** and 0.06 µg/mL for **2**. Additionally, the LOQ values were 0.30 µg/mL for **1** and 0.20 µg/mL for **2**. These results, along with other validation parameters, are summarized in Table 18.

Table 18 Method validation parameters for the determination of **1** and **2** by the proposed HPLC method.

Parameters	Values	
	1	**2**
Linearity range	1.56-200 µg/mL	1.56-200 µg/mL
Regression equation	y = 63.483x + 40.465	y = 75.954x + 20.8
Correlation coefficient (r^2)	0.9997	0.9995
Limits of detection (LOD)	0.09 µg/mL	0.06 µg/mL
Limits of quantification (LOQ)	0.30 µg/mL	0.20 µg/mL

4.4.2.3 Accuracy and precision

The analytical method established for the quantification of **1** and **2** demonstrated satisfactory accuracy, with an overall recovery falling within the range of 92.78–100.6% (Table 19). The RSD values for the intra-day and inter-day were less than 3%, demonstrating the high precision of the method (Table 20). These findings showed that the developed quantitative method was sensitive, accurate, and precise for simultaneously determining two active constituents in the *T. grandis* leaf extracts.

Table 19 Accuracy (% recovery) of **1** and **2** by the proposed HPLC method.

Concentration (µg/mL)	Recovery (%) ± SD	
	1	**2**
15	92.78 ± 0.77	99.34 ± 3.06
75	100.61 ± 0.86	98.20 ± 0.77
135	97.13 ± 2.71	98.94 ± 1.26

Table 20 The intra- and inter-day precisions of **1** and **2** by the proposed HPLC method.

Concentration (µg/mL)	Measured concentration (µg/mL)		RSD (%)			
			Intra-Day [a]		Inter-Day [b]	
	1	2	1	2	1	2
20	21.0 ± 0.10	19.17 ± 0.45	0.46	2.33	1.90	2.10
75	77.1 ± 0.09	76.08 ± 0.38	0.11	0.50	1.02	1.51
150	152.1 ± 0.03	151.39 ± 1.00	0.02	0.60	0.13	1.15

[a] Intra-day at three times in one day. [b] Inter-day on three different days.

The concentrations of the two 5α-reductase inhibitors, **1** and **2**, in both hexane and ethanolic extracts of *T. grandis* leaf were quantified using the previously validated HPLC procedure (see section 4.4.2.1 to 4.4.2.3 for comprehensive details). The presence of these constituents was confirmed by comparison their retention time with those of the standard compounds (Figure 34c). The results clearly demonstrated that the ethanolic extract contains significantly greater levels of **1** (6.18 ± 0.12 % (*w*/*w*)) and **2** (3.83 ± 0.04 % (*w*/*w*)) than the hexane extract, which contained **1** and **2** at contents of 5.60 ± 0.05 % (*w*/*w*) and 3.23 ± 0.03 % (*w*/*w*), respectively (Table 21). This observation aligns with the higher 5α-reductase inhibitory activity of ethanolic extract. In addition, it was observed that the ethanolic extract exhibited a decreased concentration of unwanted gum in comparison to the hexane extract (Figure 33a).

Table 21 The contents of **1** and **2** in *T. grandis* leaf-hexane and ethanolic extracts of and IC_{50} values against 5α-reductase of *T. grandis* leaf extracts. The results are expressed as the means ± SD in three replicates.

Samples	Contents (% *w*/*w*)		IC_{50} against 5α-reductase (µg/mL)
	1	2	
Hexane extract	5.60 ± 0.05	3.23 ± 0.03	26.45 ± 0.69
Ethanolic extract	6.18 ± 0.12*	3.83 ± 0.04*	23.91 ± 0.17*

* $p < 0.05$, significantly different compared with the hexane extract.

Furthermore, ethanol is generally recognized as safe for used in food, drugs, and cosmetics [224-226], making an attractive extraction solvent. Hence, we highly recommend the use of 95% ethanol as the preferred solvent for extracting *T. grandis* leaves. This ethanol-extracted material can then be safely utilized as an ingredient in pharmaceutical and cosmeceutical products designed for the treatment of hair loss.

4.5 Study on physicochemical properties of *T. grandis* leaf extract

4.5.1 Solubility

To determine a suitable vehicle for an *in-vitro* skin penetration study, the solubility of **1** and **2** in the crude ethanolic extract was investigated using the shake flask method at 37 ± 2 °C. Two solvents were prepared for the test: distilled water and HEPES buffer. An excess ethanolic extract was added to 1 mL of each solvent for solubility analysis, then analyzed using the HPLC method. In comparison to the solubility of **1** and **2** in the distilled water containing 0.01 ± 0.42 mg/mL of **1** and 0.01 ± 0.05 mg/mL of **2**, the solubility of these in the HEPES buffer with 2% w/v of Tween20 was found to be much higher for **1** (1.05 ± 0.04 mg/mL) and **2** (1.08 ± 0.02 mg/mL). The solubility values of **1** and **2** are shown in Table 22. Following the United States Pharmacopeia (USP) and British Pharmacopeia (BP), the classification of solubility, regardless of the solvent used, is based only on quantitative considerations [159]. Compounds **1** and **2** were defined as slightly soluble compounds when solubilized in HEPES buffer and practically insoluble compounds in distilled water [227]. These findings indicate that the HEPES buffer may be a suitable vehicle for further skin penetration studies.

Table 22 Solubility analysis of **1** and **2** contents in ethanolic extract against these two solvents

Solvents	Amounts (mg/mL)		Solubility definition
	1	**2**	
Distilled water	0.01 ± 0.42	0.01 ± 0.05	practically insoluble
HEPES buffer with 2% w/v of Tween20	1.05 ± 0.04*	1.08 ± 0.02*	slightly soluble

* $p < 0.05$, significantly different compared with the distilled water

In addition, this solubility test suggests that adding chemical enhancers to the extract, including substances like PG, glycerine, and PEG-40 hydrogenated castor oil, could potentially enhance the penetration of poorly soluble compounds [228,229]. In our investigation, the preferred chemical enhancers were PG and PEG-40 hydrogenated castor oil, which were dissolved in extracts to increase their solubility and absorption through the skin.

4.5.2 pH determination

The pH values of ethanolic extract and ethanolic extract in PG were 4.24 ± 0.01 and 5.04 ± 0.01, respectively. This result demonstrated that the ethanolic extract was more acidic than the ethanolic extract in PG. The results of the pH values of ethanolic and ethanolic extract in PG were summarized in Table 23. However, the pH values of these extracts indicated a preferable pH range for use in topical cosmetic preparations.

Table 23 The pH values of ethanolic extract and ethanolic extract in PG

Samples	pH value
Ethanolic extract	4.24 ± 0.01*
Ethanolic extract in PG	5.04 ± 0.01

* $p < 0.05$, significantly different compared with the ethanolic extract in PG

4.5.3 Color measurements

Color parameters L*, a*, and b* were measured to analyze the color of the ethanolic extract and ethanolic extract in PG (lightness (L* 0/100 black/white), redness (+a*), greenness (-a*), yellowness (+b*), and blueness (-b*)). As shown in Table 24, colorants had L*, a*, and b* values of 8.8 ± 0.9, -0.7 ± 0.1, -1.2 ± 0.2 (for crude ethanolic extract); 20.0 ± 1.7, 11.7 ± 1.0, 18.3 ± 3.4 (for ethanolic extract in PG). These results showed that the ethanolic extract in PG was lighter, redder, and yellower, while the ethanolic extract was greener. This information can be applied to the further development of natural pigments in cosmetics.

Table 24 Color appearance of *T. grandis* leaf extracts

Color values	Samples	
	Ethanolic extract	Ethanolic extract in PG
L* ((0) dark, (100) light)	8.8 ± 0.9	20.0 ± 1.7
a* ((-a) green, (+a) red)	-0.7 ± 0.1	11.7 ± 1.0
b* ((-b) blue, (+b) yellow)	-1.2 ± 0.2	18.3 ± 3.4
Visual observation color	dark green viscous	dark brown liquid

4.5.4 Zeta potential measurement

The prediction regarding the particle stability in suspension can be made by measuring the zeta potential, which is its surface charge. In the present work, the zeta potential of an ethanolic extract solubilized in water (0.5 mg/mL) was determined. Zeta potentials greater than |±30 mV| are required for the storage stability of a charge-stabilized dispersion. Our result demonstrated that the zeta potential of the ethanolic extract was found to be -17.33 ± 0.23 mV (Figure 35). This result demonstrated that the particle stability behavior of ethanolic extract solubilized in water was defined as incipient instability [166]. Our findings indicate that the particles in ethanolic extract suspension were quite easily agglomerated. Thus, the addition of potential additives to the sample might improve the zeta potential, which is useful for formulating dispersions in cosmetic products.

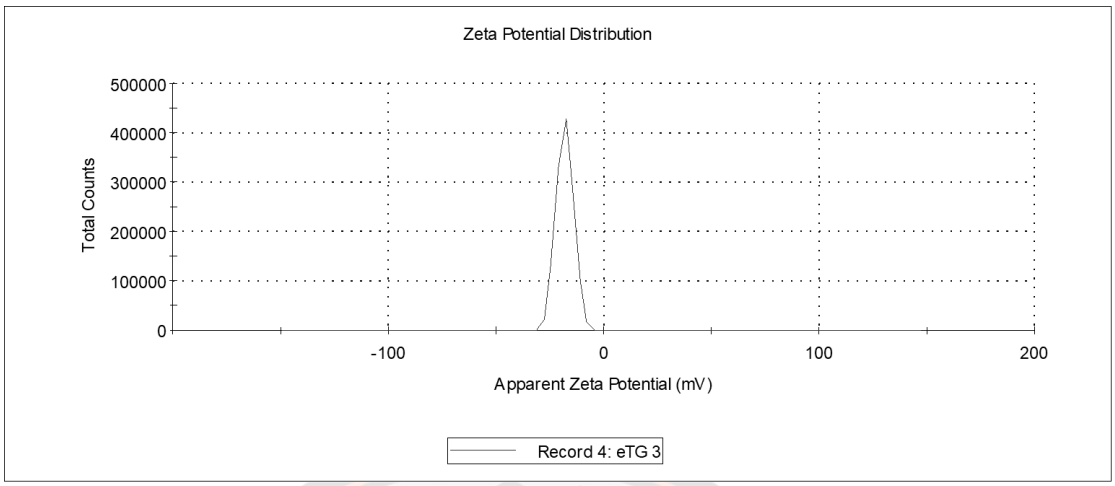

Figure 35 Zeta potential measurement of ethanolic extract using zeta potential analyzer

4.5.5 Viscosity measurement

To determine the viscosity of an ethanolic extract in PG for further formulation of topical products. Our experiment demonstrated that the viscosity of ethanolic extract in PG was 91.01 ± 0.92 cP. This extract is time and shear rate-independent and displayed Newtonian behavior [230].

4.5.6 The partition coefficient of compounds **1** and **2**

The partition coefficient (log $P_{o/w}$) describes the hydrophilicity (water liking) and hydrophobicity (lipid liking) of a compound when it is dissolved in an immiscible biphasic system between *n*-octanol and water. Therefore, the log $P_{o/w}$ value can be used as a predictive measure for the permeability of a compound across the stratum corneum (a lipid domain) and the viable epidermis (an aqueous domain) [231]. In our work, the log $P_{o/w}$ values of **1** and **2** were determined using HPLC, and the *k* values of the reference and test samples were calculated using their retention times. The log $P_{o/w}$ values of **1** and **2** are reported here for the first time. When log $P_{o/w}$ is positive or high, this indicates that the retention time is longer, resulting in a greater *k* value. The correlation coefficient (r^2) of 0.9910 for **1** (Figure 36a) and 0.9911 for **2** (Figure 36b) was calculated by plotting the relationships between log $P_{o/w}$ of reference compounds and their mean log *k*. The *k* values for **1** and **2** were 1.015 ± 0.016 and 0.992 ± 0.005, which corresponds to the log $P_{o/w}$ values of 5.767 ± 0.07 and 5.661 ± 0.02, respectively.

These results demonstrated that **1** and **2** are hydrophobic compounds. However, compound **1** was slightly more hydrophobic than **2**, making it easier to penetrate through its interaction with the lipid layer of the stratum corneum. Our findings agree with previous reports that showed that hydrophobic compounds tended to increase skin penetration more than hydrophilic compounds [169,232,233].

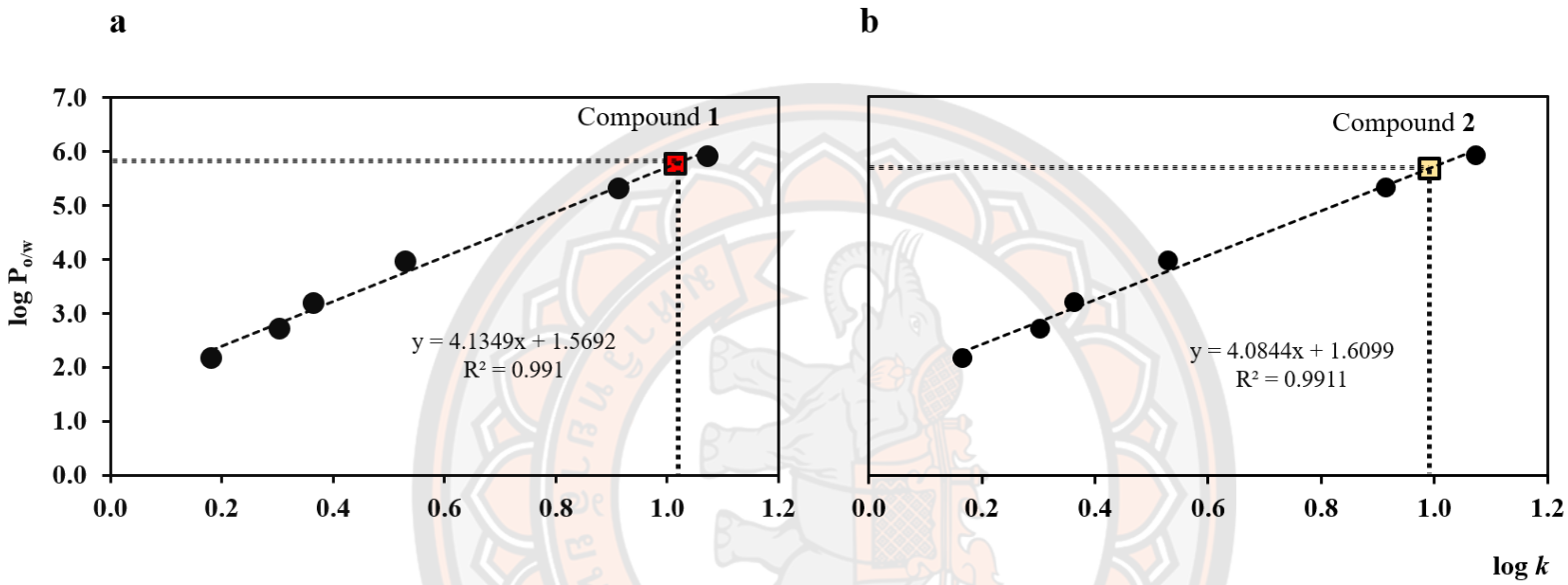

Figure 36 Correlation plotted of log $P_{o/w}$ of reference compounds against their average log *k* (n=5). The log *k* and log $P_{o/w}$ of (a) compound **1** were 1.015 ± 0.016 and 5.767 ± 0.07, respectively and (b) compound **2** were 0.992 ± 0.005 and 5.661 ± 0.02, respectively.

4.6 Stability of compounds 1 and 2 in ethanolic extract and ethanolic extract in PG

4.6.1 Effect of pH

The ethanolic extract was dissolved in buffer solutions at different pH levels (pH 2.0, 5.5, 7.4, and 9.0) and maintained at a constant temperature of 25 ± 2 ℃. Subsequently, the HPLC was employed to assessed the remaining quantities of **1** and **2** after varying incubation periods (Figure 37). Both **1** and **2** showed similar trends of degradation profiles. Compounds **1** and **2** were stable in acidic solutions (pH 2.0-5.5) for up to 30 days, while in neutral to basic environments (pH 7.4-9.0), they showed a slight but statistically significant degradation after 7 days. This finding suggests that the degradations of **1** and **2** under the basic solutions were possibly deprotonated at the carboxylic acid position to generate the carboxylate anion [234]. However, the residual contents of **1** and **2** remained above 90% at pH 2.0-9.0 for at least 30 days. As topical products in cosmetics are often designed with a pH range between 4 to 6 [235], a pH value of 5.5 was used for subsequent stability testing.

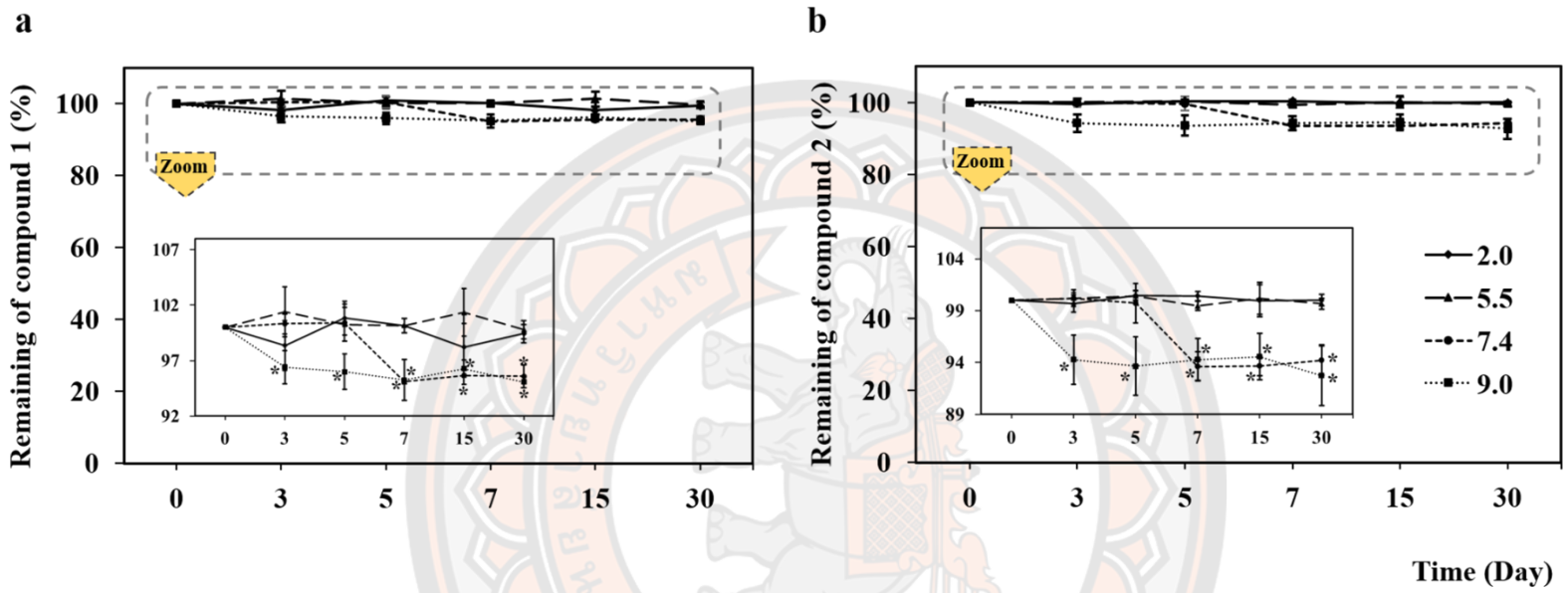

Figure 37 The effect of various pH conditions on the stability of (a) compound **1** and (b) compound **2** in *T. grandis* ethanolic extract analyzed by HPLC (* $p < 0.05$ against data of day 0)

4.6.2 Effect of temperature

The ethanolic extract and ethanolic extract in PG were stored either as the prepared extract or a buffered solution forms (at pH 5.5). These samples were subjected to storage for varying durations up to 180 days at different temperatures (50, 60, 70, and 80 °C). The degradation of **1** and **2** are depicted in Figures 38-39 and Figures 40-41, respectively. The remaining contents of **1** and **2** in both forms of ethanolic extract and ethanolic extract in PG were slightly decreased after 30 days of storage at 50 °C and 60 °C. However, after 180 days of storage, greater than 80% of **1** and **2** remained in extracts. At the higher temperatures (70 °C and 80 °C), the differences in degradation profiles of the two markers in both forms of two different extracts were clearly visible. At 80 °C, it was clear that **1** in the buffered solution form of the ethanolic extract degraded the most rapidly, with significant degradation as early as 60 days, and was completely degraded after 120 days (Figure 38b).

Similarly, after 90 days at 70 °C, there were statistically significant differences, and after 180 days, there was a complete loss (Figure 38b). On the other hand, when PG was present in the extract at 70 °C and 80 °C, the degradation was slower (Figure 39b). The stability of **1** in the ethanolic extract as the prepared extract form was found to be sensitive to temperature, particularly at 80°C. it exhibited significant degradation after 60 days of storage (Figure 38a), whereas it appeared to be more stable when dissolved in PG, with a remaining of 86.33 ± 0.76% at day 60 (Figure 39a).

After only 30 days, the stability of **2** in ethanolic in buffered solution form was highly degraded at 80°C, and it was completely degraded after 90 days (Figure 40b). Furthermore, it was found that compound **2** was unstable in the buffered solution form of ethanolic extract stored at 70°C. After 90 days in this condition, **2** began to degrade significantly. It was completely degraded after 180 days (Figure 40b), similar to what we observed in **1** (Figure 38b). The content of **2** in the buffered solution form of ethanolic extract in PG was stable over 120 days at 70 °C, with more than 80% remaining (Figure 41b). The content of **2** in the ethanolic extract significantly decreased after 30 days of storage at 80 °C in the prepared extract form, but the remaining content remained constant at more than 60% until 180 days of storage (Figure 40a). In contrast

to the remainder of **2** in ethanolic extract in PG stored in the same conditions, it was stable for at least 180 days (Figure 41a).

Specifically, **1** was more stable at high temperatures than **2**. This may be related to the number of substituents connected to the double bonds at C_8-C_9 (for **1**) and C_7-C_8 (for **2**). More substituted alkene is more stable than less substituted alkene due to hyperconjugation. Bond strength may be a second factor that contributes to alkene stability. Alkenes become more stable as substitution increases. Highly substituted alkenes are consistently more stable than less substituted alkenes because they possess a higher ratio of sp^2–sp^3 bonds to sp^3–sp^3 bonds [236]. As a result, the stability of a tetrasubstituted alkene of **1** is greater than that of a trisubstituted alkene of **2**.

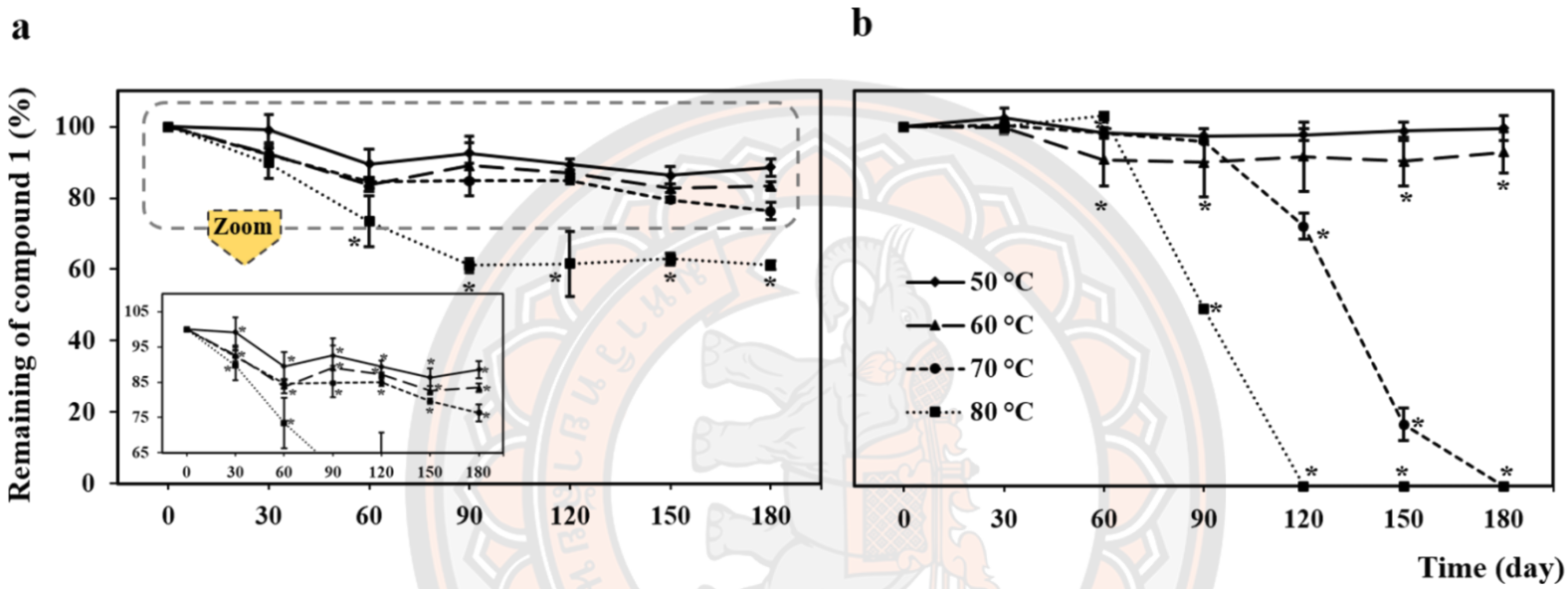

Figure 38 The effect of temperature on the stability of compound **1** in ethanolic extract of (a) prepared extract form and (b) buffered solution form (pH 5.5) during storage under different conservation conditions over 180 days. The remaining content of **1** was measured by HPLC (*$p < 0.05$ against data of day 0).

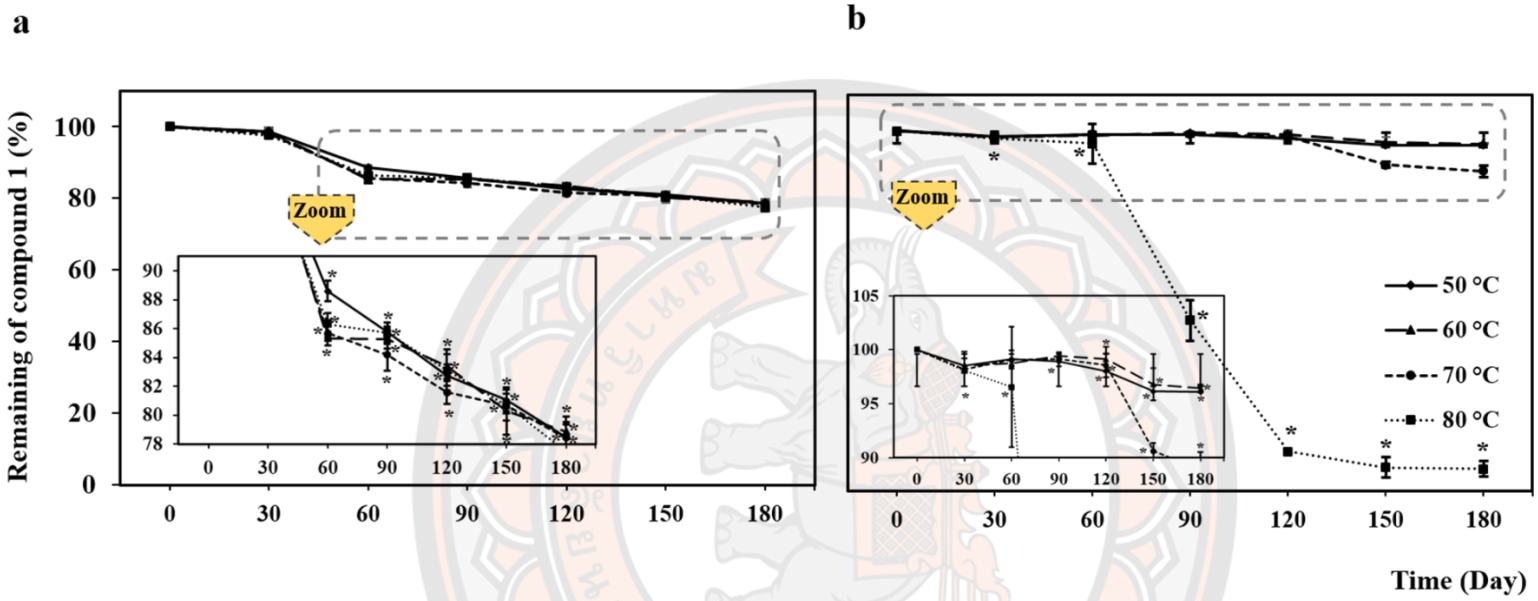

Figure 39 The effect of temperature on the stability of compound **1** in ethanolic extract in PG of (a) prepared extract form and (b) buffered solution form (pH 5.5) during storage under different conservation conditions over 180 days. The remaining content of **1** was measured by HPLC (*$p < 0.05$ against data of day 0).

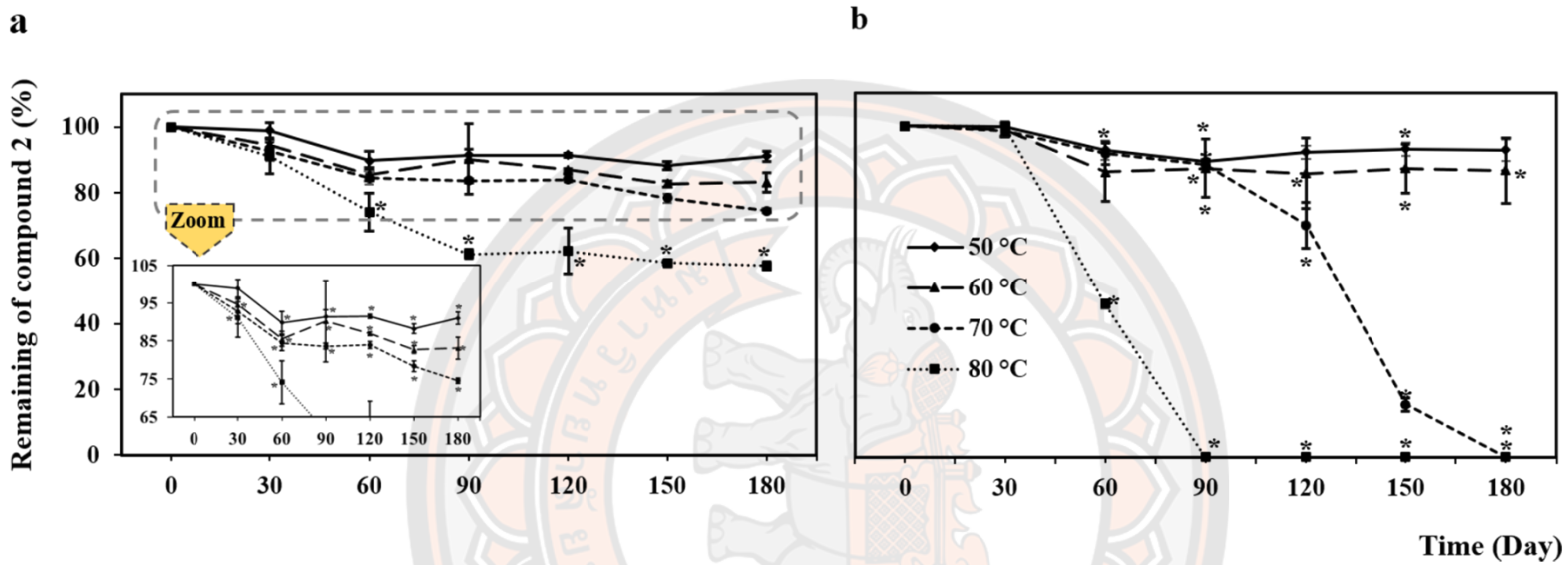

Figure 40 The effect of temperature on the stability of compound **2** in ethanolic extract of (a) prepared extract form and (b) buffered solution form (pH 5.5) during storage under different conservation conditions over 180 days. The remaining content of **2** was measured by HPLC (*$p < 0.05$ against data of day 0).

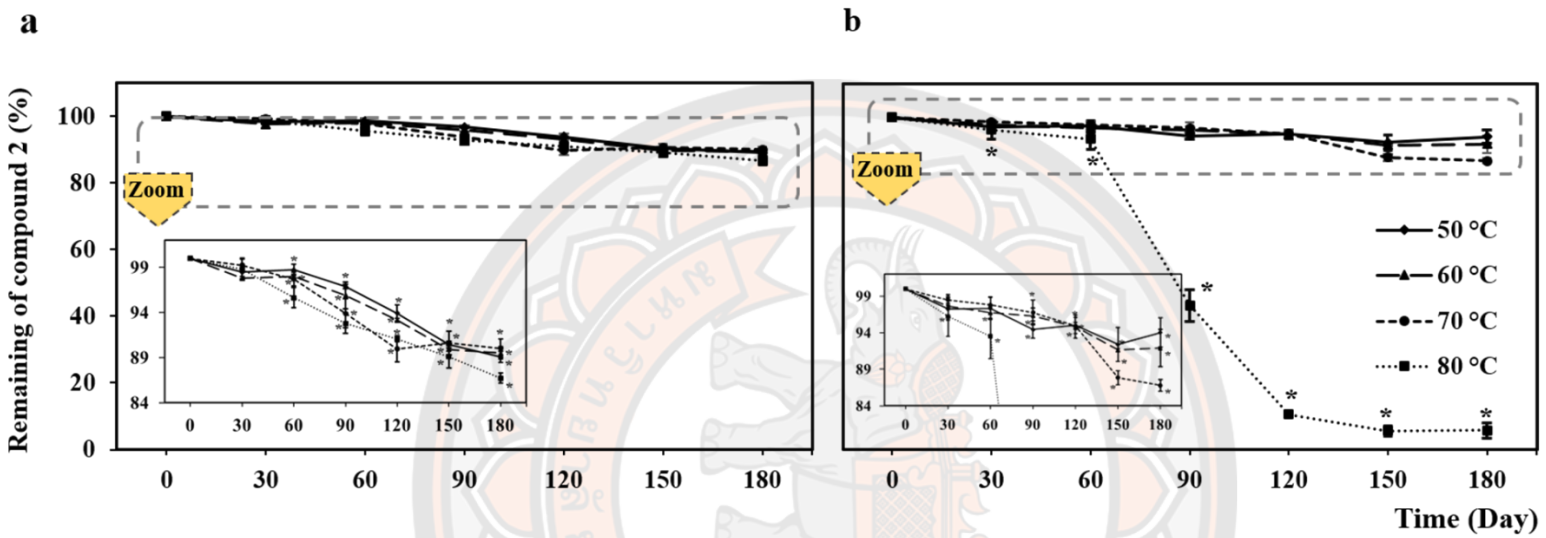

Figure 41 The effect of temperature on the stability of compound **2** in ethanolic extract in PG of (a) prepared extract form and (b)) buffered solution form (pH 5.5) during storage under different conservation conditions over 180 days. The remaining content of **2** was measured by HPLC (*p < 0.05 against data of day 0).

The stability profiles of **1** and **2** in buffered solution form of the ethanolic extract in PG were improved in our study. Our findings were consistent with the finding of Kao et al. [25], who reported that the four major components of *Scutellaria baicalensis* (baicalin, wogonoside, baicalein, and wogonin) were more stable in 20% PG than in water storage solvents. It has been postulated that two –OH groups present in PG have an extensive capacity for hydration, facilitated by the surrounding water molecules via both hydrogen bond donation and acceptance [237]. Therefore, the addition of PG may reduce water activity to prevent chemical degradation. In PG/water mixtures, the polarity of the aqueous medium and the dielectric constant were also reduced. Such a reason might be decreased the stability rate constant of degradation, thereby enhancing its stability [238].

Furthermore, adding PEG-40 to the ethanolic extract in PG may help to prevent the degradation of its bioactive compounds. This may be because the formation of a covalent bond with PEG allows active ingredients to be stabilized and solubilized, reducing their toxicity, antigenicity, and oxidation reaction by forming micelles, as well as improving cell penetration [239,240]. Additionally, our findings indicated that the prepared extract form was more thermally stable than those in the buffered solution form. This finding suggests that compounds **1** and **2** degraded more easily in buffered solution form at high temperatures, which may have accelerated oxidative reactions [241,242]. Therefore, the *T. grandis* extracts in the prepared extract forms are more suitable for storage than in the solution from in PEG-40 and buffer solution pH 5.5. Moreover, the storage temperature should be kept below 60°C.

4.6.3 Preliminary identification of temperature degradation products

To preliminary identify the degradation products, a solid mixture of compounds **1** and **2** was kept at accelerated condition (80 °C) for 14 days. A spot of unidentified polar compounds was observed on the TLC fingerprint at the R_f value of 0.43, as shown in Figure 42a. These polar degradation products were also detected in LC-MS baseline peak chromatogram (BPC) (Figure 42b). When the degradation profiles of these two samples (at days 0 and 14) were compared, it was found that the peak intensities of polar compounds increased after keeping at 80 °C for 14 days, while the peaks of compounds **1** and **2**, particularly **2**, decreased (Figure 42b, below). These

degradation products were then separated into four sub-fractions (A-D) using silica gel column chromatography. Sub-fraction C (1 mg) contained the major polar spots at R_f = 0.43, which were then preliminary identified using the LC-MS method. Two degradation products were detected at the retention time of 2.78 min for peak A and 3.55 min for peak B (Figure 43a). The ESI-MS spectra of peaks A and B revealed *m/z* 331.1934 *m/z*, 367.1707 for peak A, and *m/z* 317.2002, 335.2096 for peak B (Figure 43b), which differed from the ESI-MS spectra of **1** and **2** as shown in Figure 42c (*m/z* 303.2374 $[M-H]^-$ for **1** and *m/z* 303.2352 for **2** $[M-H]^-$). This may be the result of the direct activation of the sp^3 C–H bond at the allylic position into ketone groups, which stimulates the allylic oxidation reaction [243]. Because of the low yield of isolated degradation products, it was difficult to confirm their structures. Additional study is required to clarify the structure of degradation products.

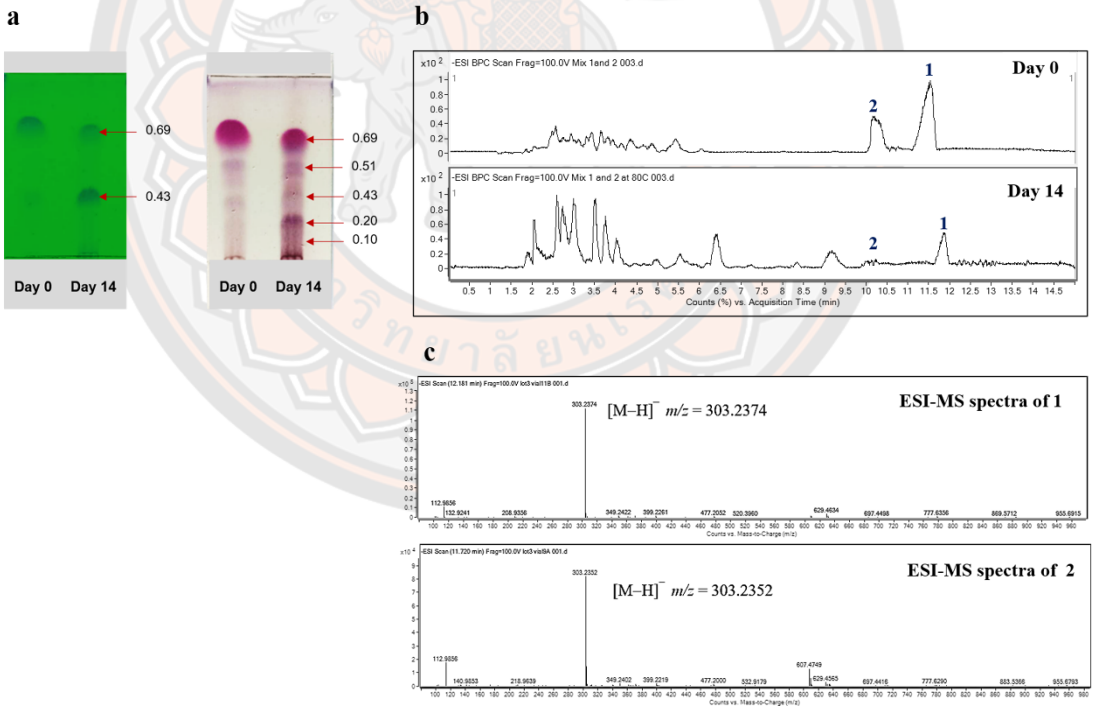

Figure 42 The degradation profiles of compounds **1** and **2** in the solid mixture were determined at day 0 (before the test) and day 14 (after being kept at 80 °C) using (a) TLC, (b) LC-MS techniques, and (c) ESI-MS spectra of **1** and **2**.

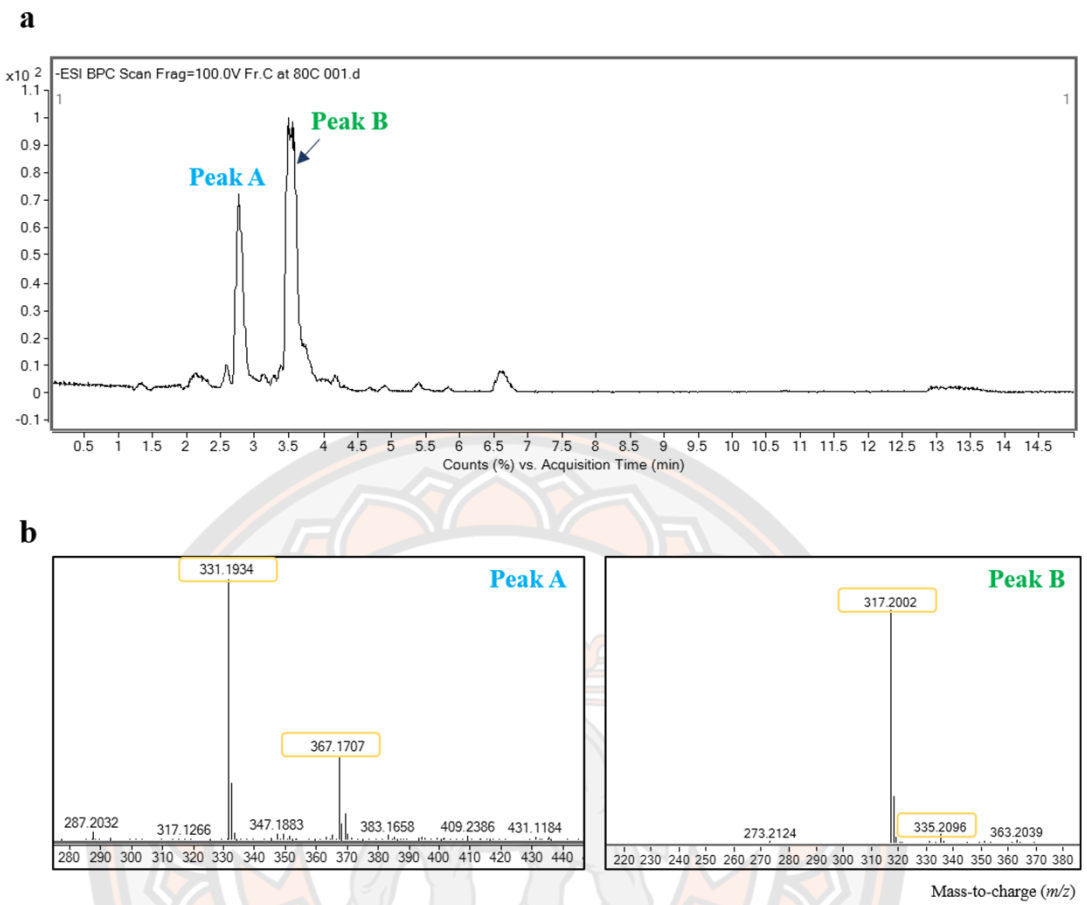

Figure 43 The (a) baseline peak chromatogram (BPC) of sub-fraction C (10 mg/mL) from LC-MS and (b) mass fragmentation (in negative mode) of peaks A and B

4.6.4 Effect of light

The prepared extracts (ethanolic extract and ethanolic extract in PG), as well as the buffered solution forms, were kept in well-closed containers and exposed to 1.21 million lux-h of light for 13.5 h during which time the presence of **1** and **2** in the ethanolic extract in PG rapidly degraded by ~ 90% for **1** and ~ 40% for **2**, whereas **1** and **2** in the prepared extract form of the ethanolic extract showed the least loss (Figure 44a). During the 13.5 h light exposure, the buffered solution form of ethanolic extract in PG lost **1** faster than that from the ethanolic extract. The remaining content of **2** was statistically significantly more stable than that of **1** (Figure 44b). The ethanolic extract in PG was more unstable than the ethanolic extract in both forms.

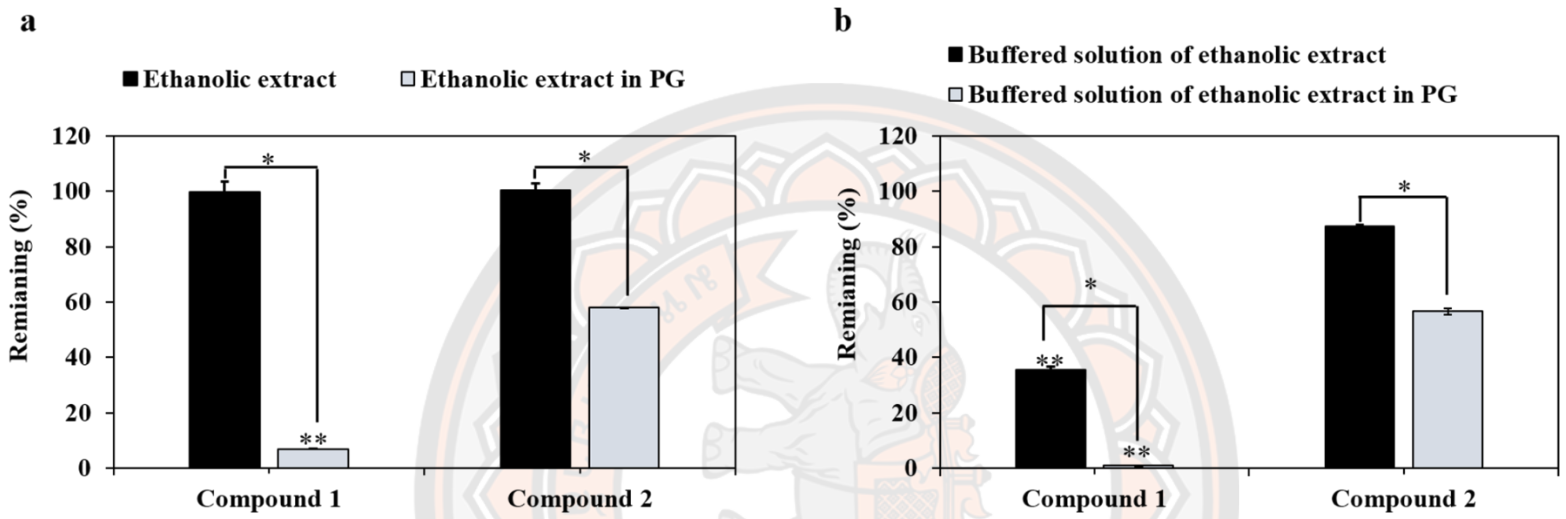

Figure **44** Degradation of compounds **1** and **2** in (a) ethanolic extract and ethanolic extract in PG, (b) buffered solution (pH 5.5) of ethanolic extract and buffered solution (pH 5.5) of ethanolic extract in PG during storage under light conditions for 13.5 h. The remaining contents of **1** and **2** were analyzed using HPLC ($^{*}p < 0.05$, $^{**}p < 0.05$ vs compound **2**).

According to the presented data, the light-sensitivity of both **1** and **2** in buffered solution form of the PG solvent was clearly observed. This may occur as a result of the ability of light components like UV to activate the PG which in turn act as a radical initiator to promote oxidation **1** and **2** in solution [244]. However, other factors may be involved in the decomposition of these compounds, which requires further investigation. These findings suggest that using light-protective packaging and UV absorbents may be able to improve the photostability of **1** and **2** in *T. grandis* extract.

4.6.5 Calculation of the shelf-life of **1** and **2** by the Q10 method

The Q10 equation, which predicts the potential shelf-life of compounds with heat-sensitive degradation was used to calculate the shelf-life estimation of **1** and **2** in ethanolic extract and ethanolic extract in PG under prepared extract forms. At 60 days, the remaining content of **1** and **2** in the ethanolic extract and ethanolic extract in PG of prepared extract forms storage at 50°C remained 90% or higher. The value of Q was set to 3 due to the activation energy of most compounds is in the range of 18-20 kcal/mol and estimated shelf life of **1** and **2** was calculated as follows:

$$t_{90}(30°C) = \frac{60}{3^{(30-50)/10}} = 540 \text{ days or } 1.48 \text{ years}$$

Therefore, with respect to the remaining amount of both **1** and **2**, the shelf-life of the prepared extract forms (ethanolic extract and ethanolic extract in PG) at 30 °C is estimated to be 1.48 years.

4.7 *In vitro* skin penetration of 1 and 2 from *T. grandis* ethanolic extract and ethanolic extract in PG

The skin penetration levels of **1** and **2** extracted with ethanol, as well as the skin penetration level of the ethanolic extract in PG, were evaluated using Franz diffusion cells. The results showed that **1** and **2** in the ethanolic extract solution were able to penetrate the receiver compartment after 4 h and had high cumulative amounts of >10% after 24 h. The cumulative amounts after 24 h were 12.20 ± 0.19 % of **1** and 10.96 ± 0.51 % of **2** (Figure 45a), whereas the ethanolic extract in PG provided superior skin penetration with the cumulative amounts of 12.72 ± 0.24% of **1** and 11.30 ± 0.35%

of **2** (Figure 45b). The sample recovery ranged from 90% to 100% (Table 25). According to these studies, **1** and **2** are more likely to penetrate the receiver compartment when PG solvent is added. However, after 24 h, the greater penetration of **1** in both the ethanolic extract solution and the ethanolic extract in PG indicated significantly larger cumulative amounts (%) than the penetration of **2**. According to the partition coefficient described above, **1** was more hydrophobic than **2**. This property makes it more likely interact with the lipid layer of the stratum corneum [245,246]. The result of this study can usefully inform the future development of cosmetic or hair loss treatments containing *T. grandis* extracts.

Several studies have shown that terpenes, particularly essential oils (e.g., 1,8-cineole, menthol, and menthone) and their constituents, can improve percutaneous absorption [228,229,247]. The study by Srivilai et al. [169] also reported the effect on minoxidil penetration of germacrone and sesquiterpene-enriched extracts from *Curcuma aeruginosa* Roxb., using Franz diffusion cells. The penetration of minoxidil alone through the human foreskin was limited, reaching only 0.9 ± 0.1 % after 8 h in the stratum corneum, but was about 10-fold higher when combined with germacrone, and 2% *C. aeruginosa* essential oil (7–8%), both of which enhance skin penetration.

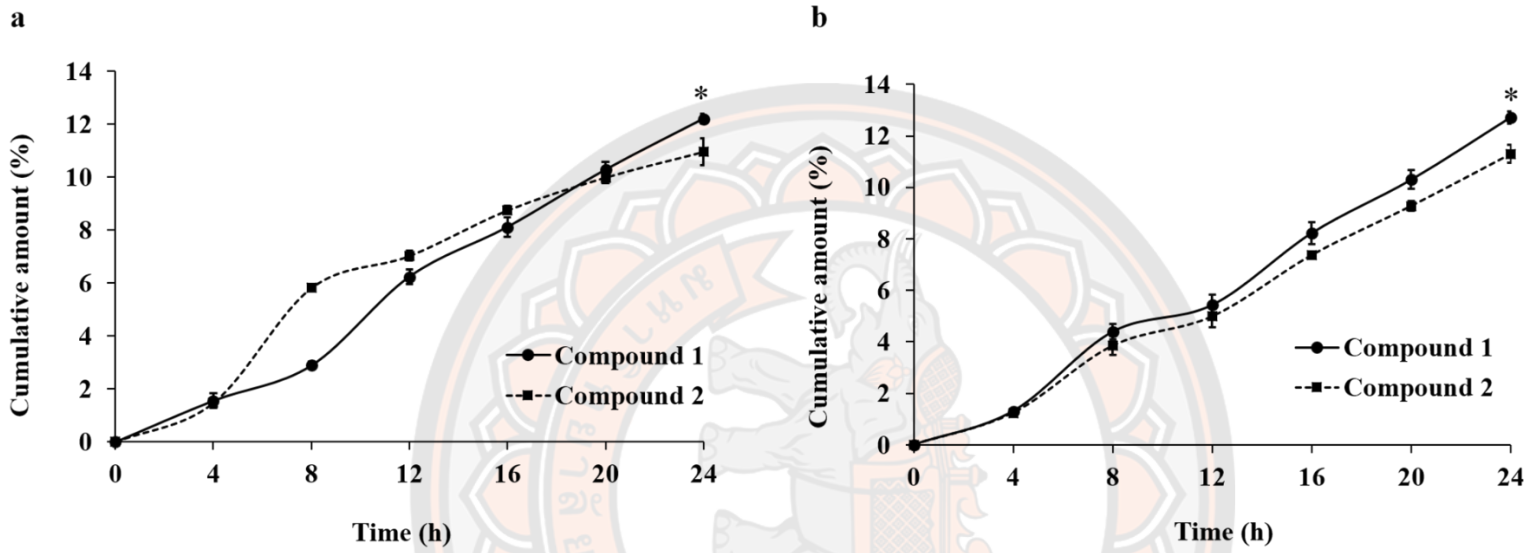

Figure 45 The skin penetration profiles of **1** and **2** after application of (a) ethanolic extract solution and (b) ethanolic extract in PG on the skin membranes for 24 h. Each point represents a percentage of **1** and **2** cumulative amounts in the receptor medium at each time point measured by the HPLC method. The values represent the mean ± SD of triplicate experiments. (*$p < 0.05$, significantly different compared with **2** at 24 h).

Table 25 *In-vitro* skin penetration of **1** and **2** after application of ethanolic extract solution and ethanolic extract in PG on the skin membranes for 24 h. The results are expressed as the mean of the percentage (%) applied dose ± SD of triplicate experiments.

Samples	Compounds	Donor (%)	Membrane (%)	Receiver (%)	Recovery (%)
Ethanolic extract solution	**1**	76.16 ± 0.99	4.47 ± 0.14	12.20 ± 0.19*	92.63 ± 0.84
	2	77.20 ± 0.77	5.70 ± 0.37	10.96 ± 0.51	93.86 ± 0.91
Ethanolic extract in PG	**1**	82.00 ± 0.63	4.11 ± 0.05	12.72 ± 0.24*	98.84 ± 0.91
	2	78.47 ± 0.55	5.03 ± 0.01	11.30 ± 0.35	94.80 ± 0.85

*$p < 0.05$, significantly different compared with compound **2** at the same extract.

Few studies have previously been conducted on the topic of diterpenes and triterpenes skin penetration [248,249]. Rizwan et al. [248] investigated the effects of several monoterpene enhancers and labdane diterpene forskolin using an automated transdermal diffusion cell sampling technique. Terpene enhancers (1% *w/w*) were shown to be effective for rat skin and human cadaver skin penetration in the following order: cineole > D-limonene > L-menthol > linalool > forskolin and cineole > D-limonene > linalool > L-menthol > forskolin. Although diterpene forskolin penetrated less than monoterpenes in both skin models, it enhanced skin permeability by disrupting and extracting stratum corneum lipid bilayers, as do other terpenes. Our findings also revealed that these two diterpenes (**1** and **2**) can penetrate the skin by interacting with the lipid layer part of the stratum corneum. However, our work is significant in that it describes the skin penetration of two 5α-reductase inhibitors (**1** and **2**) in *T. grandis* leaf extracts for the first time.

CHAPTER V
CONCLUSION

This study presents novel finding on the isolation and characterization of 5α-reductase inhibitors from the leaf extract of *T. grandis*. Specifically, compounds **1** and **2**, which are eperuane-type diterpenes, as well as compound **3**, a lupane-type triterpene, were successfully purified and identified. The quantitative HPLC analysis of **1** and **2** as the two potent 5α-reductase inhibitors in teak leaf extracts was developed, validated, and successfully applied. The 95% ethanol was used as the extraction solvent for *T. grandis* leaves and provided a higher yield of extract as well as exhibited a greater 5α-reductase inhibitory activity, in addition, the ethanolic extract showed the greater amounts of **1** and **2** than hexane extract. Our study suggested that **1** and **2** may serve as bioactive compounds for the further development of hair loss treatment products.

Various parameters, including pH, solubility, partition coefficient, color, zeta potential, and viscosity, were used to measure the physicochemical properties of the ethanolic extract and the ethanolic extract in PG, as well as the chemical constituents. According to our findings, the pH values of the two extracts indicated an acidic environment and provided a pH range acceptable for topical cosmetics. The partition coefficients of **1** and **2** were found to be positive, indicating that these compounds are hydrophobic. Therefore, compounds **1** and **2** have poor solubility in distilled water, while their solubility is slightly soluble in HEPES buffer with 2% w/v of Tween20. This result indicated that HEPES buffer containing solubilizer could serve as a suitable vehicle for further skin penetration studies. The color determination of ethanolic extract and ethanolic extract in PG showed that the ethanolic extract in PG was lighter, redder, and yellower than the ethanolic extract, which was greener. Additionally, the particle stability in the solution was found to be less than ± 30 mv, which was identified as quite easily agglomerated. Moreover, the viscosity of the ethanolic extract in PG was also investigated. Our investigation revealed that the viscosity of the ethanolic extract in PG exhibited Newtonian behavior. This study of physicochemical properties provides information for designing and developing an appropriate formulation for a more effective assessment of bioactive compounds in pre-formulation studies.

Furthermore, the pre-formulation and stability of compounds **1** and **2** in crude ethanolic extract and ethanolic extract in PG were investigated for the first time. Two 5α-reductase inhibitors (**1** and **2**) identified in an ethanolic extract were more stable in an acidic solution for at least 30 days. Compounds **1** and **2** in the buffered solution were degraded by more than 60% after 2 months for ethanolic extract and after 3 months for ethanolic extract in PG stored at 80 °C. It should be noted that the degradation process was significantly delayed when the ethanolic extract was mixed with PG (ethanolic extract in PG) or when it was maintained in prepared extract form. Using the Q10 method, the shelf-life of **1** and **2** in prepared extract forms (ethanolic extract and ethanolic extract in PG) was determined to be 1.48 years. These two 5α-reductase inhibitors in *T. grandis* were rapidly degraded when exposed to light in the buffered solution forms. Compounds **1** and **2** are presumably degraded by oxidation under conditions of heat and light exposure. Identification and profile of degradation products inhibiting 5α-reductase could be the focus of future research. To prevent the degradation of its bioactive components, our results suggest that the *T. grandis* leaf extract should be prepared in a prepared extract form, incorporation a slight acidic component, and packaged in light-protective container. According to the results of an *in vitro* skin penetration study, both **1** and **2** in ethanolic extract and ethanolic extract in PG were able to begin penetrating the skin after 4 h and exhibited high cumulative amounts >10% after 24 h, with both compounds tending more penetrates the skin when PG solvent was used. Therefore, our findings verified the efficacy of *T. grandis* ethanolic extract in PG in cosmetic applications for **1** and **2**.

REFERENCES

[1] DA Wilson. *Testosterone*. *In*: Clinical Veterinary Advisor. W.B. Saunders, Saint Louis, 2012, p. 963-4.

[2] DW Russell and JD Wilson. Steroid 5α-reductase: two genes/two enzymes. *Annu. Rev. Biochem.* 1994; **63**, 25-61.

[3] EG Occhiato, A Guarna, G Danza and M Serio. Selective non-steroidal inhibitors of 5α-reductase type 1. *J. Steroid Biochem. Mol. Biol.* 2004; **88**, 1-16.

[4] VA Randall. Role of 5α-reductase in health and disease. *Baillière's Clin. Endocrinol. Metab.*1994; **8**, 405-31.

[5] LC Sperling. Hair and systemic disease. *Dermatol. Clin.* 2001; **19**, 711-26.

[6] Olsen EA. *Androgenetic alopecia*. *In*: Disorders of hair growth: diagnosis and treatment. McGraw-Hill, New York, 1993, p. 257-83.

[7] A Rossi, C Cantisani, L Melis, A Iorio, E Scali and S Calvieri. Minoxidil use in dermatology, side effects and recent patents. *Recent Pat. Inflammation Allergy Drug Discovery* 2012; **6**, 130-6.

[8] VM Meidan and E Touitou. Treatments for androgenetic alopecia and alopecia areata: current options and future prospects. *Drugs* 2001; **61**, 53-69.

[9] N Kumar, W Rungseevijitprapa, NA Narkkhong, M Suttajit and C Chaiyasut. 5α-reductase inhibition and hair growth promotion of some Thai plants traditionally used for hair treatment. *J. Ethnopharmacol.* 2012; **139**, 765-71.

[10] K Palanisamy, M Hegde and JS Yi. Teak (*Tectona grandis* Linn. f.): A renowned commercial timber species. *Int. J. Pharm. Pharm. Sci.* 2009; **25**, 1-24.

[11] P Charoensit, F Sawasdipol, N Tibkawin, N Suphrom and N Khorana. Development of natural pigments from *Tectona grandis* (teak) leaves: Agricultural waste material from teak plantations. *Sustainable Chem. Pharm.* 2021; **19**, 100365.

[12] N Tibkawin, N Suphrom, N Nuengchamnong, N Khorana and P Charoensit. Utilisation of *Tectona grandis* (teak) leaf extracts as natural hair dyes. *Color. Technol.* 2022; **138**, 355-67.

[13] CP Khare. *Indian medicinal plants: an illustrated dictionary*. Springer Berlin Heidelberg, New York, 2008, p. 649.

[14] AM Aguinaldo, OPM Ocampo, BF Bowden, AI Gray and PG Waterman. Tectograndone, an anthraquinone-naphthoquinone pigment from the leaves of *Tectona grandis. Phytochemistry* 1993; **33**, 933-5.

[15] R Lacret, RM Varela, JM Molinillo, C Nogueiras and FA Macias. Anthratectone and naphthotectone, two quinones from bioactive extracts of *Tectona grandis. J. Chem. Ecol.* 2011; **37**, 1341-8.

[16] N Nayeem and MD Karvekar. Isolation of phenolic compounds from the methanolic extract of *Tectona grandis. Res. J. Pharm., Biol. Chem. Sci.* 2010; **1**, 221-5.

[17] FA Macias, R Lacret, RM Varela, C Nogueiras and JM Molinillo. Isolation and phytotoxicity of terpenes from *Tectona grandis. J. Chem. Ecol.* 2010; **36**, 396-404.

[18] FA Macías, R Lacret, RM Varela, C Nogueiras and JMG Molinillo. Bioactive apocarotenoids from *Tectona grandis. Phytochemistry* 2008; **69**, 2708-15.

[19] R Lacret, RM Varela, JMG Molinillo, C Nogueiras and FA Macías. Tectonoelins, new norlignans from a bioactive extract of *Tectona grandis. Phytochem. Lett.* 2012; **5**, 382-6.

[20] Z Khan, M Ali and P Bagri. A new steroidal glycoside and fatty acid esters from the stem bark of *Tectona grandis* Linn. *Nat. Prod. Res.* 2010; **24**, 1059-68.

[21] N Singh, N Shukla, P Singh, R Sharma, SM Rajendran, R Maurya and G Palit. Verbascoside isolated from *Tectona grandis* mediates gastric protection in rats via inhibiting proton pump activity. *Fitoterapia* 2010; **81**, 755-61.

[22] K Joshi, P Singh and RT Pardasani. Chemical components of the roots of *Tectona grandis* and *Gmelina arborea. Planta Med.* 1977; **32**, 71-5.

[23] D Jaybhaye, S Varma, N Gagne, V Bonde, A Gite and D Bhosle. Effect of *Tectona grandis* Linn. seeds on hair growth activity of albino mice. *Int. J. Ayurveda Res.* 2010; **1**, 211-5.

[24] Y Fachrunniza, J Srivilai, V Wisuitiprot, W Wisuitiprot, N Suphrom, P Temkitthawon, N Waranuch and K Ingkaninan. *Tectona grandis*, a potential

active ingredient for hair growth promotion. *Songklanakarin J. Sci. Technol*. 2020; **42**, 1352-9.

[25] TT Kao, MC Wang, YH Chen, YT Chung and PA Hwang. Propylene glycol improves stability of the anti-inflammatory compounds in *Scutellaria baicalensis* extract. *Processes* 2021; **9**, 894.

[26] M Canton, S Poigny, R Roe, JM Nuzillard and JH Renault. Dereplication of natural extracts diluted in propylene glycol, 1,3-propanediol and glycerin. Comparison of *Leontopodium alpinum* Cass. (Edelweiss) extracts as a case study. *Cosmetics* 2021; **8**, 10.

[27] KD Kaufman. Androgen metabolism as it affects hair growth in androgenetic alopecia. *Dermatol. Clin.* 1996; **14**, 697-711.

[28] MA Mukaddam and PJ Snyder. *Androgens*. *In*: Osteoporosis. 4th ed. Academic Press, San Diego, 2013, p. 1827-37.

[29] F Azzouni, A Godoy, Y Li and J Mohler. The 5α-reductase isozyme family: a review of basic biology and their role in human diseases. *Adv. Urol.* 2012; **2012**, 1-18.

[30] J Srivilai, G Minale, CN Scholfield and K Ingkaninan. Discovery of natural steroid 5α-reductase inhibitors. *Assay Drug Dev. Technol.* 2019; **17**, 44-57.

[31] X Li, C Chen, SM Singh and F Labire. The enzyme and inhibitors of 4-ene-3-oxosteroid 5α-oxidoreductase. *Steroids* 1995; **60**, 430-41.

[32] A Cilotti, G Danza and M Serio. Clinical application of 5α-reductase inhibitors. *J. Endocrinol. Invest.* 2001; **24**, 199-203.

[33] S Aggarwal, S Thareja, A Verma, TR Bhardwaj and M Kumar. An overview on 5α-reductase inhibitors. *Steroids* 2010; **75**, 109-53.

[34] ME Sawaya. Clinical updates in hair. *Dermatol. Clin.* 1997; **15**, 37-43.

[35] N Orentreich. Pathogenesis of alopecia. *J. Soc. Cosmet. Chem.* 1960; **11**, 479-99.

[36] GK Epstein, J Epstein and J Cohen. Hair loss in men and women: Medical and surgical therapies. *Advances in Cosmetic Surgery*, 2019; **2**, 161-76.

[37] R Grimalt. Psychological aspects of hair disease. *J. Cosmet. Dermatol.* 2005; **4**, 142-7.

[38] OT Norwood. Incidence of female androgenetic alopecia (female pattern alopecia). *Dermatol. Surg.* 2001; **27**, 53-4.

[39] D Semwal, R Kotiyal, A Chauhan, A Mishra, L Adhikari, A Semalty and M Semalty. Alopecia and the herbal drugs: an overview of the current status. *Adv. Biomed. Pharm.* 2015; **2**, 246-54.

[40] BK Patel, MAM Velasco, FT Gutierrez and D Khesin. Addressing androgenetic alopecia a complex disorder with a multilateral treatment strategy. *MOJ bioequiv. bioavailab.* 2017; **3**, 00025.

[41] AS Tully, J Schwartzenberger and J Studdiford. Androgenic alopecia. *J. Men's Health* 2010; **7**, 270-7.

[42] JB Hamilton. Patterned loss of hair in man; types and incidence. *Ann. N. Y. Acad. Sci.* 1951; **53**, 708-28.

[43] E Ludwig. Classification of the types of androgenetic alopecia (common baldness) occurring in the female sex. *Br. J. Dermatol.* 1977; **97**, 247-54.

[44] U Blume-Peytavi, K Hillmann, E Dietz, D Canfield and NG Bartels. A randomized, single-blind trial of 5% minoxidil foam once daily versus 2% minoxidil solution twice daily in the treatment of androgenetic alopecia in women. *J. Am. Acad. Dermatol.* 2011; **65**, 1126-34.e2.

[45] EA Olsen, D Whiting, W Bergfeld, J Miller, M Hordinsky, R Wanser, P Zhang and B Kohut. A multicenter, randomized, placebo-controlled, double-blind clinical trial of a novel formulation of 5% minoxidil topical foam versus placebo in the treatment of androgenetic alopecia in men. *J. Am. Acad. Dermatol.* 2007; **57**, 767-74.

[46] S Varothai and WF Bergfeld. Androgenetic alopecia: An evidence-based treatment update. *Am. J. Clin. Dermatol.* 2014; **15**, 217-30.

[47] WD James. Clinical practice. Acne. *N. Engl. J. Med*. 2005; **352**, 1463-72.

[48] GM White. Recent findings in the epidemiologic evidence, classification, and subtypes of acne vulgaris. *J. Am. Acad. Dermatol.* 1998; **39**, S34-S7.

[49] A Haider and JC Shaw. Treatment of acne vulgaris. *JAMA* 2004; **292**, 726-35.

[50] SB Clarke, AM Nelson, RE George and DM Thiboutot. Pharmacologic modulation of sebaceous gland activity: mechanisms and clinical applications. *Dermatol. Clin.* 2007; **25**, 137-46.

[51] JJ Lai, P Chang, KP Lai, L Chen and C Chang. The role of androgen and androgen receptor in skin-related disorders. *Arch. Dermatol. Res.* 2012; **304**, 499-510.

[52] SJ Berry, DS Coffey, PC Walsh and LL Ewing. The development of human benign prostatic hyperplasia with age. *J. Urol.* 1984; **132**, 474-9.

[53] SL Vignera, RA Condorelli, GI Russo, G Morgia and AE Calogero. Endocrine control of benign prostatic hyperplasia. *Andrology* 2016; **4**, 404-11.

[54] DI Kang and JI Chung. Current status of 5α-reductase inhibitors in prostate disease management. *Korean J. Urol.* 2013; **54**, 213-9.

[55] A Hohl, MF Ronsoni and Md Oliveira. Hirsutism: diagnosis and treatment. *Arq. Bras. Endocrinol. Metabol.* 2014; **58**, 97-107.

[56] D Bode, DA Seehusen and D Baird. Hirsutism in women. *Am. Fam. Physician* 2012; **85**, 373-80.

[57] AR Zappacosta. Reversal of baldness in patient receiving minoxidil for hypertension. *N. Engl. J. Med*. 1980; **303**, 1480-1.

[58] AE Buhl, SJ Conrad, DJ Waldon and MN Brunden. Potassium channel conductance as a control mechanism in hair follicles. *J. Invest. Dermatol.* 1993; **101**, S148-S52.

[59] G Tian, JD Stuart, ML Moss, PL Domanico, HN Bramson, IR Patel, SH Kadwell, LK Overton, TA Kost, RA Mook, SV Frye, KW Batchelor and JS Wiseman. 17β-(*N-tert*-butylcarbamoyl)-4-aza-5α-androstan-1-en-3-one is an active site-directed slow time-dependent inhibitor of human steroid 5α-reductase 1. *Biochemistry* 1994; **33**, 2291-6.

[60] PN Span, MC Voller, AG Smals, FG Sweep, JA Schalken, MR Feneley and RS Kirby. Selectivity of finasteride as an *in vivo* inhibitor of 5α-reductase isozyme enzymatic activity in the human prostate. *J. Urol.* 1999; **161**, 332-7.

[61] MS Irwig and S Kolukula. Persistent sexual side effects of finasteride for male pattern hair loss. *J. Sex. Med.* 2011; **8**, 1747-53.

[62] V Mysore. Finasteride and sexual side effects. *Indian Dermatol. Online J.* 2012; **3**, 62-5.

[63] M Ranjan, P Diffley, G Stephen, D Price, TJ Walton and RP Newton. Comparative study of human steroid 5α-reductase isoforms in prostate and female breast skin tissues: sensitivity to inhibition by finasteride and epristeride. *Life Sci.* 2002; **71**, 115-26.

[64] MA Levy, M Brandt, KM Sheedy, JT Dinh, DA Holt, LM Garrison, DJ Bergsma and BW Metcalf. Epristeride is a selective and specific uncompetitive inhibitor of human steroid 5α-reductase isoform 2. *J. Steroid Biochem. Mol. Biol.* 1994; **48**, 197-206.

[65] XB Ju, HF Wu, LX Hua, W Zhang and J Li. The clinical efficacy of epristeride in the treatment of benign prostatic hyperplasia. *Natl. J. Androl.* 2002; **8**, 42-4.

[66] RV Clark, DJ Hermann, GR Cunningham, TH Wilson, BB Morrill and S Hobbs. Marked suppression of dihydrotestosterone in men with benign prostatic hyperplasia by dutasteride, a dual 5α-reductase inhibitor. *J. Clin. Endocrinol. Metab.* 2004; **89**, 2179-84.

[67] M Gleave, J Qian, C Andreou, P Pommerville, J Chin, R Casey, G Steinhoff, N Fleshner, D Bostwick, L Thomas and R Rittmaster. The effects of the dual 5α-reductase inhibitor dutasteride on localized prostate cancer-results from a 4-month pre-radical prostatectomy study.*The Prostate* 2006; **66**, 1674-85.

[68] K Yamana, F Labrie and V Luu-The. Human type 3 5α-reductase is expressed in peripheral tissues at higher levels than types 1 and 2 and its activity is potently inhibited by finasteride and dutasteride. *Horm. Mol. Biol. Clin. Invest.* 2010; **2**, 293-9.

[69] WK Chan, CY Fong, HH Tiong and CH Tan. The inhibition of 3β HSD activity in porcine granulosa cells by 4-MA, a potent 5α-reductase inhibitor. *Biochem. Biophys. Res. Commun.* 1987; **144**, 166-71.

[70] A Nahata and VK Dixit. Evaluation of 5α-reductase inhibitory activity of certain herbs useful as antiandrogens. *Andrologia* 2014; **46**, 592-601.

[71] R Jain, O Monthakantirat, P Tengamnuay and W De-Eknamkul. Avicequinone C isolated from *Avicennia marina* exhibits 5α-reductase-type 1 inhibitory activity

using an androgenic alopecia relevant cell-based assay system. *Molecules* 2014; **19**, 6809-21.

[72] K Murata, F Takeshita, K Samukawa, T Tani and H Matsuda. Effects of ginseng rhizome and ginsenoside Ro on testosterone 5α-reductase and hair re-growth in testosterone-treated mice. *Phytother. Res.* 2012; **26**, 48-53.

[73] H Matsuda, N Sato, M Yamazaki, S Naruto and M Kubo. Testosterone 5α-reductase inhibitory active constituents from Anemarrhenae rhizoma. *Biol. Pharm. Bull.* 2001; **24**, 586-7.

[74] B Zhang, Rw Zhang, Xq Yin, Zz Lao, Z Zhang, Qg Wu, Lw Yu, Xp Lai, Yh Wan and G Li. Inhibitory activities of some traditional Chinese herbs against testosterone 5α-reductase and effects of *Cacumen platycladi* on hair re-growth in testosterone-treated mice. *J. Ethnopharmacol.* 2016; **177**, 1-9.

[75] EK Seo, KH Kim, MK Kim, MH Cho, E Choi, K Kim and W Mar. Inhibitors of 5α-reductase type I in LNCaP cells from the roots of *Angelica koreana*. *Planta Med.* 2002; **68**, 162-3.

[76] K Ishiguro, H Oku and T Kato. Testosterone 5α-reductase inhibitor bisnaphthoquinone derivative from *Impatiens balsamina*. *Phytother. Res.* 2000; **14**, 54-6.

[77] YH Li, YF Yang, K Li, LL Jin, NY Yang and DY Kong. 5α-reductase and aromatase inhibitory constituents from *Brassica rapa* L. pollen. *Chem. Pharm. Bull. (Tokyo)* 2009; **57**, 401-4.

[78] A Jonas, G Rosenblat, D Krapf, W Bitterman and I Neeman. Cactus flower extracts may prove beneficial in benign prostatic hyperplasia due to inhibition of 5α-reductase activity, aromatase activity and lipid peroxidation. *Urol. Res.* 1998; **26**, 265-70.

[79] J Liu, R Ando, K Shimizu, K Hashida, R Makino, S Ohara and R Kondo. Steroid 5α-reductase inhibitory activity of condensed tannins from woody plants. *J. Wood Sci.* 2008; **54**, 68-75.

[80] WS Park, CH Lee, BG Lee and IS Chang. The extract of *Thujae occidentalis* semen inhibited 5α-reductase and androchronogenetic alopecia of B6CBAF1/j hybrid mouse. *J. Dermatol. Sci.* 2003; **31**, 91-8.

[81] Y Hirano, R Kondo and K Sakai. 5α-reductase inhibitory tannin-related compounds isolated from *Shorea laeviforia. J. Wood Sci.* 2003; **49**, 339-43.

[82] K Murata, K Noguchi, M Kondo, M Onishi, N Watanabe, K Okamura and H Matsuda. Inhibitory activities of *Puerariae Flos* against testosterone 5α-reductase and its hair growth promotion activities. *J. Nat. Med*. 2012; **66**, 158-65.

[83] J Koseki, T Matsumoto, Y Matsubara, K Tsuchiya, Y Mizuhara, K Sekiguchi, H Nishimura, J Watanabe, A Kaneko, T Hattori, K Maemura and Y Kase. Inhibition of rat 5α-reductase activity and testosterone-induced sebum synthesis in hamster sebocytes by an extract of *Quercus acutissima* Cortex. *J. Evidence-Based Complementary Altern. Med*. 2015; **2015**, 1-9.

[84] J Liu, K Kurashiki, K Shimizu and R Kondo. 5α-reductase inhibitory effect of triterpenoids isolated from *Ganoderma lucidum. Biol. Pharm. Bull.* 2006; **29**, 392-5.

[85] K Shimizu, R Kondo, K Sakai, S Buabarn and U Dilokkunanant. 5α-Reductase inhibitory component from leaves of *Artocarpus altilis. J. Wood Sci.* 2000; **46**, 385-9.

[86] K Shimizu, M Fukuda, R Kondo and K Sakai. The 5α-reductase inhibitory components from heartwood of *Artocarpus incisus*: structure-activity investigations. *Planta Med.* 2000; **66**, 16-9.

[87] D Lesuisse, J Berjonneau, C Ciot, P Devaux, B Doucet, JF Gourvest, B Khemis, C Lang, R Legrand, M Lowinski, P Maquin, A Parent, B Schoot and G Teutsch. Determination of oenothein B as the active 5α-reductase-inhibiting principle of the folk medicine *Epilobium parviflorum. J. Nat. Prod*. 1996; **59**, 490-2.

[88] N Hirata, M Tokunaga, S Naruto, M Iinuma and H Matsuda. Testosterone 5α-reductase inhibitory active constituents of *Piper nigrum* leaf. *Biol. Pharm. Bull*. 2007; **30**, 2402-5.

[89] CH Cho, JS Bae and YU Kim. 5α-reductase inhibitory components as antiandrogens from herbal medicine. *J. Acupunct. Meridian Stud*. 2010; **3**, 116-8.

[90] Y Komoda. Isolation of flavonoids from *Populus nigra* as Δ^4-3-ketosteroid (5α) reductase inhibitors. *Chem. Pharm. Bull. (Tokyo)* 1989; **37**, 3128-30.

[91] JS Park, MH Yeom, WS Park, KM Joo, HS Rho, DH Kim and IS Chang. Enzymatic hydrolysis of green tea seed extract and its activity on 5α-reductase inhibition. *Biosci., Biotechnol., Biochem.* 2006; **70**, 387-94.

[92] WS Park, ED Son, GW Nam, SH Kim, MS Noh, BG Lee, IS Jang, SE Kim, JJ Lee and CH Lee. Torilin from *Torilis japonica*, as a new inhibitor of testosterone 5α-reductase. *Planta Med*. 2003; **69**, 459-61.

[93] S Liao and RA Hiipakka. Selective inhibition of steroid 5α-reductase isozymes by tea epicatechin-3-gallate and epigallocatechin-3-gallate. *Biochem. Biophys. Res. Commun.* 1995; **214**, 833-8.

[94] S Jang, Y Lee, SL Hwang, MH Lee, SJ Park, IH Lee, S Kang, SS Roh, YJ Seo, JK Park, JH Lee and CD Kim. Establishment of type II 5α-reductase over-expressing cell line as an inhibitor screening model. *J. Steroid Biochem. Mol. Biol.* 2007; **107**, 245-52.

[95] N Suphrom, G Pumthong, N Khorana, N Waranuch, N Limpeanchob and K Ingkaninan. Anti-androgenic effect of sesquiterpenes isolated from the rhizomes of *Curcuma aeruginosa* Roxb. *Fitoterapia* 2012; **83**, 864-71.

[96] Yu Kim and J Han. Steroid 5α-reductase inhibition by polymethoxyflavones. *J. Korean Soc. Appl. Biol. Chem.* 2013; **56**, 469-71.

[97] YU Kim, HK Son, HK Song, MJ Ahn, SS Lee and SK Lee. Inhibition of 5α-reductase activity by diarylheptanoids from *Alpinia officinarum. Planta Med*. 2003; **69**, 72-4.

[98] American Type Culture Collection (ATCC). LNCaP clone FGC (ATCC® CRL-1740™), Available at: https://www.atcc.org/products/all/CRL-1740.aspx#generalinformation, accessed July 2019.

[99] P Negri-Cesi, A Poletti, A Colciago, P Magni, P Martini and M Motta. Presence of 5α-reductase isozymes and aromatase in human prostate cancer cells and in benign prostate hyperplastic tissue. *The Prostate* 1998; **34**, 283-91.

[100] K Neha and B Sangeeta. Phytochemical and pharmacological evaluation of *Tectona grandis* Linn. *Int. J. Pharm. Pharm. Sci.* 2013; **5**, 923-7.

[101] P Vyas, DK Yadav and P Khandelwal. *Tectona grandis* (teak)–A review on its phytochemical and therapeutic potential. *Nat. Prod. Res.* 2018; 1-17.

[102] P Oudhia. Medicinal herbs of Chhattisgarh, India, having less known traditional uses. I Sagon *Tectona grandis*, family Verbanaceae, Available at: http://www.Botanical.com, accessed June 2019.

[103] TK Kopa, AT Tchinda, MF Tala, D Zofou, R Jumbam, HK Wabo, VPK Titanji, M Frédérich, NH Tan and P Tane. Antiplasmodial anthraquinones and hemisynthetic derivatives from the leaves of *Tectona grandis* (Verbenaceae). *Phytochem. Lett.* 2014; **8**, 41-5.

[104] FB Niamké, N Amusant, D Stien, G Chaix, Y Lozano, AA Kadio, N Lemenager, D Goh, AA Adima, S Kati-Coulibaly and C Jay-Allemand. 4′,5′-Dihydroxy-epiisocatalponol, a new naphthoquinone from *Tectona grandis* L. f. heartwood, and fungicidal activity. *Int. Biodeterior. Biodegrad.* 2012; **74**, 93-8.

[105] W Sandermann and HH Dietrichs. Untersuchungen über termitenresistente Hölzer. *Eur. J. Wood Wood Prod.* 1957; **15**, 281-97.

[106] P Singh, S Jain and S Bhargava. A 1,4-Anthraquinone derivative from *Tectona grandis*. *Phytochemistry* 1989; **28**, 1258-9.

[107] PK Gupta and P Singh. A naphthaquinone derivative from *Tectona grandis* Linn. *J. Asian Nat. Prod. Res.* 2004; **6**, 237-40.

[108] G Lukmandaru and K Takahashi. Radial distribution of quinones in plantation teak (*Tectona grandis* L.f.). *Ann. For. Sci.* 2009; **66**, 605p1-p9.

[109] RM Khan and SM Mlungwana. 5-Hydroxylapachol: a cytotoxic agent from *Tectona grandis*. *Phytochemistry* 1999; **50**, 439-42.

[110] P Vyas, BD Wadhwani, P Khandelwal, H Araya and Y Fujimoto. Tectonaquinones A, B and C: three new naphthoquinone derivatives from the heartwood of *Tectona grandis*. *Nat. Prod. Res*. 2020; 1-9.

[111] J Smith and R Thomson. Naturally occurring quinones. Part V. Spinochromes E and N. *J. Chem. Soc. (Resumed)* 1961; 1008-12.

[112] E Windeisen, A Klassen and G Wegener. On the chemical characterisation of plantation teakwood from Panama. *Holz Roh- Werkst.* 2003; **61**, 416-8.

[113] W Sandermann and MH Simatupang. Über Inhaltsstoffe aus Teak (*Tectona grandis* L.), I. Isolierung und Konstitution eines toxischen Teakchinons. *Chem. Ber.* 1963; **96**, 2182-5.

[114] W Sandermann and MH Simatupang. Über Inhaltsstoffe aus Teak (*Tectona grandis* L.), II. Konstitution and Synthese des Tectols und Dehydrotectols. *Chem. Ber.* 1964; **97**, 588-97.

[115] K Kinzô and S Keigai. On tectoquinone, the volatile principle of the teak wood. *Bull. Chem. Soc. Jpn.* 1932; **7**, 114-27.

[116] P Sumthong, RR Romero-González and R Verpoorte. Identification of anti-wood rot compounds in teak (*Tectona grandis* L.f.) sawdust extract. *J. Wood Chem. Technol.* 2008; **28**, 247-60.

[117] P Rudman. Anthraquinones of teak (*Tectona grandis* L.F.). *Chem. Ind.* 1960; **44**, 1356-7.

[118] R Thomson. *Naturally occurring quinones*. Academic Press, London and New York, 1971, p. 12.

[119] A Burnett and R Thomson. Naturally occurring quinones. Part XV. Biogenesis of the anthraquinones in *Rubia tinctorum* L.(Madder). *J. Chem. Soc. C* 1968; 2437-41.

[120] W Sandermann and M Simatupang. Neue Chinone aus Teak (*Tectona grandis* L.). *Naturwissenschaften* 1965; **52**, 262-3.

[121] R Dayal and T Seshadri. Chemical investigation of *Tectona grandis* (roots). *J. Indian Chem. Soc.* 1979; **56**, 940-1.

[122] S Bhargava, S Jain, A Suri and P Singh. Further studies on anthraquinone derivatives from *Tectona grandis. J. Indian Chem. Soc.* 1991; **68**, 631-2.

[123] B Dhruva, A Rao, R Srinivasan and K Venkataraman. Structure of quinone from a teak tissue culture. *Indian J. Chem.* 1972; **10**, 683-5.

[124] P Singh, D Pandey, J Mathur and LP Singh. Barleriaquinone-I from the heartwood of *Tectona grandis* Linn. *J. Indian Chem. Soc.* 2008; **85**, 1060-3.

[125] SC Agarwal, MG Sarngadharan and TR Seshadri. Colouring matter of teak leaves: isolation and constitution of tectoleafquinone. *Tetrahedron Lett.* 1965; **6**, 2623-6.

[126] H Rimpler and I Christiansen. Tectograndinol, a new diterpene from *Tectona grandis* L. fil. *Z. Naturforsch., C* 1977; **32**, 724-30.

[127] NKR Pathak, P Neogi, M Biswas, Y Tripathi and VB Pandey. Betulin aldehyde, an antitumour agent from the bark of *Tectona grandis. Indian J. Pharm. Sci.* 1988; **50**, 124-5.

[128] V Ahluwalia and T Seshadri. Special chemical components of commercial woods and related plant materials, Part IV- *Tectona grandis* (Teak). *J. Sci. Ind. Res.* 1957; **16B**, 323.

[129] K Yamamoto, M Simatupang and R Hashim. Caoutchouc in teak wood (*Tectona grandis* L. f.): Formation, location, influence on sunlight irradiation, hydrophobicity and decay resistance. *Holz Roh- Werkst.* 1998; **56**, 201-9.

[130] FA Macias, A Lopez, RM Varela, A Torres and JM Molinillo. Bioactive lignans from a cultivar of *Helianthus annuus. J. Agric. Food Chem*. 2004; **52**, 6443-7.

[131] SB Varma and SP Giri. Study of wound healing activity of *Tectona grandis* Linn. leaf extract on rats. *Anc. Sci. Life* 2013; **32**, 241-4.

[132] MS Krishna and AJ Nair. Antibacterial, cytotoxic and antioxidant potential of different extracts from leaf, bark and wood of *Tectona grandis. Int. J. Pharm. Sci. Rev. Res.* 2010; **2**, 155-8.

[133] N Didry, L Dubreuil and M Pinkas. Activity of anthraquinonic and naphthoquinonic compounds on oral bacteria. *Pharmazie* 1994; **49**, 681-3.

[134] A Neamatallah, L Yan, SJ Dewar and B Austin. An extract from teak (*Tectona grandis*) bark inhibited *Listeria monocytogenes* and methicillin resistant *Staphylococcus aureus. Lett. Appl. Microbiol*. 2005; **41**, 94-6.

[135] K Purushotham, P Arun, JJ Jayarani, R Vasnthakumari, L Sankar and BR Reddy. Synergistic *in vitro* antibacterial activity of *Tectona grandis* leaves with tetracycline. *Int. J. PharmTech Res.* 2010; **2**, 519-23.

[136] K Sangeetha, I Purushothaman and S Rajarajan. Spectral characterisation, antiviral activities, in silico ADMET and molecular docking of the compounds isolated from *Tectona grandis* to chikungunya virus. *Biomed. Pharmacother.* 2017; **87**, 302-10.

[137] A Kushwah. *In-vitro* antioxidant potential and phytochemical screening of *Tectona grandis* Linn. leaves. *Int. J. Pharm. Med. Res.* 2013; **10**, 33-8.

[138] M Ghaisas, V Navghare, A Takawale, V Zope, M Tanwar and A Deshpande. Effect of *Tectona grandis* Linn. on dexamethasone-induced insulin resistance in mice. *J. Ethnopharmacol*. 2009; **122**, 304-7.

[139] Pooja, V Sharma and KC Samanta. Hypoglycemic activity of methanolic extract of *Tectona grandis* linn. Root in alloxan induced diabetic rats. *J. Appl. Pharm. Sci.* 2011; **1**, 106-9.

[140] G MP, J Himanshu, B Ishwara and SC Nitte. Anthelmintic activity of *Tectona grandis* linn fruits. *Int. Res. J. Pharm.* 2011; **2**, 219-21.

[141] S Ramachandran, B Rajini kanth, A Rajasekaran and KT Manisenthil Kumar. Evaluation of anti–inflammatory and analgesic potential of methanol extract of *Tectona grandis* flowers. *Asian. Pac. J. Trop. Biomed.* 2011; **1**, S155-S8.

[142] SP Giri and SB Varma. Analgesic and anti-inflammatory activity of *Tectona grandis* Linn. stem extract. *J. Basic Clin. Physiol. Pharmacol.* 2015; **26**, 479-84.

[143] M Asif. *In vivo* analgesic and antiinflammatory effects of *Tectona grandis* Linn. stem bark extracts. *Malays. J. Pharm. Sci.* 2011; **9**, 1-11.

[144] S Rachana. Antifungal activity screening and HPLC analysis of crude extract from *Tectona grandis*, Shilajit, *Valeriana wallachi. Electron. J. Environ., Agric. Food Chem.* 2009; **8**, 218-29.

[145] K Kore, P Jadhav, R Shete and S Shetty. Diuretic activity of *Tectona grandis* leaves aqueous extract in wistar rats. *Int. J. Pharm. Res. Dev.* 2011; **3**, 141-6.

[146] S Phalphale, A Gawai, K Biyani, R Shete, K Kore, S Chaudhari and S Magar. Evaluation of diuretic activity of *Tectona grandis* Linn. in rats. *J. Pharm. Sci.* 2013; **2**, 245-52.

[147] Pooja, V Sharma, KC Samanta and K Rathore. Antipyretic activity of methanolic extract of root of *Tectona grandis* on albino rats. *J. Pharmacol. Toxicol.* 2011; **1**, 28-33.

[148] GJ Rani and NL Bhavani. Phytochemical investigation and antipyretic activity of *Tectona grandis* Linn. *Res. J. Pharm. Technol.* 2021; **14**, 4221-5.

[149] R Goel, N Pathak, M Biswas, V Pandey and A Sanyal. Effect of lapachol, a naphthaquinone isolated from *Tectona grandis*, on experimental pepticulcer and gastric secretion. *J. Pharm. Pharmacol.* 1987; **39**, 138-40.

[150] K Anoop, TK Varun, AK Ajeesh, A Aravind, MM Azharuddin, P Praveen, MPS Ali and EJ Variyar. Screening of potential inhibitors for COVID-19 main protease from phytoconstituents of *Tectona grandis* Linn: application of molecular modeling studies. *Res. Sq.* 2021.

[151] AA Bele and A Khale. An overview on thin layer chromatography. *Int. J. Pharm. Sci. Res.* 2011; **2**, 256-67.

[152] M Jayaveersinh. *Dyeing reagents for thin-layer and paper chromatography*, 2019.

[153] B Juliane, M Mareike and M Kate. HPLC basics–principles and parameters, Available at: https://www.knauer.net/en/Systems-Solutions/Analytical-HPLC-UHPLC/HPLC-Basics---principles-and-parameters, accessed July 2022.

[154] VR Meyer. *Practical high-performance liquid chromatography*. 5th ed. John Wiley & Sons, Switzerland, 2010, p. 17-57

[155] International Conference on Harmonization (ICH). Validation of analytical procedures: Text and methodology Q2(R1), Available at: https://database.ich.org/sites/default/files/Q2%28R1%29%20Guideline.pdf, accessed June 2022.

[156] GA Shabir. Step-by-step analytical methods validation and protocol in the quality system compliance industry. *J. Valid. Technol.* 2004; **10**, 314-24.

[157] S Lawan. System suitability test in chromatographic method. *Thai J. Pharm.* 2010; **5**, 1-19.

[158] H Birch, AD Redman, DJ Letinski, DY Lyon and P Mayer. Determining the water solubility of difficult-to-test substances: A tutorial review. *Anal. Chim. Acta* 2019; **1086**, 16-28.

[159] KT Savjani, AK Gajjar and JK Savjani. Drug solubility: Importance and enhancement techniques. *ISRN Pharm.* 2012; **2012**, 1-10.

[160] PB Pathare, UL Opara and FAJ Al-Said. Colour measurement and analysis in fresh and processed foods: A review. *Food Bioprocess Technol.* 2013; **6**, 36-60.

[161] J Beetsma. The CIELAB L*a*b* system – the method to quantify colors of coatings, Available at: https://knowledge.ulprospector.com/10780/pc-the-cielab-lab-system-the-method-to-quantify-colors-of-coatings/, accessed June 2022.

[162] JW Rhim, Y Wu, CL Weller and M Schnepf. Physical characteristics of a composite film of soy protein isolate and *Propyleneglycol Alginate. J. Food Sci.* 1999; **64**, 149-52.

[163] JD Clogston and AK Patri. Zeta potential measurement. *Methods Mol. Biol.* 2011; **697**, 63-70.

[164] A Barhoum, ML García-Betancourt, H Rahier and G Van Assche. *Chapter 9 - Physicochemical characterization of nanomaterials: polymorph, composition, wettability, and thermal stability*. *In*: Emerging Applications of Nanoparticles and Architecture Nanostructures, Elsevier, 2018, p. 255-78.

[165] K Pate and P Safier. *Chemical metrology methods for CMP quality*, in *Advances in Chemical Mechanical Planarization (CMP)*. Woodhead Publishing, 2016, p. 299-325.

[166] A Kumar and CK Dixit. *Methods for characterization of nanoparticles*. *In*: Advances in Nanomedicine for the Delivery of Therapeutic Nucleic Acids, Elsevier, 2017, p. 43-58.

[167] Organization for Economic Co-operation and Development (OECD), *OECD Guidelines for the Testing of Chemicals No. 114: "Viscosity of Liquids"*. OECD Publishing, Paris, France, 2012, p. 1-6.

[168] Sanjivanjit K. Bhal. LogP-making sense of the value. Available at: https://www.acdlabs.com/download/app/physchem/making_sense.pdf, accessed December 2022.

[169] J Srivilai, N Waranuch, A Tangsumranjit, N Khorana and K Ingkaninan. Germacrone and sesquiterpene-enriched extracts from *Curcuma aeruginosa* Roxb. increase skin penetration of minoxidil, a hair growth promoter. *Drug Delivery Transl. Res.* 2018; **8**, 140-9.

[170] BS Low, BH Ng, WP Choy, KH Yuen and KL Chan. Bioavailability and pharmacokinetic studies of eurycomanone from *Eurycoma longifolia*. *Planta Med*. 2005; **71**, 803-7.

[171] K Pyrkosz-Biardzka, AZ Kucharska, A Sokół-Łętowska, P Strugała and J Gabrielska. A comprehensive study on antioxidant properties of crude extracts from fruits of *Berberis vulgaris* L., *Cornus mas* L. and *Mahonia aquifolium* Nutt. *Pol. J. Food Nutr. Sci.* 2014; **64**, 91-9.

[172] G Stefan and B Chantal. The challenges of chemical stability testing of herbal extracts in finished products using state-of-the-art analytical methodologies. *Curr. Pharm. Anal.* 2005; **1**, 203-15.

[173] E Wongwad, K Ingkaninan, W Wisuitiprot, B Sritularak and N Waranuch. Thermal degradation kinetics and pH-rate profiles of iriflophenone 3,5-C-β-D-diglucoside, iriflophenone 3-C-β-D-glucoside and mangiferin in *Aquilaria crassna* leaf extract. *Molecules* 2020; **25**, 4898.

[174] S Sipahli, V Mohanlall and JJ Mellem. Stability and degradation kinetics of crude anthocyanin extracts from *H. sabdariffa. Food Sci. Technol.* 2017; **37**, 209-15.

[175] N Suphrom, J Srivilai, G Pumthong, N Khorana, N Waranuch, N Limpeanchob and K Ingkaninan. Stability studies of antiandrogenic compounds in *Curcuma aeruginosa* Roxb. extract. *J. Pharm. Pharmacol*. 2014; **66**, 1282-93.

[176] AM Oancea, C Onofrei, M Turturică, G Bahrim, G Râpeanu and N Stănciuc. The kinetics of thermal degradation of polyphenolic compounds from elderberry (*Sambucus nigra* L.) extract. *Food Sci. Technol. Int.* 2018; **24**, 361-9.

[177] AM Oancea, M Turturică, G Bahrim, G Râpeanu and N Stănciuc. Phytochemicals and antioxidant activity degradation kinetics during thermal treatments of sour cherry extract. *LWT-Food Sci. Technol.* 2017; **82**, 139-46.

[178] T Beelders, Dd Beer and E Joubert. Thermal degradation kinetics modeling of benzophenones and xanthones during high-temperature oxidation of *Cyclopia genistoides* (L.) Vent. plant material. *J. Agric. Food Chem.* 2015; **63**, 5518-27.

[179] Q-Lab Corporation. Photostability testing for cosmetics & pharmaceuticals (ICH guidelines & forced degradation), Available at: https://www.q-lab.com/documents/public/d90a3af9-543a-48a5-9285-7865e3a9a81c.pdf, accessed October 2022.

[180] AR Bilia, MC Bergonzi, F Morgenni, G Mazzi and FF Vincieri. Evaluation of chemical stability of St. John's wort commercial extract and some preparations. *Int. J. Pharm.* 2001; **213**, 199-208.

[181] SH Kopleman, LL Augsburger, A NguyenPho, WS Zito and FX Muller. Selected physical and chemical properties of commercial *Hypericum perforatum* extracts relevant for formulated product quality and performance. *AAPS PharmSciTech* 2001; **3**, 1-18.

[182] S Barrek, O Paisse and MF Grenier-Loustalot. Analysis of neem oils by LC-MS and degradation kinetics of azadirachtin-A in a controlled environment. *Anal. Bioanal. Chem.* 2004; **378**, 753-63.

[183] AD Mali. An updated review on transdermal drug delivery systems. *Int. J. Adv. Sci. Res.* 2015; **8**, 244-54.

[184] TJ Franz. Percutaneous absorption on the relevance of *in vitro* data. *J. Invest. Dermatol.* 1975; **64**, 190-5.

[185] A Haq, M Dorrani, B Goodyear, V Joshi and B Michniak-Kohn. Membrane properties for permeability testing: Skin versus synthetic membranes. *Int. J. Pharm.* 2018; **539**, 58-64.

[186] BW Barry. Modern methods of promoting drug absorption through the skin. *Mol. Aspects Med.* 1991; **12**, 195-241.

[187] A Haq, B Goodyear, D Ameen, V Joshi and B Michniak-Kohn. Strat-M® synthetic membrane: Permeability comparison to human cadaver skin. *Int. J. Pharm.* 2018; **547**, 432-7.

[188] R Neupane, SHS Boddu, J Renukuntla, RJ Babu and AK Tiwari. Alternatives to biological skin in permeation studies: Current trends and possibilities. *Pharmaceutics* 2020; **12**, 152.

[189] T Shukla, N Upmanyu, M Agrawal, S Saraf, S Saraf and A Alexander. Biomedical applications of microemulsion through dermal and transdermal route. *Biomed. Pharmacother*. 2018; **108**, 1477-94.

[190] J Hadgraft. Skin, the final frontier. *Int. J. Pharm*. 2001; **224**, 1-18.

[191] S Nafisi and HI Maibach. *Chapter 3 - Skin penetration of nanoparticles*, in *Emerging Nanotechnologies in Immunology*. Elsevier, Boston, 2018, p. 47-88.

[192] MA Bolzinger, S Briançon, J Pelletier and Y Chevalier. Penetration of drugs through skin, a complex rate-controlling membrane. *Curr. Opin. Colloid Interface Sci.* 2012; **17**, 156-65.

[193] S Supe and P Takudage. Methods for evaluating penetration of drug into the skin: A review. *Sking Res. Technol.* 2020; **00**, 1-10.

[194] J Srivilai, K Rabgay, N Khorana, N Waranuch, N Nuengchamnong and K Ingkaninan. A new label-free screen for steroid 5α-reductase inhibitors using LC-MS. *Steroids* 2016; **116**, 67-75.

[195] J Srivilai, K Rabgay, N Khorana, N Waranuch, N Nuengchamnong, W Wisuitiprot, T Chuprajob, C Changtam, A Suksamrarn, W Chavasiri, N Sornkaew and K Ingkaninan. Anti-androgenic curcumin analogues as steroid 5α-reductase inhibitors. *Med. Chem. Res.* 2017; **26**, 1550-6.

[196] ICH Q2 (R1). Validation of analytical procedures: text and methodology, Available at: https://www.ema.europa.eu/en/documents/scientific-guideline/ich-q-2-r1-validation-analytical-procedures-text-methodology-step-5_en.pdf, accessed January 2023.

[197] Organization for Economic Co-operation and Development (OECD), *OECD Guidelines for the Testing of Chemicals No. 105: "Water Solubility"*. OECD Publishing, Paris, France,1995, p. 1-7.

[198] Organization for Economic Co-operation and Development (OECD), *OECD Guidelines for the Testing of Chemicals No. 117: "Partition Coefficient (n-octanol/water), HPLC Method"*. OECD Publishing, Paris, France, 2004, p. 1-11.

[199] ICH Q1B. Stability testing: photostability testing of new drug substances and products, Available at: https://database.ich.org/sites/default/files/Q1B%20Guideline.pdf, accessed March 2023.

[200] N Ngamdokmai, K Ingkaninan, N Chaichamnong, K Chootip, N Neungchamnong and N Waranuch. Development, characterization, and stability evaluation of the anti-cellulite emgel containing herbal extracts and essential oils. *Pharmaceuticals* 2021; **14**, 1-15.

[201] KK Onyechi and CA Igwegbe. Shelf life assessment of *Picralima nitida* and glibenclamide using bio-based dose-response relationship method. *Asian J. Med. Pharm. Sci*. 2019; **6**, 1-10.

[202] Organization for Economic Co-operation and Development (OECD). *OECD Guidelines for the Testing of Chemicals No. 428: "Skin Absorption: in vitro Method"*. OECD Publishing, Paris, France, 2004, p. 1-8.

[203] W Aoki, T Ohtsuki, SK Sadhu, M Sato, T Koyano, S Preeprame, T Kowithayakorn and M Ishibashi. First isolation of three diterpenes as naturally-occurring compounds from *Sindora siamensis*. *J. Nat. Med.* 2007; **61**, 77-9.

[204] AJ Marsaioli, HFL Filho and JdP Campello. Diterpenes in the bark of *Hymenea coubaril*. *Phytochemistry* 1975; **14**, 1882-3.

[205] PM Imamura, AJ Marsaioli, LE Barata and EA Rúveda. ^{13}C NMR spectral analysis of eperuane diterpenes. *Phytochemistry* 1977; **16**, 1842-4.

[206] S Mouffok, H Haba, C Lavaud, C Long and M Benkhaled. Chemical constituents of *Centaurea omphalotricha* Coss. & Durieu ex Batt. & Trab. *Rec. Nat. Prod*. 2012; **6**, 292-5.

[207] N Ungur, M Gavagnin and G Cimino. Synthesis of diastereoisomeric *ent*-isocopalic acid glycerides. *Tetrahedron Lett.* 1996; **37**, 3549-52.

[208] N Ungur, M Gavagnin, A Fontana and G Cimino. Synthetic studies on natural diterpenoid glyceryl esters. *Tetrahedron* 2000; **56**, 2503-12.

[209] PF Vlad, N Ungur, NV Hung and VB Perutsky. Superacidic low-temperature cyclization of terpenols and their acetates. *Russ. Chem. Bull*. 1995; **44**, 2390-403.

[210] H Suzuki, M Noma and N Kawashima. Two labdane diterpenoids from *Nicotiana setchellii*. *Phytochemistry* 1983; **22**, 1294-5.

[211] JPBd Sousa, D Nanayakkara, AAB Silva and JK Bastos. Leishmanicidal and antimalarial activities of crude extracts from aerial parts of *Copaifera langsdorffii* and isolation of secondary metabolites. *J. Pharm. Res.* 2012; **5**, 4103-7.

[212] W Xiang, RT Li, QS Song, Z Na and HD Sun. *ent*-Clerodanoids from *Isodon scoparius*. *Helv. Chim. Acta* 2004; **87**, 2860-5.

[213] P Jain and S Bari. Isolation of lupeol, stigmasterol and campesterol from petroleum ether extract of woody stem of *Wrightia tinctoria. Asian J. Plant Sci*. 2010; **9**, 163-7.

[214] D Pandya and I Anand. Isolation and high-performance thin layer chromatographic estimation of Lupeol from *Oxystelma esculentum. Pharm. Methods* 2011; **2**, 99-105.

[215] K Díaz, L Espinoza, A Madrid, L Pizarro and R Chamy. Isolation and identification of compounds from bioactive extracts of *Taraxacum officinale* Weber ex F. H. Wigg. (Dandelion) as a potential source of antibacterial agents. *Evid. Based Complement. Alternat. Med.* 2018; **2018**, 1-8.

[216] J Liu, K Kurashiki, K Shimizu and R Kondo. Structure-activity relationship for inhibition of 5α-reductase by triterpenoids isolated from *Ganoderma lucidum. Bioorg. Med. Chem.* 2006; **14**, 8654-60.

[217] J Srivilai, N Khorana, N Waranuch, W Wisuitiprot, N Suphrom, A Suksamrarn and K Ingkaninan. Germacrene analogs are anti-androgenic on androgen-dependent cells. *Nat. Prod. Commun.* 2016; **11**, 1934578X1601100906.

[218] A Guarna, EG Occhiato, F Machetti, A Trabocchi, D Scarpi, G Danza, R Mancina, A Comerci and M Serio. Effect of C-ring modifications in benzo[c]quinolizin-3-ones, new selective inhibitors of human 5 alpha-reductase 1. *Bioorg. Med. Chem*. 2001; **9**, 1385-93.

[219] JA Sánchez-Burgos, M Ramírez-Mares, J Gallegos-Infante, R González-Laredo, M Moreno-Jiménez, MH Cháirez-Ramírez, L Medina-Torres and N Rocha-Guzmán. Isolation of lupeol from white oak leaves and its anti-inflammatory activity. *Ind. Crops Prod*. 2015; **77**, 827-32.

[220] J Fotie, DS Bohle, ML Leimanis, E Georges, G Rukunga and AE Nkengfack. Lupeol long-chain fatty acid esters with antimalarial activity from *Holarrhena floribunda. J. Nat. Prod*. 2006; **69**, 62-7.

[221] L Martini. How to defeat male pattern alopecia in a trompeur de femmes, who loves to abuse of libido boosters?. *Our Dermatology Online* 2018; **9**, 207-9.

[222] AAM Sohag, MT Hossain, MA Rahaman, P Rahman, MS Hasan, RC Das, MK Khan, MH Sikder, M Alam, MJ Uddin, MDH Rahman, M Tahjib-Ul-Arif, T

Islam, IS Moon and MA Hannan. Molecular pharmacology and therapeutic advances of the pentacyclic triterpene lupeol. *Phytomedicine* 2022; **99**, 154012.

[223] HR Siddique, SK Mishra, RJ Karnes and M Saleem. Lupeol, a novel androgen receptor inhibitor: implications in prostate cancer therapy. *Clin. Cancer Res*. 2011; **17**, 5379-91.

[224] DW Lachenmeier. Safety evaluation of topical applications of ethanol on the skin and inside the oral cavity. *J. Occup. Med. Toxicol*. 2008; **3**, 1-16.

[225] J Oh and MK Kim. Effect of alternative preservatives on the quality of rice cakes as halal food. *Foods* 2021; **10**, 2291.

[226] AR Mansur, J Oh, HS Lee and SY Oh. Determination of ethanol in foods and beverages by magnetic stirring-assisted aqueous extraction coupled with GC-FID: A validated method for halal verification. *Food Chem.* 2022; **366**, 130526.

[227] S Stegemann, F Leveiller, D Franchi, H de Jong and H Lindén. When poor solubility becomes an issue: from early stage to proof of concept. *Eur. J. Pharm. Sci.* 2007; **31**, 249-61.

[228] AC Williams and BW Barry. Penetration enhancers. *Adv. Drug Delivery Rev.* 2004; **56**, 603-18.

[229] AC Williams and BW Barry. Penetration enhancers. *Adv. Drug Delivery Rev.* 2012; **64**, 128-37.

[230] DB Braun and MR Rosen. *Part 1 - Practical Rheology*, in *Rheology Modifiers Handbook*. William Andrew Publishing, Oxford, UK, 1999, p. 1-69.

[231] H Zhu, EC Jung, X Hui and H Maibach. Proposed human stratum corneum water domain in chemical absorption. *J. Appl. Toxicol*. 2016; **36**, 991-6.

[232] F Hafeez and H Maibach. Occlusion effect on *in vivo* percutaneous penetration of chemicals in man and monkey: partition coefficient effects. *Skin Pharmacol. Physiol.* 2013; **26**, 85-91.

[233] E Wongwad, K Ingkaninan, W Wisuitiprot and N Waranuch. The fabric facial mask enhanced skin permeation of hydrophilic bioactive compounds in *Aquilaria crassna* leaf extract. *Songklanakarin J. Sci. Technol.* 2021; **43**, 1335-41.

[234] A Ornelas, N Zacharias-Millward, DG Menter, JS Davis, L Lichtenberger, D Hawke, E Hawk, E Vilar, P Bhattacharya and S Millward. Beyond COX-1: the

effects of aspirin on platelet biology and potential mechanisms of chemoprevention. *Cancer Metastasis Rev.* 2017; **36**, 289-303.

[235] M Lukić, I Pantelić and SD Savić. Towards optimal pH of the skin and topical formulations: From the current state of the art to tailored products. *Cosmetics* 2021; **8**, 69.

[236] J McMurry. *Organic chemistry with biological applications*. 2nd ed. Brooks/Cole Cengage Learning, USA, 2007, p. 223-6.

[237] NH Rhys, RJ Gillams, LE Collins, SK Callear, MJ Lawrence and SE McLain. On the structure of an aqueous propylene glycol solution. *J. Chem. Phys.* 2016; **145**, 224504.

[238] PJ Sinko. *Martin's physical pharmacy and pharmaceutical sciences*. 6th ed. Lippincott Williams and Wilkins, USA, 2006, p. 409.

[239] R Cassano, T Ferrarelli, MV Mauro, P Cavalcanti, N Picci and S Trombino. Preparation, characterization and *in vitro* activities evaluation of solid lipid nanoparticles based on PEG-40 stearate for antifungal drugs vaginal delivery. *Drug Deliv.* 2016; **23**, 1037-46.

[240] A Wichit, A Tangsumranjit, T Pitaksuteepong and N Waranuch. Polymeric micelles of PEG-PE as carriers of all-trans retinoic acid for stability improvement. *AAPS PharmSciTech.* 2012; **13**, 336-43.

[241] GW McGraw, RW Hemingway, LL Ingram, CS Canady and WB McGraw. Thermal degradation of terpenes: camphene, Δ^3-carene, limonene, and alpha-terpinene. *Environ. Sci. Technol.* 1999; **33**, 4029-33.

[242] SA Khayyat and LS Roselin. Recent progress in photochemical reaction on main components of some essential oils. *J. Saudi Chem. Soc.* 2018; **22**, 855-75.

[243] V Srivastava, PK Singh and PP Singh. Visible Light Promoted Allylic C-H Oxidation. *Croat. Chem. Acta.* 2017; **90**, 435-42.

[244] Bharat Petroleum. Preliminary feasibility report for polyol/propylene glycol/mono ethylene glycol petrochemical project, Available at: https://environmentclearance.nic.in/writereaddata/Online/TOR/24_Nov_2017_175437307BRBUXERUPreliminaryFeasibilityReport.pdf, accessed July 2023.

[245] T Haque and MMU Talukder. Chemical Enhancer: A Simplistic Way to Modulate Barrier Function of the Stratum Corneum. *Adv. Pharm. Bull.* 2018; **8**, 169-79.

[246] QD Pham, S Björklund, J Engblom, D Topgaard and E Sparr. Chemical penetration enhancers in stratum corneum - Relation between molecular effects and barrier function. *J. Control Release* 2016; **232**, 175-87.

[247] A Herman and AP Herman. Essential oils and their constituents as skin penetration enhancer for transdermal drug delivery: a review. *J. Pharm. Pharmacol*. 2015; **67**, 473-85.

[248] M Rizwan, M Aqil, A Ahad, Y Sultana and MM Ali. Transdermal delivery of valsartan: I. Effect of various terpenes. *Drug Dev. Ind. Pharm.* 2008; **34**, 618-26.

[249] T Imura, T Morita, T Fukuoka, M Ryu, K Igarashi, Y Hirata and D Kitamoto. Spontaneous vesicle formation from sodium salt of acidic sophorolipid and its application as a skin penetration enhancer. *J. Oleo Sci.* 2014; ess13117.

APPENDIX

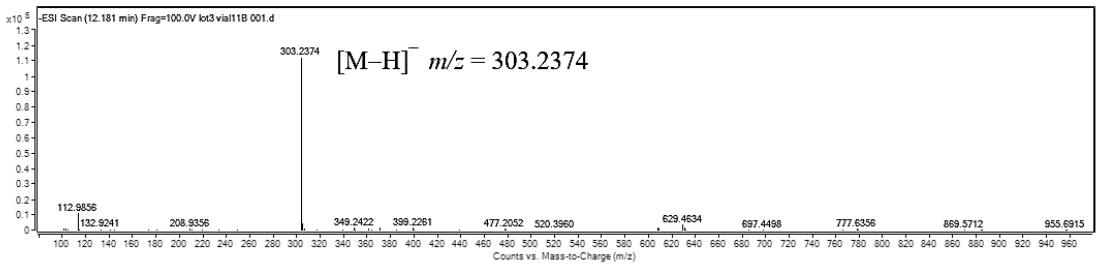

Figure 46 HRESI–MS (negative ion mode) spectrum of **1**

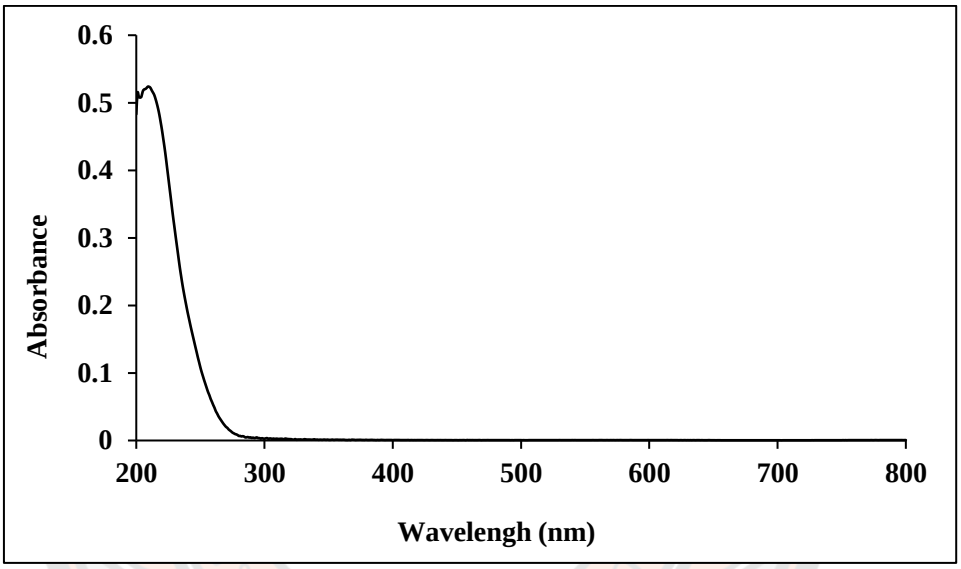

Figure 47 UV absorption spectrum of **1**

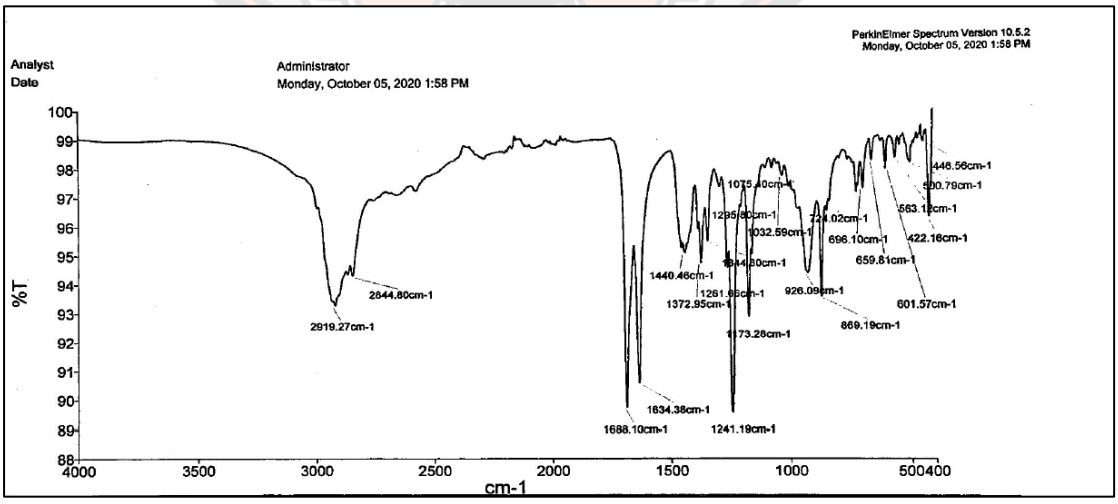

Figure 48 FT–IR (ATR mode) spectrum of **1**

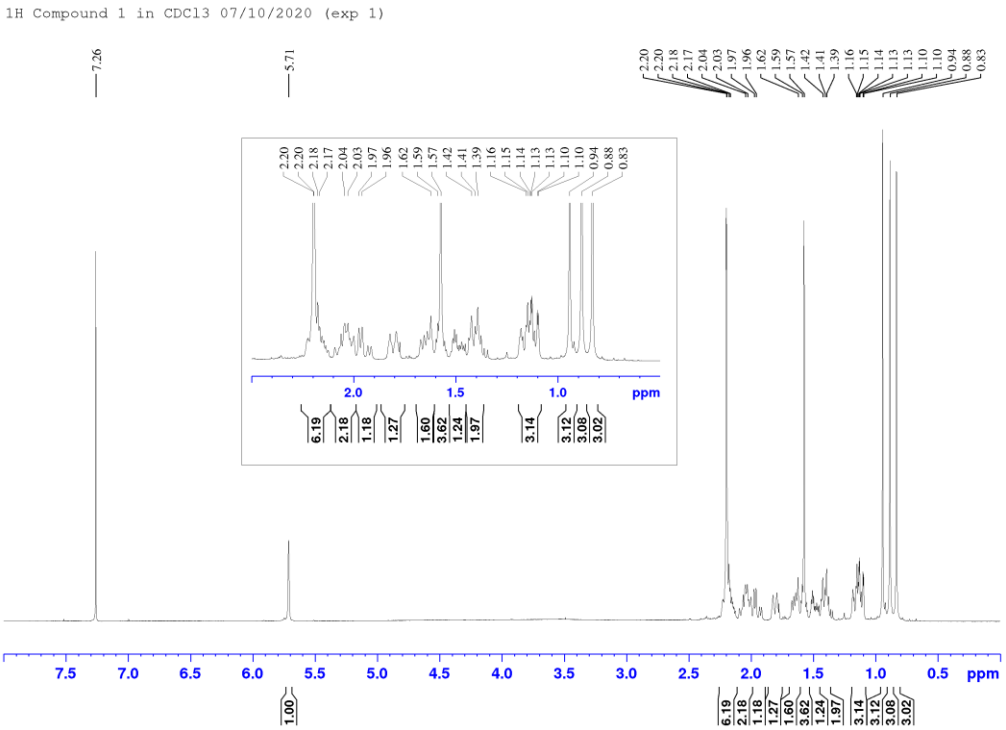

Figure 49 ^{1}H–NMR spectrum of **1** (400 MHz, $CDCl_3$)

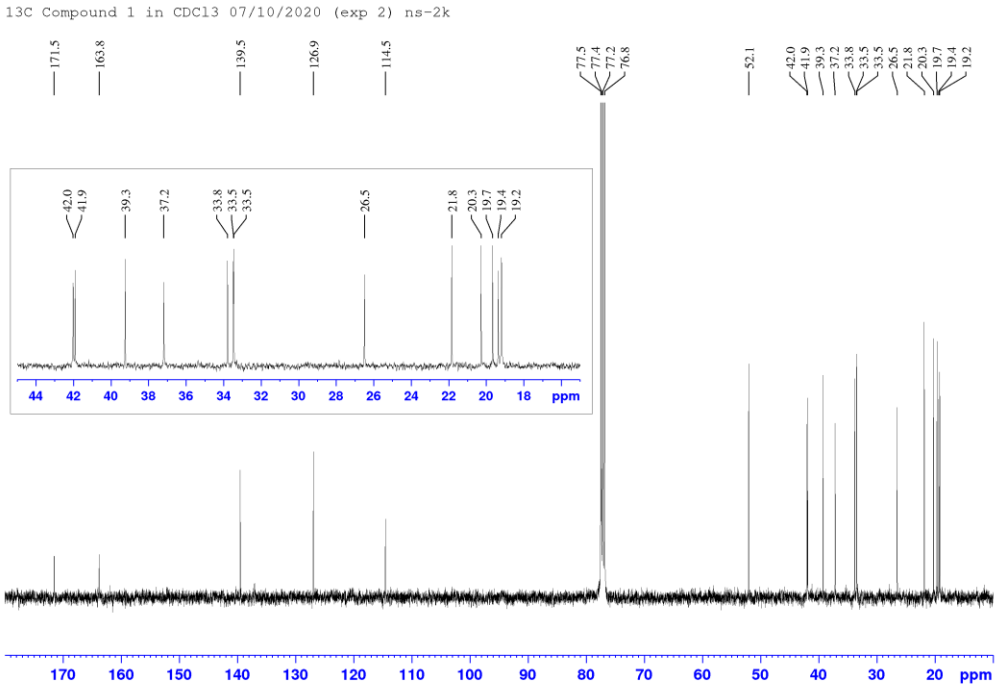

Figure 50 ^{13}C–NMR spectrum of **1** (100 MHz, $CDCl_3$)

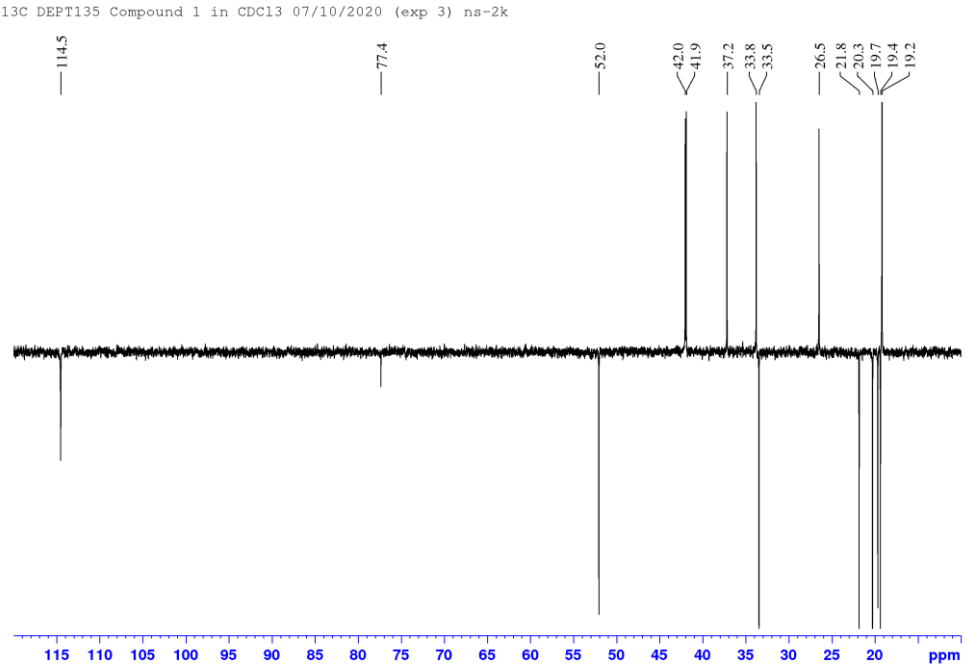

Figure 51 DEPT 135 spectrum of **1** (100 MHz, $CDCl_3$)

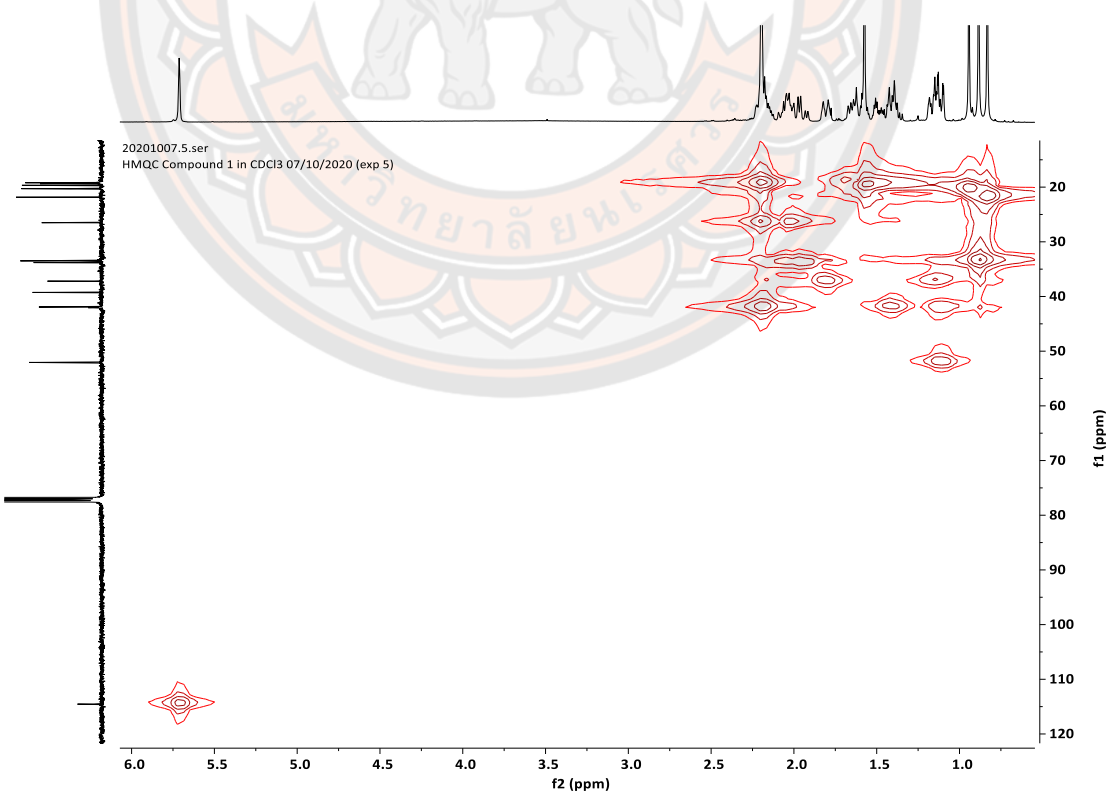

Figure 52 HMQC spectrum of **1** (400 MHz for ^{1}H and 100 MHz for ^{13}C, $CDCl_3$)

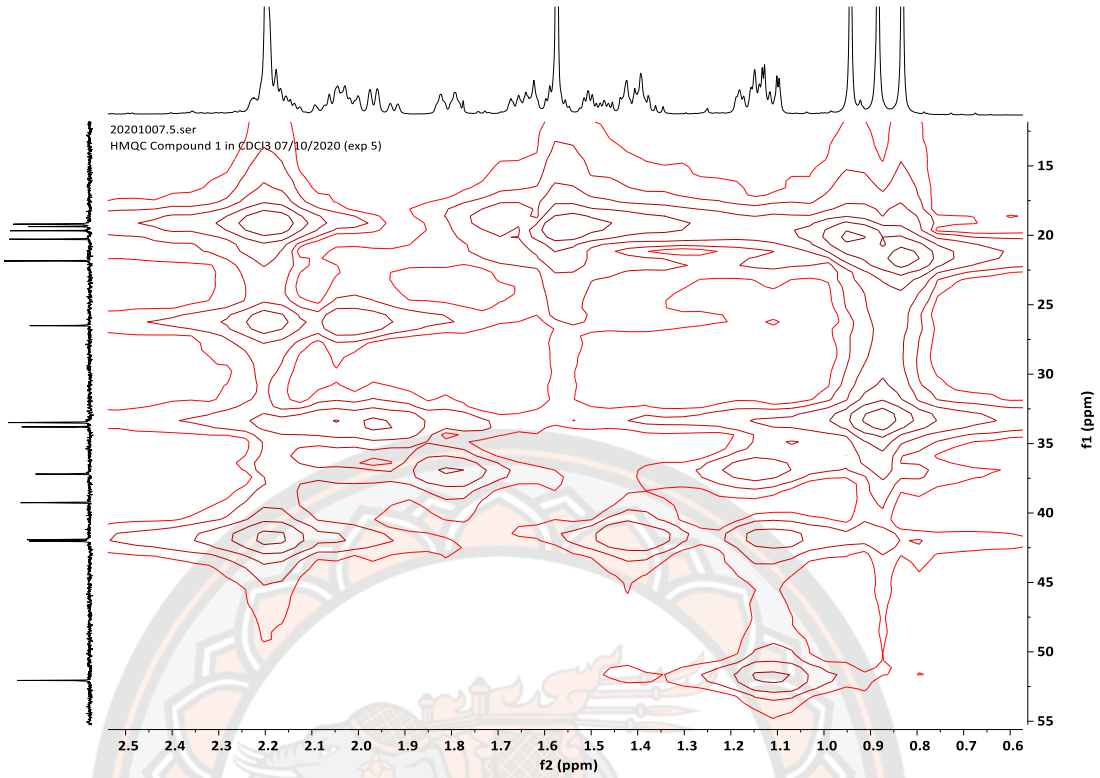

Figure 53 Enlarged HMQC spectrum of **1** (400 MHz for ^{1}H and 100 MHz for ^{13}C, $CDCl_3$)

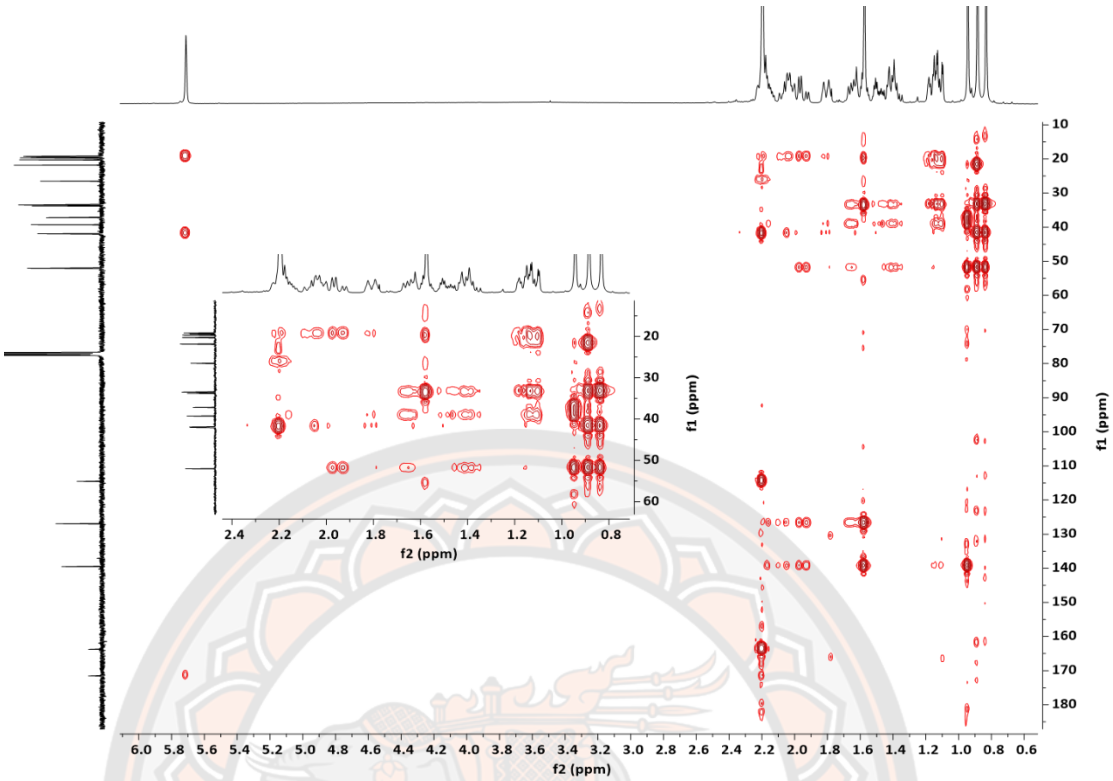

Figure 54 HMBC spectrum of **1** (400 MHz for ^{1}H and 100 MHz for ^{13}C, $CDCl_3$)

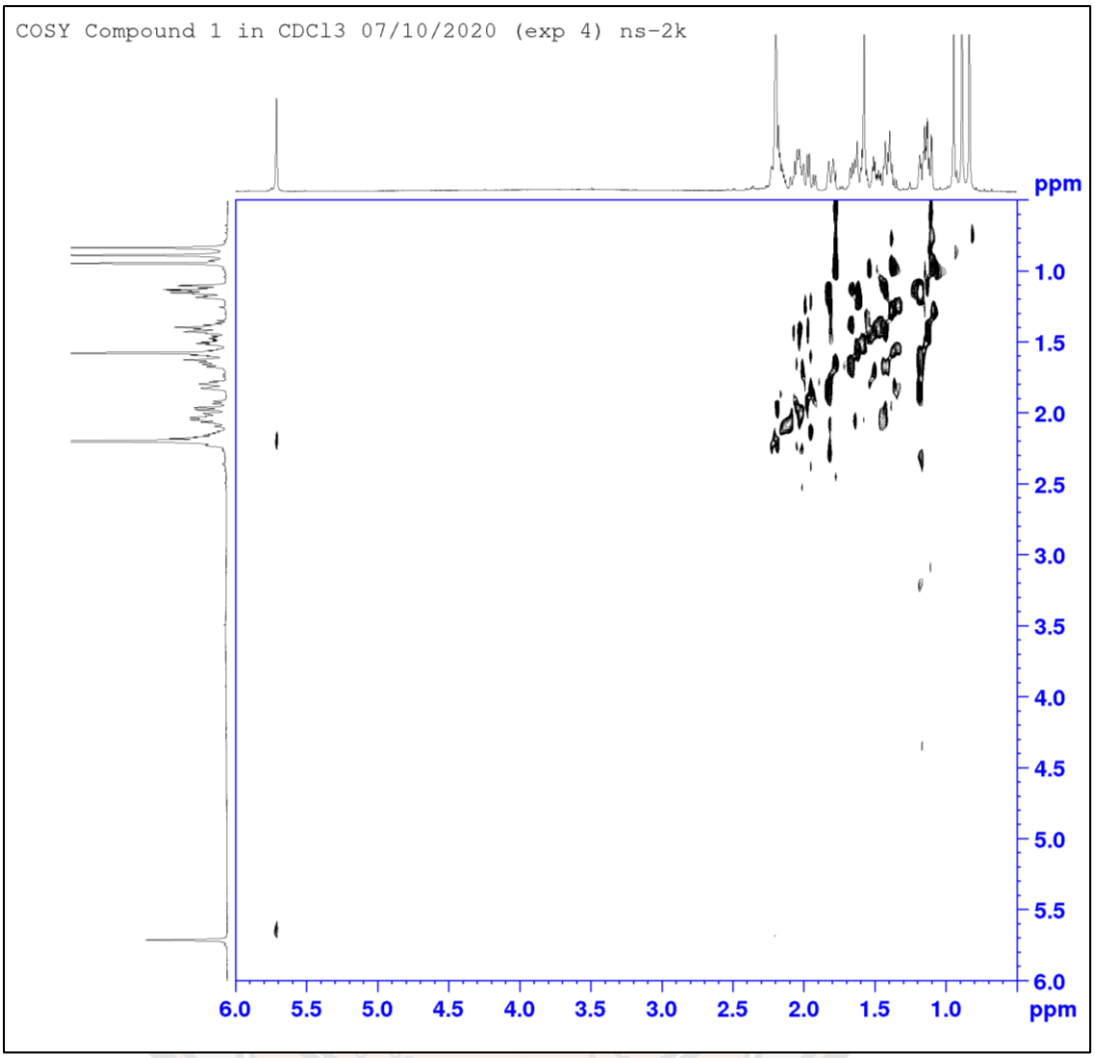

Figure 55 COSY spectrum of **1** (400 MHz, $CDCl_3$)

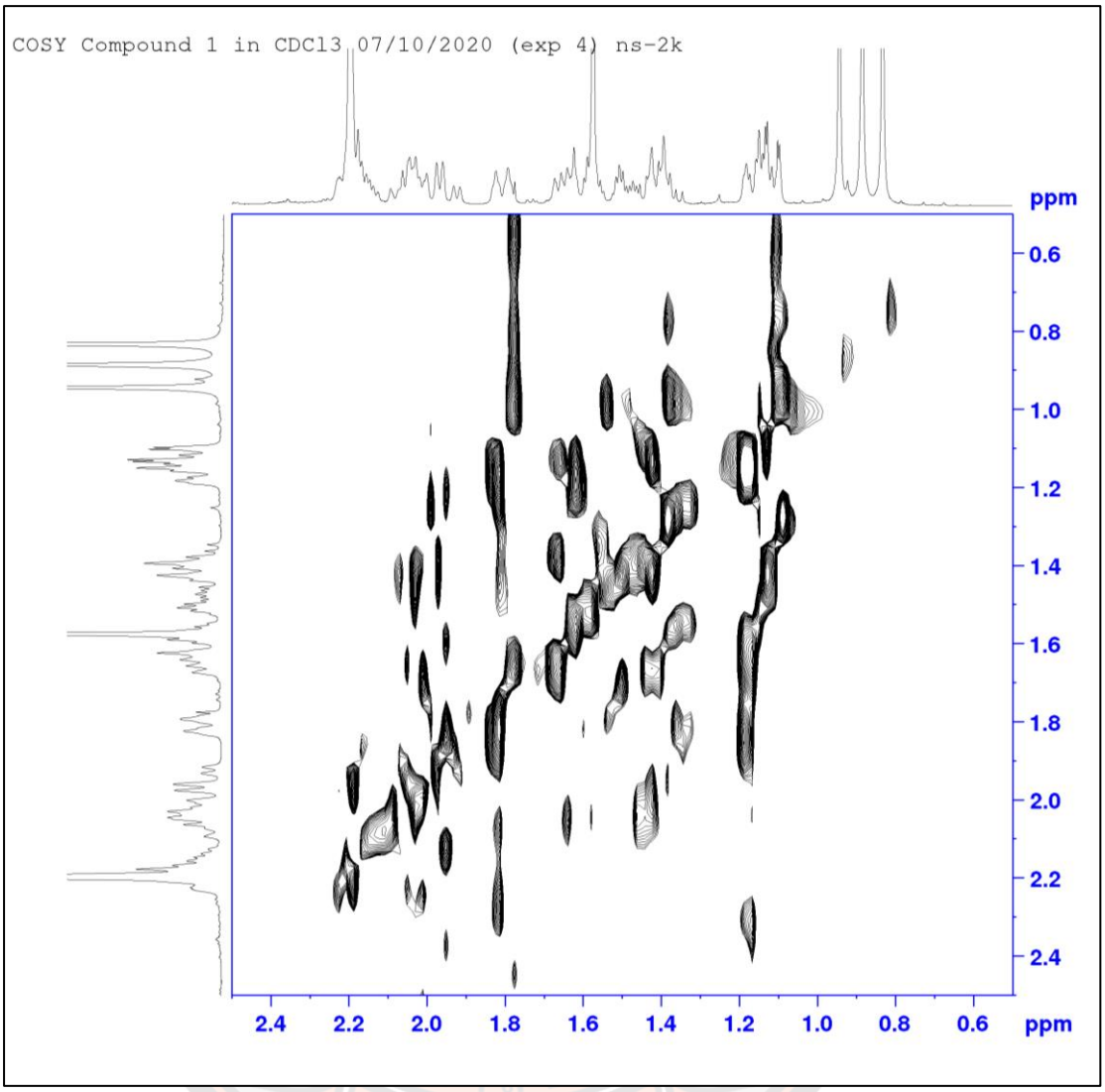

Figure 56 Enlarged COSY spectrum of **1** (400 MHz, $CDCl_3$)

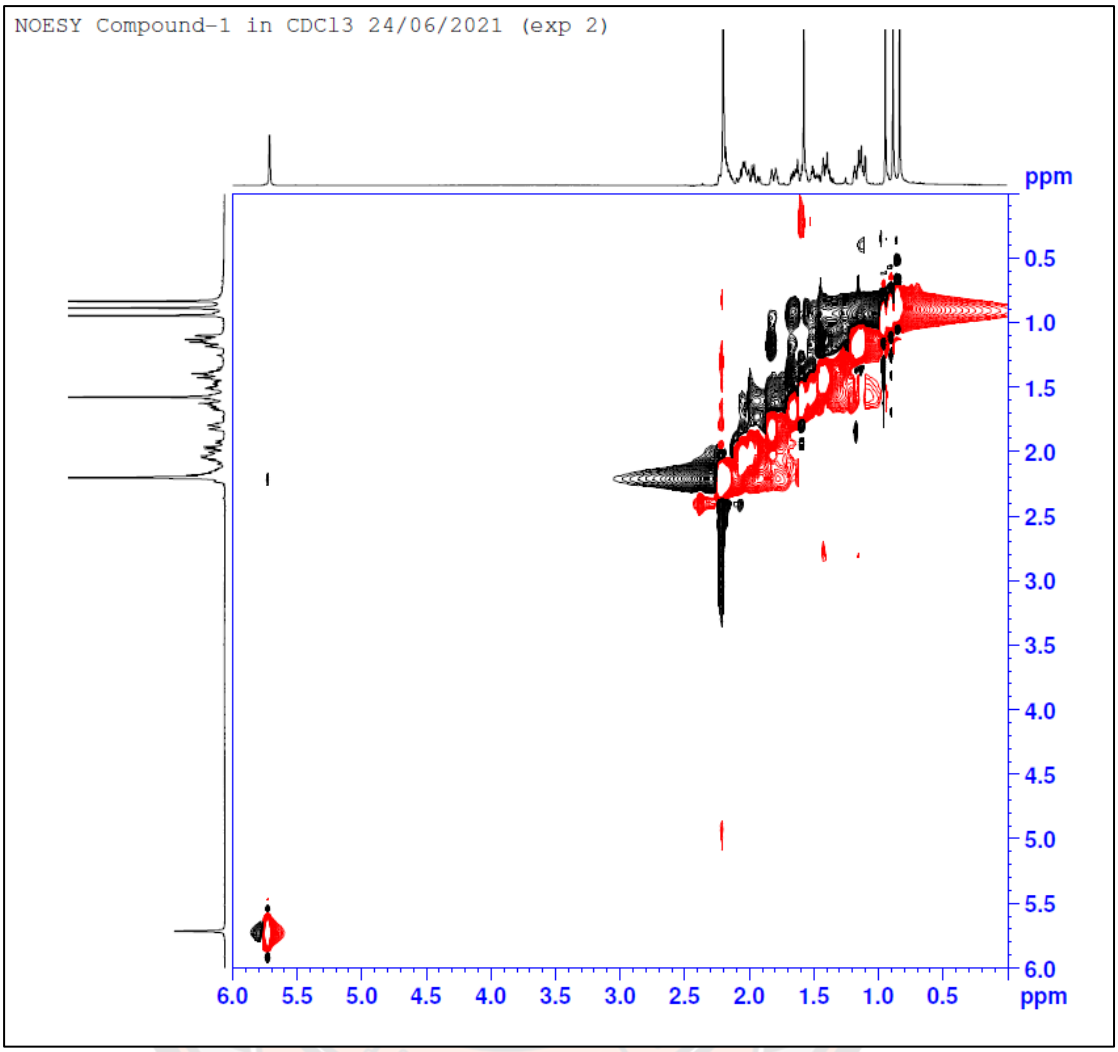

Figure 57 NOESY spectrum of **1** (400 MHz, $CDCl_3$)

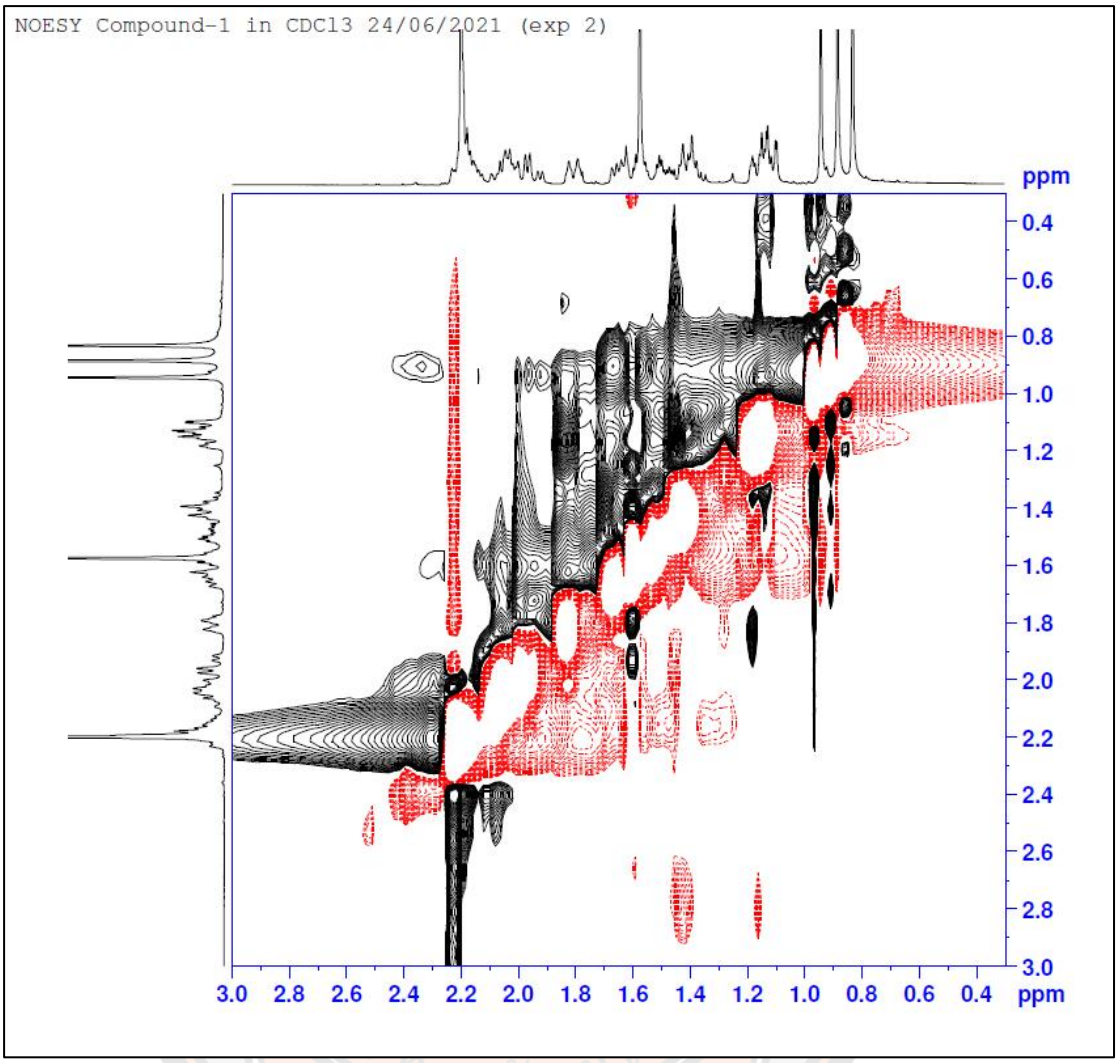

Figure 58 An expanded region NOESY spectrum of **1** (400 MHz, $CDCl_3$), the chemical shift at 0.3-3.0 ppm

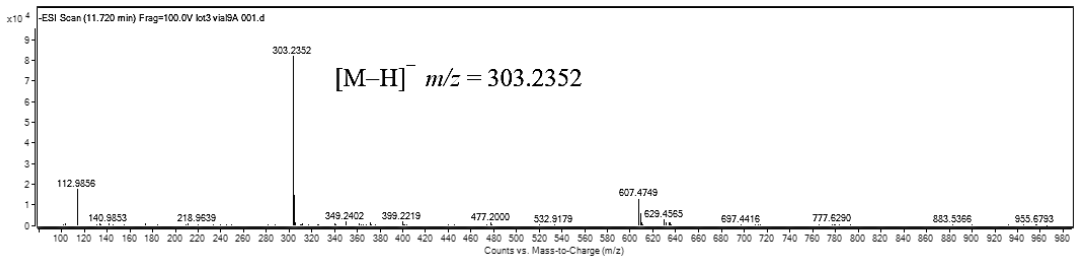

Figure 59 HRESI–MS (negative ion mode) spectrum of **2**

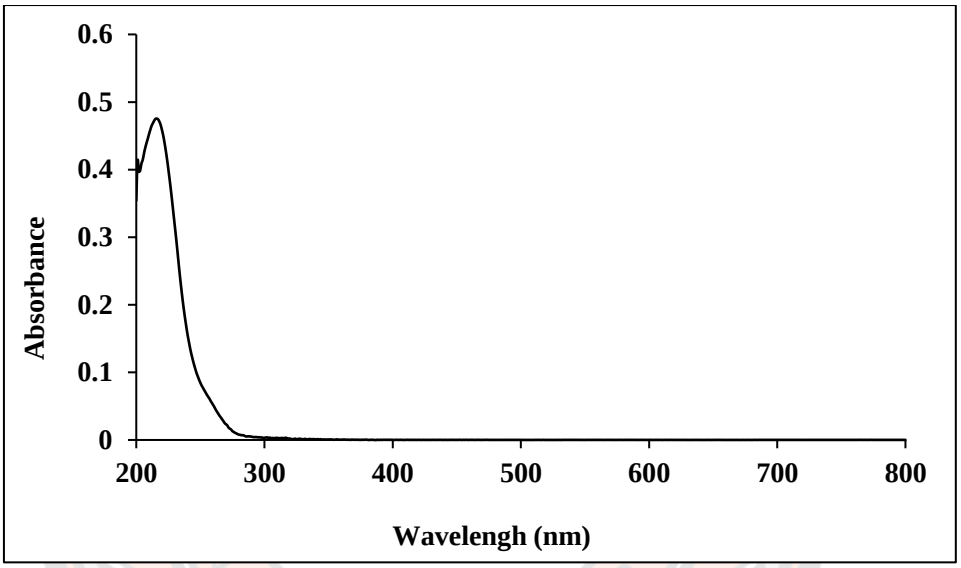

Figure 60 UV absorption spectrum of **2**

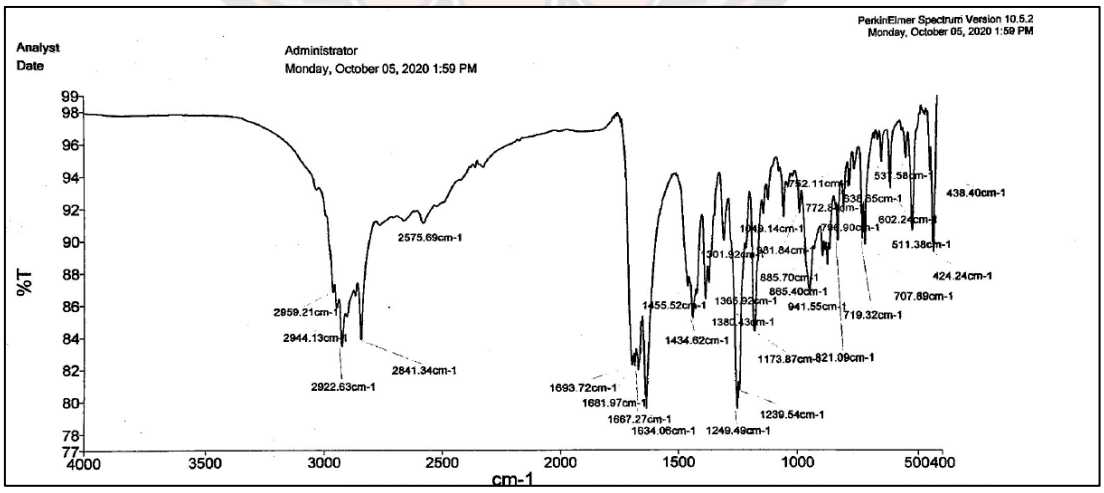

Figure 61 FT–IR (ATR mode) spectrum of **2**

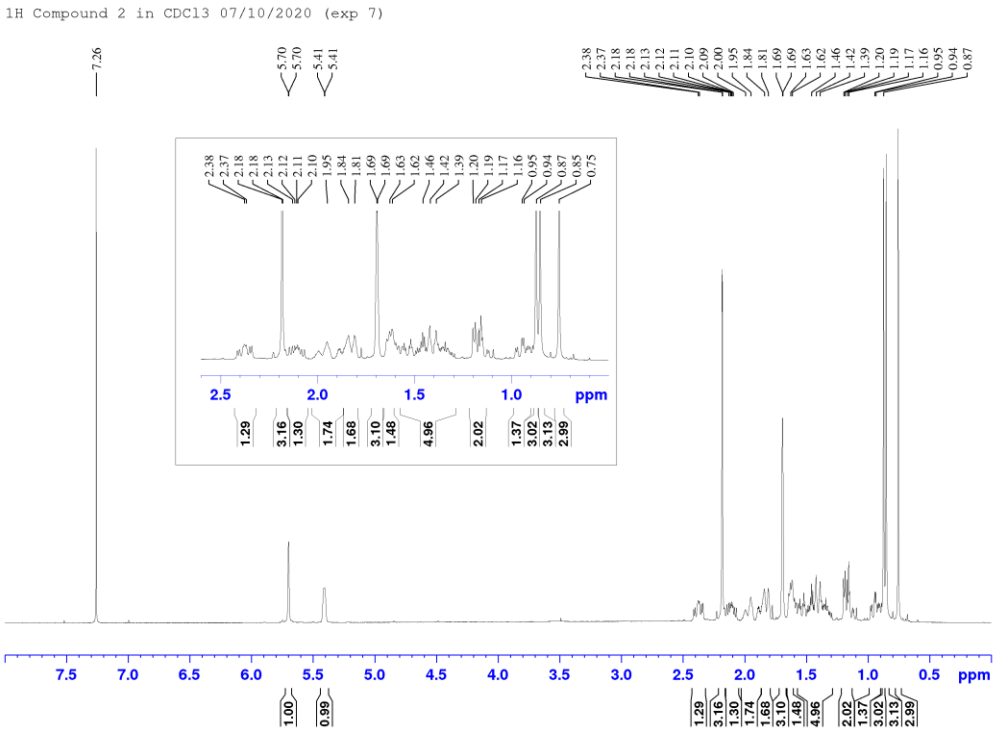

Figure 62 ^{1}H–NMR spectrum of **2** (400 MHz, $CDCl_3$)

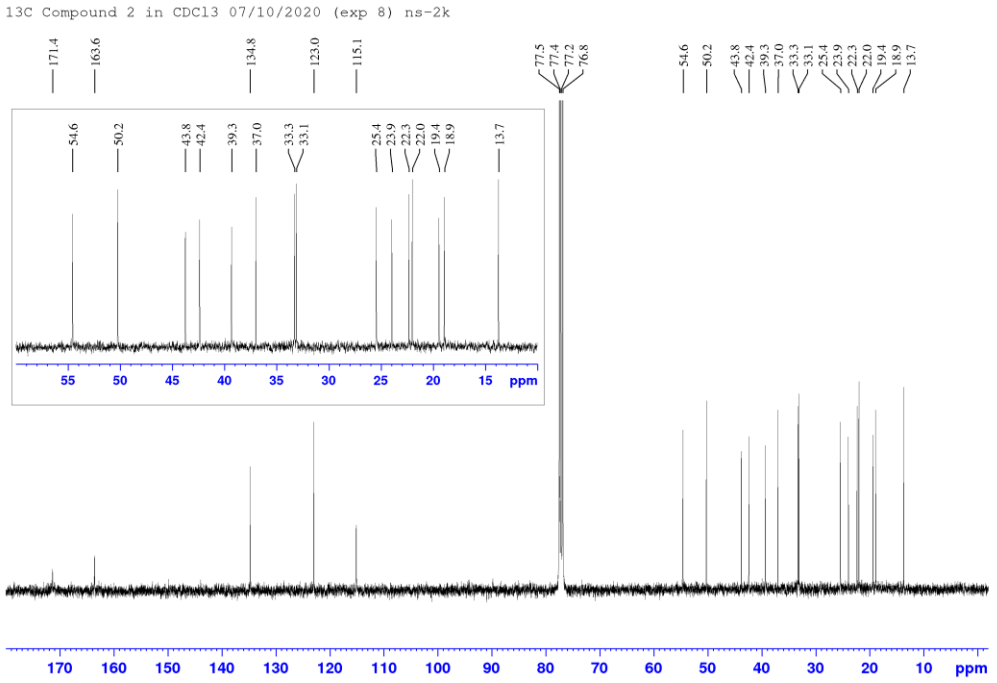

Figure 63 ^{13}C–NMR spectrum of **2** (100 MHz, $CDCl_3$)

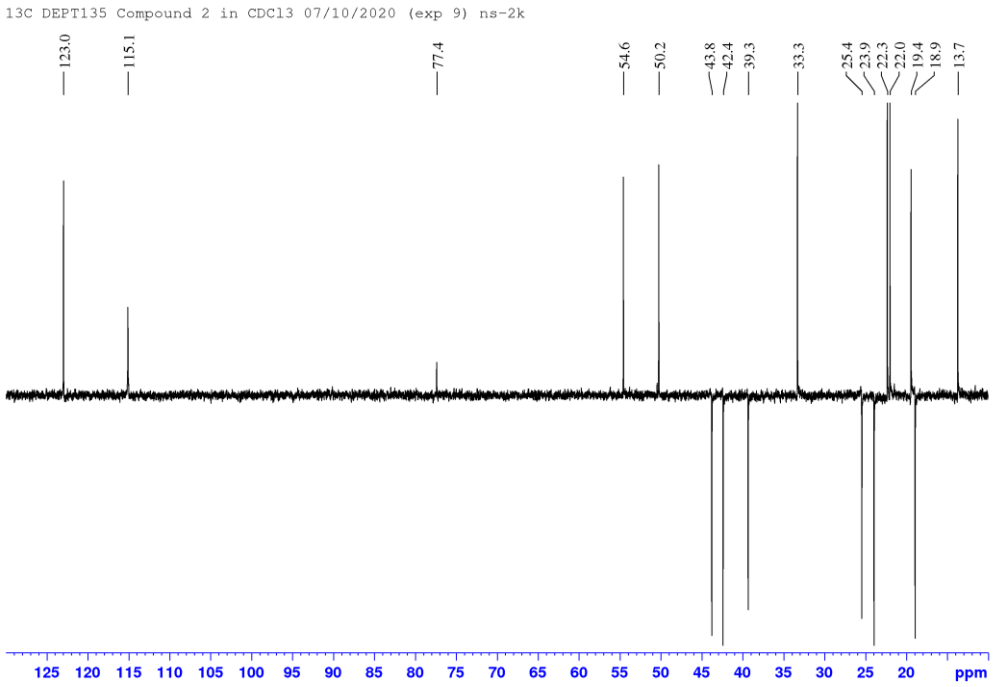

Figure 64 DEPT 135 spectrum of **2** (100 MHz, $CDCl_3$)

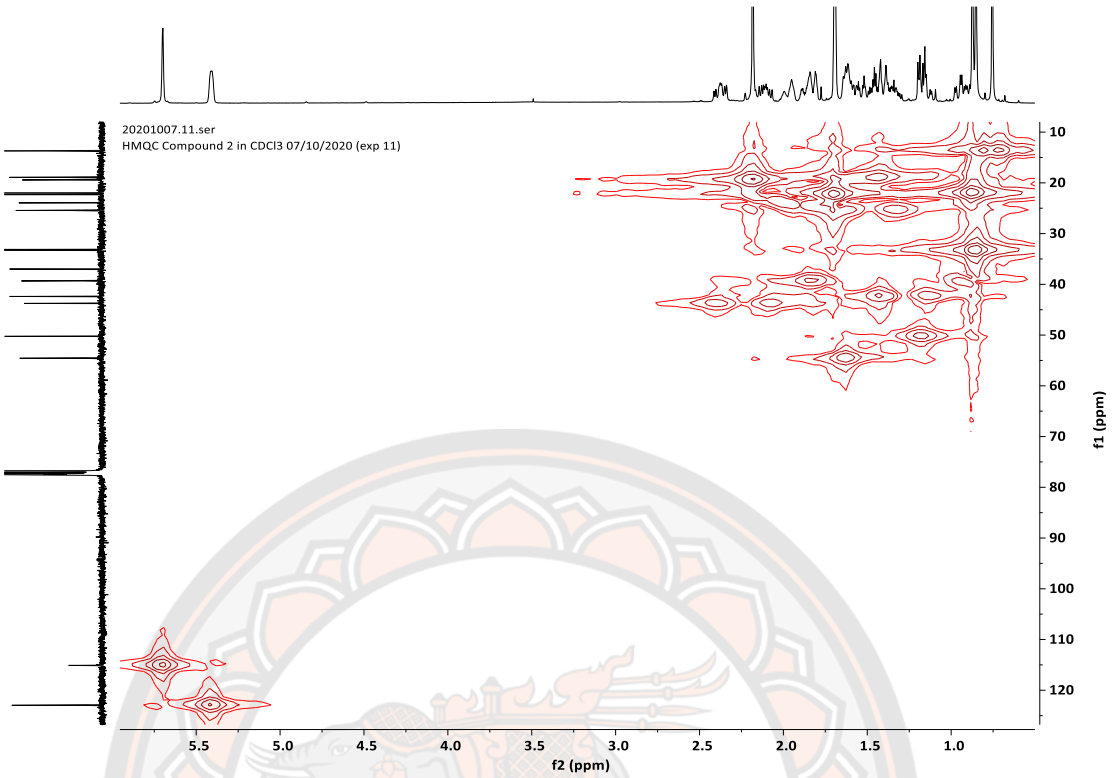

Figure 65 HMQC spectrum of **2** (400 MHz for ^{1}H and 100 MHz for ^{13}C, $CDCl_3$)

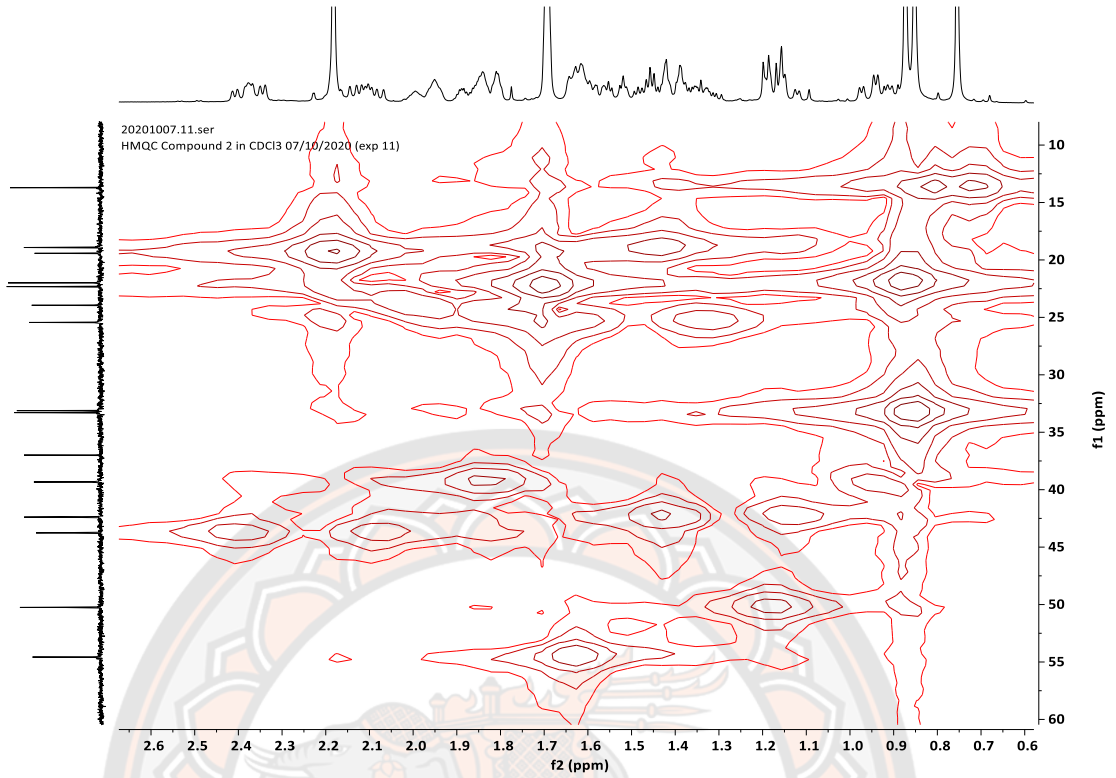

Figure 66 Enlarged HMQC spectrum of **2** (400 MHz for ^{1}H and 100 MHz for ^{13}C, $CDCl_3$)

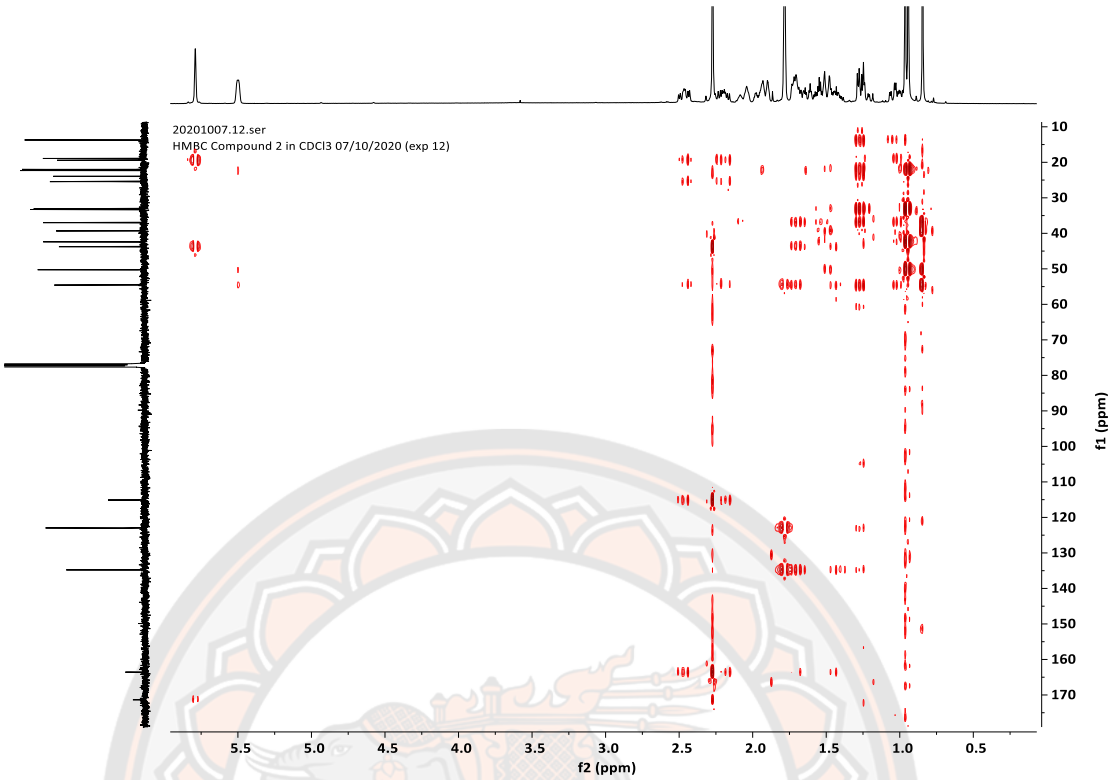

Figure 67 HMBC spectrum of **2** (400 MHz for ^{1}H and 100 MHz for ^{13}C, $CDCl_3$)

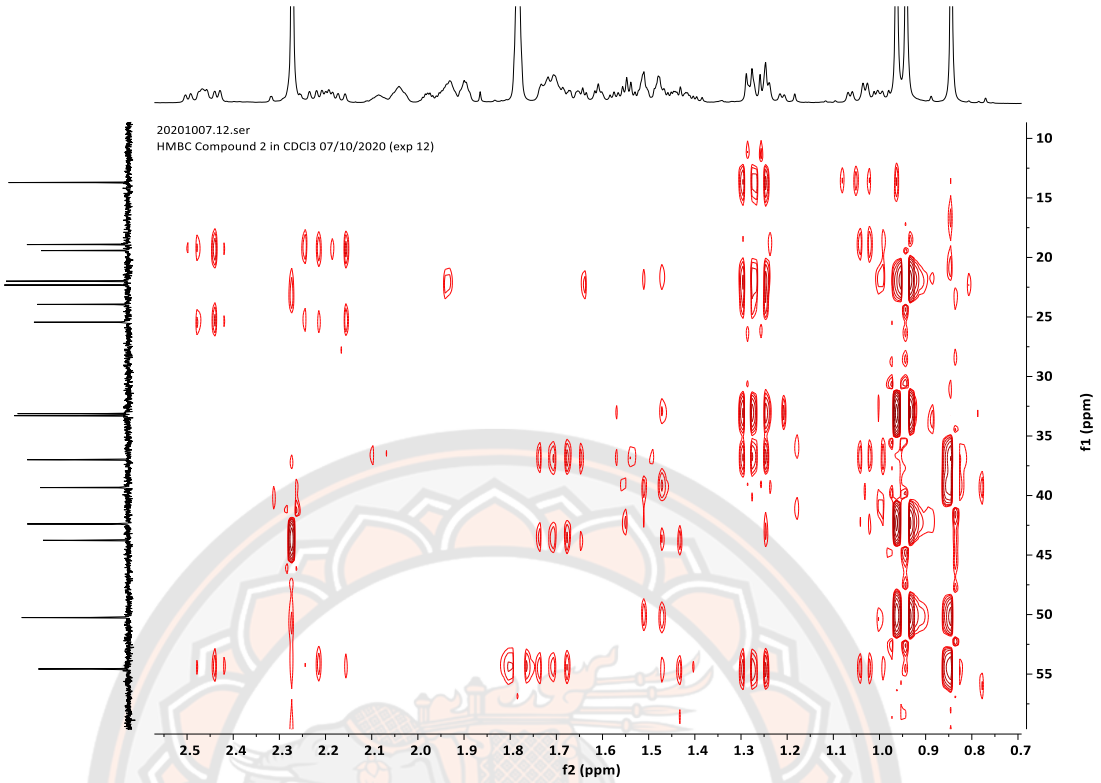

Figure 68 Enlarged HMBC spectrum of **2** (δ_H 0.7-2.6 ppm and δ_C 10-60 ppm) at 400 MHz for ^{1}H and 100 MHz for ^{13}C, $CDCl_3$

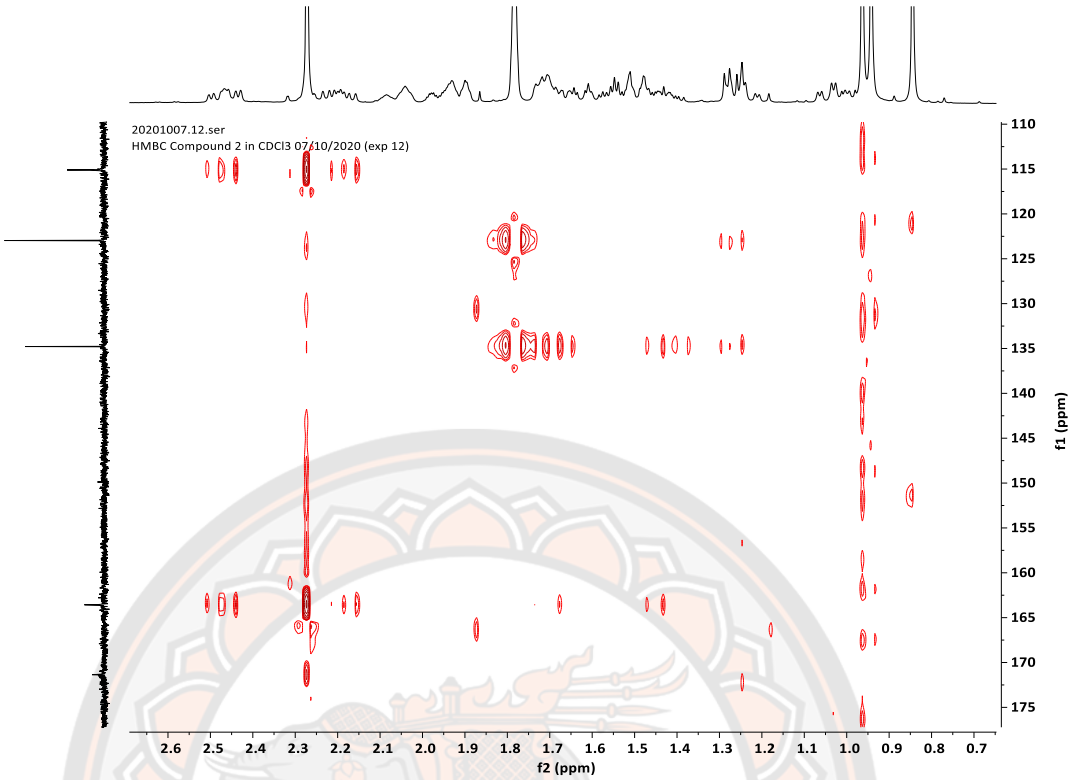

Figure 69 Enlarged HMBC spectrum of **2** (δ_H 0.7-2.7 ppm and δ_C 110-180 ppm) at 400 MHz for ^{1}H and 100 MHz for ^{13}C, $CDCl_3$

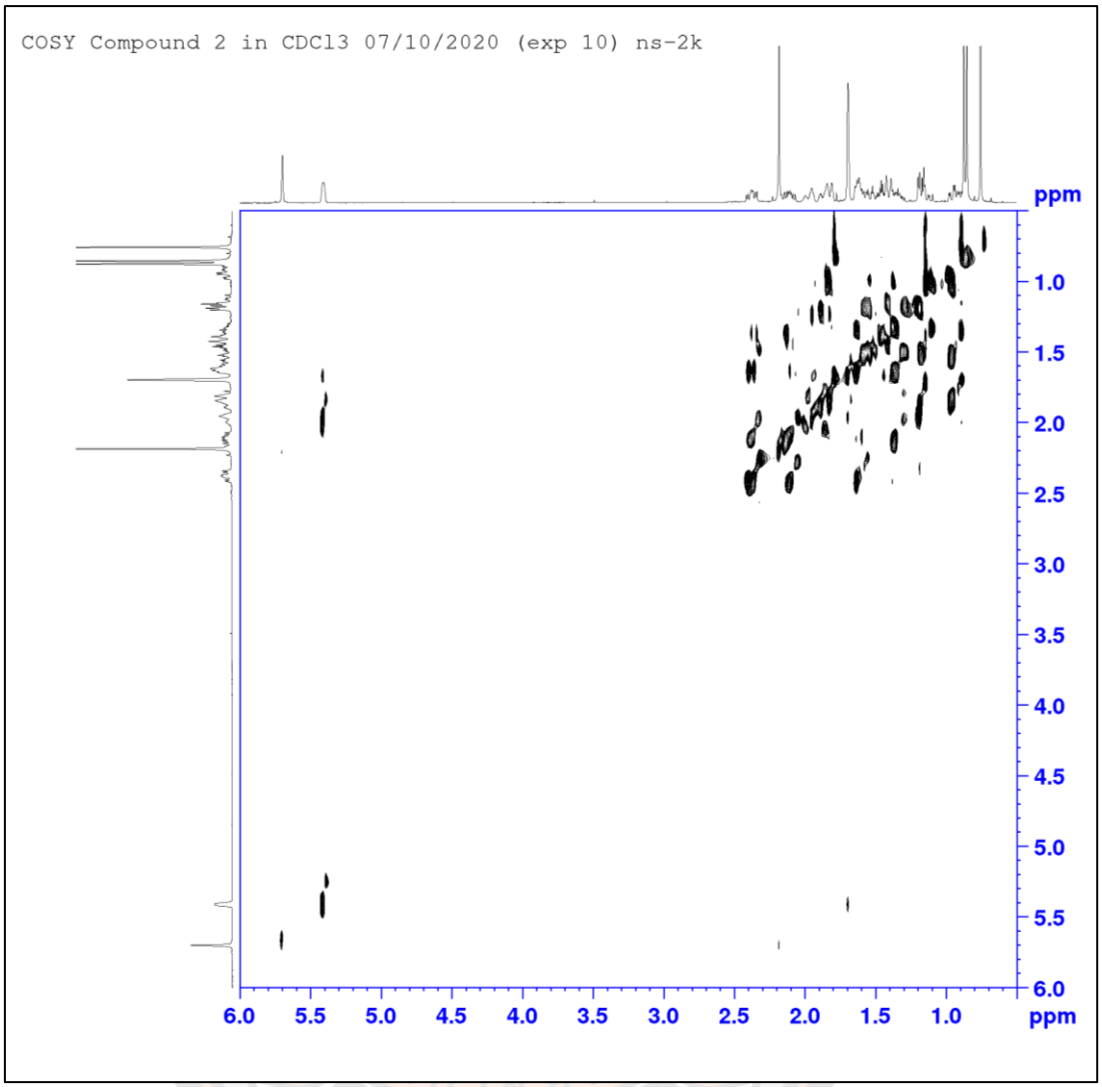

Figure 70 COSY spectrum of **2** (400 MHz, $CDCl_3$)

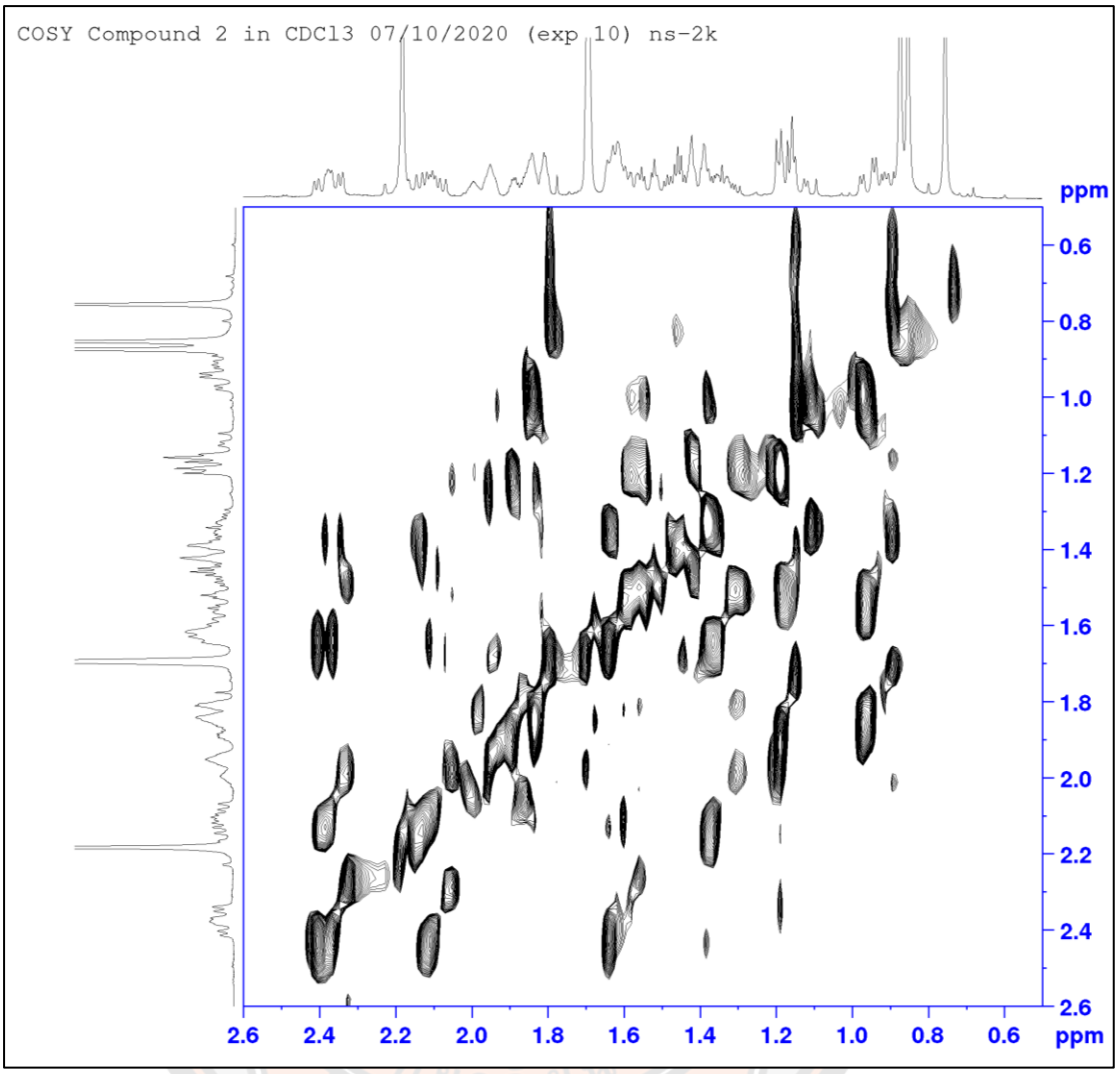

Figure 71 Enlarged COSY spectrum of **2** (400 MHz, $CDCl_3$)

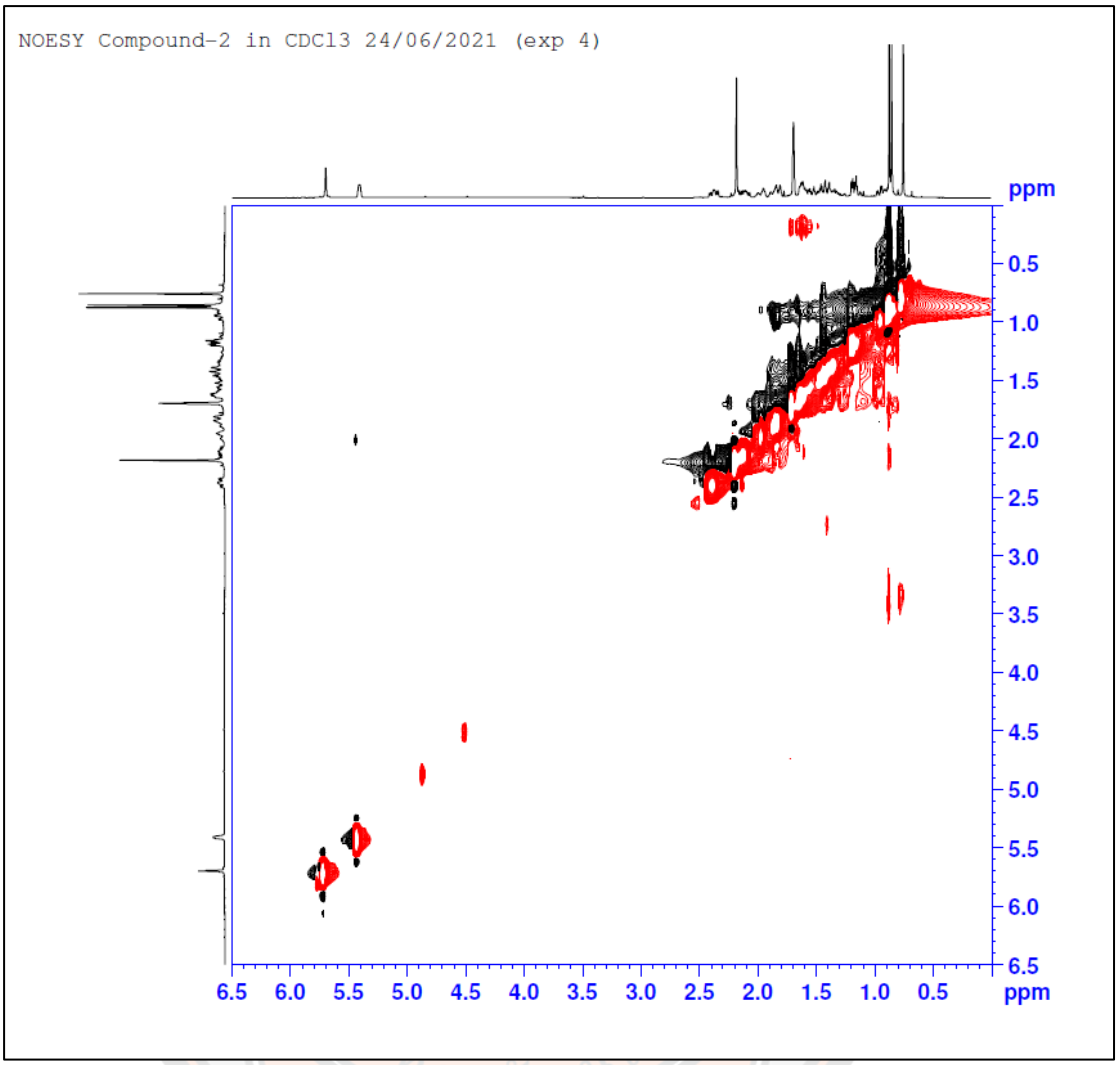

Figure 72 NOESY spectrum of **2** (400 MHz, $CDCl_3$)

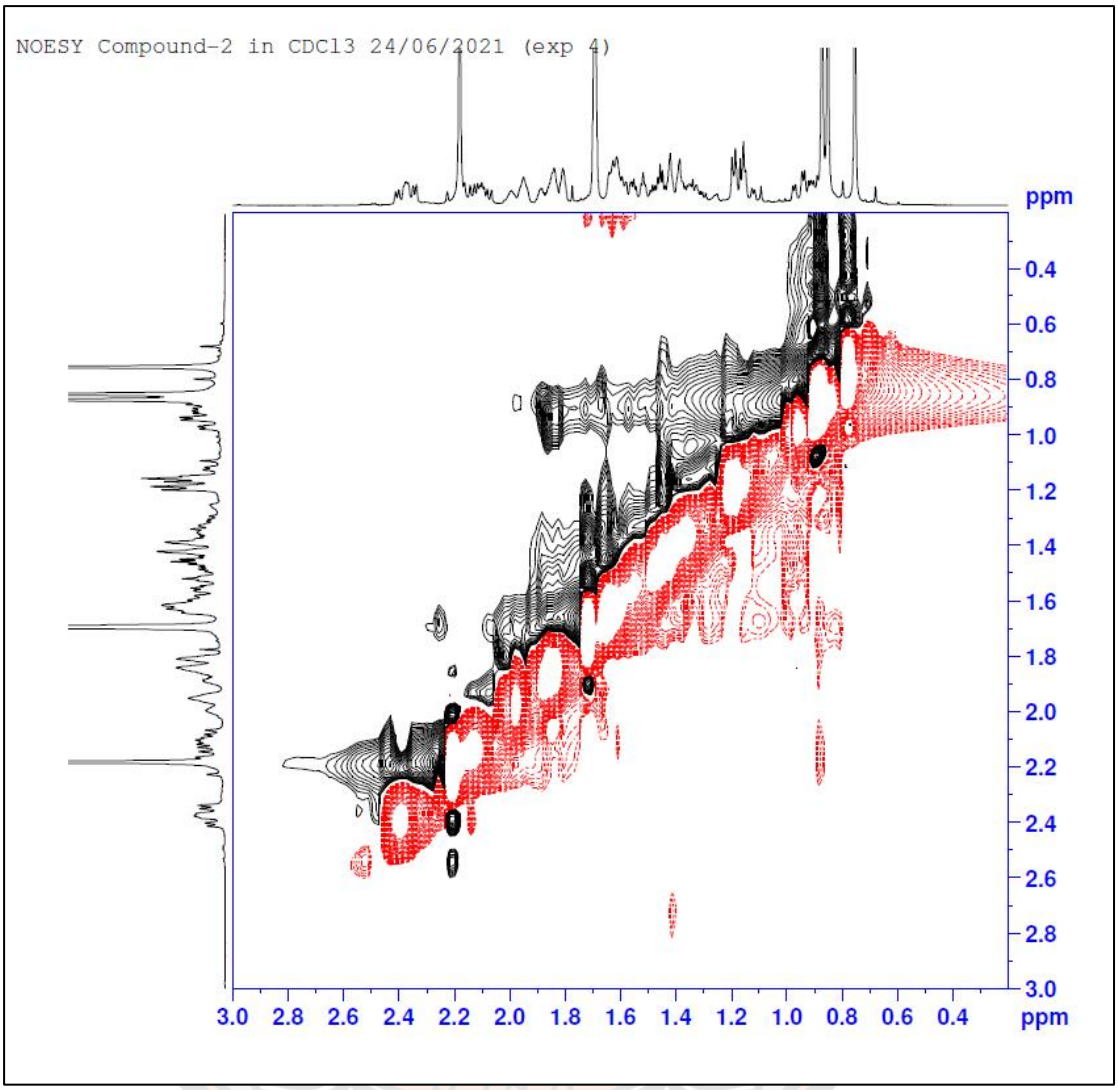

Figure 73 An expanded region NOESY spectrum (δ_H 0.3-3.0 ppm) of **2** (400 MHz, $CDCl_3$)

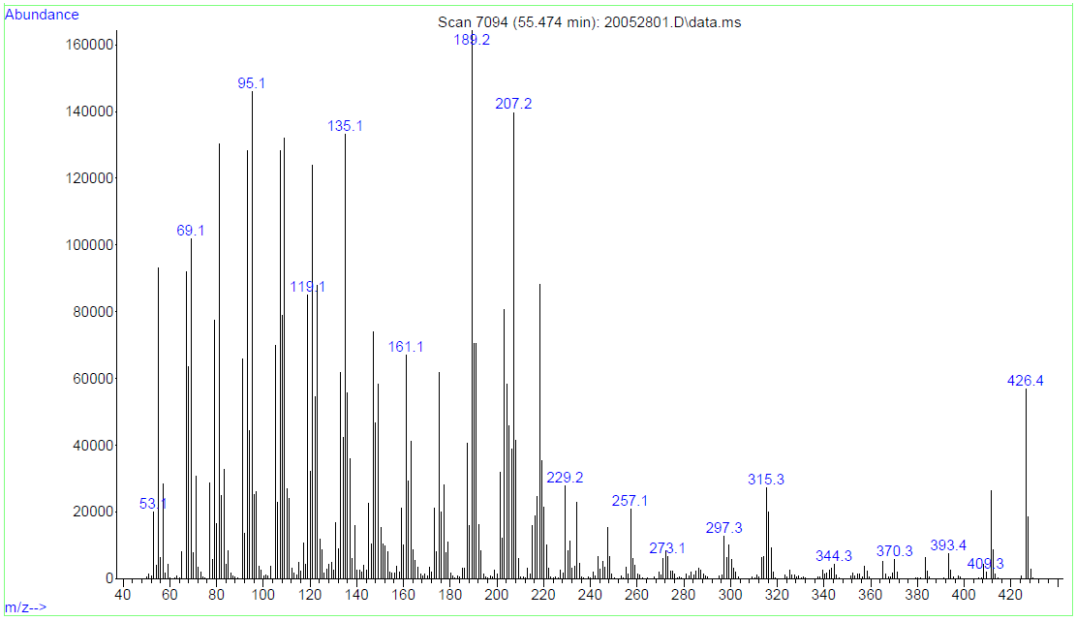

Figure 74 EI–MS spectrum of **3**

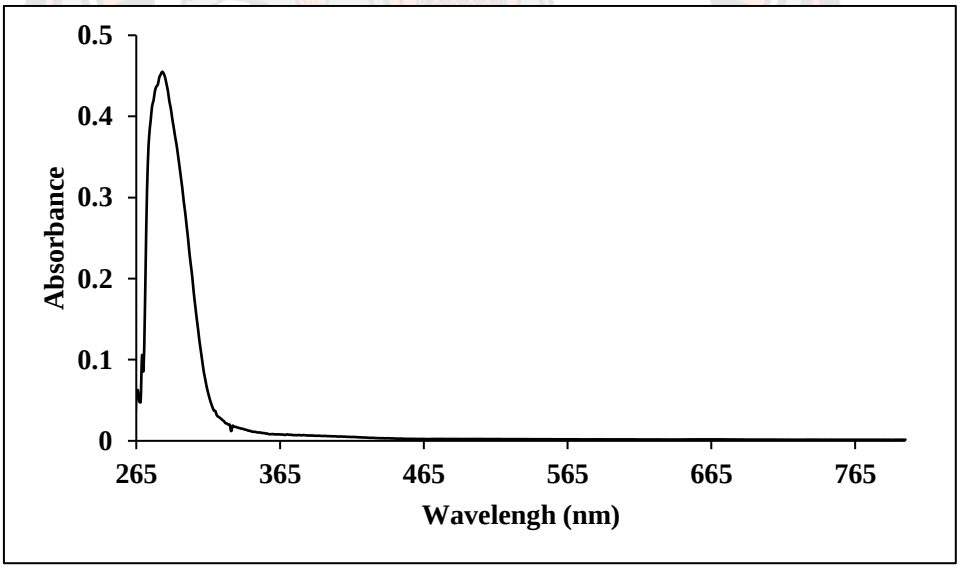

Figure 75 UV absorption spectrum of **3**

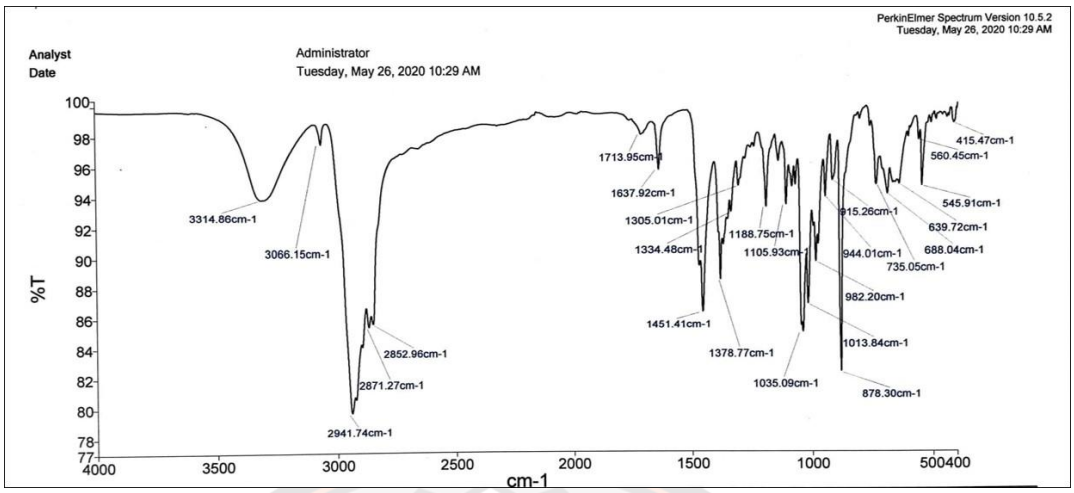

Figure 76 FT–IR (ATR mode) spectrum of **3**

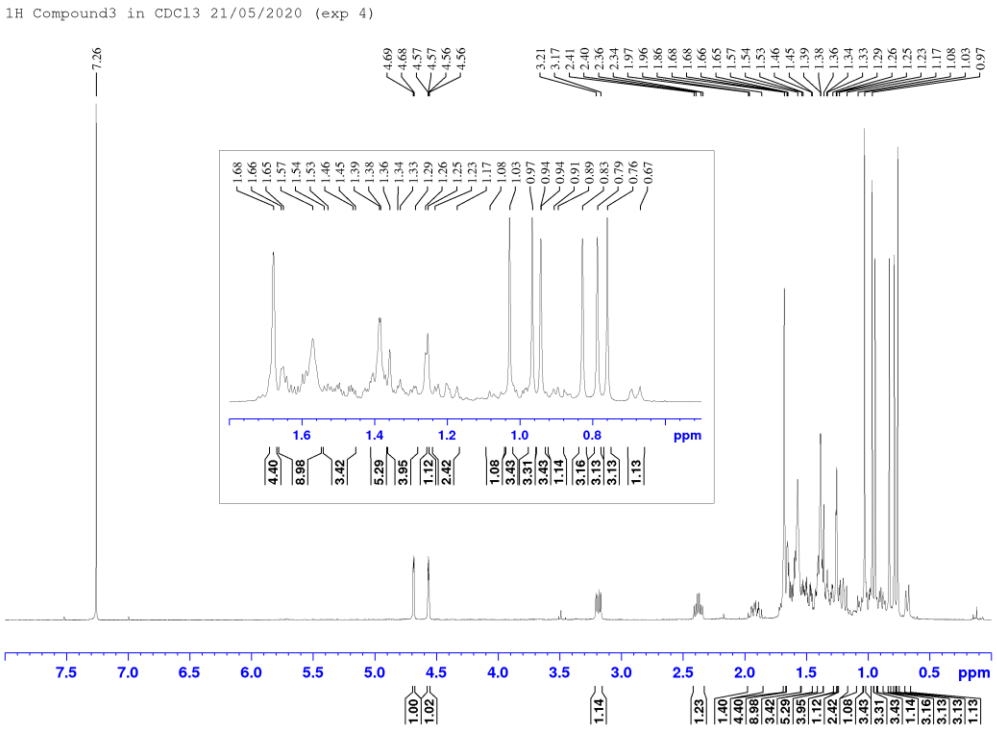

Figure 77 ^{1}H–NMR spectrum of **3** (400 MHz, $CDCl_3$)

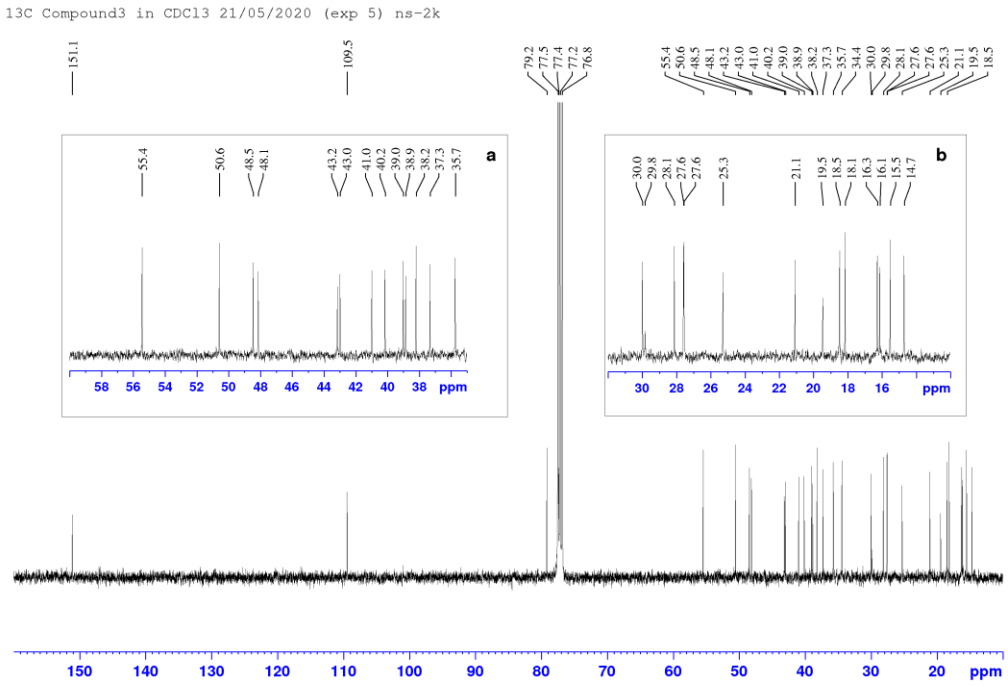

Figure 78 ^{13}C–NMR spectrum of **3** (100 MHz, $CDCl_3$)

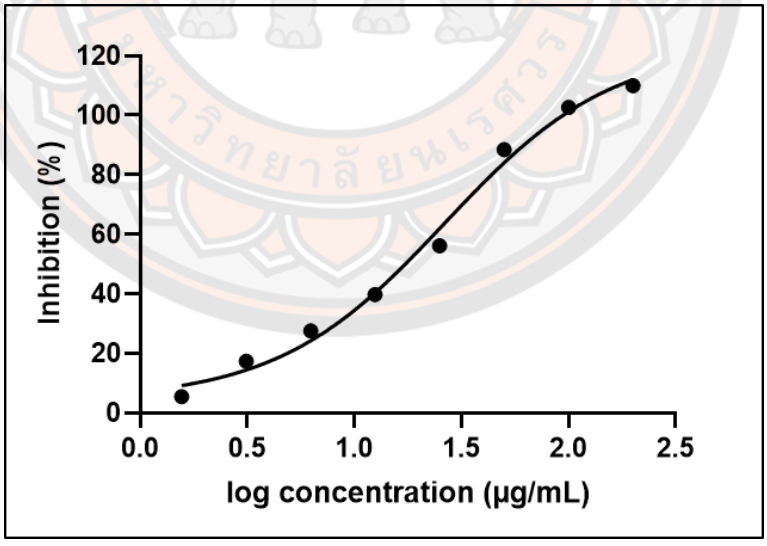

Figure 79 IC_{50} graph of hexane extract as determined by enzymatic 5α-reductase inhibition assay (n=3)

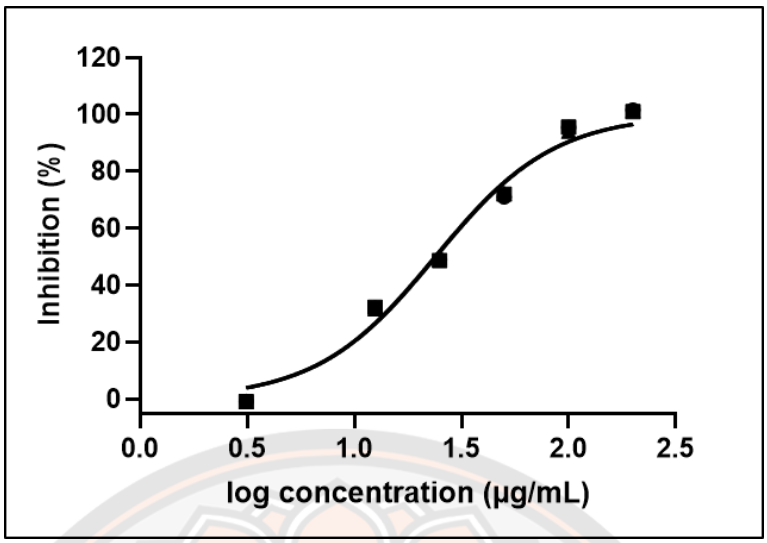

Figure 80 IC_{50} graph of ethanolic extract as determined by enzymatic 5α-reductase inhibition assay (n=3)

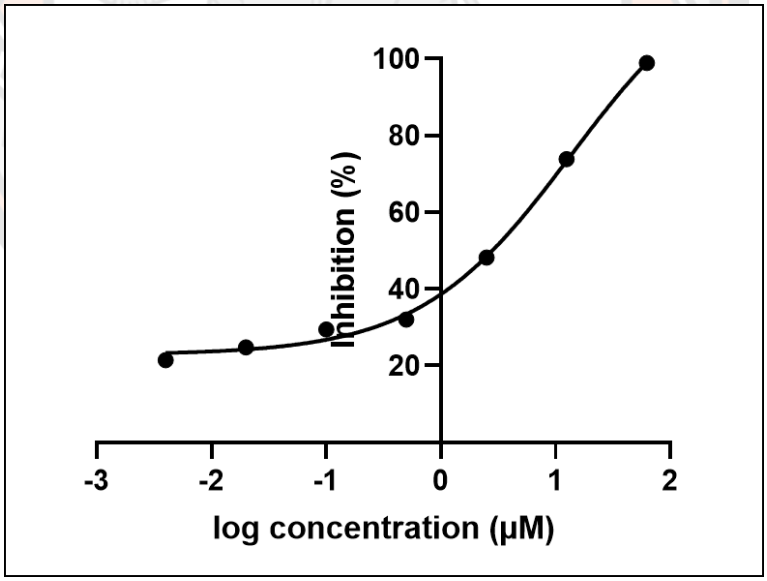

Figure 81 IC_{50} graph of compound **1** as determined by enzymatic 5α-reductase inhibition assay (n=3)

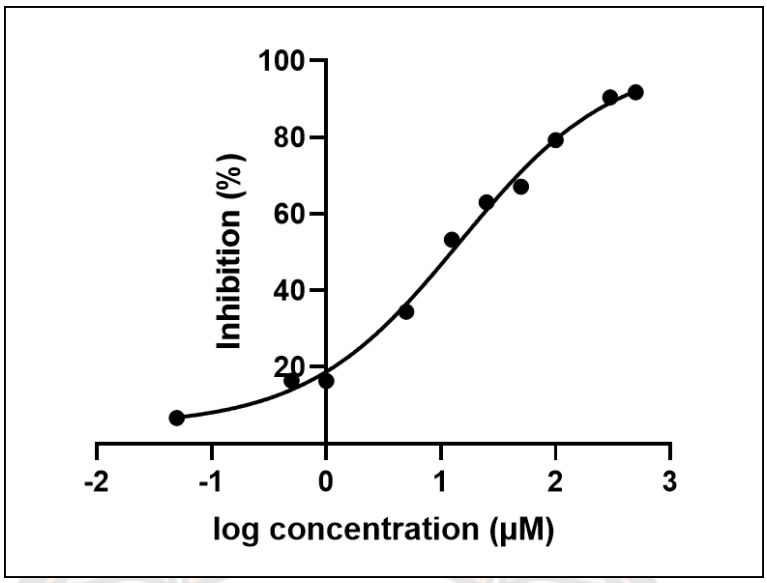

Figure 82 IC_{50} graph of compound **2** as determined by enzymatic 5α-reductase inhibition assay (n=3)

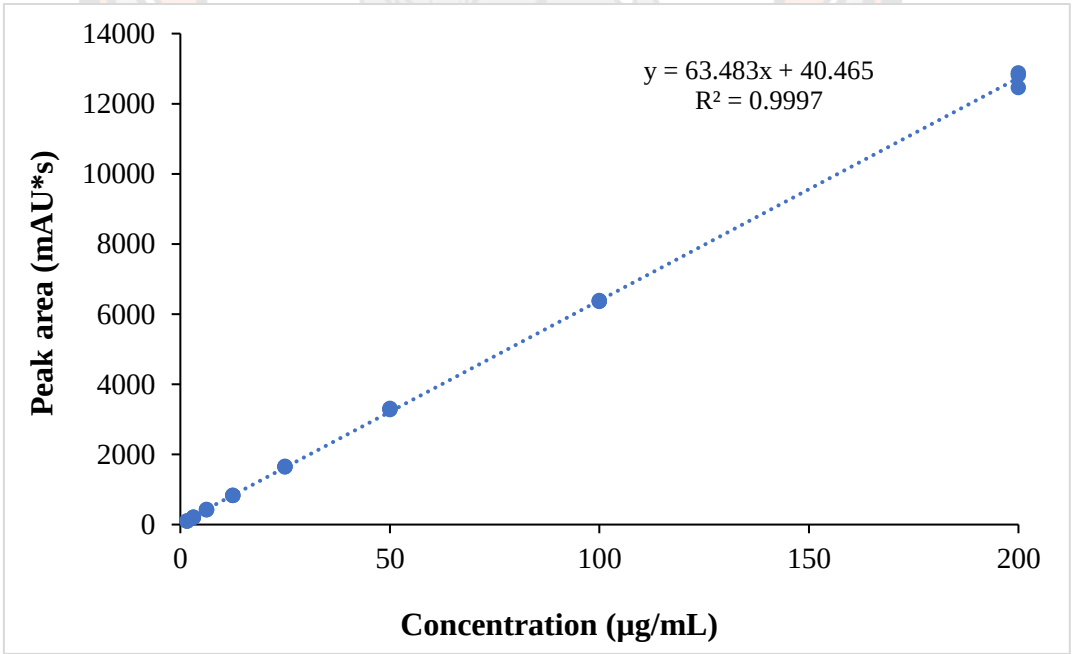

Figure 83 The plot of peak area versus the concentrations (1.56–200 µg/mL) of **1**.

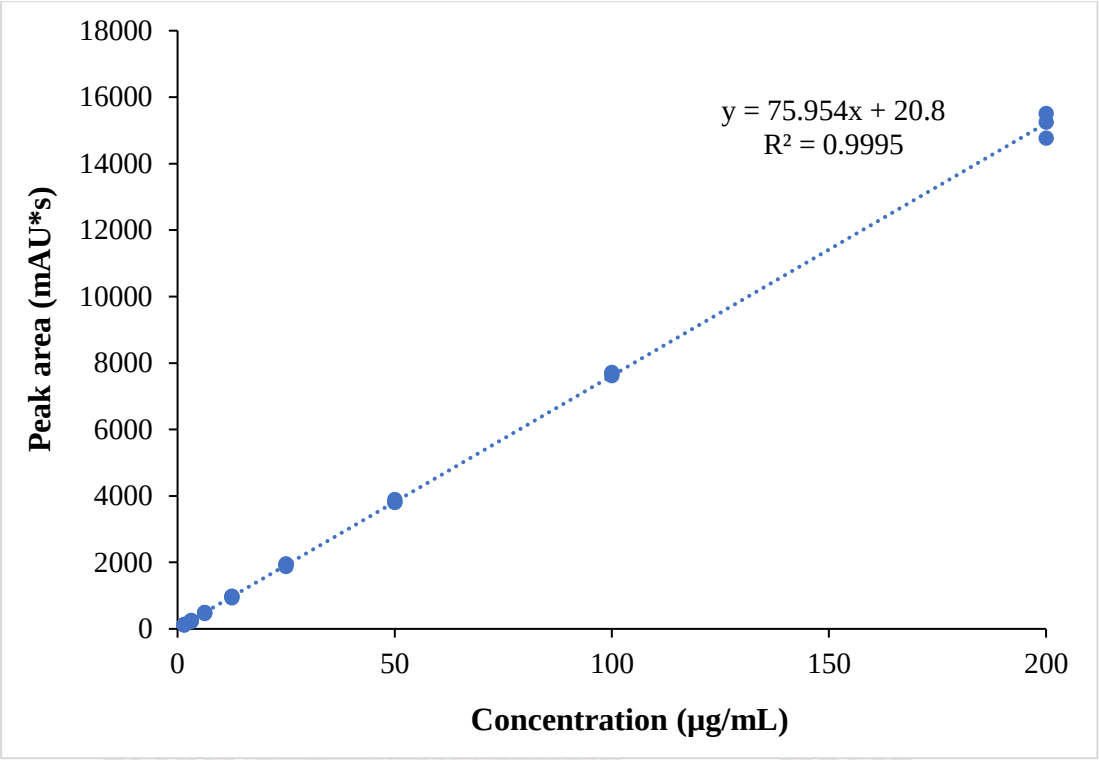

Figure 84 The plot of peak area versus the concentrations (1.56–200 µg/mL) of **1**.

AF 04-09/5.0

COE No. 030/2021

IRB No. P10046/64

คณะกรรมการจริยธรรมการวิจัยในมนุษย์ มหาวิทยาลัยนเรศวร

99 หมู่ 9 ตำบลท่าโพธิ์ อำเภอเมือง จังหวัดพิษณุโลก 65000 เบอร์โทรศัพท์ 05596-8752

หนังสือรับรองการยกเว้นพิจารณาจริยธรรมโครงการวิจัย

คณะกรรมการจริยธรรมการวิจัยในมนุษย์ มหาวิทยาลัยนเรศวร ดำเนินการให้การรับรองโครงการวิจัยตามแนวทางหลักจริยธรรมการวิจัยในคนที่เป็นมาตรฐานสากล ได้แก่ Declaration of Helsinki, The Belmont Report, CIOMS Guideline และ International Conference on Harmonization in Good Clinical Practice หรือ ICH-GCP

ชื่อโครงการ : สารยับยั้งสเตอรอยด์ไฟว์แอลฟารีดักเทส คุณสมบัติทางเคมีกายภาพ และการศึกษาก่อนการตั้งตำรับของสารสกัดใบสัก

ผู้วิจัยหลัก : นางสาวกมลลักษณ์ อินสำโรง

สังกัดหน่วยงาน : คณะวิทยาศาสตร์

ผู้ร่วมวิจัย : ผศ.ดร.หนึ่งฤทัย สุพรม

วิธีทบทวน : แบบยกเว้น (Exemption Review)

รายงานความก้าวหน้า : ไม่ต้องส่ง รายงานความก้าวหน้า (Progress Report)

ลงนาม:.....

(นายแพทย์สมบูรณ์ ตันสุภสวัสดิกุล)

ประธานคณะกรรมการจริยธรรมการวิจัยในมนุษย์

มหาวิทยาลัยนเรศวร

วันที่รับรองการยกเว้นพิจารณาจริยธรรม : 5 เมษายน 2564

หมายเหตุ

1. ไม่ต้องส่ง รายงานความก้าวหน้า (Progress Report) และรายงานสรุปผลการวิจัย (Final Report)
2. หากมีการแก้ไขโครงการวิจัยภายหลังการรับรอง ให้ผู้วิจัยดำเนินการส่งส่วนแก้ไขเพิ่มเติมโครงการวิจัย (Amendment) หรือจัดทำเป็นโครงการวิจัยใหม่